Preparation of Submicron Lignin Particles from Different Lignocellulosic Biomass and Their Modification

A Dissertation Submitted for Partial Fulfillment of the degree of Doctor of Philosophy in Chemistry

Submitted by

Swapan Kumer Ray
Examination Roll No: 01
Registration Number: 01/2018-19
Session: 2018-19

Physical Chemistry Research Laboratory
Department of Chemistry
University of Dhaka
Dhaka-1000

February, 2024

Declaration

We hereby state that the research presented in the thesis is all original work. It has never been a part of another thesis, dissertation, or application for a degree, diploma, or other qualifications, either at this institution or any other.

We are responsible for carrying out the research in accordance with the University's Committee's directions after reading the most recent version of the university's research ethical policies. In doing this, we have made every effort to account for any potential dangers, and we are aware of both our responsibilities and the rights of the participants.

…….

(Dr. Md. Qamrul Ehsan)
Professor and Chairman
Department of Chemistry
University of Dhaka
Dhaka-1000
&
Supervisor

……

(Dr. Tanvir Muslim)
Professor
Department of Chemistry
University of Dhaka
Dhaka-1000
&
Joint Supervisor

……

(Swapan Kumer Ray)
Examination Roll No: 01
Registration Number: 01/2018-19
Session: 2018-19

Dedicated

To

My Parents, Wife and Son

Acknowledgement

This has been an amazing journey for me and hereby I would like to thank everyone who held my hand and supported me a lot during the past four years. Regarding the outcome of this thesis work, I would like to express my heartiest gratitude and sincere appreciation to my research supervisor and reverend teacher **Professor Md. Qamrul Ehsan, D. Sc.,** Chairman, Department of Chemistry, University of Dhaka, who was not only my academic advisor, but also a great mentor for life. I cannot ever thank him enough for everything that he taught me, which are countless. I specially express my sincere thanks to him for his valuable suggestion and sincere supervision for completing this research work, successfully.

I deeply express gratitude to my research Joint Supervisor **Dr. Tanvir Muslim**, Professor, Department of Chemistry, University of Dhaka for his continuous support, encouragement, guidance, suggestions and valuable advices during the course of this research work.

It is my great honor to convey my sincere gratitude to the Chairman of BCSIR and respected teacher professor **Dr. Md. Aftab Ali Shaikh**, Professor, Department of Chemistry, University of Dhaka for giving me wonderful opportunity and support to move through the academic processes during PhD program.

I am thankful to **Dr. Md. Sarwar Jahan**, respected director of BCSIR Dhaka Laboratories, for continuous support and encouragement throughout my research period. I am also thankful to the respected **course teachers and other teachers of the Department of Chemistry, University of Dhaka**, for their valuable support and recommendations. I would also like to thank all of the officers and staffs of the Department of Chemistry, University of Dhaka, for their sincere effort during my study period.

I am highly thankful to the **scientists of Fibre & Polymer Fibre & Polymer Research Division**, BCSIR Dhaka Laboratories for their kind co-operation and valuable support during my research work.

My deepest gratitude and thanks to the **scientists of BCSIR Dhaka laboratories, Institute of Energy Research & Development, Institute of Glass & Ceramic Research & Testing, Institute of National Analytical Research & Services, Biomedical & Toxicological Research Institute and Leather Research Institute** for different instrumental analysis along with other research support. Special thanks to BCSIR

authority for allowing me to work at Fibre & Polymer Research Division, BCSIR Dhaka laboratories with modern laboratory facilities.

Thanks to the **Ministry of Science & Technology, Govt. of Bangladesh** for giving me permission to complete my PhD research work in **Fibre & Polymer Research Division of BCSIR Dhaka Laboratories, BCSIR, Dhaka, Bangladesh and Department of Chemistry, University of Dhaka, Dhaka**, Bangladesh along with a great research support by providing me an Annual Development Project entitled "Development of Fibre & Polymer Laboratory of BCSIR" as Project Director from July-2012 to June-2016 and also allocated me some special allocation projects, as Principle Investigator.

Finally, I would like to express my heartiest indebtedness and profound gratitude to my beloved mother **Milon Rani Ray**, my wife **Anindita**, my only son **Swapnoduti Anindo Rhivu** and all my family members for their continuous inspiration and immeasurable sacrifices throughout the period of my study. Specially, I want to wholeheartedly thank my beloved wife **Anindita** for endless love and support. This life changing experience was impossible without her tremendous sacrifices. Most importantly none of this could have happened without whose inspiration is my most favorite personality, my world, my father **Abani Mohan Ray**. But it's my misfortune that he is no more.

The author

Table of Contents

Chapter 1: General Introduction

Chapter 2: Research Methodology

Chapter 3: Development of a material-driven phase III lignocellulosic feedstock biorefinery: Isolation of lignin and characterization

Chapter 4: Chemical Modification of Alkali-lignin Submicron Particles through Acetobromination

Chapter 5: Recovery of Pretreatment Chemicals from Waste Liquors of the Biorefinery

Chapter 6: Atom Economy and Sustainability of the Material-driven Phase III Lignocellulosic Feedstock Biorefinery

Appendix

Abstract

A very straightforward and technologically and economically viable Material-driven Phase III Lignocellulosic Feedstock Biorefinery (LCF Biorefinery) system has been developed for separating alkali-lignin that complies with the principles of green chemistry. The system has been designed based on a sequential acid-base pretreatment on extractive-free lignocellulosic biomass at the temperature range 150 to 170 ^{o}C and successfully applied to fractionate non-woods, e.g., Coconut fibre and Bagasse and woody biomasses, e.g., *Trema orientalis* and *Dipterocarpus turbinatus*. Simple operation process and easy separation of the main structural components, i.e., hemicelluloses (22.66 to 27.06% w/w), cellulosic pulps (29.80 to 40.06% w/w), lignin (17.46 to 26.00% w/w) and the recovery of used chemicals, i.e., acid and base (about 100%) along with the degraded organic and inorganic residues from black liquors as valuable nitrogen, phosphorus and potassium (NPK) containing materials in crystalline and liquid forms have made the process as green. Phosphoric acid and potassium hydroxide were used as the acid and base. Isolation and subsequent recoveries of phosphoric acid precipitated alkali-lignin (ALs) from the black liquors were 84.48% for Coconut fibre (CF_AL), 79.56% for Bagasse (BG_AL), 79.34% for *Trema orientalis* (TO_AL) and 75.22% for *Dipterocarpus turbinatus* (GW_AL) based on their Klason lignin contents. These amounts were higher than lignin isolated using different ionic liquids, e.g., pyrrolidinium acetate, 1-ethyl-3-methylimidazolium acetate and 1-butyl-3-methylimidazolium chloride. The particle sizes of ball milled alkali-lignin were in submicron range, with medium dispersities (D) ranging from 0.299 to 0.594, as determined by dynamic light scattering (DLS) experiments. Intrinsic viscosities of alkali-lignin in dimethylsulfoxide at 25 ^{o}C were 22.7 mL/g for CF_AL; 4.0 mL/g for BG_AL; 16.8 mL/g for TO_AL and 13.1 mL/g for GW_AL. C_9-formula of four alkali-lignin samples were $C_9H_{7.45}O_{5.88}(OCH_3)_{1.06}$ for Coconut fibre; $C_9H_{8.09}O_{3.23}(OCH_3)_{1.03}$ for Bagasse; $C_9H_{7.88}O_{3.50}(OCH_3)_{1.13}$ for *Trema orientalis* and $C_9H_{7.80}O_{3.60}(OCH_3)_{1.02}$ for *Dipterocarpus turbinatus*. X-ray photoelectron spectroscopic (XPS) study showed the alkali-lignin samples were pure with oxygen to carbon ratios ranging from 0.177 to 0.291. Sulfur was absent in all lignin samples as the characteristics of alkali-lignin, but a trace amounts of nitrogen and silicon were present. Based on the high resolution deconvoluted XPS spectra, percentages of carbon and oxygen in C1s and O1s components were estimated using corresponding peak areas and assigned accordingly. Fundamental, overtone and combination bands of the alkali-lignin samples were examined

by Fourier transform mid and near infrared (FT-MIR-NIR) spectroscopic technique. Some agglomeration in the milled lignin samples were observed from Field emission-scanning electron microscopic (FE-SEM) study. All lignin samples showed a weight loss about 15% upto 200 ^{o}C and about 30% upto 375 ^{o}C. About 20 to 42% carbon materials, i.e., char obtained at 850 ^{o}C from the degradation of alkali-lignin samples under inert atmosphere. All lignin samples showed a glass transition temperature of approximately 75 ^{o}C, which was suggestive of degraded lignin. Ultraviolet diffuse reflectance spectroscopic (UV-DRS) analysis showed that the powdered lignin samples absorbed radiation in the ultraviolet region. Kubelka-Munk function and apparent absorbance of alkali-lignin samples showed a good agreement with the reference values and exhibited higher absorption coefficient in UV regions, i.e., UV-A 315 to 400 nm; UV-B 280 to 315 nm and UV-C 200 to 280 nm. Surprisingly, CF_AL showed the highest Kubelka-Munk function with the highest apparent absorbance value and absorbed strongly in UV regions, i.e., 224 to 428 nm. Antioxidant activity of all lignin samples were measured by 2,2-diphenyl-1-picrylhydrazyl (DPPH) method and half-maximal inhibitory concentration (IC_{50}) values ranging from 6.02 to 19.57 μg/mL were obtained, whereas ascorbic acid showed IC_{50} value of 9.52 μg/mL. Overall evaluation of thermal characteristics, antioxidant activity, and ultraviolet light absorption properties of alkali-lignin samples also produced encouraging findings for high-value applications.

Depending on the intended applications, lignin's structure could be transformed using a variety of reagents and different conditions, e.g., chemical modifications of lignin. It is known that acetyl bromide (AcBr) has been used to acetobrominate lignin, analytically, in acetic acid medium and subsequently quantify and elucidate the structural features of lignin, including molar mass determination and compositions of monolignols applying derivatization followed by reductive cleavage (DFRC) methodology. Acetyl bromide can modify the lignin structure in mainly three ways, e.g., acetylation, benzylic bromination and potential cleavage of α-ether bonds. No report yet published on the lignin acetobromination, where bromination in the lignin's aromatic ring occurred concurrently with acetylation and benzylic bromination. On the other hand, in-depth research into the physicochemical properties of acetobrominated lignin has not yet been performed, nor has there been any straightforward method for synthesizing acetobrominated lignin with higher bromine contents. In this investigation we have described a new synthetic route (utilizing a flow chemistry approach) for producing acetobrominated alkali-lignin with higher bromine contents by acetylation, benzylic bromination and the bromination in

aromatic ring of the monolignols, concurrently, using acetic anhydride and bromine in the presence or absence of acetic acid. Bromine levels in the synthesized products were substantially higher (17 to 22% w/w) in comparison to acetobrominated lignin made using conventional method, e.g., reaction with acetyl bromide in acetic acid medium (about 5% w/w). In contrast to conventional method, the new method dramatically increased the percentage of C-Br bonds in lignin, while the amounts of the aromatic rings' C-H bonds reduced, indicating the aromatic ring bromination. Increased amounts of acetyl group in the lignin structure were also observed. High resolution deconvoluted X-ray photoelectron spectroscopic (XPS) analysis supported these facts. ^{1}H-^{13}C Heteronuclear single quantum coherence (HSQC) Nuclear magnetic resonance (NMR) spectroscopic study also showed no significant correlation in the aromatic range. Fourier transform mid and near infrared (FT-MIR-NIR) spectroscopic studies revealed that bromine and acetyl groups replaced the hydroxyl groups from lignin structure and thus the polarity of lignin macromolecule decreased. The acetobrominated samples were highly soluble in acetone, dioxane, tetrahydrofuran and dimethylsulfoxide, but partially soluble in ethanol and insoluble in water. Dilute solution viscometry (DSV), Scanning electron microscopy-energy dispersive X-ray spectroscopy (SEM-EDX), X-ray diffraction analysis, Simultaneous thermal analysis (STA), UV-Vis spectroscopic analysis, etc., were applied to evaluate and compare the molecular properties of acetobrominated products. Mechanism of the new acetobromination reaction of lignin has also been elucidated. Overall studies demonstrated the potential of new acetobromination method as a lignin modification tool for the commercialization of technical lignin.

As the sustainability of lignocellulosic biomass conversion processes largely depend on the minimization of environmental pollution in any forms, thus an efficient conversion of lignocellulosic biomasses into their main structural components, i.e., cellulose, hemicelluloses and lignin with no waste generation is of great importance. To ensure the sustainability of the Material-driven Phase III LCF Biorefinery System, the used pretreatment chemicals, i.e., phosphoric acid and potassium hydroxide along with degraded organics from waste liquors have been recovered as valuable nitrogen, phosphorus and potassium (NPK) containing materials in crystalline and liquid forms. The recovery steps were performed after the separation of alkali-lignin from black liquors by adding ammonium hydroxide and crystallized the acid and bases as salts at room temperature. The salts were characterized by XRD, XPS and SEM-EDX techniques. Analyses showed that the salts crystallized from black liquors were $K(NH_4)HPO_4$,

$(NH_4)_2HPO_4$, KH_2PO_4 and $(K,NH_4)H_2PO_4$. The spent liquors obtained after the crystallization step might be used as liquid-fertilizer containing potassium, ammonium and phosphate ions and hydrolyzed biomass constituents. Properties of the liquid fertilizer were also evaluated by different physicochemical methods, including viscosity measurement, moisture content determination, etc. SEM-EDX analysis of the solid contents of liquid fertilizers confirmed the presence of nitrogen, potassium, phosphorus, carbon and oxygen in the materials. Thus, all solids and liquids involved in the biomass conversion process were recovered to achieve higher atom economy (greater than 96%) and ensure economic viability of the biorefinery system. Principles of green chemistry were obeyed in every step of the work. The developed material-driven phase III LCF biorefinery system might add a new dimension in the conversion of lignocellulosic biomass to structural components, i.e., hemicelluloses, cellulose, and alkali-lignin along with the recovery of pretreatment chemicals from waste liquor as valuable NPK containing materials/fertilizers for agricultural applications.

List of Symbols, Abbreviation and Nomenclature

CHEMICALS and OTHER SYMBOLS

AcBr	Acetyl bromide
[Pyrr][Ac]	Pyrrolidinium acetate
[C_2C_1im][OAc]	1-Ethyl-3-methylimidazolium acetate
[BmimCl]	1-Butyl-3-methylimidazolium chloride
AQ	Anthraquinone
NPK	Nitrogen, phosphorus, potassium
THF	Tetrahydrofuran
DMSO	Dimethylsulfoxide
DPPH	2,2-diphenyl-1-picrylhydrazyl
AA	Acetic acid
AAn	Acetic abhydride
Br	Bromine
AH	Ammonium hydroxide
PH	Potassium hydroxide
PA	Phosphoric acid
DI water	Deionized water
g	Gram
µg	Microgram
mg	Miligram
Kg	Kilogram
kDa	Kilodalton
nm	Nanometer
µm	Micrometer
mm	Milimeter
m	Meter
sec	Second
min	Minute
h	Hour
µL	Microlitre
mL	Mililitre
L	Litre
(v/v)	Volume per volume e.g.. (mL/mL)
(w/v)	Weight per volume e.g., (mL/mL)
ppm	Parts per million
%	Percentage
^oC	Degree celsius
ODW	Oven dried weight
i.e.	That is
e.g.	For example
et al.	And others
α	Alpha
β	Beta
γ	Gamma
η	Eta

MATERIALS

LCF	Lignocellulosic feedstock
CF	Coconut fibre
BG	Bagasse
TO	*Trema orientalis (Nalita wood)*
GW	Gurjan wood (*Dipterocarpus turbinatus*)
CF_AL	Coconut fibre alkali-lignin
BG_AL	Bagasse alkali-lignin
TO_AL	*Trema orientalis* alkali lignin
GW_AL	Gurjan wood alkali lignin
CF_AL_AcBr	Acetobrominated coconut fibre alkali-lignin (Conventional method)
BG_AL_AcBr	Acetobrominated bagasse alkali-lignin (Conventional method)
TO_AL_AcBr	Acetobrominated trema orientalis alkali lignin (Conventional method)
GW_AL_AcBr	Acetobrominated gurjan wood alkali lignin (Conventional method)
CF_AL_AcBr-1-5	Acetobrominated coconut fibre alkali-lignin samples (1 to 5) synthesized in the absence of acetic acid (New method: Preparative mehod-1)
CF_AL_AcBr_AA	Acetobrominated coconut fibre alkali-lignin sample synthesized in the presence of acetic acid (New mehod: Preparative mehod-2)
CF_SF	Coconut fibre_Crystallized salt
BG_SF	Bagasse_ Crystallized salt
TO_SF	Trema orientalis_ Crystallized salt
GW_SF	Gurjan wood_ Crystallized salt
CF_LF	Coconut fibre_liquid NPK-fertilizer
BG_LF	Bagasse_liquid NPK-fertilizer
TO_LF	Trema orientalis_liquid NPK-fertilizer
GW_LF	Gurjan wood_liquid NPK-fertilizer
CF_LF-S	Coconut fibre_liquid NPK-fertilizer's solid content
BG_LF-S	Bagasse_liquid NPK-fertilizer's solid content
TO_LF-S	Trema orientalis_liquid NPK-fertilizer's solid content
GW_LF-S	Gurjan wood_liquid NPK-fertilizer's solid content

CHARACTERIZATION

ASE	Accelarated solvent extraction
EA	Elemental analysis
PSA	Particle size analysis
XPS	X-ray photoelectron spectroscopy
FT-MIR	Fourier transform mid infrared spectroscopic analysis
FT-NIR	Fourier transform near infrared spectroscopic analysis
TGA	Thermogravimeric analysis
DTGA	Differential thermogravimetric analysis
DSC	Differential scanning calorimetry
DDSC	Derivative differential scanning calorimetry
FE-SEM	Field emission-Scanning electron microscopy

EDX/EDS	Energy dispersive X-ray spectroscopy
UV-Vis	Ultraviolet-visible spectroscopy
UV-DRS	Uitaviolet diffuse reflectance spectroscopy
DSV	Dilute solution viscometry
DLS	Dynamic light scattering
XRD	X-ray diffraction analysis
NMR	Nuclear magnetic resonance spectroscopy
HSQC	Heteronuclear single quantum coherence
DFRC	Derivatization followed by reductive cleavage

PROPERTIES

AOA	Antioxidant activity
η	Dynamic viscosity
η_r	Relative viscosity
$[\eta]$	Intrinsic viscosity
IC_{50}	Half maxmum inhibitory concentration
T_g	Glass transion temperature
D	Dispersiy
O/C	Oxygen to carbon ratio
$F(R_\alpha)$	Kubelka-Munk function
R_α	Absolute remittance

List of Tables

List of Figures and Illustrations

List of Schemes

Chapter 1: General Introduction

1.1. Background

Conversion of lignocellulosic biomasses into their structural components is getting more attention, day by day, due to their availability, renewable nature and increasing environmental concern generated by petrochemicals. It is now considered as an important field of research for producing valuable and green products to ensure sustainable industrial production and development. Biomass converted products, i.e., cellulose, hemicelluloses and lignin as a source of fine chemicals and advanced materials, etc. are increasingly used in widespread conventional, high-performance, and smart applications [1, 2]. Biomasses are also valuable for the production of biofuel and energy by applying appropriate and feasible conversion technologies (Figure 1.1 and Figure 1.2).

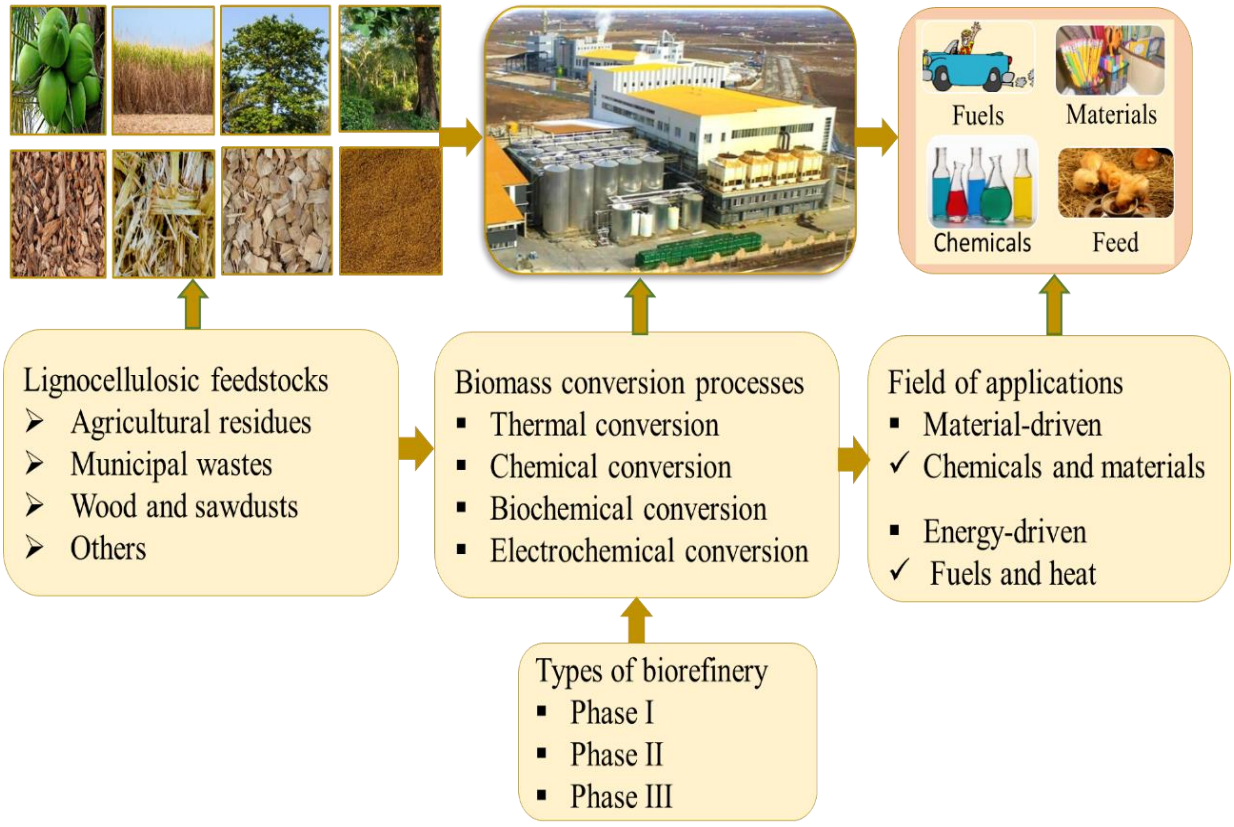

Figure 1.1: Lignocellulosic feedstock biorefinery and field of applications

However, value addition to technical lignin is still limited. At present, lignin is being produced in a large quantity as a by-product of different pulping industries and biorefinery systems. According to the International Lignin Institute, more than 50 million tonnes of Kraft lignin are produced every year, globally.

There are no significant high value applications of lignin except burning and heat generation or land filling. Management and utilization of lignin containing waste liquors generated from pulp industries and different biorefinery processes is still a challenging issue towards sustainable development. A green and efficient utilization of these waste liquors have been considered as an important field for the economic feasibility and also sustainability of different pulping processes and biorefinery systems.

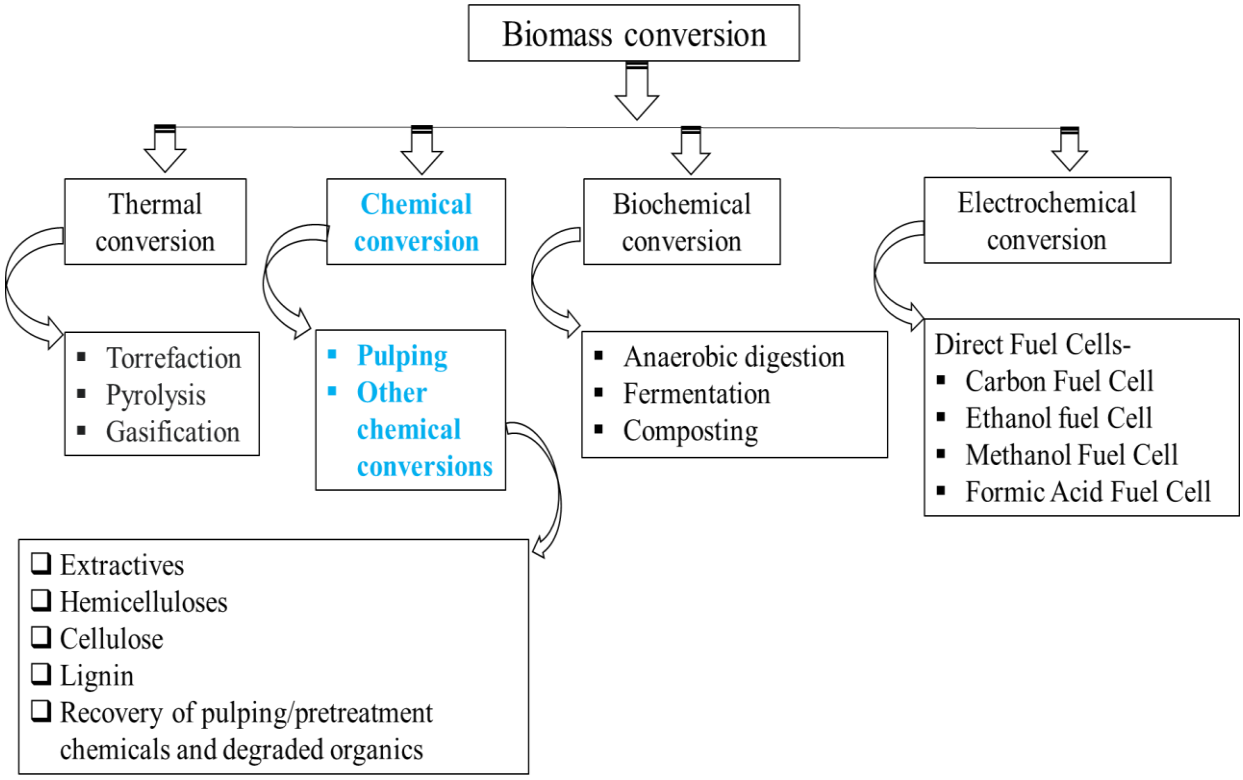

Figure 1.2: Commonly used technologies for biomass conversion

As a natural and renewable raw material and obtainable at an affordable cost, lignin's substitution potential can be extended to many products currently sourced from petrochemicals. Lignin shows some excellent physicochemical properties, e.g., biodegradability, antioxidant activity, flame retardancy, reinforcing capability with various materials, etc. These properties with multi-functional nature make lignin as a potential candidate for the production of high value bio-aromatic chemicals, bio-based polymeric materials, e.g., resins and polymers, dispersants/super-plasticizers, asphalt modifiers, carbon fibres for use as reinforcement fillers in thermoplastic polymers, light-weight composite materials, as well as graphene for use in super-capacitors for energy storage and other suitable applications, etc.

Many studies have been conducted on the utilization of lignin since last few decades. Some attractive and very promising results have been obtained. To achieve industrial sustainability, e.g., environmental, economic and social point of view, greener conversions of lignocellulosic biomasses including their waste forms are of paramount importance. Thus, the following research and development activities need special consideration based on the overall context-

(i) Development of green and innovative biorefinery technique that successfully converts different lignocellulosic biomasses, e.g., woods and non-woods to their structural components, i.e., cellulose, hemicelluloses and lignin and non-structural components, e.g., extractives, etc. with no waste generation and thus no environmental pollution.
(ii) A straightforward method to isolate and prepare lignin from the biorefinery in pure form and determination of physicochemical properties for potential applications.
(iii) Chemical modification(s) of lignin by suitable technique for high value applications.
(iv) Recovery of pretreatment chemicals from waste liquors, after the separation of lignin, as valuable forms for industrial applications.
(v) Applications of unmodified and modified lignin in different industries, e.g., rubber, plastics, resins, bitumen, biomedical, agriculture, etc.

However, a research on creating a sustainable supply of non-food biomass to support a "resource-efficient" bioeconomy in Europe was recently issued by Imperial College of London [3]. This project was aimed to use five types of lignocellulosic biomass, e.g., wood from forest, other forest biomass, agricultural residues, wastes, and cropped biomass (Figure 1.3).

Main focus has been given to switch to sophisticated biomass conversion technologies in order to mobilize indigenous lignocellulosic biomass in a sustainable and resource-efficient manner for the promotion of bio-based economy in Europe. The most common type of renewable bioresources on the planet is plant biomasses (Figure 1.4), i.e., lignocellulosic feedstock that includes softwood like pine, spruce, etc. are common, while hardwood like aspen, beech, birch, *Trema orientalis (*Nalita wood), and *Dipterocarpus turbinatus (*Gurjan wood), etc. Most agricultural crops and grasses, including bamboo, wheat straw, rice straw, sugarcane bagasse, cereal crops, oilseed crops, etc. make up the category of herbaceous biomass.

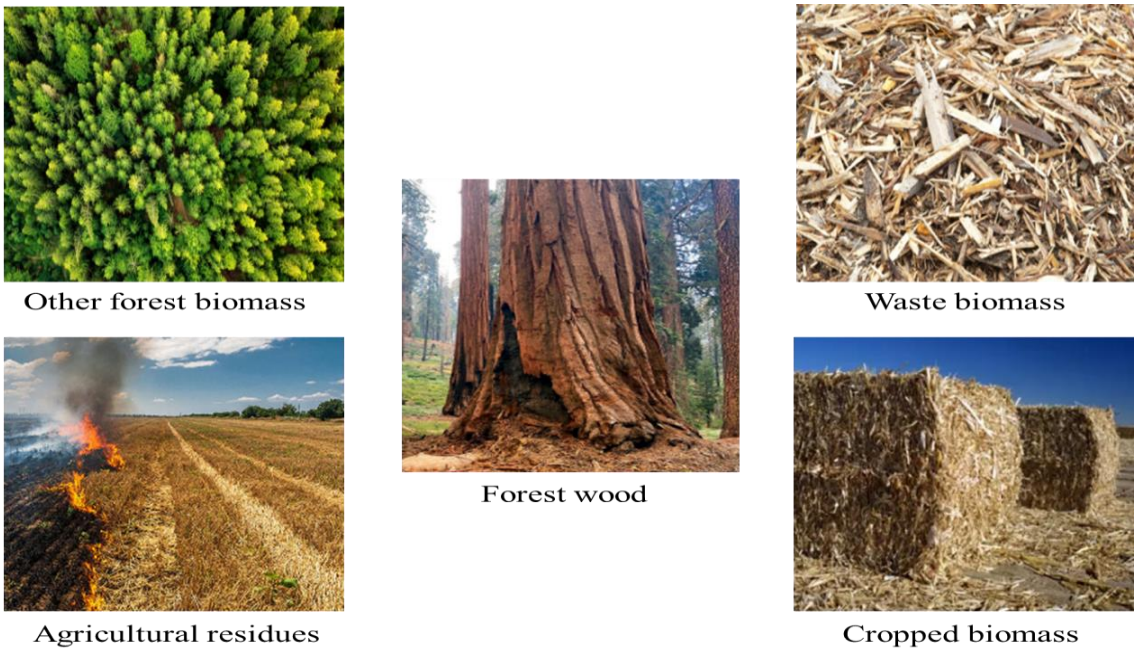

Figure 1.3: Different lignocellulosic feedstock for the development of bio-based economy

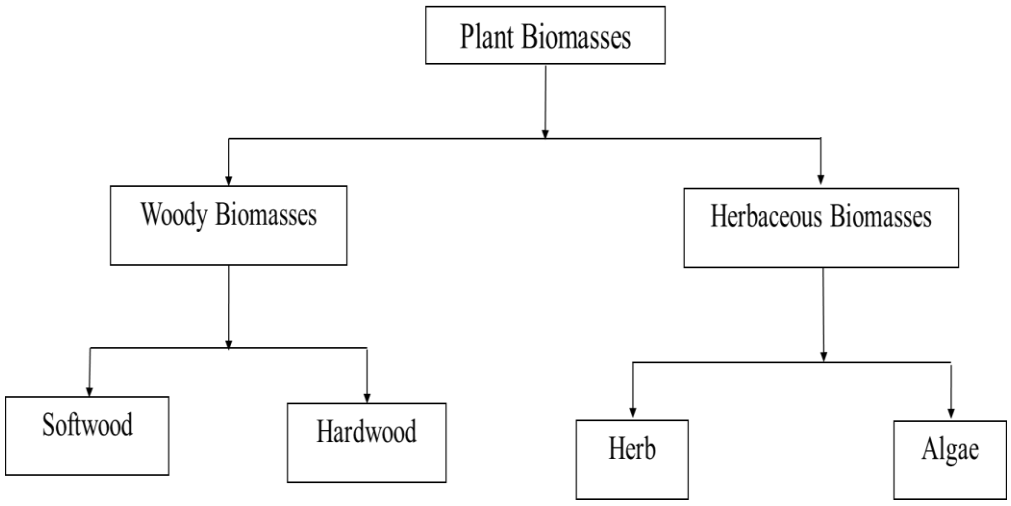

Figure 1.4: A brief classification of plant biomasses/lignocellulosic feedstock

As cereal crop residues, the plant's dried stems, pods, and husks can used as lignocellulosic feedstock individually and in combination. The grasslands are described as the home of stems, shells, and their mixtures. However, lignocellulosic-feedstock mainly composed of two types of biopolymers, i.e., lignin and holocellulose. The holocellulose component is also composed of two different polymers, cellulose and hemicelluloses [4]. Structural and non-structural constituents of lignocellulosic-feedstock have been summarized briefly in Figure 1.5 and the amounts of structural components in some biomasses have been given in Table 1.1.

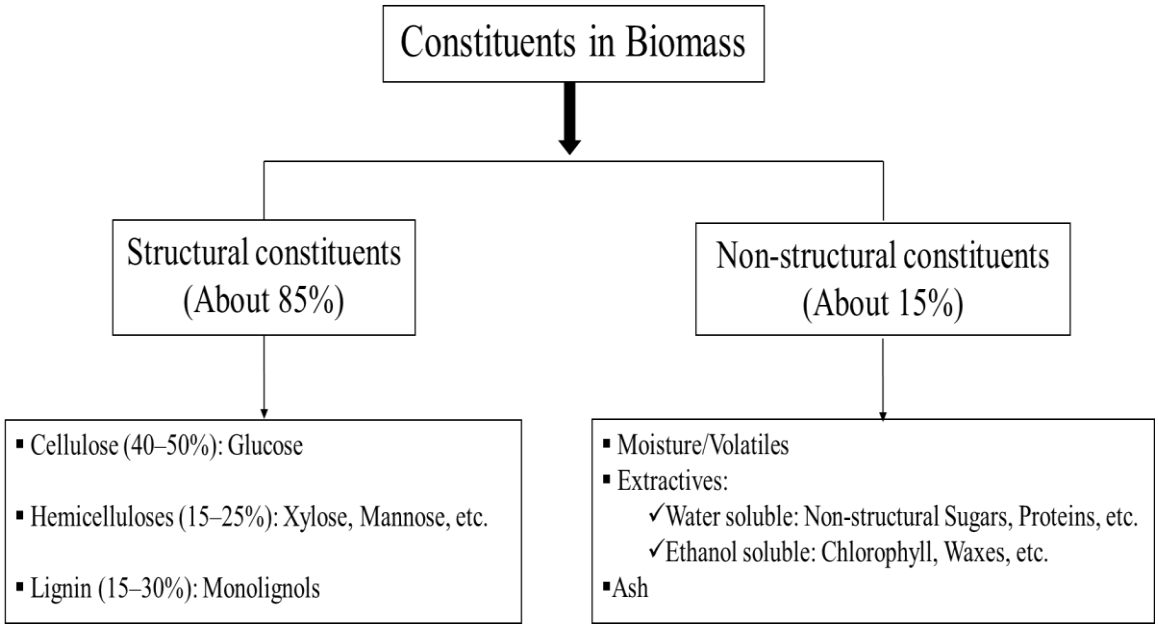

Figure 1.5: Structural and nonstructural constituents of plant biomass

Table 1.1: Principle structural components, i.e., cellulose, hemicelluloses and lignin in common lignocellulosic feedstock [5].

Lignocellulosic feedstock	Cellulose	Hemicelluloses	Lignin
Hardwood	40–55	24–40	18–25
Softwood	45–50	25–35	25–35
Sugar cane bagasse	42	25	20
Sweet sorghum	45	27	21
Rice Straw	32	24	18
Nut shells	25–30	25–30	30–40
Grasses	25–40	25–50	10–30
Wheat straw	29–35	26–32	16–21
Agricultural residues	5–15	37–50	25–50

Besides pulping raw materials and agricultural feedstock, there are enormous amounts of biomasses, e.g., waste green coconut husk, bagasse, different wood residues, etc. being discarded every day in the municipal areas of some Asian countries [6-8]. Conversion of this feedstock by following green chemistry principles may add a higher value with respect to the economy and also environment. To achieve industrial sustainability, e.g., environmental, economic and social point of view, greener conversions of lignocellulosic biomasses including their waste forms are of paramount importance [9]. Many scientific efforts have been made over the past few decades to provide more environmentally friendly conversion

techniques for the manufacture of cellulose, lignin, and hemicelluloses as well as for the recoveries of compounds utilized in the pretreatment procedures [10-13]. Mainly two pathways (Figure 1.6) are being followed to convert lignocellulosic biomasses into their most abundant structural components, i.e., cellulose and lignin [14].

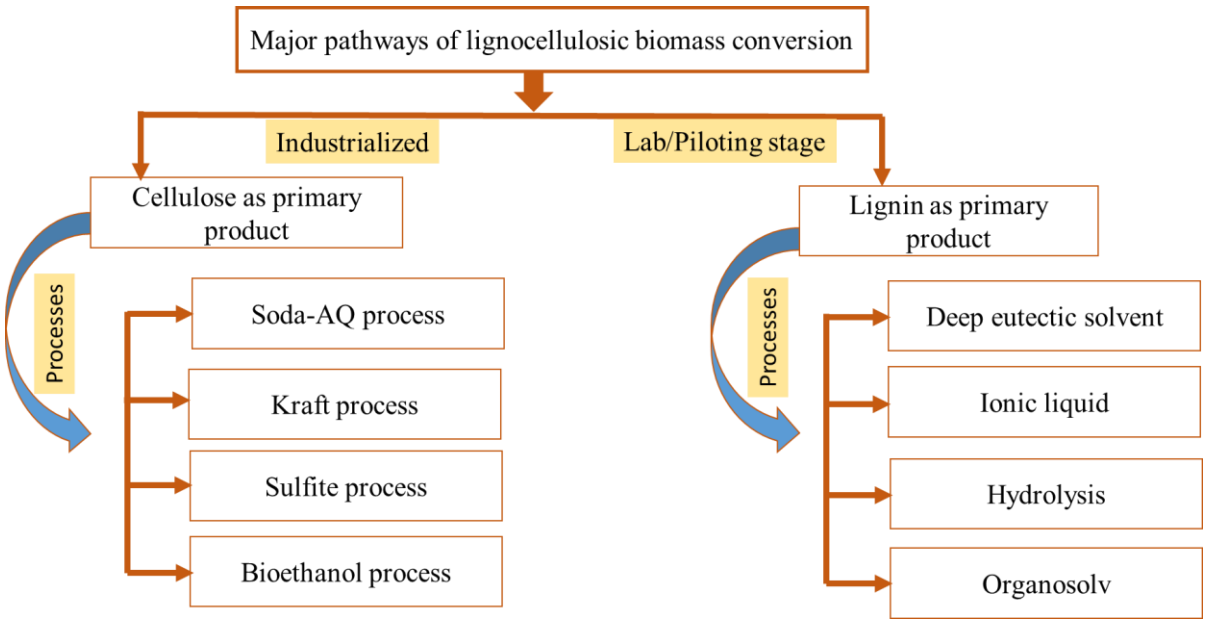

Figure 1.6: Two main pathways are used to convert lignocellulosic biomass into their componants

The biomass conversion system includes a prehydrolysis step that is being examined as a viable method for the recovery of hemicelluloses and converts them to mono and oligosaccharides using the right procedures in order to manufacture materials and fine chemicals, etc. [2, 15-18]. A lot of research and development is still needed to create a sustainable and financially successful model lignocellulosic-feedstock biorefinery system, such as an integrated biorefinery [19-25].

National Renewable Energy Laboratory (NREL) defines the biorefinery as “A biorefinery is a facility that integrates biomass conversion processes and equipment to produce fuels, power, and chemicals from biomass. The biorefinery concept is analogous to today’s petroleum refineries, which produce multiple fuels and products from petroleum. Industrial biorefineries have been identified as the most promising route to the creation of a new domestic bio-based industry” [26].

A formal definition of a biorefinery was just released by the International Energy Agency (IEA), which describes it as "the sustainable processing of biomass into a spectrum of bio-based goods (food, feed, chemicals, and/or materials) and bioenergy (biofuels, power, and/or heat)" [27].

There are many concepts to classify biorefinery systems. Based on the types of final uses, such as energetic and non-energetic products, two primary classes of biorefinery system have been described [28-30]. These are (i) energy-driven biorefinery, which produce biofuels, power and/ or heat and (ii) material-driven biorefinery that produce biomaterials, lubricants, chemicals, food, feed, etc. In addition to this, three different types of biorefineries based on feedstock and product categories have been identified in the literature [30]. Phase I biorefineries use a single feedstock, a single processing step, and a single major product. Phase II biorefineries use a single feedstock, multiple processing steps, and multiple major products. Phase III biorefineries use multiple feedstock, multiple processing steps, and multiple major products (Table 1.2).

Table 1.2: Different types of biorefineries based on feedstock and product categories

Name	Feedstock and product	Example
Phase I Biorefinery	Single feedstock, single process and single major product	Biodiesel from vegetable oil, pulp and paper mills, and the production of ethanol from corn grain
Phase II Biorefinery	Single feedstock, multiple processes and multiple major products	Production of various chemicals from starch; Production of multiple carbohydrate derivatives and bioethanol from cereal grains
Phase III Biorefinery	Multiple feedstock, multiple processes and multiple major products	Phase III Biorefineries are advanced biorefineries and can utilize various types of feedstock, processing technologies and produce multiple types of products.

However, the following issues should be considered to develop any Biorefinery System-

(i) Selection of lignocellulosic feedstock: The careful selection of feedstock for a biorefinery system should be done based on their composition, availability, and potential value. Agricultural waste, forestry waste, algae, and other biomass sources can all be used as feedstock. The choice could be made depending on the final products that are desired as well as feedstock's specific makeup, which may include the amount of protein, lignin, lipids, or carbohydrates.

(ii) Pretreatment of feedstock: The pretreatment of the feedstock is an essential step in a biorefinery system. By increasing the biomass's accessibility and reactivity, it aims to make it more open for subsequent conversion processes. Size reduction, thermal treatment, chemical

solubilization, or enzymatic hydrolysis, etc. are some examples of physical, chemical, or biological pretreatment methods.

(iii) Fractionation and separation methods: Fractionating the feedstock to separate out each component is the next step. Valuable fractions like carbohydrates, lignin, proteins, and lipids are isolated using a variety of separation processes. Techniques like extraction, hydrolysis, solvent fractionation, membrane separation, and chromatographic procedures can all be used as fractionation methods.

(iv) Conversion processes: After fractionation and separation of the feedstock, different parts are put through particular conversion procedure to produce the desired products. These can be thermochemical processes like pyrolysis, gasification, or liquefaction as well as fermentation, enzymatic conversion, chemical reactions, and others. The components are supposed to be converted into high-value chemicals, biofuels, biopolymers, or other beneficial products.

(v) Process integration and optimization: In order to optimize overall process efficiency and maximize the value generated from the feedstock, biorefineries focus a strong emphasis on the integration of several processing techniques.

(vi) Product diversification and value addition: Producing a wide range of valuable products from the feedstock is another essential aspect of the biorefineries. Products include specialized chemicals, biopolymers, nutraceuticals, and biofuels (such as ethanol, biodiesel, or biojet fuel). The viability and sustainability of the biorefinery system can be improved by the extraction of numerous high-value products.

(vii) Circular economy approach: By using biomass feedstock and turning them into useful products, biorefinery complies with the concepts of a circular economy and reduces waste production.

1.2. Literature review

Since the current biorefineries employ sophisticated conversion techniques to provide the needed products and energy, a financially viable biorefinery must meet two key criteria, (i) simple separation and fractionation technologies for high-throughput systems that will produce value-added products and no waste streams, and (ii) generic solutions that will apply across multiple feedstock [31]. “The primary objective of traditional lignocellulosic biorefineries, first and foremost, is to harvest valuable products from the carbohydrate fractions. Until now, only a few lignin-first approaches have been well disclosed. Because there is no such thing as a universal or one size-fits-all biorefinery, further research is of paramount importance to expand the portfolio of potential valorization routes, both with respect to the lignin fraction as to the residual pulp. Lignin is no longer treated as a subordinate biomass constituent, but instead as a primary valorization target, without compromising the carbohydrate fraction” [32].

In fact, lignin is the second largest polymer obtained from lignocellulosic biomasses and highly important natural polymer containing aromatic rings. It is a highly cross-linked, three dimensional, amorphous and water insoluble complex polymer that comprised of three lignin precursors termed as monolignols, i.e., *p*-Coumaryl alcohol, Coniferyl alcohol and Sinapyl alcohol (Figure. 1.7). At present, the pulping and bioethanol industries create more than 70 million tons of technical lignin every year. Complicated and condensed structure of lignin limits its direct industrialization. About 95% of technical lignin is being burnt as fuel in heat and power plants. The remaining 5% of lignin being modified by different processes to be used for potential applications, such as additives, binders, dispersants, and surfactants [33].

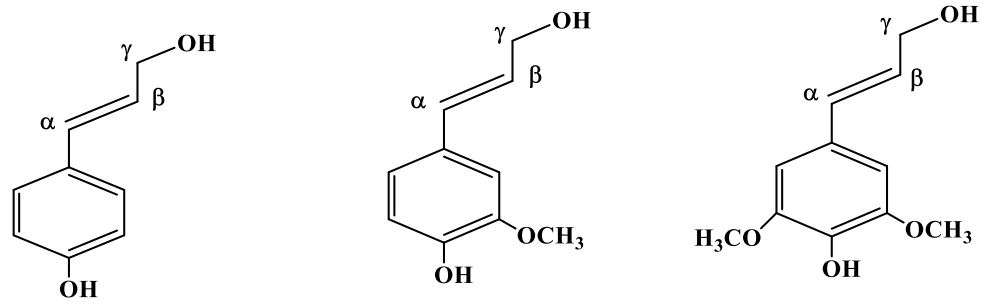

Figure 1.7: Three main precusors of lignin, i.e., monolignols (a) P-Coumaryl alcohol (b) Coniferyl alcohol and (c) Sinapyl alcohol

These monomers are linked together by enzyme-mediated dehydrogenetive polymerization process in plant cell walls through phenylpropanoid units, i.e., *p*-hydroxyphenyl (H), guaiacyl (G) and syringyl (S) units (Figure 1.8).

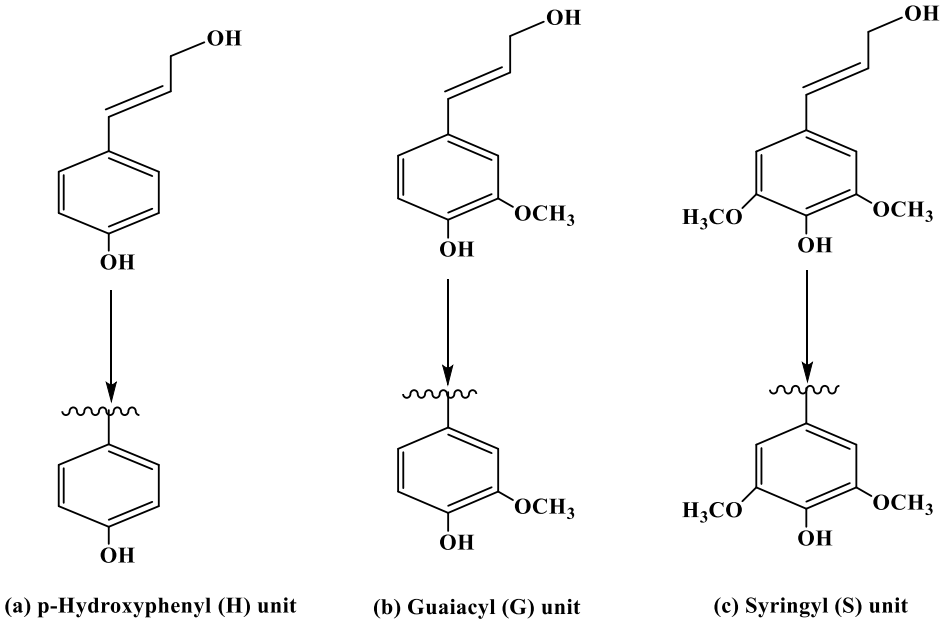

Figure 1.8: Structural units of lignin polymer derived from three monolignols, (a) p-Hydroxyphenyl (H) unit (b) Guaiacyl (G) unit and (c) Syringyl (S) unit

Lignin polymerization is a combinatorial radical coupling process, primarily in an endwise fashion, and produces a series of substructures with a small variety of interunit linkages within the polymer, including β-O-4, α-O-4, β-5, β-1, 4-O-5, 5-5 and β-β, etc. (Figure 1.9) [33, 34]. Units that are trifunctionally linked to adjacent units represent branching sites which gives rise to the network structure characteristics of lignin (Table 1.3). As the interunit carbon-carbon linkages of the lignin are difficult to break without excessively fragmenting the carbon skeleton, solvolysis of the ether linkages is often utilized as the best approach for the degradation to structures which retain some characteristic features of original lignin. Unlike cellulose, the largest natural aliphatic polymer with a well-defined sequence of monomeric units and linked by regular β-1,4-glycosidic bonds, lignin is characterized by a variety of chemically different bonding patterns and needs different conditions, e.g., a number of thermochemical and biochemical conversion processes for the cleavage of the bonds.

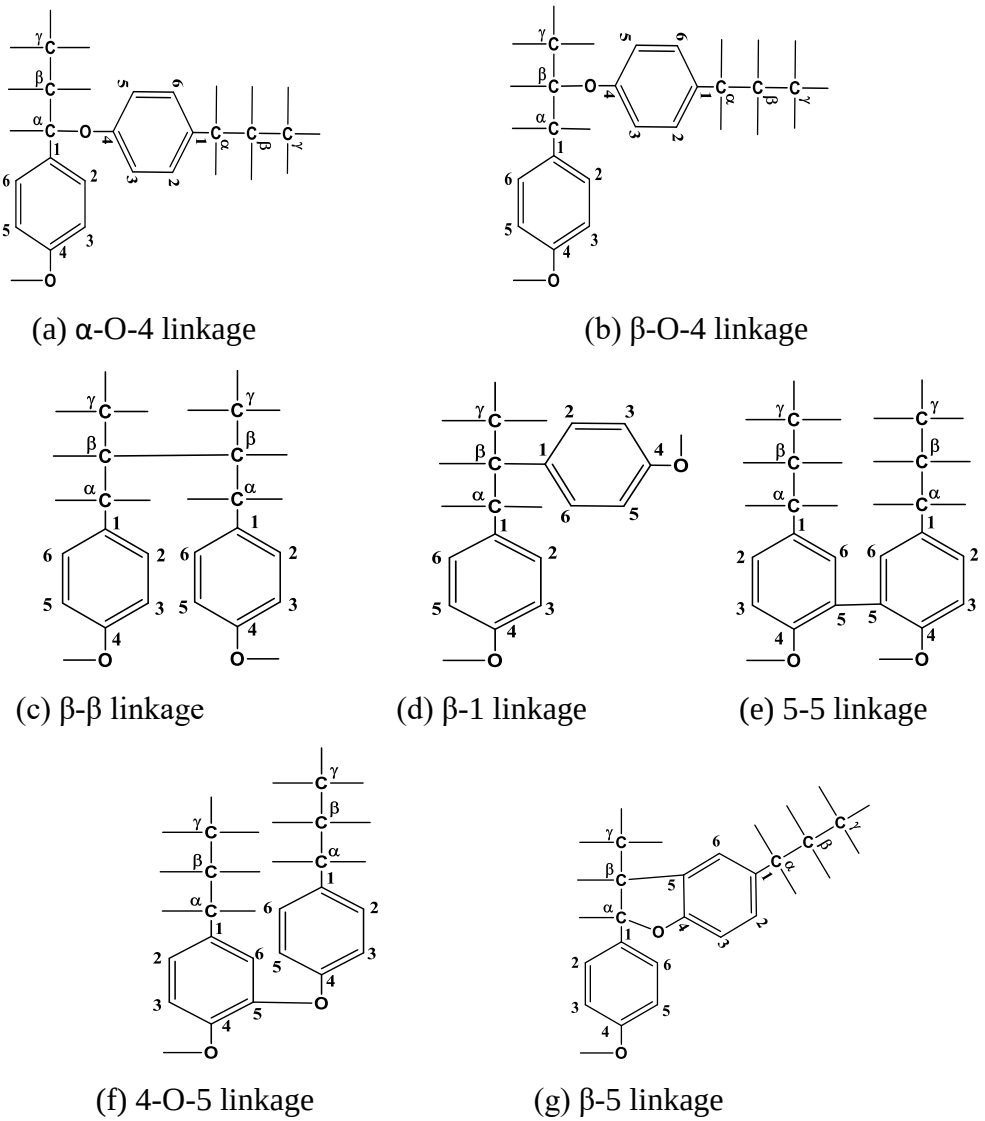

Figure 1.9: Different interunit linkages generally present in lignin macromolecule (a) α-O-4 linkage (b) β-O-4 linkage (c) β-β linkage (d) β-1 linkage (e) 5-5 linkage (f) 4-O-5 linkage and (g) β-5 linkage

Of the functional groups attached to the basic phenylpropanoid skeleton, those having the greatest impact on the reactivity of lignin include phenolic hydroxyl, benzylic hydroxyl and carbonyl groups. Methoxyl group is comparatively unreactive than hydroxyl or carbonyl groups, but serve the useful function by providing an approximate measure of the phenylpropanoid content of particular lignin. The frequency of these groups may vary according to the morphological location of the lignin, wood species and also the method of isolation [35].

Table 1.3: Interunitary linkages in lignin preparations (linkages/100 C_9-units)

Linkage	Erickson et. al. (1973) (Softwood; spruce lignin)	Nimz (1974) (Hardwood; beech lignin)	Names of the bonds
β-O-4	49-51	65	Aryl glycerol-β-aryl ether
α-O-4	6-8	-	Non-cyclic benzyl aryl ether
β-5	9-15	6	Phenylcoumaran
β-1	2	15	1,2-diarylpropane
5-5	9.5	2.3	Biphenyl
4-O-5	3.5	1.5	Diarylether
β-β	2	5.5	Linked through side chain

Several factors limit the applications of lignin, namely (i) a non-uniform structure, (ii) high molecular weight and (iii) broad dispersity. The reactivity of lignin is very low due to the steric hindrance in its complex molecular architecture. Reactivity of lignin could be enhanced by applying chemical modifications and thermochemical de-polymerization processes. Multifunctional nature of lignin macromolecule is still the main attraction for suitable chemical conversions or polymer modifications for high value applications. Amount of these functional groups in different lignin preparation (Table 1.4) were also studied by many researchers [36, 37]. Multifunctionality of lignin includes free positions of aromatic ring, phenolic and aliphatic hydroxyl groups, methoxyl and carbonyl groups, etc. A schematic representation of lignin macromolecule has been given in Figure 1.10.

Table 1.4: Contents of functional groups (%, w/w) in lignin prepared by different methods [36-37]

Functional group	Kraft	Soda-AQ	Ethanol process	Organosolv	Lignosulfonate	Method
Aliphatic hydroxyl	10.09	3.10	4.73	3.50	-	^{1}H-NMR
Phenolic hydroxyl	4.10	4.50	3.33	2.65	-	^{1}H-NMR
Methoxyl	10.47	19.30	10.10	15.20	8.70	Gas chromatography
Carbonyl	2.35 *(0.32)	1.94 (0.25)	5.20 (0.23)	2.90 (0.19)	4.70 (0.27)	UV-spectroscopy
Carboxylic	7.06 (0.15)	6.91 (0.22)	2.02 (0.27)	3.15 (0.20)	4.63 (0.21)	Non-aqueous potentiometric titration
Sulfonate	-	-	-	-	12.23 (0.39)	

* () standard deviation

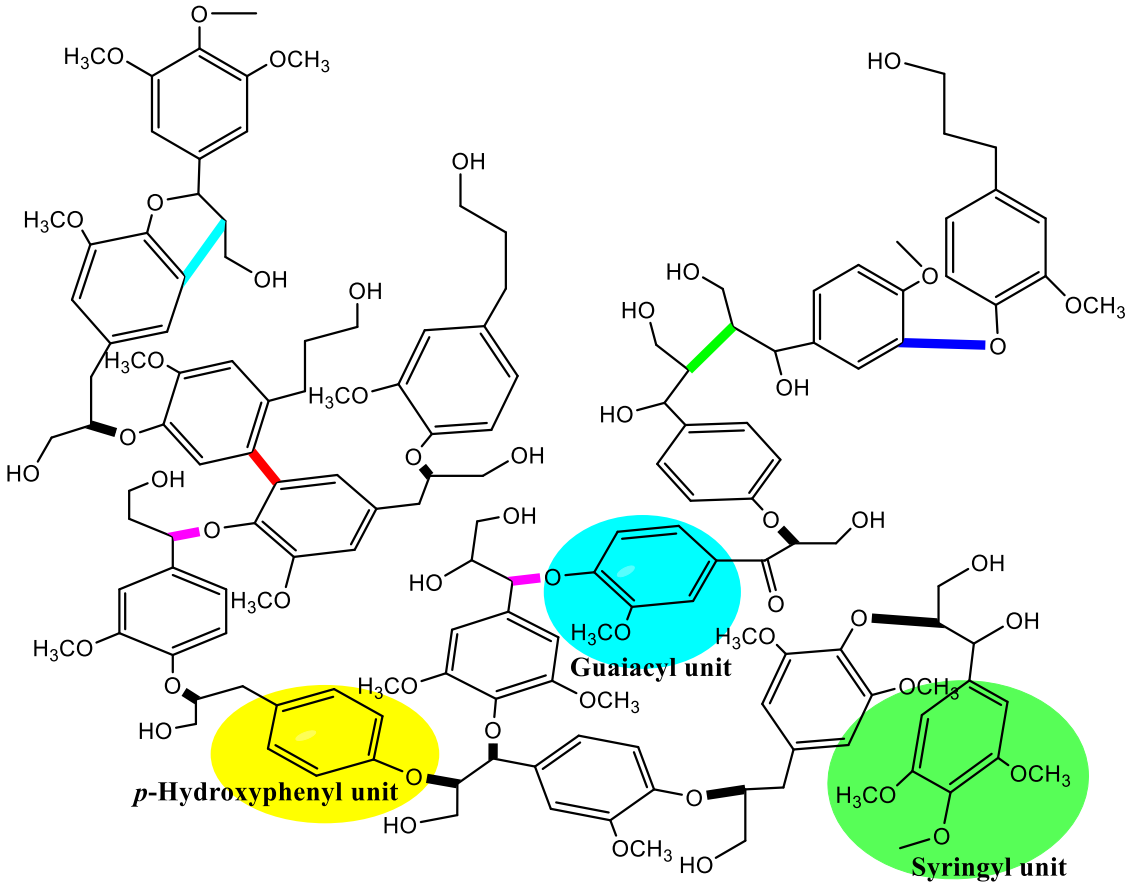

Figure 1.10: A schematic representation of lignin macromolecule. Color bonds in bold form represent different interunit linkages, i.e., β-O-4 (black), α-O-4 (pink), β-β (green), β-5 (light blue), 5-5 (red), 4-O-5 (deep blue), etc. in lignin.

Modifications of lignin

Lignin has been subjected to a vast array of reactions for both fundamental and applied studies. There are two broad classes for the modification of lignin, i.e., physical and chemical modifications. These classes could further be classified into subclasses based on the nature of modification technique applied, as given briefly in Figure 1.11.

Physical modifications of lignin

Physical strategies for lignin modification involve physical processes in order to provide the transformed substance new and distinct features as compared to direct reactions between functional groups present in lignin and other chemical compounds [40]. During lignin isolation process, black liquor is usually acidified at lower pH to precipitate lignin particles, which are then collected through filtration and rinsed out using water. Previous work

suggested that wet ball-milling using a small milling medium is the most reliable method in terms of processing efficiency and the controllability particle-size and distribution [41].

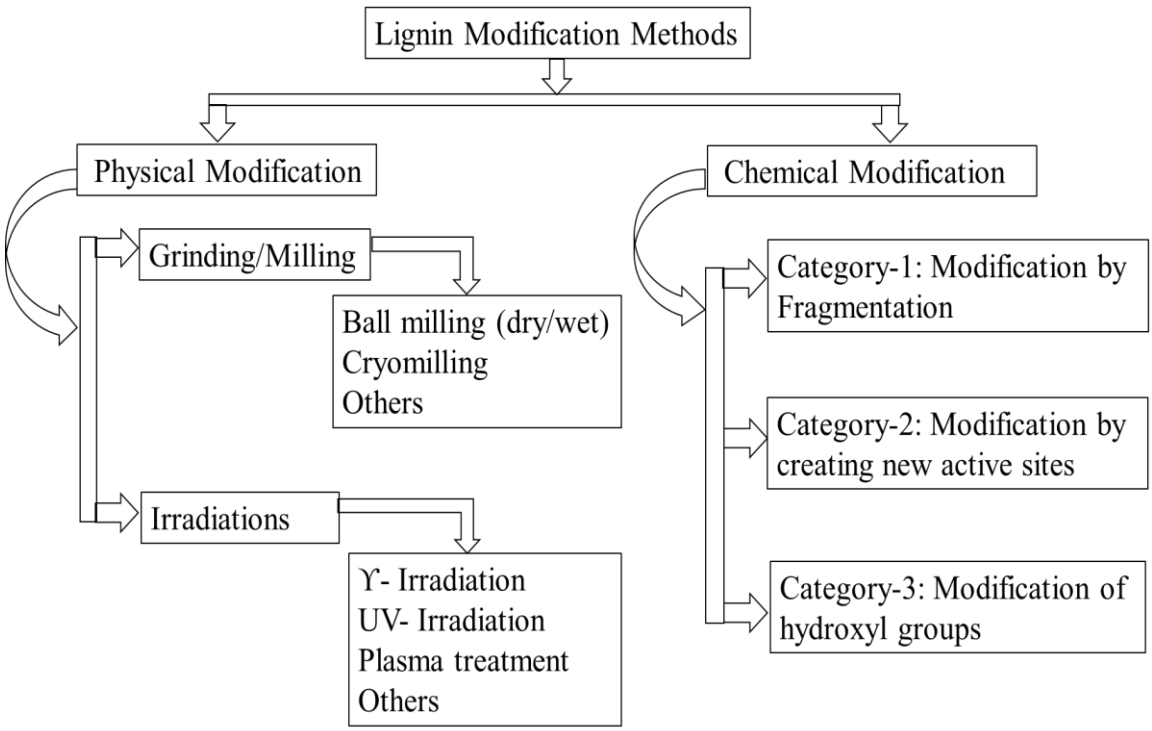

Figure 1.11: Modification of lignin by different physical and chemical methods

Manual mortar and pestle grinding showed that acid precipitated lignin exhibited hydrodynamic radius larger than 10 microns with broad particle size distribution. Ball milling techniques, i.e., dry and wet milling processes were also applied to reduce particle size of the acid precipitated lignin. It was observed that an easy operation and cost effective ball milling techniques could decrease lignin particle size at the submicron levels and can meet the requirements of a wide variety of applications. A detail study on the effect of ball milling on the structure of lignin as analyzed by derivatization followed by reductive cleavage method (DFRC) methodology and indicated that vibratory ball milling had no significant effect on the lignin structure, if toluene is used in the milling technique [42]. On the other hand, dry vibratory ball milling under a nitrogen atmosphere causes substantial structural changes in lignin including condensation reaction. Cryomilling study on lignin showed that the technique could be used to increase the number of phenolic ends and with external force, intramolecular covalent bonds of lignin can be broken and reactive ends by homolytic bond cleavage occurred [43]. Cryo conditions in the milling process could prevent the sample from thermal changes and enhance some physicochemical properties [44]. Irradiation of γ-rays on lignin

showed substantial structural changes, e.g., lowering the molecular weight, changes in the glass transition temperature and enhanced the free radical scavenging activity, etc. [45]. Ultraviolet light treatment on lignin sample also showed the formation of smooth coatings and contributed to the suppression of OH band intensity and the formation of C=O bonds and imparted hydrophilic properties to the lignin surface. On the other hand, SF_6 plasma treatment caused substantial changes in the surface structure, causing roughness and incorporation of CF_x groups, which improved hydrophobicity of the lignin [46].

Chemical modifications of lignin

The chemical modification of lignin could be classified into three main categories and stated in Table 1.5. Apart from different chemical modification methods, acetobromination of lignin received more attention only for analytical works on lignocellulosic biomass [42, 49, 50]. The physicochemical characteristics of acetobrominated lignin or acetobromination of lignin as a method of lignin valorization have not yet been thoroughly studied. In fact, brominated organic compounds are an important class of compounds that have a wide range of industrial applications [51, 52].

Some marine and terrestrial plants, bacteria, fungi, insects, marine animals, etc. could produce naturally occurring organic bromine compounds, but synthetic organic bromine compounds are the predominant in terms of bromine consumption, industrially and account for 80% of the total bromine production [53]. Organobromine compounds are being used as biocide for polymer latex preparation, cleaning agents, coating materials, flame retardants, cosmetic industries, medical disinfectants, pharmaceuticals, dyes, wood and paper industries, glues and sealants and metal processing works, etc. [54].

Management and utilization of black liquors

Management and utilization of waste liquors generated from pulp industries and different biorefinery processes is still a challenging issue towards the sustainable development [55, 56]. Among the industrialized lignocellulosic biomass conversion processes, chemical conversion produce waste liquors, e.g., black liquor in kraft and soda pulping, brown liquor in sulfite pulping, etc. [57]. Usually, these liquors contain degraded lignin, hemicelluloses and extractives along with other processing chemicals, e.g., alkali, sulfur compounds, etc.

Table 1.5: Three possible categories of chemical modifications of lignin [47-48]

SN	Category	Modification route
1	Fragmentation or lignin depolymerization to use lignin as a carbon source or to cleave lignin structure into aromatic macromers.	Hydrogenation Pyrolysis Hydrolysis Oxidation Gasification Enzymatic oxidation Microbial conversion
2	Modification by creating new chemical active sites	Halogenation Nitration Amination Sulfoalkylation Sulfonation Hydroxyalkylation Alkylation/de-alkylation
3	Chemical modification of hydroxyl groups	Esterification Urethanization Phenolation Oxidation Reduction Etherification Polymer grafting

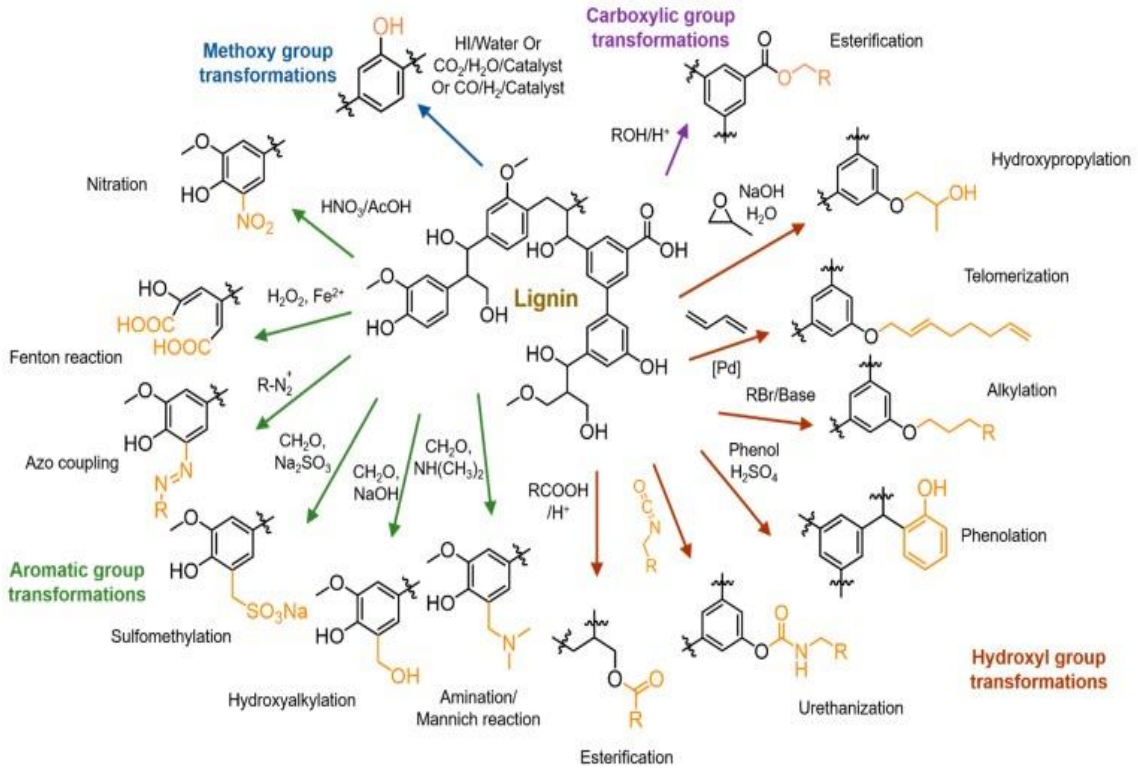

Figure 1.12: Chemical modifications of lignin by different pathways: Adapted/reproduced from Ganewatta, M. S., Lokupitiya, H. N., & Tang, C. (2019). Lignin biopolymers in the age of controlled polymerization. Polymers 11: 1176. Creative Commons license and disclaimer available from: http://creativecommons.org/licenses/by/4.0/legalcode.18

Generally, a significant portion of black liquors are burnt in a recovery boiler to generate steam and electricity as required for the pulp mills and the remaining portion might be utilized to develop added-value products and fuels, etc. [58]. About 15 million dry tons of solid wastes and byproduct solids being generated annually in the United States pulp and paper mills. These wastes contain about 50% solid materials and 50% water [59]. At the same time, 11 million tonnes of waste being produced yearly by the European pulp and paper industries, of which 70% originates from the production of deinked recycled paper [60].

Large amounts of water, energy, chemicals, and wood are needed to make pulp and paper, and can generate a variety of pollutants and emissions that need to be managed or treated. Environmental effects could result from solid wastes, thermal loading of natural streams, odor-causing substances, air pollutants from combustion, and emissions of poisonous and hazardous chemicals into air and water. By increasing the use of recycled paper, enhancing energy efficiency, and making capital investments for efficient compliance with regulations, the sectors have been making efforts to reduce its negative environmental effects [61].

The environmental problems of pulp and paper industry are not limited by the high water consumption. Wastewater generation, solid wastes including sludge from wastewater treatment plants and air emissions are other problems. Thus, effective disposal and treatment approaches for wastewater are essential.

Different treatment processes have been applied to manage and utilize the solid waste generated from the pulp industries and biorefineries. Mainly two approaches are followed to minimize the wastes, i.e., chemical recovery and recycling and minimization of waste production by applying the best available techniques, according to the Integrated Pollution, Prevention and Control Regulation [62]. A study showed that pulp and paper mills are approaching the ‘zero waste’ goal. Such a situation can be achieved primarily by reducing waste generation and encouraging internal recycling, which is a desirable situation considering the cleaner production concept [63]. These wastes could be suitably processed into by-products and then sent to external recycling agencies. The materials produced by subsequent processing steps could be used in agriculture, construction, energy and environmental technology, etc.

The production of added value materials from waste streams, e.g., acid pretreatment liquor is essential to improve the economics of lignocellulosic bioethanol production applying innovative techniques for the detoxification and recovery of valuable chemicals [64]. Some attempts were also taken by the researchers to valorize the spent liquor of sulfite pulping process using biorefinery concept [65].

Thus, the development of a green conversion process of lignocellulosic biomass into their main structural components, i.e., cellulose, hemicelluloses and lignin with no waste generation is of great importance. This could be ensured by recovering pretreatment chemicals and degraded organics from spent liquor into usable materials, e.g., fertilizers. The recovery of pretreatment chemicals from spent liquor, i.e., lignin removed black liquor might be considered as an innovative solution to green and sustainable industry, e.g., integrated biorefinery.

The following objectives have been developed taking into account all of the challenges in the conversion of lignocellulosic biomass and their utilization for sustainable industrialization.

1.3. Objective of the research

The objective of the research is to investigate the structural features and constituents of lignocellulosic biomass; their pretreatment and subsequent recoveries of the constituents with specific attention given to lignin polymer and its modifications; recoveries of pretreatment chemicals, etc. Principles of green chemistry are followed in overall investigations. The objective includes-

(i) Quantitative assessment of the constituents of selected lignocellulosic biomasses, e.g., woods (*Trema orientalis* and *Dipterocarpus turbinatus*) and non-woods (Coconut fibre/husk and Bagasse) including their waste forms by applying National Renewable Energy Laboratory (NREL)/ Technical Association of the Pulp and Paper Industry (TAPPI) or other methods.

(ii) Establishment of suitable conditions for the isolation of lignin from different lignocellulosic biomasses through material-driven biorefinery technique by obeying the principles of green chemistry.

(iii) Preparation of alkali-lignin particles by physical method, e.g., vibratory ball milling; determination of particle sizes, molecular weights/intrinsic viscosity and dispersity by standard methods.

(iv) Detail characterization of alkali-lignin particles by different instrumental/standard methods including X-ray photoelectron spectroscopic analysis.

(v) Chemical modifications of alkali-lignin samples, characterization and examination physicochemical properties.

(vi) To explore the fields of application of submicron alkali-lignin and modified alkali-lignin products.

1.4. Present work

This dissertation presents a straightforward material-driven phase III lignocellulosic-feedstock biorefinery system that is based on a simple and innovative acid-base pretreatment technique. The sequential acid-base pretreatments on lignocellulosic biomasses, e.g., woods and non-woods in order to recover their structural components, i.e., cellulose, hemicelluloses, and lignin, as well as beneficial fertilizer production facilities from black/waste liquors have been focused to solve some existing problems on the conversion of lignocellulosic biomass in a greener way.

Phosphoric acid was utilized as acid in the acid pretreatment step followed by potassium hydroxide digestion in the presence of anthraquinone. Degraded hemicelluloses were recovered from the acid pretreatment step, whereas cellulosic pulps and alkali-lignin were recovered from the residues and spent liquors in the base pretreatment step, respectively. A straightforward and easy separation of the main structural components, i.e., cellulosic pulps, hemicelluloses and lignin and about 100% recovery of used acid and base with degraded organics into valuable forms, e.g., nitrogen, phosphorus and potassium (NPK) containing materials/fertilizers might add a significant value to the biorefinery system.

Special attention was given to develop an easy isolation method for alkali-lignin, purification and modification by physical method, e.g., vibratory ball milling and characterized applying different instrumental methods. The alkali-lignin particles were then chemically altered using new preparative acetobromination techniques (i.e., Preparative method-1 and Preparative-2) in order to incorporate more bromine atom in the lignin structure along with acetylation. Flow chemistry pathway was followed to perform the acetobromination in a safe and sound mode. Characterization of acetobrominated products was carried out using different instrumental methods and properties were evaluated.

All of the work under the thesis presented henceforth was conducted in Fibre & Polymer Research Division, Bangladesh Council of Scientific & Industrial Research (BCSIR), Dhanmondi, Dhaka-1205, Bangladesh and Physical Chemistry Laboratory, Department of Chemistry, University of Dhaka (DU), Bangladesh with the permissions of authorities of the organizations.

Raw materials, e.g., lignocellulosic biomasses used in this work were of Bangladesh origin. Different chemicals and reagents, solvents, analytical standards, etc. were purchased from renowned manufacturers and stated in materials and methods sections. Deionized water was produced in Fibre & Polymer Laboratory of BCSIR using a deionized water plant (MRC, UK). Experiments were performed by taking appropriate health and safety measures.

Principles of green chemistry were followed throughout the works. The methods used in the thesis were of standard methods, which were published by different international organizations, e.g., National Renewable Energy Laboratory (NREL), Technical Association of the Pulp and Paper Industry (TAPPI), etc. Some methods were adopted from different peer reviewed journals. Necessary references were stated at the end of each chapter. Instrumental analyses were done by a number of modern instruments and stated in materials and methods sections. Schematic diagram of the instruments have been given in the Appendix. Secondary data have been obtained by using OriginPro 2022 software, incorporated in the thesis and explained in details. ChemDraw professional softwere was used to draw the reaction schemes, chemical structures, etc.

1.5. References

[1] C. Huang, C. Xu, X. Meng, L. Wang and X. Zhou, Isolation, Modification, and Characterization of the Constituents (Cellulose, Hemicellulose, Lignin, et al.) in Biomass and Their Bio-Based Applications, *Front. Bioeng. Biotechnol*. 2022 , doi: 10.3389/fbioe.2022.866531

[2] P. Gallezot, Conversion of biomass to selected chemical products, *Chem. Soc. Rev*., 2012, 41, 1538–1558, DOI: 10.1039/c1cs15147a

[3] Delivery of sustainable supply of non-food biomass to support a "resource-efficient" Bioeconomy in Europe; https://www.s2biom.eu/images/Publications/ D8.2_S2Biom_Vision_for_1_billion_ tonnes_ biomass_2030.pdf (Last accessed 30.07.2022)

[4] S. M. Dean, Understanding Lignocellulose: Synergistic Computational and Analytic Methods, ACS Symposium Series; American Chemical Society: Washington, DC, 2019. Vol 1338, Ch 1, pp. 1-15, doi:10.1021/bk-2019-1338.ch001

[5] A. K. Kumar and S. Sharma, Recent updates on different methods of pretreatment of lignocellulosic feedstocks: a review, *Bioresources and Bioprocessing*, 2017, 4(1), 7, doi: 10.1186/s40643-017-0137-9

[6] K. M. Nazmul Islam, Municipal Solid Waste to Energy Generation in Bangladesh: Possible Scenarios to Generate Renewable Electricity in Dhaka and Chittagong City, *Journal of Renewable Energy*, 2016, 1-16 doi.org/10.1155/2016/1712370

[7] M. A. Habib, M.M. Ahmed, M. Aziz, M. R. A. Beg and M. E. Hoque, Municipal Solid Waste Management and Waste-to-Energy Potential from Rajshahi City Corporation in Bangladesh. *Applied Sciences*, *11*(9), 3744. doi.org/10.3390/app11093744

[8] M. Alamgir and A. Ahsan, MUNICIPAL SOLID WASTE AND RECOVERY POTENTIAL: BANGLADESH PERSPECTIVE, *Iran. J. Environ. Health. Sci. Eng*., 2007, 2, 67-76

[9] W. Den, V. K. Sharma, M. Lee, G. Nadadur and R. S. Varma, Lignocellulosic Biomass Transformations via Greener Oxidative Pretreatment Processes: Access to Energy and Value-Added Chemicals, *Frontiers in chemistry*, 2018, 6, 141. doi.org/10.3389/fchem.2018.00141

[10] R. Roy, M. S. Rahman and D. E. Raynie, Recent Advances of Greener Pretreatment Technologies of Lignocellulose, *Current Research in Green and Sustainable Chemistry*, 2020, 3, 100035, doi:10.1016/j.crgsc.2020.100035

[11] G. K. Gupta and P. Shukla, Lignocellulosic biomass for the synthesis of nanocellulose and its eco-friendly advanced applications, *Frontiers in Chemistry*, 2020, 8, 1203, doi: 10.3389/fchem.2020.601256

[12] H. Wanga, Y. Pud, A. Ragauskas and B. Yang, From lignin to valuable products-strategies, challenges, and prospects, *Bioresource Technology*, 2019, 271, 449-461, DOI: 10.1016/j.biortech.2018.09.072

[13] P. Kumar, D. M. Barrett, M. J. Delwiche and P. Stroeve, Methods for Pretreatment of Lignocellulosic Biomass for Efficient Hydrolysis and Biofuel Production, *Industrial & Engineering Chemistry Research*, 2009, 48, 3713–3729, doi.org/10.1021/ie801542g

[14] E. Melro, A. Filipe, D. Sousa, B. Medronho and A. Romano, Revisiting lignin: a tour through its structural features, characterization methods and applications, *New Journal of Chemistry*, 2021, 16, 6986-7013, doi.org/10.1039/D0NJ06234K

[15] V. D. Buck, M. Polanska and J. V. Impe, Modeling Biowaste Biorefineries: A Review, *Front. Sustain. Food Syst.*, 2020, 4, doi.org/10.3389/fsufs.2020.00011

[16] A. Bassani, C. Fiorentini, V. Vadivel, A. Moncalvo and G. Spigno, Implementation of Auto-Hydrolysis Process for the Recovery of Antioxidants and Cellulose from Wheat Straw, *Applied Sciences*, 2020, 17, 6112, doi.org/10.3390/app10176112

[17] K. Kucharska, P. Rybarczyk, I. Hołowacz, R. Łukajtis, M. Glinka and M. Kamiński, Pretreatment of Lignocellulosic Materials as Substrates for Fermentation Processes, *Molecules*, 2018, 11, 2937, DOI: 10.3390/molecules23112937

[18] E. C. Bensah, M. Mensah and E. Antwi, Status and prospects for household biogas plants in Ghana: lessons, barriers, potential, and way forward, *International journal of energy and environment*, 2011, 5, 887-898

[19] F. Cherubini, G. Jungmeier, M. Wellisch, T. Willke, I. Skiadas, R. V. Ree and E. de. Jong, Toward a common classification approach for biorefinery systems, *Biofuels Bioprod. Bioref.*, 2009, 3, 534-546, doi.org/10.1002/bbb.172

[20] L. J. Konwar, J. Mikkola, N. Bordoloi, R. Saikia, R. S. Chutia and R. Kataki, Sidestreams From Bioenergy and Biorefinery Complexes as a Resource for Circular Bioeconomy, *Waste Biorefinery*, 2018, 85-125. doi.org/10.1016/B978-0-444-63992-9.00003-3

[21] F. H. Isikgor and C. R. Becer, Lignocellulosic biomass: a sustainable platform for the production of bio-based chemicals and polymers, *Polymer Chemistry*, 2015, 25, 4497–4559, doi.org/10.1039/C5PY00263J

[22] Chemical and material biorefineries in the EU and beyond, https://publications.jrc.ec.europa.eu/repository/handle/JRC124809 (Last accessed 16.08.2022)

[23] H. Chen, Lignocellulose biorefinery feedstock engineering, *Lignocellulose biorefinery engineering*, 2015, 1, 37-86, doi:10.1016/B978-0-08-100135-6.00003-X

[24] Z. H. Liu, N. Hao, Y. Y. Wang, C. Dou, F. Lin, R. Shen, R. Bura, D. B. Hodge, B. E. Dale, A. J. Ragauskas and B. Yang, Transforming biorefinery designs with 'Plug-In Processes of Lignin' to enable economic waste valorization, *Nature Communications*, 2021, 12(1), 1-13, doi.org/10.1038/s41467-021-23920-4

[25] S. K. Maity, Opportunities, recent trends and challenges of integrated biorefinery: Part I, *Renewable and Sustainable Energy Reviews*, 2015, 43, 1427–1445, doi.org/10.1016/j.rser.2014.11.092

[26] National Renewable Energy Laboratory (NREL), http://www.nrel.gov/biomass/ biorefinery.html (Last accessed 30.07.2022)

[27] Task 42: Biorefining in a Circular Economy**,** https://task42.ieabioenergy.com/ (Last accessed 30.07.2022)

[28] B. Kamm, P. R. Gruber and M. Kamm, Biorefineries-Industrial Processes and Products, WILEY-VCH Verlag GmbH & Co. KGaA, Germany, 2006, doi.org/10.1002/9783527619849.ch1

[29] F. Cherubini, The Biorefinery Concept: Using Biomass Instead of Oil for Producing Energy and Chemicals, *Energy conversion and management*, 2010, 51, 1412-1421, doi.org/10.1016/j.enconman.2010.01.015

[30] J. Clark and F. Deswarte, Introduction to chemicals from biomass, *Biomass as a Feedstock*, 2015, 31–52, doi:10.1002/9781118714478.ch2

[31] B. Kamm and M. Kamm, Biorefineries – Multi Product Processes, *Adv Biochem Eng Biotechnol*, Springer-Verlag Berlin Heidelberg, 2007, 105: 175-204, doi: 10.1007/10_2006_040

[32] Z. H. Liu, N. Hao, Y. Y. Wang, C. Dou, F. Lin, R. C. Shen, R. Bura, D. B. Hodge, B. E. Dale, A. J. Ragauskas, B. Yang and J. S. Yuan, *Nature Communications*, 2021, 1, 1-13

[33] R. C. Sun, Lignin Source and Structural Characterization, *ChemSusChem*, 2020, 13, 1-10, doi:10.1002/cssc.202001324

[34] R. Parthasarathi, R. A. Romero, A. Redondo and S. Gnanakaran, Theoretical Study of the Remarkably Diverse Linkages in Lignin, *The Journal of Physical Chemistry Letters*, 2011, 2(20), 2660–666, doi:10.1021/jz201201q

[35] O. Faix, Methods in Lignin Chemistry, (ed. S. Y. Lin and C. W. Dence), Springer-Verlog, Berlin Heidelberg, First edition, 1992, 4, 81-106

[36] N. E. Mansouri and J. Salvadó, Analytical methods for determining functional groups in various technical lignins, *Industrial Crops and Products*, 2007, 26(2), 116–124, doi:10.1016/j.indcrop.2007.02.006

[37] N. E. Mansouri and Joan Salvadó, Structural characterization of technical lignins for the production of adhesives: Application to lignosulfonate, kraft, soda-anthraquinone, organosolv and ethanol process lignins, *Industrial Crops and Products*, 2006, 24(1), 8–16, doi:10.1016/j.indcrop.2005.10.002

[38] E. Adler, Lignin chemistry—past, present and future, 1977, 11(3), 169–218. Doi:10.1007/bf00365615

[39] R. D. Hatfield, D. M. Rancour and J. M. Marita, Grass Cell Walls: A Story of Cross-Linking. *Front. Plant Sci*., 2017, 7:2056., doi: 10.3389/fpls.2016.02056

[40] K. Komisarz, T. M. Majka and K. Pielichowski, Chemical and Physical Modification of Lignin for Green Polymeric Composite Materials., 2023, *Materials*, 16(1), 16, doi.org/10.3390/ma16010016

[41] C. Miao and W. Y. Hamad, Controlling lignin particle size for polymer blend applications, *Journal of Applied Polymer Science*, 2017, 134(14), doi:10.1002/app.44669

[42] T. Ikeda, K. Holtman, J. F. Kadla, H. Chang and H. Jameel, Studies on the Effect of Ball Milling on Lignin Structure Using a Modified DFRC Method, *J. Agric. Food Chem*. 2002, 50(1), 129–135, Doi:10.1021/jf010870f

[43] C. C. Piras, S. Fernández-Prieto and W. M. De Borggraeve, Ball milling: a green technology for the preparation and functionalisation of nanocellulose derivatives, *Nanoscale Advances*, 2019, 937-947, doi.org/10.1039/c8na00238j

[44] D. Fatma, Formation and characterization of mechanochemically generated free lignin radicals from olive seeds, *Turk J Chem*, 2021, 45: 282-294, doi:10.3906/kim-2008-19

[45] N. R. Rao, T. V. Rao, S. V. S. R. Reddy and B.S. Rao, The effect of gamma irradiation on physical, thermal and antioxidant properties of kraft lignin, J. Radiat. *Res. Appl. Sci*. 2015, 8, 621–629, doi.org/10.1016/j.jrras.2015.07.003

[46] J. R. Souza, J. R. Araujo, B. S. Archanjo and R.A. Simão, Cross-linked lignin coatings produced by UV light and SF6 plasma treatments, *Progress in Organic Coatings*, 2018, 128, 82-89. doi.org/10.1016/j.porgcoat.2018.12.017

[47] S. Laurichesse and L. Avérous, Chemical modification of lignins: Towards biobased polymers, Progress in Polymer Science, 2014, 39(7), 1266–1290, doi:10.1016/j.progpolymsci.2013.11.004

[48] M. S. Ganewatta, H. N. Lokupitiya and C. Tang, Lignin Biopolymers in the Age of Controlled Polymerization, *Polymers*, 2019, 11(7), 1176, doi.org/10.3390/polym11071176

[49] F. Lu and J. Ralph, DFRC Method for Lignin Analysis. 1. New Method for β-Aryl Ether Cleavage: Lignin Model Studies, *J. Agric. Food Chem*. 1997, 45, 12, 4655–4660, doi.org/10.1021/jf970539p

[50] T. Partovi, A. H. Massoudi and S. A. Mirshokraie, Investigation of structure of milled wood and dioxane lignins of Populus nigra and Cupressus sempervirens using the DFRC method, *Chem. Pap.*, 2012, **66**, 800–804, doi.org/10.2478/s11696-012-0178-7

[51] D. Ioffe and R. Frim, Kirk-Othmer Encyclopedia of Chemical Technology, 2000, Bromine, Organic Compounds (2nd ed.), doi: 10.1002/ 0471238961. 0218151325150606

[52] A. Mehran, A. Pedro, S. Andreas and A. Bergman, An overview of commercially used brominated flame retardants, their applications, their use patterns in different countries/regions and possible modes of release, 2003, 29(6), 683-689, doi:10.1016/s0160-4120(03)00121-1

[53] S. Indranirekha, J. B. Arun and P. Prodeep, Use of Bromine and Bromo-Organic Compounds in Organic Synthesis, *Chemical reviews*, 2016, 16(12): 6837-7042., doi:10.1021/acs.chemrev.5b00400

[54] K. Smith, Advances in the synthesis and applications of organobromine compounds, *Advances in Organobromine Chemistry II*, 1995, Volume 7, 49–64, doi:10.1016/s0926-9614(05)80009-7

[55] M. Dixit, G. Kumar, S. Guddu and Pratyoosh, Insights into the resources generation from pulp and paper industry wastes: challenges, perspectives and innovations, *Bioresource Technology*, 2019, 1-50, doi:10.1016/j.biortech.2019.122496

[56] H. Y. Leong, C. K. Chang, K.S. Khoo, K. W. Chew , S. R. Chia , J. W. Lim , J. Chang and P. L. Showet, Waste biorefinery towards a sustainable circular bioeconomy: a solution to global issues, Biotechnology for Biofuels, *Biotechnol Biofuels*, 2021, 14:87, doi.org/10.1186/s13068-021-01939-5

[57] M. S. T. Amândio, J. M. Pereira, J. M. S. Rocha, L. S. Serafim and A. M. R. B. Xavier, Getting Value from Pulp and Paper Industry Wastes: On the Way to Sustainability and Circular Economy, *Energies*, 2022, 15, 4105, doi.org/10.3390/ en15114105

[58] D. D. Mandal, G. Singh, S. Majumdar and P. Chanda., Challenges in developing strategies for the valorization of lignin—a major pollutant of the paper mill industry, *Environ Sci Pollut Res*, 2023, 30, 11119–11140, doi.org/10.1007/s11356-022-24022-4

[59] Bajpai, P., Generation of Waste in Pulp and Paper Mills, Management of Pulp and Paper Mill Waste, 2014, 9–17, Chapter, doi:10.1007/978-3-319-11788-1_2

[60] M.C. Monte, E. Fuente, A. Blanco and C. Negro, Waste management from pulp and paper production in the European Union, 2009, 29(1), 293–308, doi:10.1016/j.wasman.2008.02.002

[61] Dixit M, Gupta GK, Liu H, Shukla P, Pulp and paper industry based pollutants, their health hazards and environmental risks, *Current Opinion in Environmental Science & Health*, 2019, doi.org/10.1016/j.coesh.2019.09.010

[62] K. I. Bahar, C. Zeynep and I. Orhan, Pollution Prevention in the Pulp and Paper Industries, *Environmental Management in Practice*, 2011, Chapter, doi. 10.5772/23709

[63] L. Simão, D. Hotza, F. Raupp-Pereira, J. A. Labrincha, O. R. K. Montedo.,Wastes from pulp and paper mills- a review of generation and recycling alternatives, *Cerâmica*, 2018, 64(371), 443–453, doi:10.1590/0366-69132018643712414

[64] M. Christopher, M. Anusree, A. K. Mathew, K. Nampoothiri, K. Madhavan, R. K. Sukumaran and A. Pandey, Detoxification of acidic biorefinery waste liquor for production of high value amino acid, *Bioresource Technology*, 2016, doi:10.1016/j.biortech.2016.03.054

[65] C. Rueda, P. A. Calvo, G. Moncalián, G. Ruiz and A. Coz, Biorefinery options to valorize the spent liquor from sulfite pulping, *Journal of Chemical Technology & Biotechnology*, 2014, doi:10.1002/jctb.4536

CHAPTER 2

RESEARCH METHODOLOGY

Chapter 2: Research Methodology

2.1. Introduction

The methodology applied for the conversion of lignocellulosic biomass to isolate and subsequently modify alkali-lignin has been stated in Figure 2.1. Briefly, a sequential acid-base pretreatment was performed to deconstruct the extractive-free lignocellulosic biomass matrices and recovered the structural components, i.e., cellulose, hemicelluloses and lignin from the system, efficiently. The isolated alkali-lignin samples were physically modified by ball milling and then chemically modified through acetobromination. The alkali-lignin samples and chemically modified products were characterized by different instrumental techniques. The pretreatment chemicals, i.e., acid and base were also recovered from the waste/spent liquor as nitrogen, phosphorus and potassium (NPK) containing materials/fertilizers and subsequently characterized. An overview on the research methodology used in this dissertation has been presented in subsections 2.1.1 to 2.1.8 with necessary schemes and figures.

2.1.1. Collection of raw materials and sample preparation

Two woods, i.e., *Trema orientalis and Dipterocarpus turbinatus* and two non-woods, i.e., coconut fibre and bagasse were collected from Dhaka, Bangladesh and prepared for compositional analyses by following the procedure described elsewhere [66].

2.1.2. Characterization of raw materials

Compositional analyses of the lignocellulosic biomass were done by following the standard and published methods-

(i) Water and ethanol soluble extractives were removed from the samples by accelerated solvent extraction method [NREL/TP-510-42619] [67].

(ii) Total ash contents were determined by heating of each sample in furnace at 575 ± 25 ^{o}C for 4 h [NREL/TP-510-42622] [68].

(iii) Klason lignin and acid insoluble ash were measured by NREL method [NREL/TP-510-42618] [69].

(iv) Amount of holocelluloses were determined by Chlorite bleaching method [TAPPI–T 9 wd-75] [70].

(v) α-cellulose contents were measured by 17.5% and then 9.45% alkali treatment of dried holocellulose [TAPPI T 203 cm-09] [71].

(vi) Hemicellulose contents were found from the difference between holocellulose and α-cellulose contents of each biomass [72].

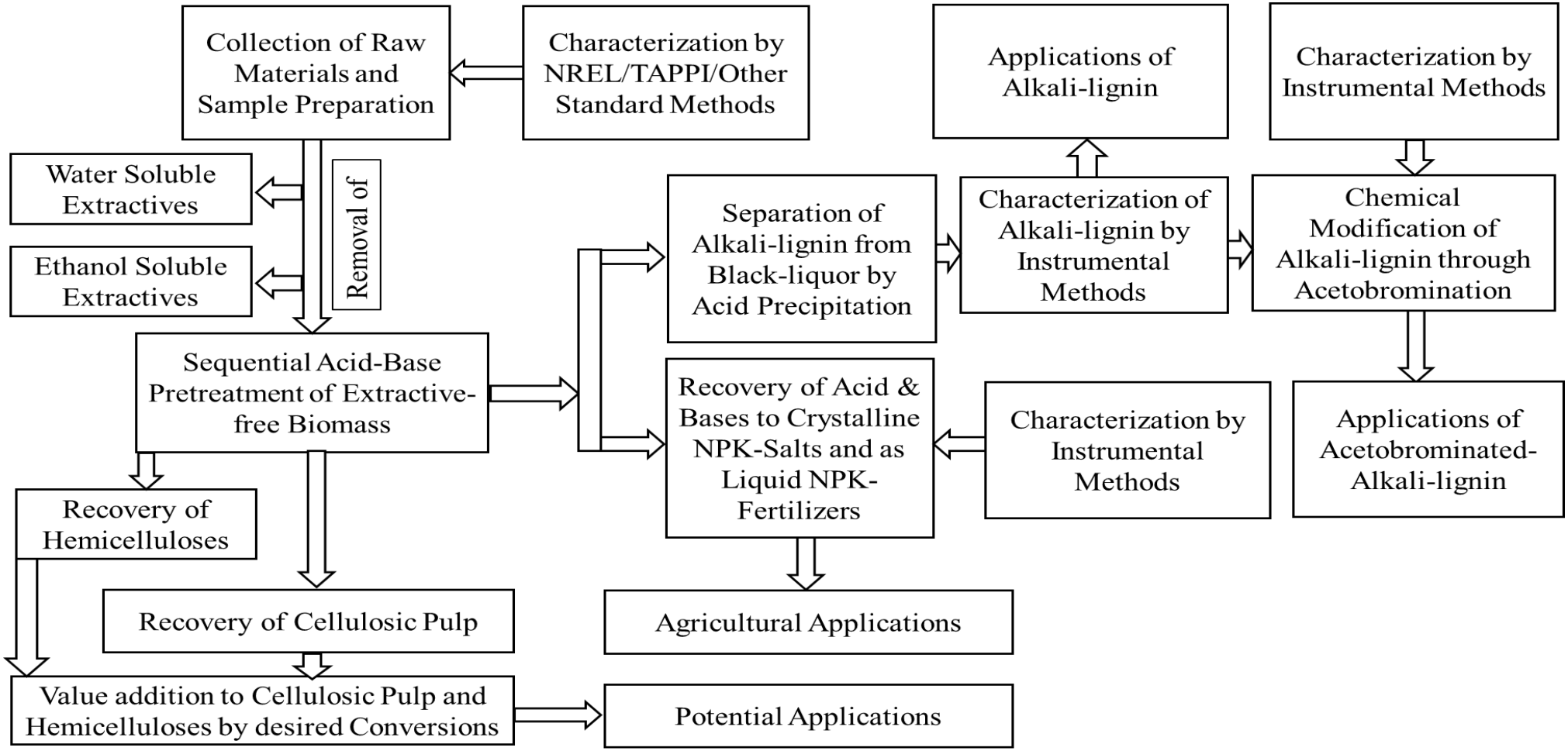

Figure 2.1: Research methodology for the conversion of lignocellulosic biomass and modifications of lignin

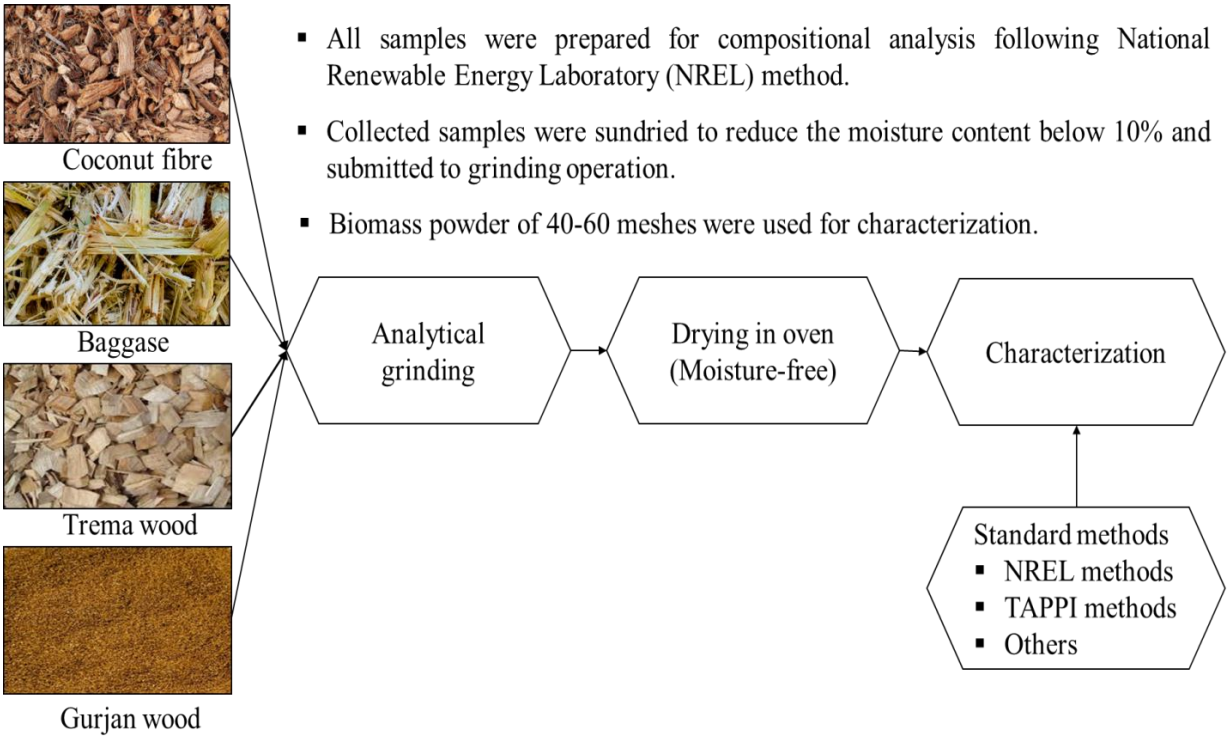

Figure 2.2: Scheme for the sample preparation and analyses of lignocellulosic biomass

2.1.3. Isolation of alkali-lignin by sequential acid-base pretreatment following biorefinery approach

After removal of the extractives, a sequential acid-base pretreatment was applied on the lignocellulosic biomass and subsequently recovered the structural constituents through following steps-

Steps for the preparation of extractive-free lignocellulosic biomass

$$\text{Lignocellulosic biomass} + \text{Water} \xrightarrow{\text{Reflux}} \text{Water soluble extractives (WSE)} + \text{WSE-free lignocellulose}$$

$$\text{WSE-free lignocellulose} + \text{Ethanol} \xrightarrow{\text{Reflux}} \text{Ethanol soluble extractives (ESE)} + \text{ESE-free lignocellulose}$$

Sequential acid-base pretreatments on extractive-free lignocellulosic biomass

$$\text{ESE-free lignocellulose} + \text{Water} \xrightarrow[\text{Heat}]{\text{Acid}} \text{Hemicelluloses (HCell)} + \text{HCell-free lignocellulose}$$

$$\text{HCell-free lignocellulose} + \text{Water} \xrightarrow[\text{Heat}]{\text{Base}} \text{Cellulose/pulp} + \text{Alkali-lignin}$$

Scheme 2.1: Removal of water and ethanol soluble extractives and sequential acid-base pretreatment on lignocellulosic biomass to deconstruct the structure

2.1.4. Physical modification of alkali-lignin by ball milling technique

The isolated alkali-lignin samples were dried under vacuum and then physically modified by ball-milling to prepare alkali-lignin particles [73].

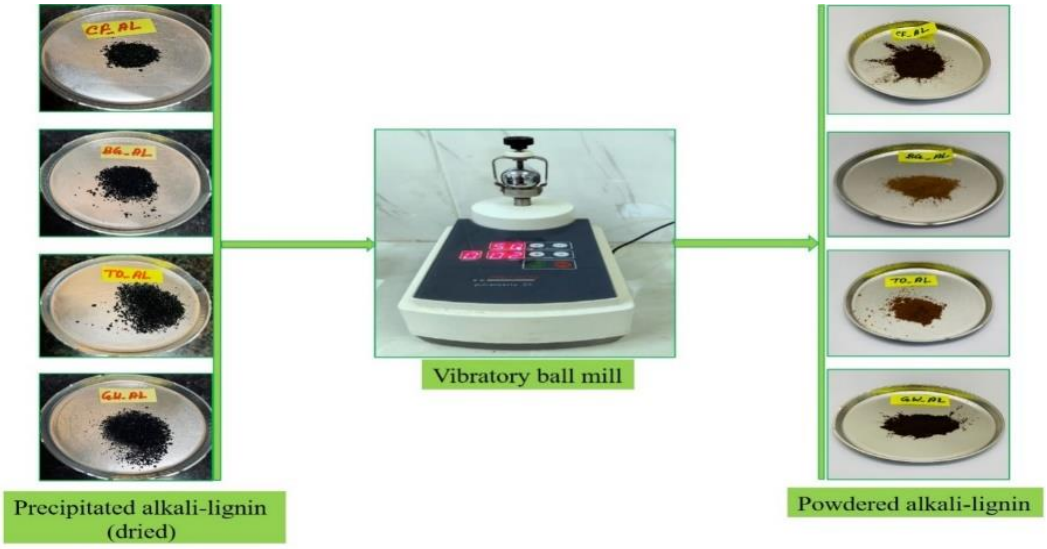

Figure 2.3: Physical modification of alkali-lignin by vibratory ball milling technique.

2.1.5. Characterization of alkali-lignin particles

Alkali-lignin samples were characterized by different instrumental techniques and then submitted for chemical modifications. Instrumental techniques included the Elemental analysis (EA); Particle size analysis (PSA) by Dynamic light scattering (DLS) technique; X-ray photoelectron spectroscopic analysis (XPS); Fourier transform mid and near infrared spectroscopic analysis (FT-MIR-NIR); Simultaneous thermal analysis (STA), e.g., Thermogravimetric analysis (TGA) and Differential scanning calorimetry (DSC); Field emission-scanning electron microscopic analysis (FE-SEM); Ultraviolet-Visible (UV-Vis) spectrophotometric analysis, e.g., determination of antioxidant activity (AOA), determination of Intrinsic viscosity (IV) by Dilute solution viscometric analysis (DSV) and Ultraviolet-diffuse reflectance spectroscopic analysis (UV-DRS), etc. (Figure 2.4). Schematic diagram of some instruments used in the research work have been given in Appendix A 6.

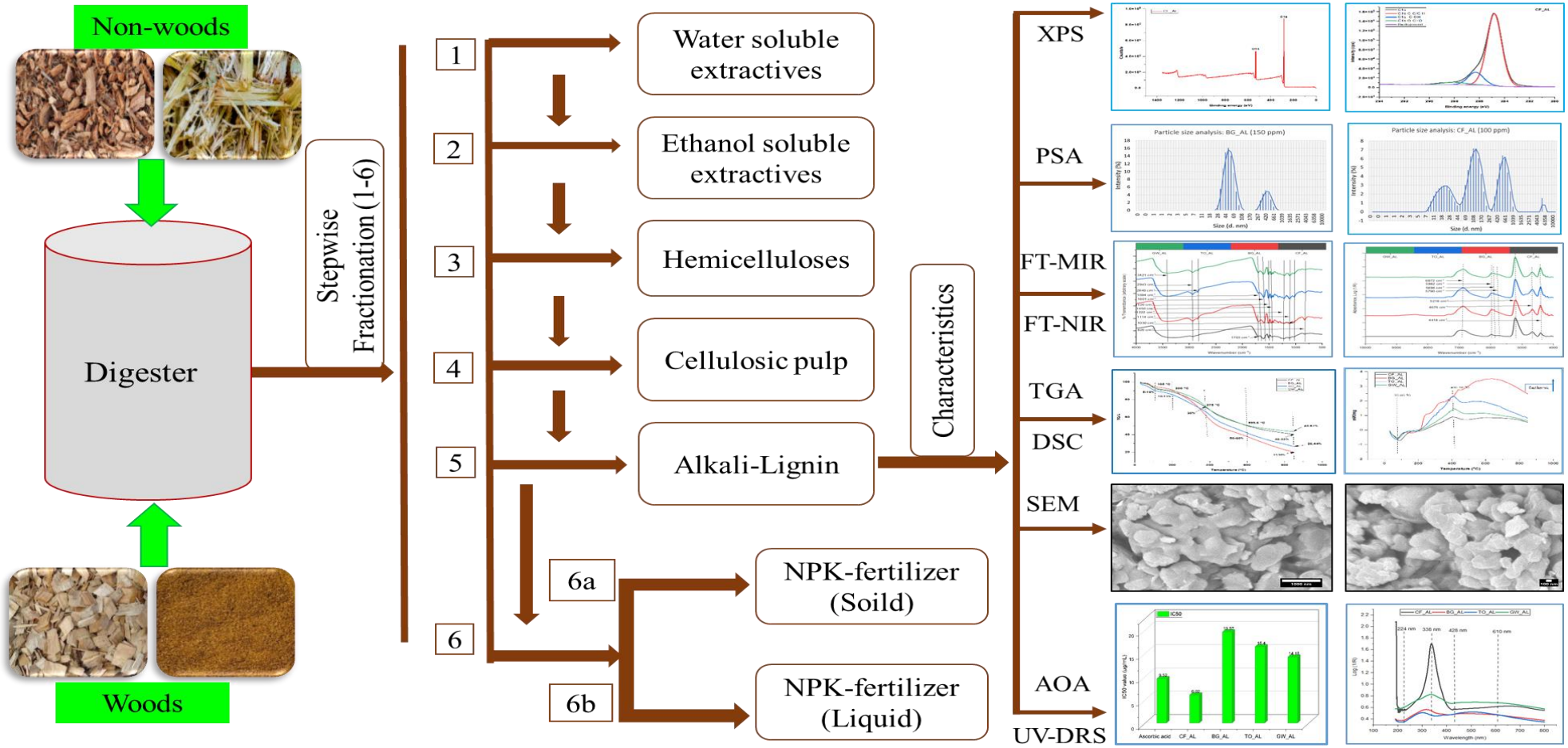

Figure 2.4: Scheme of stepwise fractionation (from 1 to 6) to isolate non-structural and structural components of lignocellulosic-feedstock and the characterization of alkali-lignin by using different instrumental techniques.

2.1.6. Chemical modification of submicron alkali-lignin particles through acetobromination and characterization of acetobrominated products

Well characterized alkali-lignin particles were acetobrominated by conventional [74] and new methods (i.e., Preparative method-1 and Preparative method-2). The products were separated, purified and then characterized by different instrumental techniques (Figure 2.5).

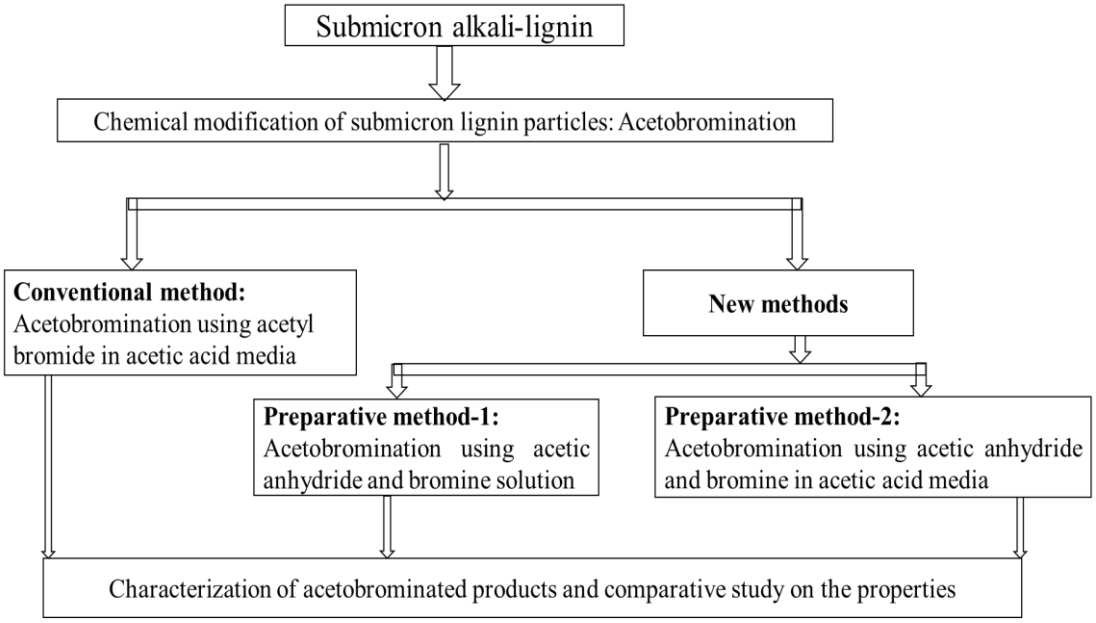

Figure 2.5: Scheme for chemical modification of alkali-lignin: Acetobromination by Conventional and New methods (applying flow chemistry approach)

2.1.7. Recovery of pretreatment chemicals from the biorefinery: As NPK fertilizers and their characterization

After the separation of alkali-lignin from black/waste liquors, the filtrates (i.e., spent liquors) were used for the recovery of pretreatment chemicals along with degraded lignocelluloses to maximize the atom economy of the biorefinery system (Figure 2.6).

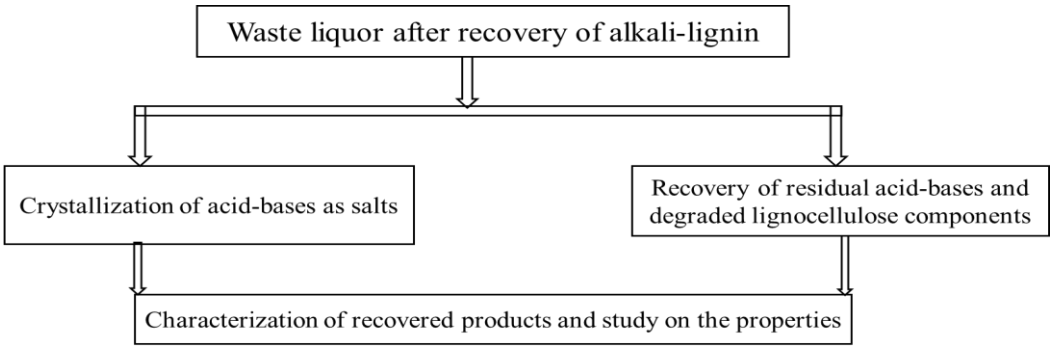

Figure 2.6: Recovery of pretreatment chemicals, i.e., acid and base from waste liquors along with degraded lignocelluloses

2.1.8. Evaluation of applicability of alkali-lignin and modified alkali-lignin in different fields

Detail analyses of the alkali-lignin and modified alkali-lignin products were evaluated for potential applications in different fields of polymer and material chemistry (Figure 2.7).

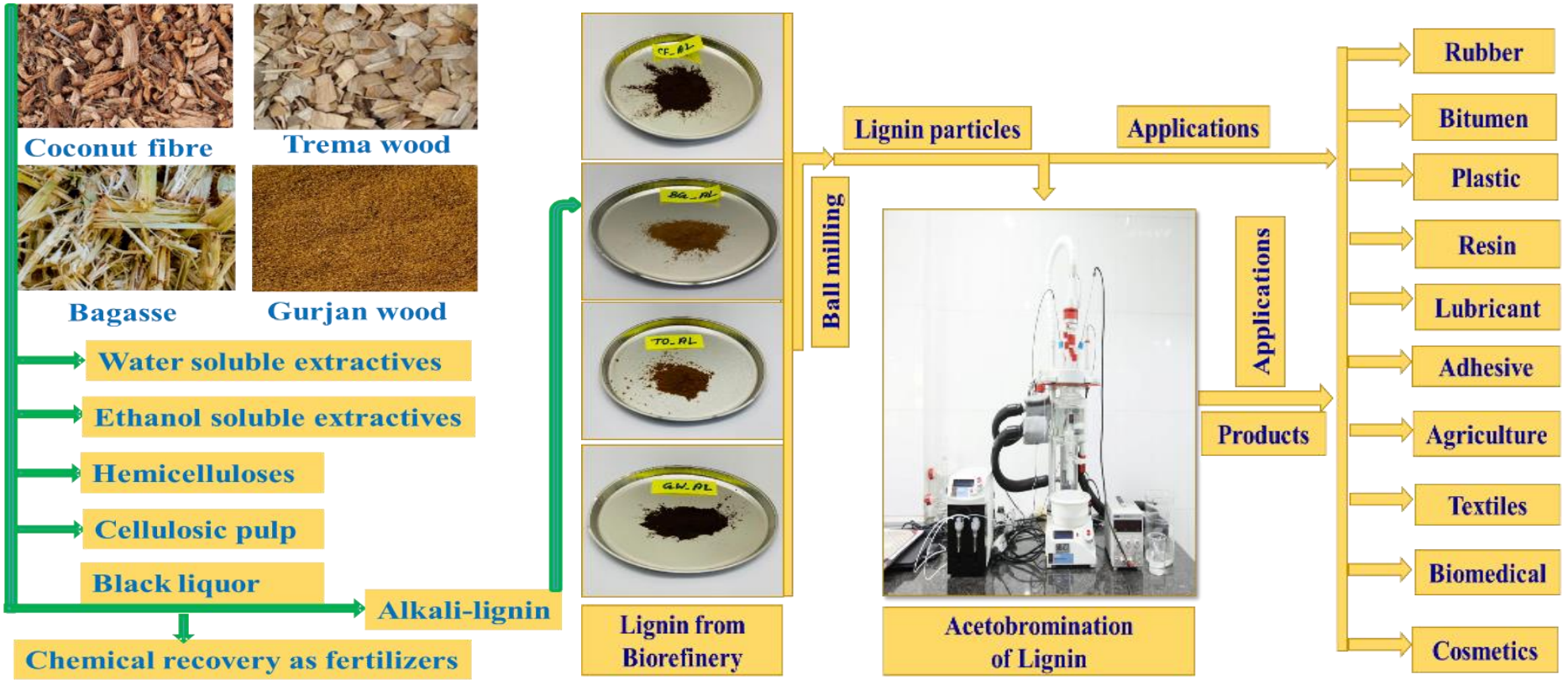

Figure 2.7: A scheme representing isolation of lignin from biorefinery, modifications of alkali-lignin and potential fields of applications

2.2. References:

[66] NREL/TP-510-42620, Preparation of Samples for Compositional Analysis, Technical Report, https://www.nrel.gov/docs/gen/fy08/42620.pdf (last accessed 07.08.2022)

[67] NREL/TP-510-42619, Determination of Extractives in Biomass, Technical Report, https://www.nrel.gov/docs/gen/fy08/42619.pdf (Last accessed 07.08.2022)

[68] NREL/TP-510-42622, Determination of Ash in Biomass, Technical Report, https://www.nrel.gov/docs/gen/fy08/42622.pdf (Last accessed 07.08.2022)

[69] NREL/TP-510-42618, Determination of Structural Carbohydrates and Lignin in Biomass, Technical Report, https://www.nrel.gov/docs/gen/fy13/42618.pdf (Last accessed 07.08.2022)

[70] TAPPI. T 9 wd-75, Holocellulose in Wood

[71] TAPPI. T 203 cm-22, Alpha-, beta- and gamma-cellulose in pulp

[72] B. Waliszewska, M. Grzelak, E. Gaweł, A. Spek-Dźwigała, A. Sieradzka and W. Czekała, Chemical Characteristics of Selected Grass Species from Polish Meadows and Their Potential Utilization for Energy Generation Purposes, *Energies*, 2021, doi:10.3390/en14061669

CHAPTER 3

DEVELOPMENT OF A MATERIAL-DRIVEN PHASE III LIGNOCELLULOSIC FEEDSTOCK BIOREFINERY: ISOLATION OF LIGNIN AND CHARACTERIZATION

Chapter 3: Development of a material-driven phase III lignocellulosic feedstock biorefinery: Isolation of lignin and characterization

3.1. Introduction

Lignin could be extracted from lignocellulosic biomass using a variety of techniques. These techniques are divided into two main categories, e.g., techniques that solubilize lignin from lignocellulosic biomasses and remove it by separating the solid residue from the wasted liquid; and techniques that selectively hydrolyze polysaccharides to leave lignin residue. Kraft, sulfite, soda or organosolv pulping processes have been considered as the representative examples of first group, whereas dilute acid hydrolysis of lignocellulosic biomasses can be considered as the second [79-80]. The first group includes the most widely used techniques for isolating and recovering lignin (Table 3.1).

Table 3.1: Different processes for isolating sulfur-free and sulfur containing lignin

Technical lignin	Isolation process	Treatment medium	Purity
Sulfur-free lignin	Alkali lignin	Alkali	Moderate-low
	Organosolv lignin	Acid	High
	Hydrolysis lignin	Acid	Moderate-low
Sulfur containing lignin	Kraft lignin	Alkali	Moderate
	Lignosulphonates	Acid	Low

However, dilute acid pretreatment can remove hemicelluloses from the lignocellulose matrices by breaking the Lignin Carbohydrate Complex (LCC) bonds. Previous studies have demonstrated that hemicelluloses are more sensitive to acid hydrolysis than cellulose, and the rate of hydrolysis of β-(1-4) linked polymers in homogeneous solutions changes depending to the component sugars in the following sequences- Glucose <Mannose < Xylose < Galactose [81]. In fact, cellulose's highly organized and crystalline structure makes it significantly more resistant to acid hydrolysis than other polysaccharides. Treatment of cellulose with 72% sulfuric acid at 20 ^{o}C caused a rapid degradation to some accessible and amorphous regions of

cellulose structure and can remove about 10% of its initial weight. A substantial reduction in the degree of polymerization was also observed. However, a two stage acid hydrolysis of wood to fermentable sugars has been created, where the first stage, or prehydrolysis stage, used diluted sulfuric acid to selectively remove the hemicelluloses at 160 ^{o}C, and the second stage, or hydrolysis stage, used 230 ^{o}C to degrade the lignocellulosic structure. From the second stage, concentrated glucose (10–12%) was obtained with a yield of roughly 50% [82]. Compared to acid hydrolysis, the cleavage of polysaccharide glycosidic bonds in alkali is slow enough, yet hemicelluloses can undergo alkaline glycosidic bond cleavage. Since cellulose is crystalline, alkaline hydrolysis is extremely slow at temperatures between 150 and 190 ^{o}C. The cleavage of α-ether and β-ether bonds in phenolic units and of β-ether bonds in non-phenolic units of the lignin structure, on the other hand, makes lignin more vulnerable to alkaline degradation of lignocellulose and allows it to be removed as soluble form [83-84]. Alkaline degradation of lignocellulose can also cause end-wise degradation of cellulose, e.g., peeling reactions, which could be minimized by adding anthraquinone in soda-anthraquinone pulping process.

However, after recovery of the cellulosic pulps from different pulping/pretreatment processes, e.g., Kraft and Soda processes, a huge volume of black/waste liquors generated that contains solubilized lignin, degraded hemicelluloses and cellulose with the pretreatment chemicals, etc. These highly alkaline black/waste liquors are usually considered as a major source of environmental pollutions, if remain untreated.

To support the industrialization of different lignocellulosic biomasses and their waste forms, this work has aimed to develop a green biomass conversion process, e.g., lignocellulosic feedstock biorefinery (based on a sequential acid-base pretreatment) to seperate the main structural components, i.e., cellulose, hemicelluloses and lignin and produce fertilizer from waste liquor. A schematic diagram on the structural changes of lignocellulosic biomass during sequential acid-base pretreatment has been presented in Figure 3.1. Potential products from the biorefinery have been given in Table 3.2. This type of material-driven phase III lignocellulosic-feedstock biorefinery approach would support the agriculture and other industrial sectors by providing necessary raw materials and products to ensure sustainable development.

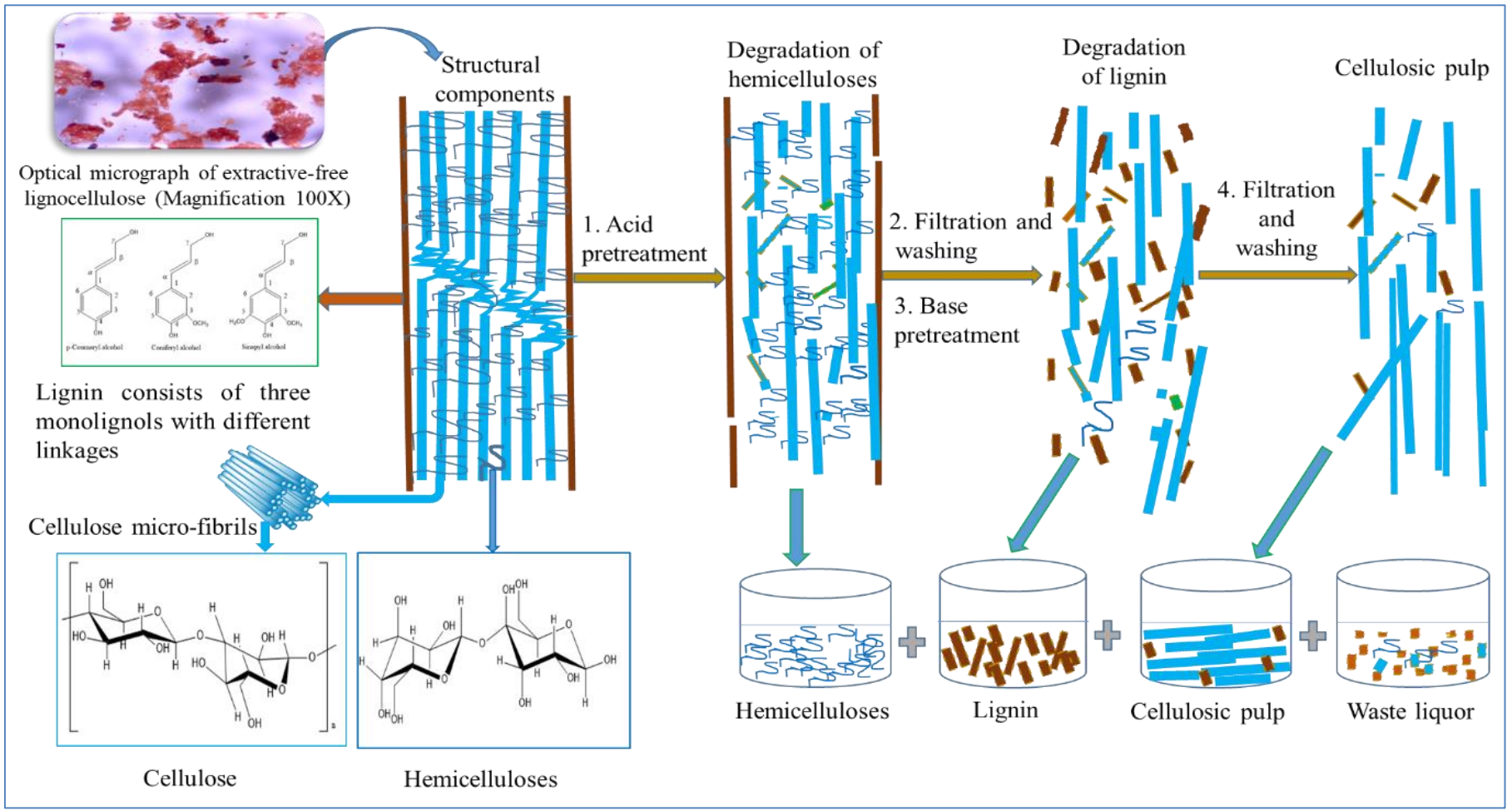

Figure 3.1: Structural changes of extractive-free lignocellulosic biomass during sequential acid-base pretreatment and the recoveries of structural components, e.g., hemicelluloses, cellulosic pulp and lignin. Used acid and base could be recovered from waste liquor.

Table 3.2: Structural components of lignocellulosic-feedstock used in the biorefinery and their modified products.

Feedstock	Components	Modified products
Different wood and non-woody biomasses	Hemicelluloses	Hemicellulose-based hydrogels; preparation of furfural, hydroxymethylfurfural, levolinic acid, etc.
	Cellulose	Preparation of nanocellulose; cellulose derivatives; cellulose-based hydrogels; emulsion stabilizer, etc.
	Lignin	Preparation of submicron lignin particles including nanolignin; lignin-based hydrogels; UV-stabilizer, antioxidants, emulsifiers; composites; bitumen modification; dye dispersants; concrete admixtures; etc.
	Fertilizer from black/waste liquor	Phosphate-based fertilizers from waste liquor in solid and liquid forms.

3.2. Materials and methods

3.2.1. Materials

All lignocellulosic biomass samples, including waste green Coconut fibre (CF) and Bagasse (BG) representing non-wood sources, as well as Trema orientalis (known locally as Nalita wood) and Dipterocarpus turbinatus (known locally as Gurjan wood) representing hardwood sources, were of Bangladesh origin. The selection of these specimens was based on their ready availability and status as archetypal representatives of non-wood and hardwood materials, respectively. The chemicals utilized in this study encompassed phosphoric acid (Merck), sulfuric acid (Merck), glacial acetic acid (Sigma-Aldrich), sodium hydroxide (Merck), potassium hydroxide (Merck), anthraquinone (Sigma-Aldrich), 95% ethanol (Merck), sodium chlorite (Sigma-Aldrich), acetate buffer of pH of 4 (Hach) and deionized water with a resistivity of 18.2 megohm.

3.2.2. Methods

Compositional analysis of lignocellulosic biomass

The collected samples were prepared for compositional analyses according to National Renewable Energy Laboratory Technical Procedure (NREL/TP), i.e., NREL/TP-510-42620 [66]. Water and ethanol soluble extractives were removed by solvent extraction method, NREL/TP-510-42619 [67]. Total ash contents were

determined by heating of each sample in furnace at 575 ± 25 ºC for 4 h following the procedure, NREL/TP-510-42622 [68]. Klason lignin and acid insoluble ash were measured by NREL method, NREL/TP-510-42618 [69]. Amount of holocelluloses were determined by Technical Association of the Pulp and Paper Industry (TAPPI) method, i.e., TAPPI–T 9 wd-75 [70]. Contents of α-cellulose were measured by 17.5% (w/v) and then 9.45% (w/v) alkali treatment of dried holocellulose by TAPPI- T 203 cm-09 [71]. Contents of hemicelluloses were found from the difference between holocellulose and α-cellulose contents of each biomass [72]. Acid soluble lignin contents were determined using a simple non-standard gravimetric technique. After six months preservation of the stored filtrates after separation of klason lignin, acid soluble lignin was precipitated and settled down. The precipitates were collected by vacuum filtration using Gooch type III crucibles, washed with deionized water and dried in a convection oven at 105 ± 5 ºC until constant weight achieved. The residues were reported as acid soluble lignin in Table 3.3. The methods applied for the analyses were discussed in Appendix A 3.

Isolation of alkali-lignin through phase III lignocellulosic-feedstock biorefinery approach

Removal of extractives and subsequent recoveries

About 75 g of each biomass samples (oven-dried; 50-60 mesh) were taken in the Soxhlet apparatus and then exhaustive extractions were performed by deionized water followed by 95% ethanol in order to remove the water and ethanol soluble extractives, respectively. The samples were oven-dried at 105 ºC and submitted for sequential acid-base pretreatment. The extractives could be recovered by distilling the solvents, e.g., deionized water and 95% ethanol and stored for reuse.

Phosphoric acid pretreatment

Extractives-free oven-dried biomass samples, i.e., Coconut fibre, Bagasse and Sawdusts of *Trema orientalis* and *Dipterocarpus turbinatus* (about 15 g each; 50-60 mesh) were digested using a sealed custom made digester (stainless steel-316 volume: 250 mL; Bangladesh) with 2% (v/v) phosphoric acid maintaining sample: liquor 1:15 at 150 ± 10 ºC for 2 h. The digested samples were cooled and then vacuum filtered by Gooch type II crucible (pore sizes: 40-90 microns). Residues were washed with deionized water and then dried under vacuum at 45 ºC until constant weight achieved.

Liquids generated from the acid hydrolysis of each biomass were stored for the recovery and valorization of hemicelluloses (final volume 250 mL; pH<2 at 25 ^{o}C).

Potassium hydroxide-anthraquinone pretreatment

2% (v/v) phosphoric acid treated oven-dried residues (about 10 g each) were digested at 160 ± 10 ^{o}C for 2 h with 4% (w/v) potassium hydroxide maintaining sample to liquor ratio of 1:15 in presence of 0.1% (w/w) anthraquinone by weight of dried residues. After cooling, the slurries were filtered by Gooch type II crucible and washed the residues with deionized water up to filtrate volume 250 mL. Then the filtrates or black liquors were stored (250 mL; pH13.00-13.50 at 25 ^{o}C) for the separation of alkali-lignin. The cellulosic pulps were oven-dried at 105 ^{o}C and then stored for valorization.

Phosphoric acid precipitation of alkali-lignin from black liquor

pH of the black liquors were adjusted to about 8.5 by dilute phosphoric acid, settled for 24 hours and then filtered. pH of the filtrates were further reduced to 2.5 by adding 42.5% (v/v) phosphoric acid followed by warming at 75 ± 5 ^{o}C for 1 h. Acid insoluble lignin, i.e., alkali-lignin were precipitated and recovered by vacuum filtration using Gooch type II crucible, washed with deionized water up to filtrate volume 250 mL and then vacuum dried at 45 ^{o}C until constant weight achieved. The alkali-lignin samples, i.e., CF_AL, BG_AL, TO_AL and GW_AL were then stored for analysis. The filtrates, i.e., spent liquors were stored for the recovery of pretreatment chemicals along with degraded organics (Table 3.4).

Effects of extractives and dilute phosphoric acid pretreatment on the isolation of alkali-lignin

To investigate the effect of extractives and dilute phosphoric acid pretreatment on the isolation of alkali-lignin, the oven-dried coconut fibre (CF), e.g., raw, extractive-free, acid pretreated and extractive-free acid pretreated samples (considering as the representative biomass) (about 5 g; 50-60 mesh) were digested in a sealed digester (stainless steel-316; volume: 100 mL; Bangladesh) following the procedure as described. Alkali-lignin samples were collected from black liquors by adding 42.5% (v/v) phosphoric acid to pH 2.5 and subsequently filtered, washed and vacuum dried (Table 3.5).

Preparation of alkali-lignin particles by ball milling technique

The vacuum dried alkali-lignin samples were ball milled (Vibratory ball mill; Poluerisette 23; FRITSCH; Germany) for 30 minutes using 30 tungsten carbide balls (speed 50 oscillation/sec). The free flowing alkali-lignin powders, i.e., CF_AL, BG_AL, TO_AL and GW_AL were then collected, vacuum dried and submitted for characterization.

3.3. Characterization and examination of physicochemical properties of alkali-lignin particles

Elemental analysis

Elemental analyses of lignin samples, i.e., CF_AL, BG_AL, TO_AL and GW_AL were done by an elemental analyzer (Elmentar, Germany). The instrument measured the amounts of carbon, hydrogen, nitrogen and sulfur present in the samples. Amounts of oxygen were calculated by difference. For simplifications, trace amounts of nitrogen have been excluded and the elemental compositions, e.g., percentages of C, H and O in the samples have been used for the determination of empirical formula on a C_9-basis. Methoxyl group contents were determined by following the empirical correlation developed based on ultimate analysis of lignin via the multiple regression method for predicting the methoxyl contents in lignin macromolecule [73].

$$[OCH_3] = -18.5769 + 4.0658\,[H] + 0.34543\,[O] \qquad (3.1)$$

Empirical formula of the alkali-lignin samples was deduced applying the rules given in literature [74] and related calculations were given in Appendix A 1.

Table 3.3: Compositional analysis of lignocellulosic biomasses (Based on 100 grams of their oven-dried weight)

Biomass	Non-structural constituents (%)				Structural constituents (%)				Grand total (g)
	Extractives		Ash		Holocellulose		Lignin		
	Water soluble	95% Ethanol soluble	Total ash	Acid insoluble ash	Alpha-cellulose	Hemicelluloses	Klason lignin	Acid soluble lignin	
CF	12.41	2.27	3.69	0.98	22.46	29.41	31.52	1.89	103.65
BG	8.31	3.45	1.70	0.55	39.41	29.11	17.76	2.69	102.43
TO	7.04	1.29	1.17	0.19	42.28	27.65	23.19	2.14	104.76
GW	3.69	5.68	1.28	0.23	43.04	24.58	23.21	1.93	103.41

Table 3.4: Recovery of structural components of lignocellulosic biomass from the biorefinery. Waste/spent liquor containing acid, base and degraded organics were stored for the recovery of pretreatment chemicals.

LCF biomass	Structural constituents			Recovered structural constituents from sequential acid-base pretreatment			Waste/spent liquor containing acid, base and degraded organics	
Ex-free biomass sample	Hemicelluloses (%)	α-cellulose (%)	Klason lignin (%)	Hemicelluloses (%)	Cellulosic pulp (%)	Alkali-lignin (%)	Volume in mL (pH)	Degraded organics (%)
CF	29.41	22.46	31.52	22.66	29.80	26.00	250 (2.5)	21.53
BG	29.11	39.41	17.76	25.66	30.40	14.13	250 (2.5)	29.80
TO	27.67	42.42	23.19	27.06	37.37	18.40	250 (2.4)	16.80
GW	24.58	43.04	23.21	21.41	40.06	17.46	250 (2.5)	21.06

Table 3.5: Effects of extractives and dilute phosphoric acid pretreatment on the isolation of alkali-lignin from Coconut fibre (CF) by dilute potassium hydroxide-anthraquinone pretreaatment

Sample	Recovered cellulosic pulp and alkali-lignin	
	Cellulosic pulp (%)	Alkali-lignin (%)
Raw coconut fibre	57.22	16.63
Extractive-free coconut fibre	46.78	18.28
Acid pretreated coconut fibre	32.98	22.60
Extractive-free and acid pretreated coconut fibre	31.57	24.24

Particle size analysis

Dynamic Light Scattering (DLS) measurements were performed at 298 K using a Malvern Light Scattering Instrument (Zetasizer Nano ZS, UK) to determine the particle size of alkali-lignin samples and their size distributions. The instrument maintained the duel measurement angle of 13° and 173°. He-Ne laser of power 4 mW and wavelength 632.8 nm was used as monochromatic light source and an avalanche photodiode (APD) was used as the detector. Antisolvent precipitation/solvent shifting method was applied to form alkali-lignin particles in the dispersion [75]. At first, the alkali-lignin samples (CF_AL, BG_AL, TO_AL and GW_AL) were dissolved in DMSO at 1 mg/mL concentration and then mixed well by using an ultrasonic bath for 15 minutes at 30 ^{o}C. Three different concentrations of each type of alkali-lignin samples, e.g., 0.1 mg/mL, 0.15 mg/mL, and 0.20 mg/mL were prepared by diluting the stock 1 mg/mL alkali lignin-DMSO mixtures with deionized water. These aqueous dispersions were used to measure the hydrodynamic diameters of alkali-lignin powder after 15 min ultrasonication at 25 ^{o}C. No extra chemical was used to stabilize the dispersions. All samples were analyzed without applying any filtration or dialysis steps. The Z-average sizes were accepted as the final hydrodynamic diameter of alkali-lignin particles.

X-ray photoelectron spectroscopic analysis

Surfaces of all alkali-lignin samples, e.g. CF_AL, BG_AL, TO_AL and GW_AL were analyzed by X-ray photoelectron spectrometer (K-Alpha_KAN, Thermo Fisher Scientific Inc., USA) under high vacuum $2x10^{-9}$ mbar and at room temperature. The moisture-free alkali-lignin particles were drop-casted using acetone and dried under vacuum before analysis. The wide scans (200 eV pass energy) were performed to determine the surface elemental composition of lignin samples. The narrow or high

resolution scans (50 eV pass energy) were conducted to evaluate the chemical states or bonding nature of the elements in the samples. The trace elements, e.g., nitrogen, phosphorus and silicon were excluded from high resolution scanning and not considered their contribution in the bond formation in complex molecular architecture of lignin. Gaussian peak profiles were used for the deconvolution of C1s and O1s spectra. The C1s peak at 284.82 eV was used as reference to calibrate the binding energy scale. All spectra were reconstructed using OriginPro 2022 software. The wide and narrow scan high resolution deconvoluted spectra were assigned and discussed in result and discussion section.

Fourier transform mid and near infrared spectroscopic analysis

The moisture-free alkali-lignin samples were analyzed in transmission mode using a FT-MIR-NIR spectrometer (Frontier, Perkin-Elmer, UK). The spectral range of IR analysis was 600 to 4000 cm^{-1} at a spectral resolution of 4 cm^{-1} and number of scans was 12. About 13 mm pellets were prepared by pressing 3 mg moisture-free lignin samples with 325 mg KBr. Spectrum was recorded and stored in computer memory. The spectra were reconstructed using OriginPro 2022 software and tentatively assigned. The samples were also analyzed in diffuse reflectance mode by using Near Infrared Reflectance Accessory (NIRA) attached with the spectrometer. The NIR spectral range was 4,000 to 10,000 cm^{-1} at a spectral resolution of 16 cm^{-1} and numbers of scans were 32. NIR transparent glass vial was used as sample container. Spectrum was recorded and stored in computer memory. The spectra were reconstructed using OriginPro 2022 software, overtone and combination bands of the alkali-lignin samples were assigned and discussed in result and discussion section.

Nuclear magnetic resonance spectroscopic analysis

^{1}H-NMR spectra of CF_AL, BG_AL, TO_AL and GW_AL samples were obtained in d_6-DMSO following a method with some modifications [76]. 600 MHz NMR spectrometer, Ascend, Bruker (or otherwise stated) was used to capture the spectra. Concentrations of the samples were 25 mg/0.5 mL and experimental temperature was 25 ^{o}C in the FT mode with the pulse width 10.5 sec (90^{o} pulse), the data acquisition time about 2.75 sec without a pulse delay, and the number of scans were 16. Qualitative assessments, e.g., evaluation of aromatic and other protons in the samples were done. To assess the spectral resolution of important lignin functionality, acetylation of CF_AL was

performed by taking 100 mg of moisture-free sample in a 50 mL round bottomed flask and then acetylated using 5 mL 1:1 (v/v) acetic anhydride in fresh distilled pyridine solution for 24 hours at ambient temperature [131]. Ethanol (25 mL) was added and stirred magnetically. After 30 min, the solvents were removed by film evaporation. Repeated addition and removal of ethanol (5-10 times) results in the removal of acetic acid and pyridine from the sample. The sample was then dried in vacuum over KOH and P_2O_5. The acetylated lignin sample was dissolved in 5 mL chloroform and the solution was dripped into 100 mL magnetically stirred anhydrous ether. The precipitate (CF_AL_acetylated) was collected by centrifugation and washed several times with ether. The precipitate was then dried in vacuum at 45 ^oC for 12 h.

Field emission- scanning electron microscopic analysis

Analyses of the size and morphology of prepared alkali-lignin particles were done by Field Emission Scanning Electron Microscope (JEOL JSM-7610F, Japan) applying electron voltage 5kV. The moisture-free powdered samples were set/mounted on carbon tape with adhesive and sputter-coated with platinum before analysis. Observation was done with the help of charge compensator. The FE-SEM images of the samples were presented and discussed in result and discussion section.

Examination of thermal properties

Thermal analyses of the moisture-free alkali-lignin powdered samples were analyzed by Simultaneous Thermal Analyzer (JupiterF3, Netzsch, Germany). The instrument simultaneously measured the sample's weight change and the energy input required for keeping the sample and reference material at the same temperature as a function of temperature. In order to elucidate the physicochemical properties, about 10 mg of each sample was introduced for measurement under nitrogen atmosphere (50 ml/min) at a heating rate of 10 ^oC/min from 30 to 850 ^oC. TG and DSC thermograms have been presented separately and discussed in result and discussion section.

Determination of antioxidant activities

The antioxidant activity of prepared alkali-lignin samples, i.e., CF_AL, BG_AL, TO_AL and GW_AL were determined in DMSO medium using the free radical, 2,2-Diphenyl-1-picrylhydrazyl (DPPH*), where the absorption band of the radical at 517 nm was disappeared upon reduction by alkali-lignin samples and compared with ascorbic acid following the method described by Brand-Williams with some modifications [77].

Accurate amounts of ascorbic acid and each alkali-lignin samples (2 mg) were dissolved in 2 mL DMSO to prepare stock solutions. Concentrations of these solutions were 1000 µg/mL. Different concentrations were made by serial dilution of these stock solutions with DMSO. 20 µg/mL DPPH solutions were prepared by dissolving 5 mg DPPH in 250 mL DMSO. For assay, 1 mL of each solution (samples and control) were mixed well with 1 mL fresh DMSO and 3 mL DPPH solution in amber color vial (5 mL) and kept for 25 minutes in a dark place. Then, the absorbances of the solutions were measured at 517 nm against DMSO by a double-beam UV-Vis Spectrophotometer attached with 8-sample changer (Lambda 35, Perkin Elmer, Singapore). Blank determinations were also made using all components of the solutions except samples. Percent inhibitions or Radical scavenging activities were determined by following equation 3.2 [77] using absorbance data of the sample ($Absorbance_{sample}$) and blank ($Absorbance_{blank}$) as given in Appendix A 2.

$$\% \text{ Inhibition} = [1 - (Absorbance_{sample} / Absorbance_{blank})] \times 100 \qquad (3.2)$$

IC_{50} value of the samples was calculated by plotting %Inhibition or Radical scavenging activity Vs Log concentrations of the samples.

Diffuse reflectance Ultraviolet-Visible spectroscopic analysis

The submicron alkali-lignin powder samples were analyzed by Perkin-Elmer UV-Vis spectrophotometer (Lambda 35, Perkin Elmer, Singapore) equipped with a 60 mm integrating sphere. Uniform flat surfaces and identical packing densities of the samples were ensured by taking 250 mg of each powder samples into the dedicated sample cell and then fixed with hand press [78]. The UV-Vis diffuse reflectance spectra were acquired from 190 to 800 nm, step 1 nm. Calibration was performed by means of Spectralon® standard.

Determination of Intrinsic Viscosity

An automated microviscometer (Lovis 2000M, Anton-paar, Austria) was used for single-concentration intrinsic viscosity measurement of prepared alkali-lignin samples. At first, the samples (20 mg) were dissolved in dimethyl sulfoxide (10 mL) and then ultrasonicated at 30 ^{o}C for 15 minutes. Density of DMSO was reconfirmed (1.09594 g/mL) using an automated density meter (Model: DMA 5000M; Anton-paar; Austria).

Viscosity measurements were performed using capillary, ø 1.59 steel and maintaining the temperature at 25 ^{o}C and inclination 35^{o} with 1^{o} steps. The automated microviscometer have the ability to measure the absolute/dynamic viscosity of solutions ranging from 0.3 mPa.s to 10,000 mPa.s with up to 0.5% accuracy, temperature accuracy 0.02 ^{o}C and accuracy of measuring time up to 0.05%. Billmeyer equation 3.3 was used to calculate approximate intrinsic viscosity of alkali-lignin-

$$[\eta] = 0.25 \frac{(\eta_r - 1) + 3 \ln \eta_r}{c} \quad (3.3)$$

here,

$[\eta]$= Intrinsic viscosity

η_r = Relative viscosity

c = Concentration

3.4. Results and discussion

Compositional analysis of lignocellulosic biomasses

To establish the material-driven phase III lignocellulosic feedstock biorefinery with easy lignin isolation facility, the most relevant compositional analysis of four lignocellulosic biomasses could provide a clear insight on the conversion yields and process economics [85-86].

The main structural and non-structural components of four lignocellulosic biomasses, i.e., Coconut fibre, Bagasse, *Trema orientalis* and *Dipterocarpus turbinatus* were analysed and presented in Figure 3.2 (Table 3.4). Amounts of α-cellulose, hemicelluloses, klason lignin, total extractives and ash contents in the samples showed some variations as found in the literature [87-93]. The variation of the constituents could be explained based on the origins, forms, structural diversities, growth conditions, etc. of used lignocellulosic biomasses [85]. α-cellulose contents of *Trema orientalis* and *Dipterocarpus turbinatus* were greater than coconut fibre and sugarcane bagasse as the characteristics of wood.

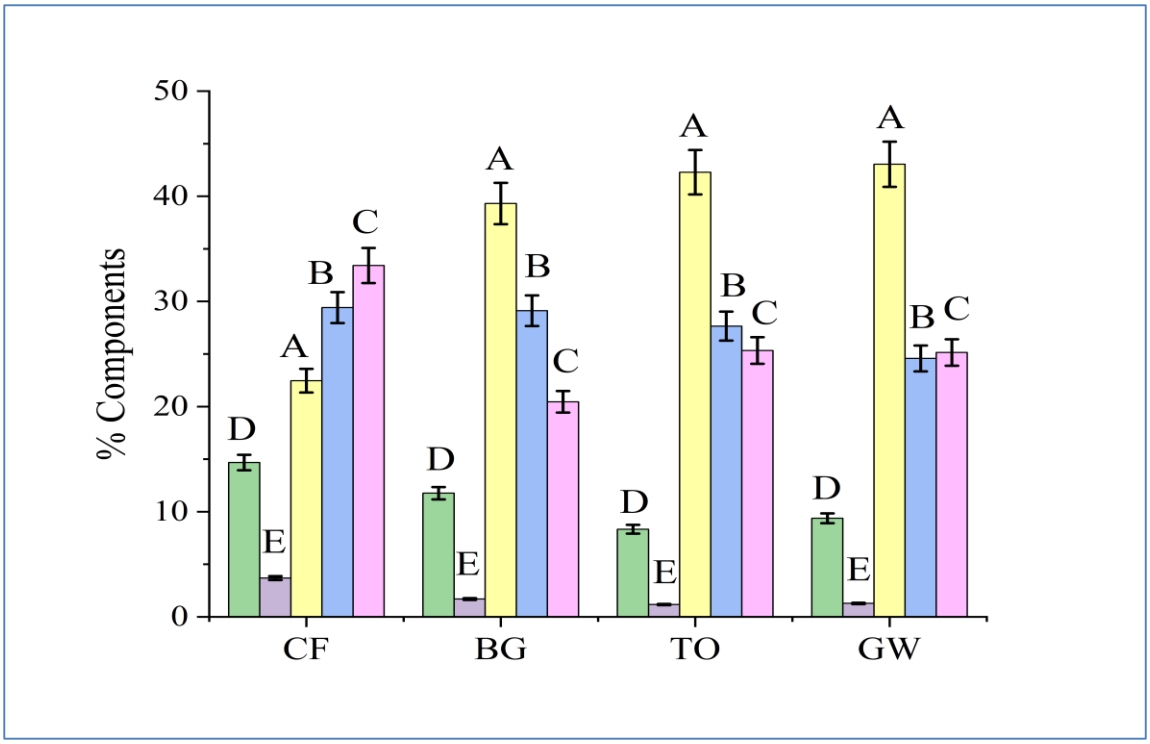

Figure 3.2: Compositional analysis of four lignocellulosic biomasses, i.e., Coconut fibre (CF), Bagasse (BG), *Trema orientalis* (TO) and *Dipterocarpus turbinatus* (GW); A = α-cellulose, B = hemicelluloses; C = klason lignin, D = extractives and E = total ash.

Coconut fibre had the lowest α-cellulose content among four samples, but the highest amount of klason lignin. In fact, coconut fibre is the most lignin rich biomass and lignin content may reach more than 50% of its oven-dried weight as reported in previous work [94]. Amounts of Klason lignin in green coconut fibre could be lower (31.52%) than their mature counterpart. It was due to aging process or growth Conditions [95]. Bagasse had the lowest klason lignin contents but higher α-cellulose content than coconut fibre. *Trema orientalis* and *Dipterocarpus turbinatus* had similar amounts of α-cellulose and Klason lignin contents, as characteristics of hardwood [96]. Coconut fibre and bagasse had higher amounts of extractives than *Trema orientalis* and *Dipterocarpus turbinatus.* Among the biomasses, green coconut fibre had the highest extractive contents, e.g. water and 95% ethanol soluble extractives, combindly. Coconut fibre showed the highest amount of total ash content (3.69%) among four samples. Acid insoluble ash contents were less than 1% in all cases. As far as we have concerned, no studies were conducted on the compositional analysis of *Dipterocarpus turbinatus* (Gurjan wood), but there have been few studies conducted on the tropical timber wood species of the Dipterocarpacea [93] and *Trema orientalis* families (Nalita wood) [91-92].

Recovery of structural components from the biorefinery

Amounts of phosphoric acid precipitated alkali-lignin (AL) from the black or spent liquors of coconut fibre (CF), bagasse (BG), *Trema orientalis* (TO) and *Dipterocarpus turbinatus* (GW) along with other structural components have been presented in Figure 3.3. As can be seen, the yields of alkali-lignin were lower than the biomasses' klason lignin concentrations, i.e., CF_AL 84.48%, BG_AL 79.56%, TO_AL 79.34% and GW_AL 75.22%.

Dilute phosphoric acid hydrolyzed the hemicelluloses from extractive-free samples by breaking the bonds in lignin carbohydrate complexes and could be recovered from the filtrates, i.e., 22.66% (w/w) from coconut fibre, 25.66% (w/w) from bagasse, 27.06% (w/w) from *Trema orientalis* and 25.86% (w/w) from *Dipterocarpus turbinatus* based on oven-dried biomass. The amounts of hydrolyzed hemicelluloses were 77.04, 88.14, 97.79 and 87.10 % (w/w) of actual hemicelluloses contents of coconut fibre, bagasse, *Trema orientalis and Dipterocarpus turbinatus*, respectively. Although dilute acid hydrolysis can selectively remove the hemicelluloses from extractive-free lignocellulose, minor amounts of cellulose may be hydrolyzed [82]. In a study, sequential treatments on dewaxed bamboo (D. sinicus) samples with 80% ethanol containing 0.025M HCl, 80% ethanol containing 0.5% NaOH, and alkaline aqueous solutions containing 2.0, 5.0, and 8.0 % NaOH at 75 ^{o}C for four hours while maintaining solid to liquid ratio of 1:25 (g/mL) resulted in 16.6% soluble hemicelluloses, accounting for 94.3% of total hemicelluloses [97]. Additionally, autohydrolysis was used to extract hemicelluloses from lignocellulosic biomasses, and pine wood was autohydrolyzed at 170 °C for 60 minutes, yielding roughly 60% hemicelluloses [98]. In acid catalyzed extraction of hemicelluloses, H_2SO_4, HCl, HF, and HNO_3 are commonly used. To recover hemicellulose sugars, a dilute acid hydrothermal fractionation technique was also devised [99]. A maximum xylose yield of 74.75% was recorded using 0.3 wt% H_2SO_4 at 180°C for 10 min. Acid content, temperature, and reaction time all played a big impact on how well hemicelluloses were removed. Using a 1.76 wt% H_2SO_4 solution at 152.6 °C for 21 minutes, the sugar recovery was 85.5%, with xylan, mannan, and galactan accounting for 78.9% of the total sugars recovered [100].

In a different investigation, hemicelluloses were extracted from birch sawdust using hot water and formic acid [101]. By combining the yields of xylose and furfural at 170 °C, the addition of formic acid increased the extraction rate of hemicelluloses from birch

wood compared to standard hydrothermal methods, reaching nearly 70 mol%. However, phosphoric acid is a weak acid as indicated by its first dissociation constant, Ka_1 = 7.5×10^{-3} and it is stronger than acetic acid, but weaker than sulfuric and hydrochloric acids. Further dissociation step of phosphoric acid occurs with decreasing ease.

Using dilute phosphoric acid for the pretreatment of lignocellulosic biomass to prepare sugars and other added-value by-products, several works were reported and showed that solubilisation of hemicelluloses could reach at 96-98% under applied digestion conditions [102-103]. Although acid hydrolysis makes it possible to extract large amounts of sugars, the yield and molecular weight of the recovered hemicelluloses are relatively low as a result of the ease with which they can be hydrolyzed in an acidic environment. Therefore, monosaccharides rather than xylan make up the majority of the product's ingredients. Additionally, severe corrosivity and side effects are also a part of the acid pretreatment process [99]. Modern biorefineries as well as the Soda and Kraft pulping processes for the production of dissolving pulp recently added a prehydrolysis stage for the removal of hemicelluloses prior to delignifying lignocellulosic biomasses [106-107]. Even though this treatment decreases the pulp output, the higher price of dissolving pulp and the recovered hemicelluloses can be utilized to make sugar-based chemicals or fuels to make more money. Considering the experimental results and facts as discussed above, we have included the dilute phosphoric acid pretreatment on extractive-free lignocellulosic biomass under pressurized conditions for the development of the material-driven phase III biorefinery system (Figure 3.4 and Figure 3.5).

After 4% (w/v) potassium hydroxide-anthraquinone pretreatment on the extractives and hemicelluloses-free lignocellulosic residues, cellulosic pulps, e.g., 29.80, 30.40, 37.37 and 40.06% (w/w) were recovered from coconut fibre, bagasse, *Trema orientalis* and *Dipterocarpus turbinatus*, respectively. These amounts were lower than the α-cellulose contents of the samples except coconut fibre, as it is considered as highly recalcitrant lignocellulosic biomass with the highest lignin content [94].

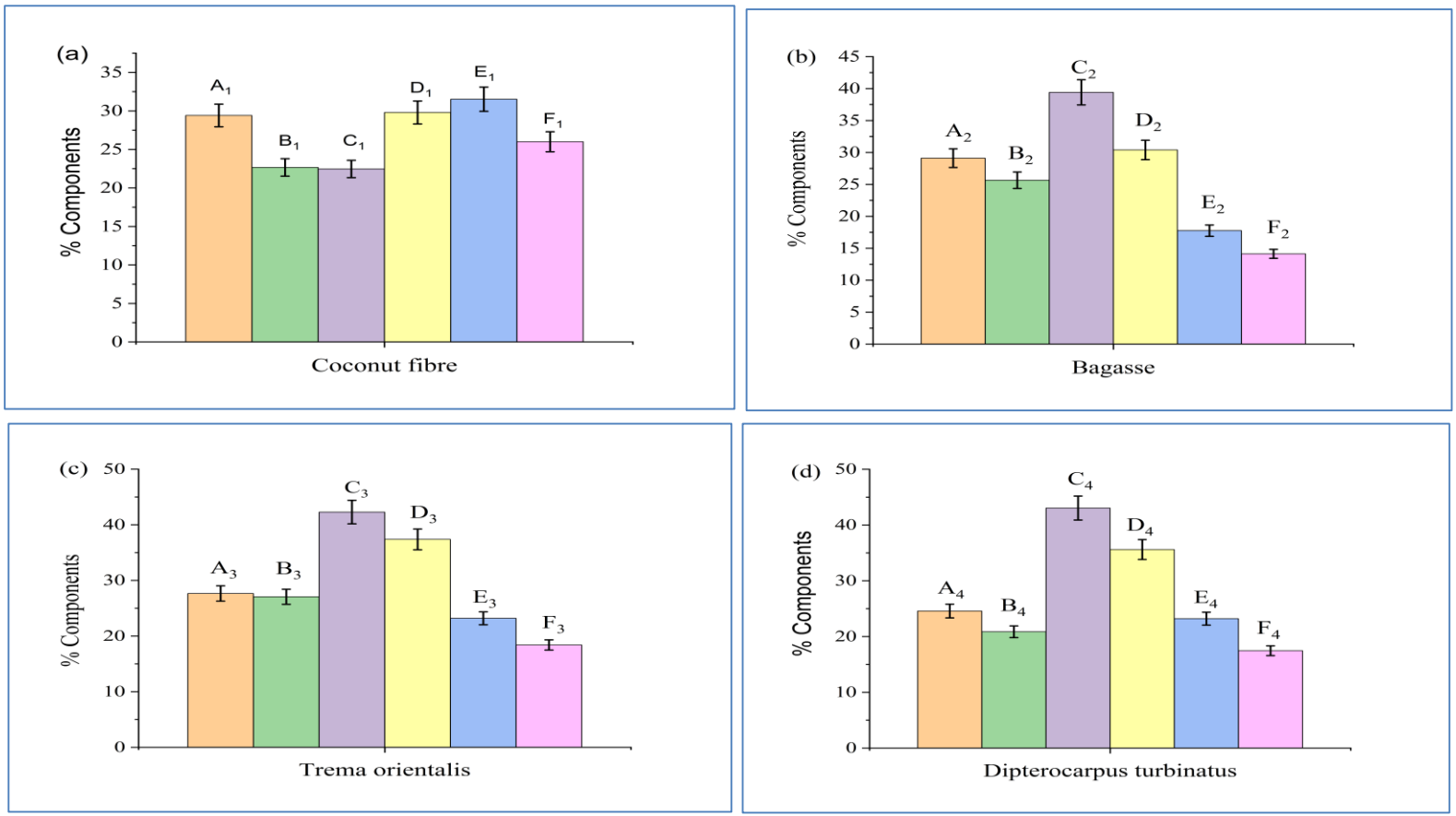

Figure 3.3: Comparison among actual and recovered structural components of used lignocellulosic biomass by sequential acid-base pretreatment (a) Coconut fibre (b) Bagasse (c) *Trema orientalis and* (d) *Dipterocarpus turninatus.* A_1, A_2, A_3 and A_4 = actual hemicelluloses; B_1, B_2, B_3 and B_4 = recovered hemicelluloses; C_1, C_2, C_3 and C_4 = actual α-celluloses; D_1, D_2, D_3 and D_4 = recovered pulps; E_1, E_2, E_3 and E_4 = klason lignin contents and F_1, F_2, F_3 and F_4 = recovered alkali-lignin from the samples, respectively.

Recovery of lower amounts of cellulosic pulps indicated the degradation and subsequent solubilisation of some cellulose and residual hemicelluloses along with lignin in the spent liquors. About 80 % alkali-lignin could be precipitated using phosphoric acid and then recovered by vacuum filtration of the spent liquors of nonwood samples, whereas slightly lower amounts of lignin (above 75 %) were obtained from the woods. This could be explained in terms of recalcitrant nature of hardwood than nonwoody biomasses towards alkali-anthraquinone pulping process [108-110]. Degraded hemicelluloses and cellulose residues in the spent liquor could be hydrolyzed into their respective mono or oligomeric sugars, while warming at pH 2.5 and then filtered out leaving the precipitated alkali-lignin in pure forms.

The acidic filtrates (pH about 2.5) were neutralized by adding necessary amounts of ammonium hydroxide (or mixture of ammonium and potassium hydroxides) to crystallize the chemicals as NPK-fertilizer. After separation of the crystals, the remaining liquids could be used as NPK-fertilizer in liquid form containing residual potassium, ammonium and phosphate ions and degraded organics, e.g., cellulose, hemicelluloses and lignin in the forms of mono or oligomers. The cellulosic pulps might be used for different industrial applications upon modifications.

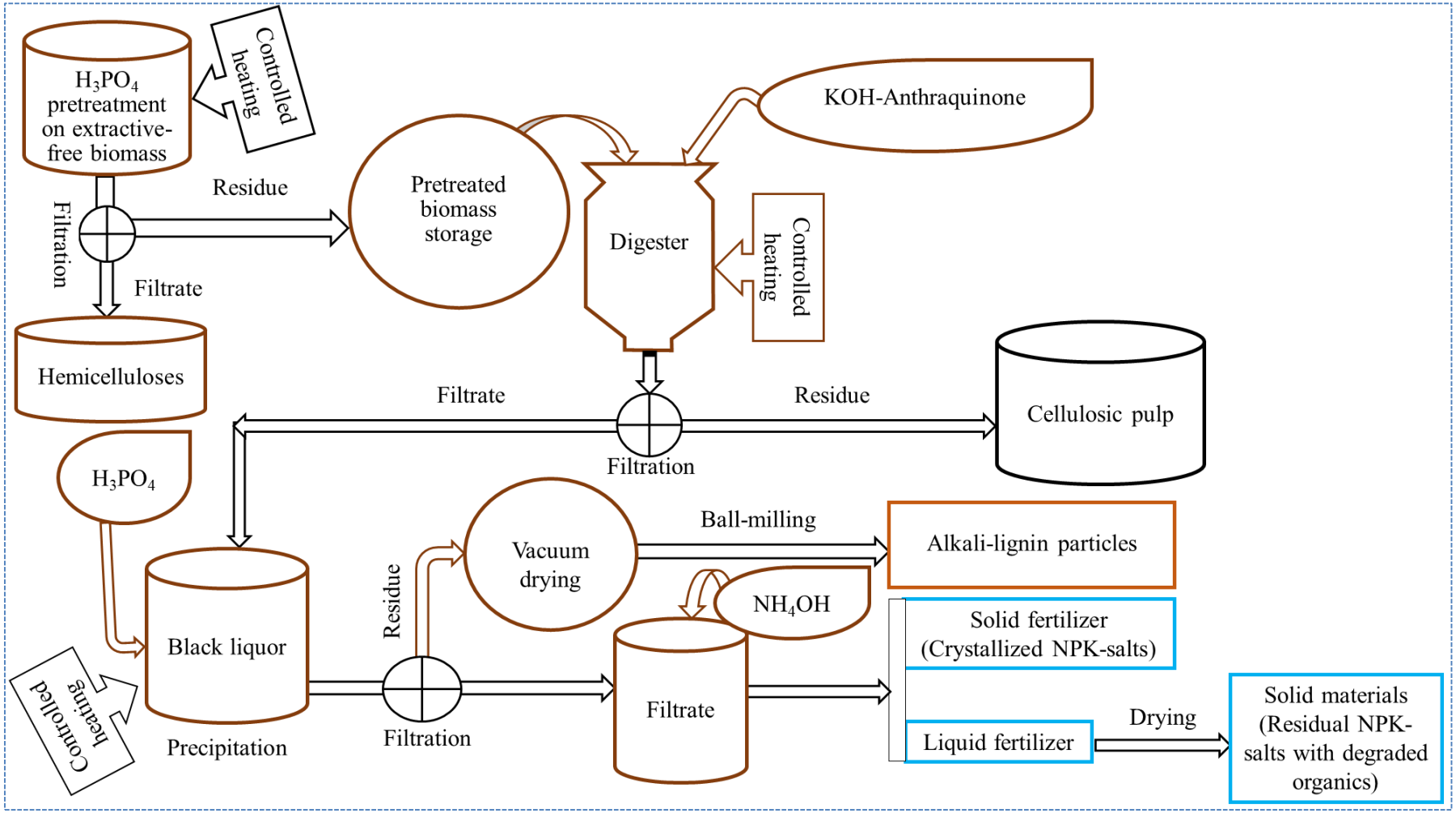

Figure 3.4: Schematic diagram of phosphoric acid, potassium hydroxide and ammonium hydroxide based Material-driven Phase III Lignocellulosic Feedstock Biorefnery for the conversion of different lignocellulosic biomass without generating any waste material.

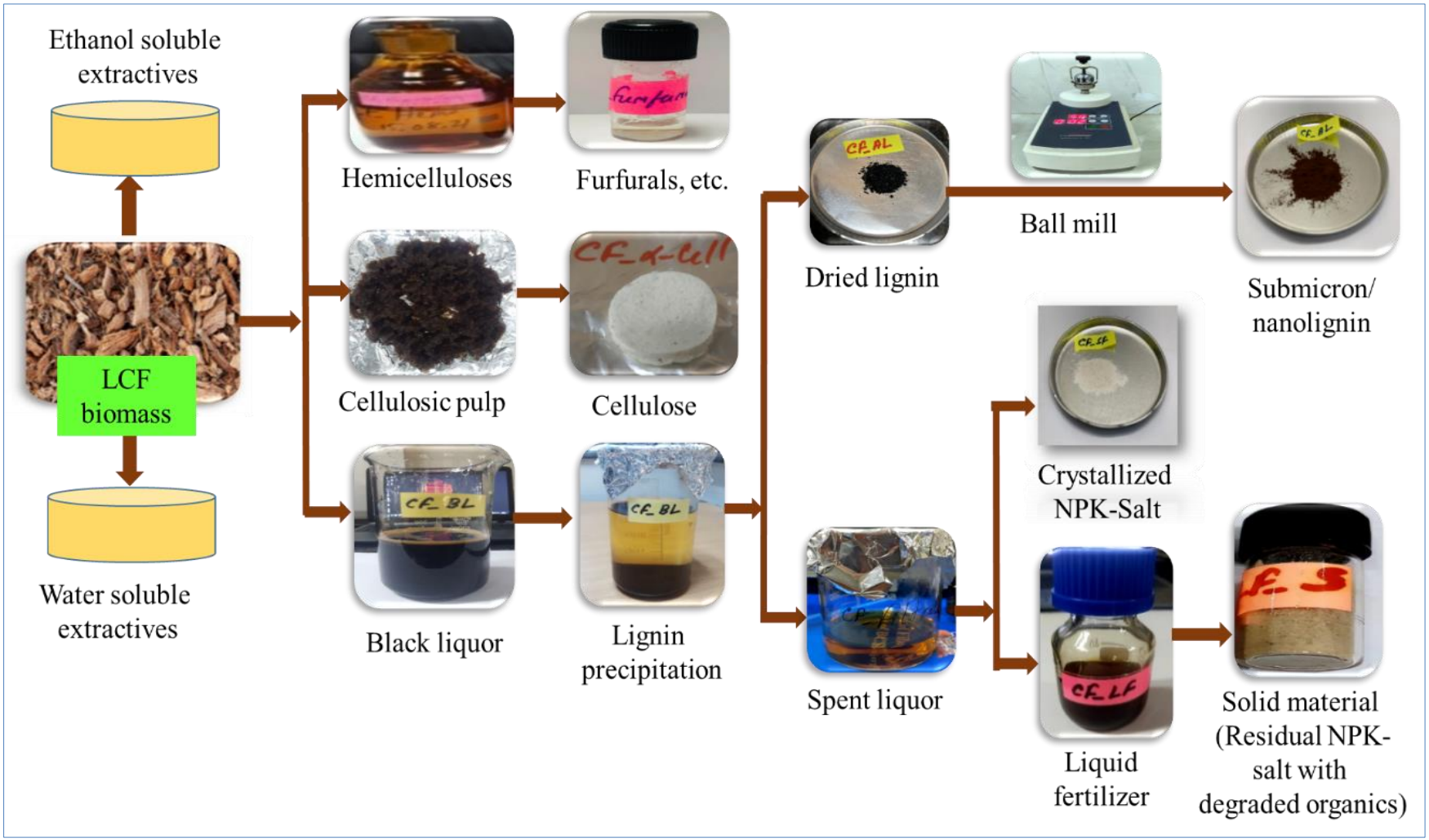

Figure 3.5: Conversion routes and some potential products from the Material-driven Phase III LCF Biorefinery System

Effects of extractives and dilute phosphoric acid pretreatment on the isolation of Alkali-lignin

As shown in Figure 3.6, the presence of extractives and dilute acid pretreatment had a substantial impact on the isolation of alkali-lignin. Due to the extensive physical and chemical interactions between lignin and the other components of the plant cell wall, an easy separation of lignin from lignin-carbohydrate complexes has typically been regarded as one of the most difficult procedures [111-112].

Previous research demonstrated that extractive-free corn stover could be heated at 90 °C for 24 hours with an affordable protic ionic liquid, [Pyrr][Ac], made from pyrrolidine and acetic acid, to isolate around 75% of the lignin [114]. The use of ionic liquid (IL), $[C_2C_1im][OAc]$ with microwave assisted extraction could isolate about 50% lignin from Eucalyptus at 140 ^oC [115]. Another research showed that alkali and IL pretreatments with 5.00 grams of sample and 40 mL of 10 g/g NaOH solution at 125 ^oC and 5.00 grams of sample and 100 grams of [BmimCl] at 110 ^oC, respectively, could extract about 42% (w/w) and 11% (w/w) of acid-insoluble lignin from bamboo [116].

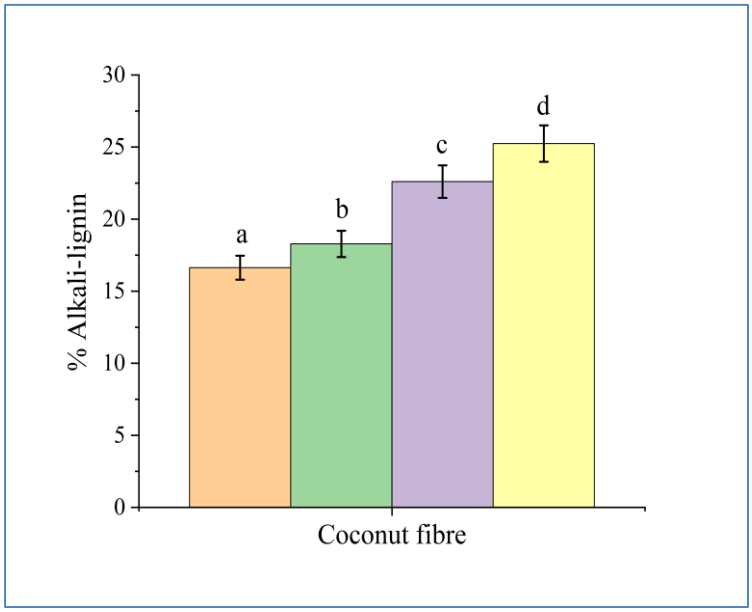

Figure 3.6: Alkali-lignin recovered from (a) raw coconut fibre (b) extractive-free coconut fibre (c) acid pretreated coconut fibre and (d) extractive-free and acid pretreated coconut fibre

It is obvious that the non-structural and structural components form complex lignocellulose matrices through different primary and secondary chemical bonding and provide highly recalcitrant nature [113]. After removal of non-structural components, e.g., resinous materials, waxes, dyes and pigments, etc., the surface of the lignocellulose

turns to more open for chemical attack. Distinct chemical processes, such as sequential acid and base hydrolysis, have different effects on the principal structural components such as hemicelluloses, cellulose, and lignin. Removal of hemicelluloses by acid pretreatment caused significant disruption of the lignocellulose matrices. When 4% (w/v) potassium hydroxide-anthraquinone pretreatment was performed on the raw, extractive-free, acid-pretreated and extractive-free acid-pretreated coconut fibre samples, different amounts of alkali-lignin, i.e., 16.63, 18.28, 22.6 and 25.24% and cellulosic pulps, i.e., 57.22, 46.78, 32.98 and 31.57% could be recovered based on oven-dried weight, respectively. Extractive-free and acid-pretreated coconut fibre sample produced the highest amount of lignin as expected, whereas lower amounts of lignin were isolated from the raw or untreated samples. Acid pretreated sample yielded comparatively higher amount of alkali-lignin than raw and extractive-free coconut fibre, as acid hydrolyzed the hemicelluloses by breaking the bonds in lignin-carbohydrate complexes as discussed earlier.

Physicochemical properties of alkali-lignin

Elemental analysis of alkali-lignin and empirical formula determination

Quantitative determination of the elements in lignin samples is the most important task to characterize lignin, e.g., determination of empirical formula, etc. Elemental compositions and empirical formula of four alkali-lignin samples have been given in Table 3.6. Elemental analyzer measured the carbon, hydrogen, nitrogen and sulfur contents, but no sulfur was detected as the samples were isolated by sulfur-free alkali-anthraquinone pulping method. Nitrogen (0.49-1.06%), generated from the degradation of protein, was present in all samples. The calculated average C_9-formula of the samples showed similarity as found in the literature [91-92]. Contribution of nitrogen in the empirical formula was not considered, as the element present at trace amount in the samples.

Table 3.6: Elemental compositions and empirical formulas of alkali-lignin samples

Sample	%C	%H	%N	%S	%O	%OCH_3	Empirical formula
CF_AL	54.55	4.87	0.56	-	40.02	15.05	$C_9H_{7.45}O_{5.88}(OCH_3)_{1.06}$
BG_AL	59.73	5.62	-	-	34.16	16.07	$C_9H_{8.09}O_{3.23}(OCH_3)_{1.03}$
TO_AL	57.66	5.47	1.06	-	35.81	17.03	$C_9H_{7.88}O_{3.50}(OCH_3)_{1.13}$
GW_AL	58.01	5.31	0.60	-	36.07	15.49	$C_9H_{7.80}O_{3.60}(OCH_3)_{1.02}$

Particle size analysis in DMSO-Water system by dynamic light scattering technique

The dynamic light scattering (DLS) technique is typically used to analyze particle size in the submicrometer size range and assess the hydrodynamic mobility of the particles. The cumulants approach can produce a dispersed light intensity-weighted harmonic mean diameter, or "Z-average diameter" of particles in the submicron ranges. Particle sizes of ball milled alkali-lignin samples in DMSO-water system at 0.1 mg/mL concentrations were in submicron ranges and showed multimodal distributions as depicted in Figure 3.8. Other particle size distribution curves have been given in Appendix A 5.

It was observed that the antisolvent precipitation/solvent shifting method successfully generated submicron lignin particles with the addition of deionized water to alkali-lignin solutions in DMSO by decreasing their solubility [117-120]. All of the samples showed particle size ranging from 102 to 660 nm with medium dispersity (D) ranging from 0.299 to 0.594 (Table 3.7). Only GW_AL at 200 ppm dispersion showed D value of 0.899, as indicative of very broad distribution. D values typically ranging from 0.01 for monodispersed particles to 0.5–0.7 for medium polydispersed samples. Generally, dispersity of greater than 0.7 indicates a broad particle size distribution in the samples [121].

Table 3.7: Particle sizes and dispersity (D) of alkali-lignin particles prepared by vibratory ball milling technique

Sample	Concentration (mg/mL)	Particle size (Z-average, nm)	Dispersity
CF_AL	0.10	240.3	0.452
	0.15	453.0	0.543
	0.20	354.5	0.521
BG_AL	0.10	281.0	0.375
	0.15	175.0	0.299
	0.20	224.9	0.594
TO_AL	0.10	541.7	0.545
	0.15	141.5	0.355
	0.20	659.8	0.536
GW_AL	0.10	188.5	0.439
	0.15	202.3	0.333
	0.20	102.2	0.899

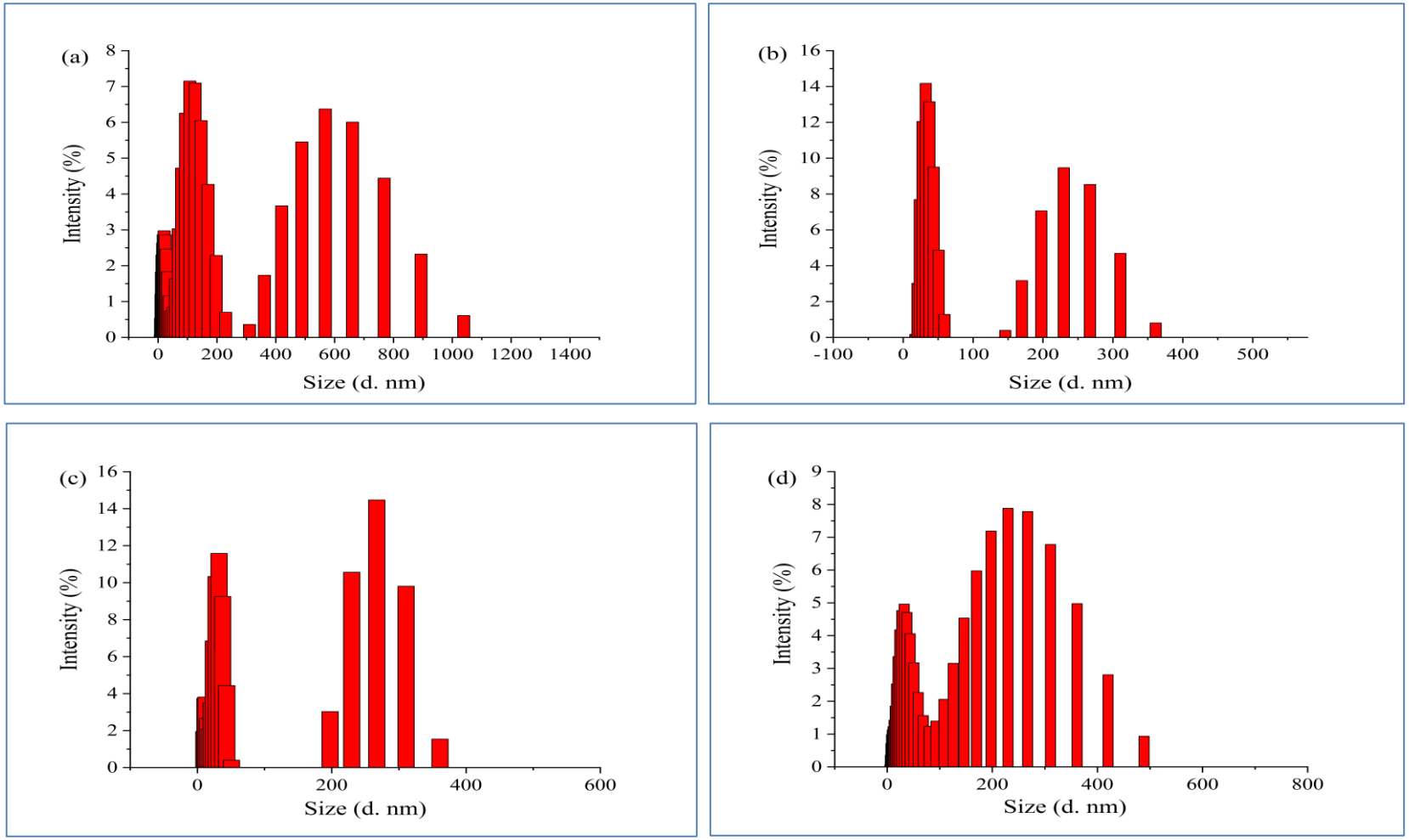

Figure 3.7: Particle sizes and distributions of alkali-lignin samples in DMSO-Water system at 0.10 mg/mL concentration, (a) CF_AL, (b) BG_AL, (c) TO_AL and (d) GW_AL.

According to several reports, mechanical processes, such as dry and wet milling procedures, can reduce particle size to the nanoscale range and are frequently employed to prepare lignin nanoparticles [119, 122]. Although the dry milling technique has the drawback of having non-uniform particle size and wide particle size dispersion, it is nonetheless regarded as a straightforward procedure for the manufacture of nanoparticles [118]. However, the mechanical treatments and antisolvent precipitation/solvent shifting methods were reported for the production of hollow-shaped to spherical-like solid lignin particles in the nanometer to micrometer ranges. There are also several techniques and settings that can produce solid lignin particles that resemble spheres, including those that employed water as an antisolvent and tetrahydrofuran (THF), acetone/water, dimethyl sulfoxide (DMSO), etc. as solvents [123].

Unmodified softwood Kraft lignin was dissolved in THF (lignin concentrations ranged from 1 to 20 mg/mL), and then water was added through dialysis. This straightforward and scalable procedure produced spherical lignin nanoparticles with an average diameter between 200 and 500 nm and dispersity (D) ranging from 0.15 to 0.56 on a scale of 0 to 1. The 20 mg/mL lignin concentration yielded the highest dispersity value, and there were no noticeable changes in dispersity between lignin concentrations of 0.1 and 10 mg/mL [117, 123]. No definite trends were observed in the particle sizes, distribution patterns and also dispersity values in alkali-lignin/DMSO/water system at 0.1 to 0.2 mg/mL concentrations, in this work. The various forms of diffusion, particle-particle interaction, multiple scattering, as well as sample fluorescence, etc., could have an impact on the apparent particle diameter derived from the dynamic light scattering experiment. The pre-dialysis lignin concentration, however, was shown to have a substantial impact on the lignin particle sizes, and the smallest particle sizes were recorded with a lignin concentration of 1 mg/mL [117]. Similar results were also reported in which lignin hollow nanocapsules had been produced by the precipitation of enzymatic hydrolysis lignin in THF solutions with the addition of water [124]. The measured particle sizes ranged from 419 to 566 nm, whereas the initial enzymatic hydrolysis lignin content increased from 0.5 to 2.0 mg/mL.

X-Ray photoelectron spectroscopic analysis and chemical states of the elements

X-ray photoelectron spectroscopic (XPS) analysis was performed on the four alkali-lignin samples. Results from the wide scan have been presented in Figure 3.8 and Table 3.8 and narrow scan high resolution deconvoluted spectra in Figure 3.9, Figure 10 and Table 3.9 to 3.16, respectively.

Table 3.8: Surface elemental compositions of alkali-lignin samples by X-ray photoelectron spectroscopy

Elemental compositions of alkali-lignin samples by XPS wide scan (%atom)								
Sample	C	O	N	P	S	K	Si	O/C
CF_AL	84.96	15.04	-		-	-	-	0.177
BG_AL	83.64	14.94	0.85	0.19	-	-	0.38	0.178
TO_AL	79.80	18.84	0.76		-	-	0.59	0.236
GW-AL	76.81	22.39	-		-	-	0.81	0.291

Results from the C1s and O1s wide scan spectra revealed that the two main elements found on the surfaces of the alkali-lignin sample were carbon and oxygen. Trace amounts of nitrogen in BG_AL and TO_AL, phosphorus in BG_AL and silicon in BG_AL, TO_AL and GW_AL were present as impurities and considered as negligible to simplify the investigations. Sulfur was not detected, as the lignin samples were prepared through alkali pulping process.

Table 3.8 provides the results of quantitative analyses of the O/C ratio in the alkali-lignin samples. In lignocellulosic materials, such as wood surfaces, the O/C ratios were previously reported to be 0.83 for cellulose, 0.80 for hemicelluloses, and 0.33 for lignin. A high O/C value therefore suggests a high relative content of carbohydrates, and a low value indicates a high relative quantity of lignin [125-128]. O/C ratio of prepared alkali-lignin samples were 0.177 for CF_AL, 0.178 for BG_AL, 0.236 for TO_AL and 0.291 for GW_AL, which were significantly lower than 0.33. Thus, the O/C ratios indicated no cellulose and hemicelluloses residues in the alkali-lignin preparations and could be considered as pure alkali-lignin.

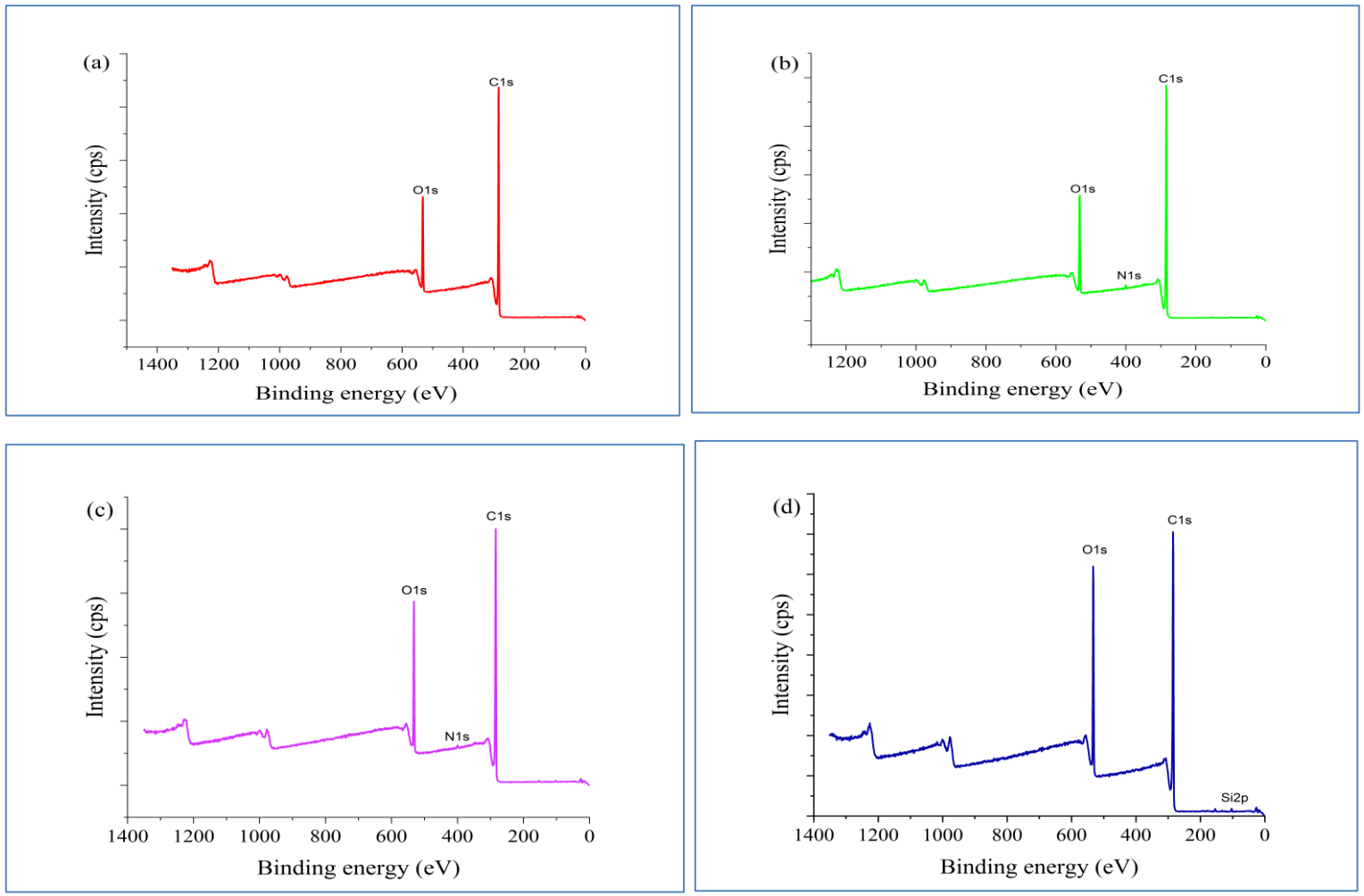

Figure 3.8: XPS wide scan spectra of alkali-lignin samples isolated from the developed biorefinery proccess, (a) CF_AL (b) BG_AL (c) TO_AL and (d) GW_AL

Narrow or high resolution scans were carried out to examine the specific bonding nature and chemical states of the surface elements, such as carbon and oxygen in the alkali-lignin samples. The binding energy scale was calibrated using the C1s peak at 284.82 eV, and the C1s and O1s spectra were deconvolved using Gaussian peak profiles as shown in Figure 3.9 and Figure 3.10, corresponding spectral data and assignment in Table 3.9 to Table 3.16. Based on how many oxygen atoms are bound to carbon, the C1s signal may typically be deconvoluted into four classes [127, 128]:

The C_1 class corresponds to carbon atoms bonded only with carbon as C-C/C=C or hydrogen atoms as -C-H/=C-H, and it is usually pointed out at a binding energy, BE of 284.6 eV.
The C_2 class reveals the carbon atoms bonded with one oxygen atom as -C-O-C/-C-O-H, and it appears at a higher BE compared to C_1 (Δ_{BE} = +1.5 ± 0.2 eV).
The C_3 class corresponds to carbon atoms bonded to a carbonyl, C=O or two non-carbonyl oxygen atoms as O-C-O (Δ_{BE} = +2.8 ± 0.2 eV).
Finally, the C_4 class is associated with carbon atoms bonded to a carbonyl and a non-carbonyl oxygen atom as -O-C=O (Δ_{BE} = +3.75 ± 0.2 eV).

Similar to this, the samples' O1s signals have been divided into three classes based on whether oxygen is bonded to carbon or hydrogen. Organic compound O1s binding energy measurements are inconsistent, and there is still disagreement about how to assign the various functional groups [129,130-132]. The binding energy of O1s could be represented as follows-

The O_1 class correspond to oxygen atoms double bonded with carbon as carbonyl, C=O or carboxyl, O-C=O would located at about 531.60 eV
The O_2 class correspond to oxygen atom single bonded with carbon as hydroxyl C-O-H or ether, C-O-C or carboxyl, O-C=O would appear at about 533.20 eV.
The O_3 class correspond to phenolic oxygen atom bonded to carbon in phenol, C=O would appear at about 534.30 eV (or chemisorbed water).

High resolution deconvoluted spectra of CF_AL, BG_AL, TO_AL and GW_AL could be grouped into C_1 to C_4 for C(1s) and O_1 to O_3 for O(1s) classes. Based on the deconvoluted spectra obtained, percentage of C(1s) in C_1 to C_4 components and O(1s) in

O_1 to O_3 components could be estimated using corresponding photoelectron (PE) peak areas by applying equations 3.4 and results were stated in Table 3.17.

$$\%Xx = \frac{Ax}{\sum_{i=1}^{n} Ai} \text{ X } 100 \qquad (3.4)$$

here,

$\%\ Xx =$ Percentage of a component, x of an element, X in a compound

$Ax =$ Area of the Photoelectron (PE) peak of component, x

$Ai =$ The sum of areas of all PE peaks of the components associated with element, X

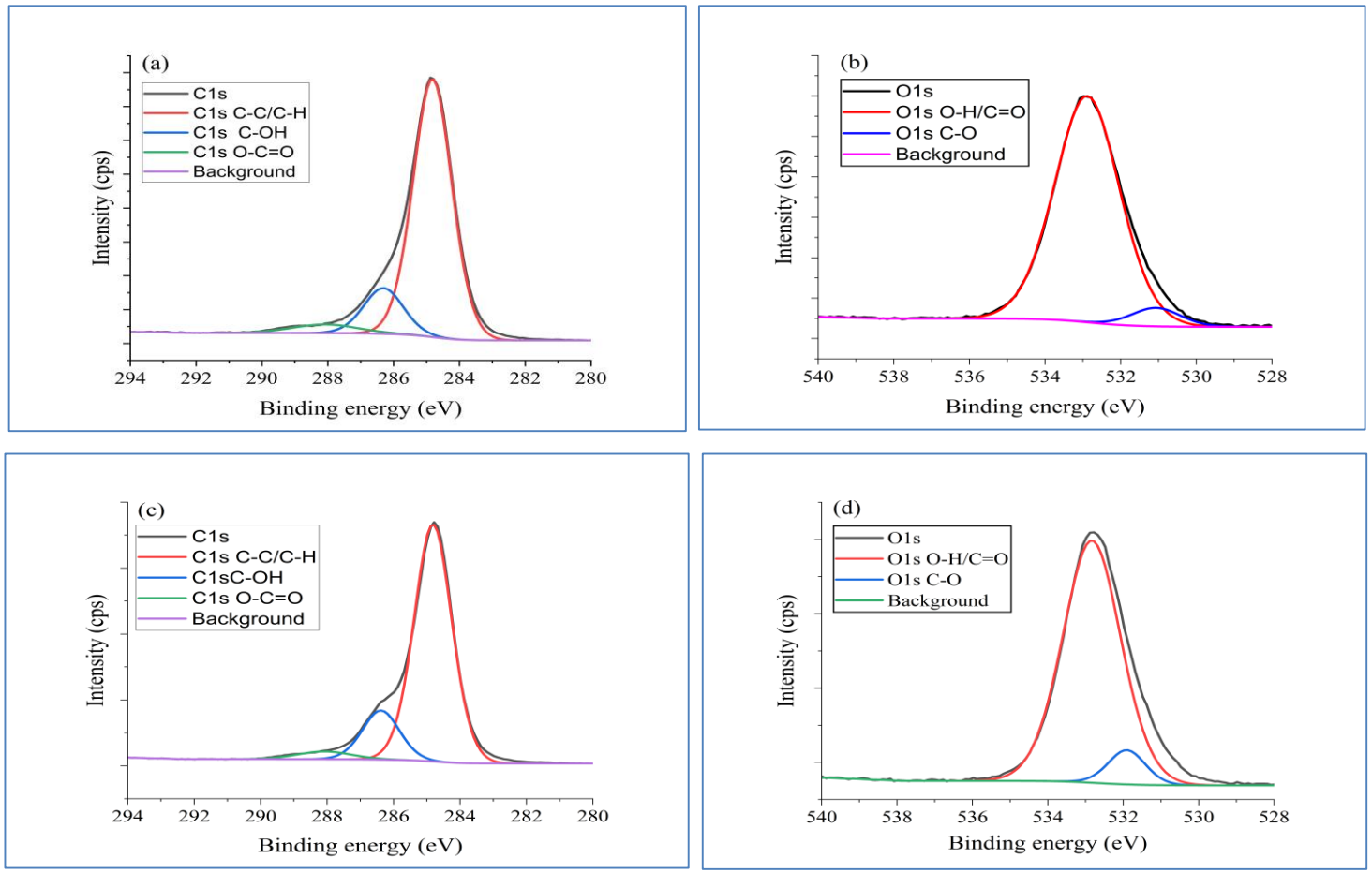

Figure 3.9: High resolution deconvoluted XPS spectra of alkali-lignin samples. Chemical states of the elements, i.e., carbon and oxygen were assigned and indicated by colored lines. XPS photoelectron peaks of (a) C1s of CF_AL (b) O1s of CF_AL (c) C1s of BG_AL and (d) O1s of BG_AL. C1s in (C-C, C-H) and (C=C, =C-H) has been mentioned as C1sC-C/C-H in spectral curves.

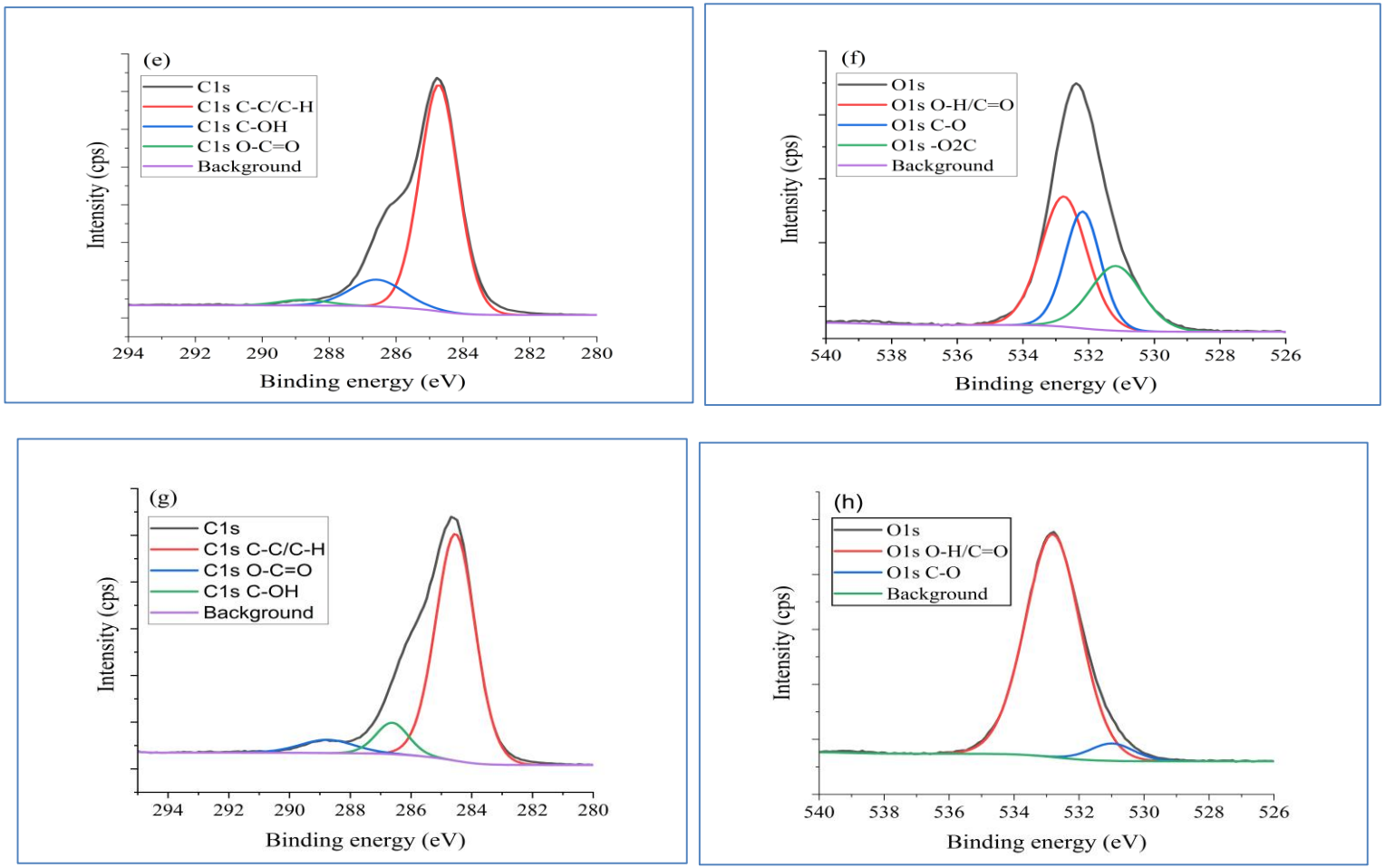

Figure 3.10: High resolution deconvoluted XPS spectra of alkali-lignin samples. Chemical states of the elements, i.e., carbon and oxygen were assigned and indicated by colored lines. XPS photoelectron peaks of (e) C1s of TO_AL (f) O1s of TO_ AL (g) C1s of GW_AL and (h) O1s of GW_AL. C1s in (C-C, C-H) and (C=C, =C-H) has been mentioned as C1sC-C/C-H in spectral curves.

Table 3.9: High resolution C1s and O1s XPS data of Coconut fibre alkali-lignin

Scan	Peak BE (eV)	Height (CPS)	Height ratio	Peak area (CPS.eV)	Area ratio	Chemical state
C_1	284.82	152560.85	1	228972.02	1	C1s , C-C/C-H
C_2	286.31	27030.99	0.18	41399.49	0.18	C1s, C-OH
C_3	288.08	5094.79	0.03	12823.13	0.06	C1s, O-C-O/C=O
C_4	288.35	-	-	-	-	C1s, O-C=O/O=COR
O_1	531.07	4564.28	0.08	7486.17	0.06	O1s, C-O
O_2	532.89	55970.53	1	122401.16	1	O1s, -OH/C=O

Table 3.10: Tentative assignment of high resolution XPS C1s components of Coconut fibre alkali-lignin

Scan	Assignment of chemical states of carbon in CF_AL	% Carbon
C_1	Binding energy of C1s electron in hydrocarbon skeleton of alkali-lignin (C=C/=C-H bond in aromatic ring and C-C/C-H in aliphatic portion)	76.32
C_2	Binding energy of C1s electron in alcoholic/phenolic/ether bonds (C-OH/C-O-C)	18.08
C_3	Binding energy of C1s electron in carbonyl/carboxylic acid/ester bonds (C=O/O-C-O)	5.60

Table 3.11: High resolution C1s and O1s XPS data of Bagasse alkali-lignin

Scan	Peak BE (eV)	Height (CPS)	Height ratio	Peak area (CPS.eV)	Area ratio	Chemical state
C_1	284.81	179975.04	1	259254.95	1	C1s , C-C/C-H
C_2	286.38	37293.91	0.21	52849.27	0.2	C1s, C-OH
C_3	288.08	5850.98	0.03	12071.35	0.05	C1s, O-C-O/C=O
C_4	288.35	-	-	-	-	C1s, O-C=O/O=COR
O_1	531.91	9220.59	0.14	11564.86	0.09	O1s, C-O
O_2	532.83	65199.74	1	127906.57	1	O1s, -OH/C=O

Table 3.12: Tentative assignment of high resolution XPS C1s components of Bagasse alkali-lignin

Scan	Assignment of chemical states of carbon in BG_AL	% Carbon
C_1	Binding energy of C1s electron in hydrocarbon skeleton of alkali-lignin (C=C/ =C-H) bond in aromatic ring and C-C/C-H in aliphatic portion)	74.97
C_2	Binding energy of C1s electron in alcoholic/ phenolic/ether bonds(C-OH/C-O-C)	20.38
C_3	Binding energy of C1s electron in carbonyl/ carboxylic acid/ester bonds (C=O/O-C-O)	4.65

Table 3.13: High resolution C1s and O1s XPS data of *Trema orientalis* alkali-lignin

Scan	Peak BE (eV)	Height (CPS)	Height ratio	Peak area (CPS.eV)	Area ratio	Chemical state
C_1	284.72	120168.76	1	176227.48	1	C1s , C-C/C-H
C_2	286.57	14197.95	0.12	29063.05	0.16	C1s, C-OH
C_3	288.08	-	-	-	-	C1s, O-C-O/C=O
C_4	288.77	3078.09	0.03	5736.57	0.03	C1s, O-C=O/O=COR
O_1	532.18	36625.46	0.9	51002.94	0.7	O1s, C-O/-O_2C
O_2	532.76	40778.81	1	72634.15	1	O1s, -OH/C=O
O_3	531.17	20259.65	0.5	40678.72	0.56	O1s, O_2C-/Ph-O

Table 3.14: Tentative assignment of high resolution XPS C1s components of *Trema orientalis* alkali-lignin

Scan	Assignment of chemical states of carbon in TO_AL	% Carbon
C_1	Binding energy of C1s electron in hydrocarbon skeleton of alkali-lignin (C=C/=C-H bond in aromatic ring and C-C/C-H in aliphatic portion)	80.26
C_2	Binding energy of C1s electron in alcoholic/ phenolic/ether bonds (C-OH/ C-O-C)	16.49
C_3	Binding energy of C1s electron in carbonyl/ carboxylic acid/ester bonds (C=O/ O-C-O)	3.25

Table 3.15: High resolution C1s and O1s XPS data of *Dipterocarpus turbinatus* alkali-lignin

Scan	Peak BE (eV)	Height (CPS)	Height ratio	Peak area (CPS.eV)	Area ratio	Chemical state
C_1	284.84	97129.06	1	161365.31	1	C1s , C-C/C-H
C_2	286.62	13458.73	0.14	18511.44	0.11	C1s, C-OH
C_3	288.08	-	-	-	-	C1s, O-C-O/C=O
C_4	288.76	5673.22	0.06	12916.01	0.08	C1s, O-C=O/O=COR
O_1	530.99	6328.09	0.08	10813.81	0.06	O1s, C-O
O_2	532.81	81094.46	1	174736.31	1	O1s, -OH/C=O

Table 3.16: Tentative assignment of high resolution XPS C1s components of *Dipterocarpus turbinatus* alkali-lignin

Scan	Assignment of chemical states of carbon in GW_AL	% Carbon
C_1	Binding energy of C1s electron in hydrocarbon skeleton of alkali-lignin (C=C/=C-H bond in aromatic ring and C-C/C-H in aliphatic portion)	80.53
C_2	Binding energy of C1s electron in alcoholic/ phenolic/ether bonds (C-OH/C-O-C)	11.47
C_3	Binding energy of C1s electron in carbonyl/carboxylic acid/ester bonds (C=O/O-C-O)	8.00

Table 3.17: Percentages of C1s and O1s components of carbon and oxygen and their chemical states in alkali-lignin samples

C1s and O1s components	Chemical states of the elements	Binding energy, eV [124-126]	Percentages of C1s and O1s components in alkali-lignin			
			CF_AL	BG_AL	TO_AL	GW_AL
C_1	C-C,C=C/ C-H, =C-H	284.72-284.84 (285.00)	80.85	79.97	83.50	83.70
C_2	C-O-C, C-O-H	286.31-286.62 (286.50)	14.61	16.30	13.77	9.60
C_3	C=O/ O-C-O	288.08-288.35 (288.00)	4.53	3.72	-	-
C_4	O-C=O/O=COR	- (289.35)	-	-	2.71	6.70
O_1	C=O/ O-C=O	530.78-531.91 (531.60)	5.76	6.89	*24.75	5.83
O_2	C-O-H, C-O-C, $-O_2C$	532.18-532.89 (533.20)	94.24	93.11	75.24	94.17
O_3	C=O or chemisorbed water	- (534.30)	-	-	-	-

*O_3 component of TO_AL (Table 3.13) has been included in the O_1 component.

Fourier transform mid and near infrared spectroscopic analysis: Evaluation of fundamental, overtone and combination bands

Fourier transform mid infrared (FT-MIR) and Fourier transform near infrared (FT-NIR) spectroscopic investigations provide useful information on how the functional groups, overtone, and combination bands, and other structural constituents of biomass [83] change during various processing steps. FT-MIR spectra of four moisture-free alkali-lignin samples, i.e., CF_AL, BG_AL, TO_AL and GW_AL have been given in Figure 3.11 and absorption data in Table 3.18 and Table 3.19, respectively. Reference FT-NIR spectral data have been given in table 3.20.

The major FT-MIR absorption bands assigned to the corresponding functional groups showed almost similar absorption patterns due to their similar structural features with minor peak shifting. All samples showed a broad absorption band centered at about 3421 cm^{-1} in their spectra and could be assigned as hydrogen-bonded hydroxyl stretching vibrations of alcoholic and phenolic hydroxyl group. Peaks of aliphatic C-H stretching were seen at 2943 and 2840 cm^{-1}, with the latter perhaps produced by methoxyl groups [134]. Unconjugated ketones, carbonyls, and ester groups in lignin typically have the ability to absorb infrared radiation between 1738 and 1709 cm^{-1}. Additionally, conjugated aldehydes and carboxylic acids absorb between 1700 and 1700 cm^{-1} [133]. The stretching vibration of the carbonyl group from unconjugated ketones, carbonyls, and in ester groups can therefore be attributed to the absorption peaks at 1694 cm^{-1}. In case of CF_AL and BG_AL, the peaks were shifted to 1703 cm^{-1}. Peaks at 1601 and 1520 cm^{-1} were caused by aromatic C-H skeletal vibrations; nonetheless, the latter peak might be regarded as pure bands. Aliphatic C-H asymmetric deformation exhibited an absorption peak at 1450 cm^{-1} [133-135]. It is more challenging to interpret the bands below 1430 cm^{-1}, and nearly all of the absorption bands are complicated with contributions from multiple vibration modes in the lignin structures [133]. In guaiacyl-syringyl (G-S) type lignin, an absorption band caused by syringyl ring breathing with C-O stretching could be seen at 1235 to 1230 cm^{-1}. All samples showed the band at about 1222 cm^{-1} and could be originated from C-C, C-O, and C=O stretches [136]. A few IR-absorption bands that could be generated from guaiacyl (G) or guaiacyl-syringyl (G-S) type lignin structures have been documented by several publications. For example, the guaiacyl ring breathing with C-O stretching band at 1270 cm^{-1} by G-type and at 1275 cm^{-1} by G-S type lignin, respectively [133].

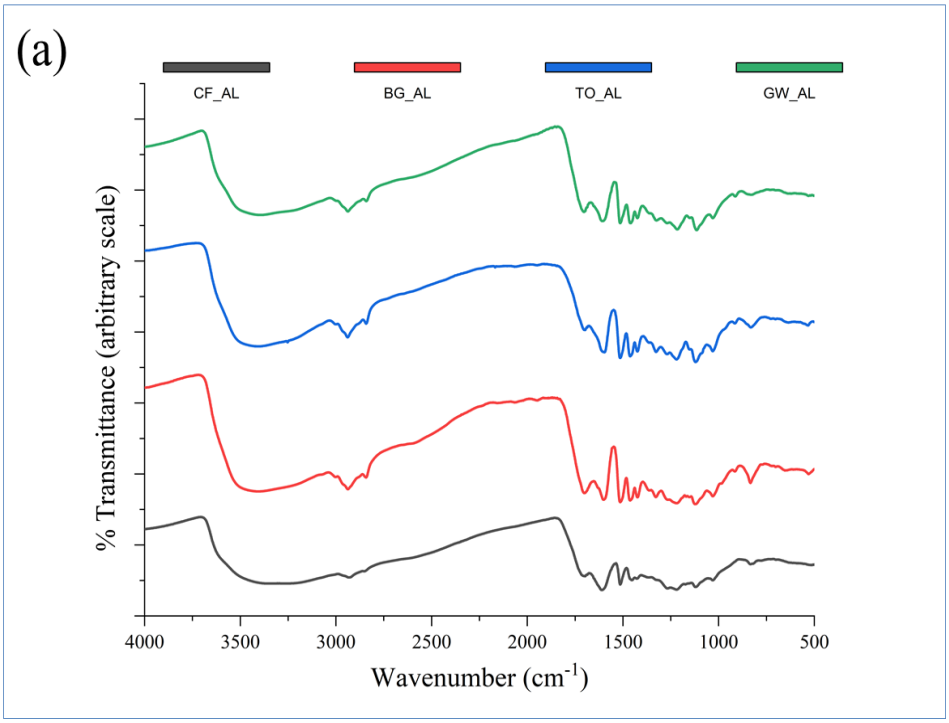

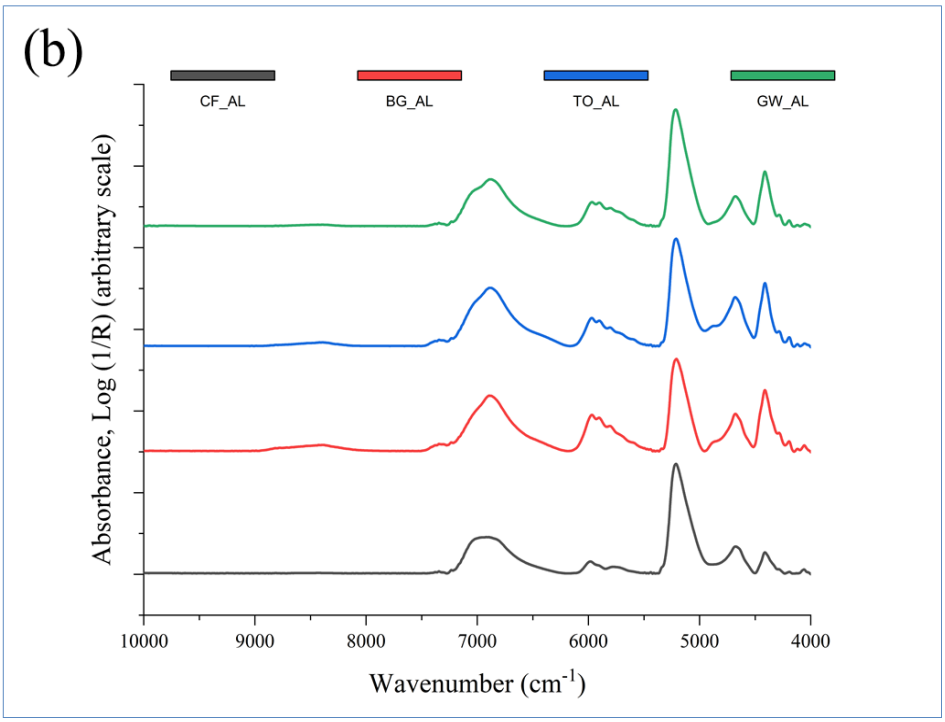

Figure 3.11: FT-MIR-NIR spectroscopic analysis of four alkali-lignin samples, i.e., CF_AL, BG_AL, TO_AL and GW_AL (a) FT-MIR spectra and (b) FT-NIR spectra

Table 3.18: FT-MIR absorption bands of alkali-lignin samples and tentative assignment of the bands

Wavenumber range (cm^{-1})	Obtained band (cm^{-1})	Band assignment
4000-3000	3421	O-H stretching, H-bonded
3000-2000	2943	$-CH_3$/ $-CH_2-$ (asymmetric stretch + deformation overtone)/ Out of plane stretching
	2840	$-CH_2-$ in plane stretching; twisting
2000-1000	1694	C=O stretching (aliphatic)
	1601	Aromatic skeletal vibrations plus C=O stretching
	1520	Aromatic skeletal vibrations (pure band)
	1450	C-H deformation combined with aromatic ring vibration/ C-C stretch in a ring
	1270-1275	C-O stretching in guaiacyl type (guaiacyl ring breathing with C-O stretching band at 1270 cm^{-1} by G-type and at 1275 cm^{-1} by G-S type lignin)
	1222	C-C, C-O, and C=O stretches
	1140-1145	G-type rings often displayed a C-H deformation band
	1122	Aromatic C-H in-plane deformation in an S-type ring
	1030	Aromatic C-H in-plane deformation plus C-O deformation in primary alcohols
1000-500	826	C-H bending/out of plane in position 2 and 6 of S and all positions of H units/Di or tetra-substituted aromatic ring (Aromatic C-H out of plane deformation).

The samples showed very weak absorptions in these regions. The weak absorption bands at 1122 cm^{-1}, however, were present in all samples and were thought to be the result of aromatic C-H in-plane deformation in an S-type ring. G-type rings often displayed a C-H deformation band at 1140–1145 cm^{-1}. The aromatic C-H in-plane deformation and C-O deformation in primary alcohol could be attributed to the absorption band at 1030 cm^{-1}. All samples demonstrated the presence of absorption bands at 825 cm^{-1} caused by aromatic C-H out of plane deformation.

The FT-NIR spectrum, which has numerous bands because of various overtones and combination modes, typically exhibits highly overlapping, broad, and frequently very low absorption. In order to acquire usable information from NIR spectroscopy,

multivariate mathematical approaches are typically used because direct spectrum interpretation is constrained. Although absorption bands in the high wave number range, such as those between 12500 and 7000 cm^{-1}, have rarely been employed for qualitative evaluation of overtones and combination bands, absorption bands between 7000 and 4000 cm^{-1} could be used [136, 137]. Overtones and combination bands of C-H and O-H made up all of the absorption bands in alkali-lignin samples. NIR band assignments for biomasses and their components, i.e., cellulose, hemicelluloses, lignin, and extractives, were explored in several literatures [136-140]. FT-NIR spectra of isolated components, i.e., cellulosic pulp, holocellulose, α-cellulose and alkali-lignin samples have been given in Appendix A 4.

It was observed that (Figure 3.11b) a strong and broad absorption band exhibited by all samples with the absorption peak maxima at about 6872 cm^{-1} and could be assigned as the first overtone of phenolic hydroxyl group of lignin with intermolecular H-bonding [136, 141]. While aliphatic C-H first overtone band could be seen at 5896 cm^{-1} in the shoulder, medium-strong and broad absorption bands were identified at 5982 cm^{-1} and could be created from aromatic C-H first overtone. The samples absorbed NIR radiation at 5204 to 5208 cm^{-1} and showed a strong and sharp band which could be assigned as the combination band of hydroxyl stretching and hydroxyl deformation of strongly absorbed moisture in the samples [136].

Aromatic C-H plus C=C combination bands (medium to weak and broad) were observed at 4676 cm^{-1}. All lignin samples showed another medium strong and sharp band at 4418 cm^{-1} and could be assigned as C=O plus O-H combination band. Milled wood lignin from spruce and aspen also showed similar absorption bands [138]. Interestingly, alkali-lignin samples showed almost identical absorption bands with very minor peak-shifting in the NIR region and the information could be used primarily in the identification and quality analysis of alkali-lignin. Structural change due to chemical modifications of alkali-lignin, e.g., changes in intensity of C-H or O-H overtone bands or C-H plus C=C or C=O plus O-H combination bands will be reflected in the NIR spectrum and thus could be used as a reaction monitoring tool during lignin modifications.

Table 3.19: FT-NIR spectral bands of alkali-lignin samples and tentative assignment

Wavenumber range (cm^{-1})	Sample	Obtained band (cm^{-1})	Functional group	Reference band (cm^{-1})
7000-6000	CF_AL BG_AL TO_AL GW_AL	6874 6872 6870 6876	First overtone of phenolic hydroxyl stretching in lignin with intermolecular H-bonding to an ether group in ortho-position confirmed by milled wood lignin spectra of beech and spruce woods.	6874
6000-5000	CF_AL BG_AL TO_AL GW_AL	5960 5966 5960 5962	First overtone of aromatic skeletal C-H stretching	5963-5980
	CF_AL BG_AL TO_AL GW_AL	5896 5897 5896 5897	First overtone of aliphatic C-H stretching	5890
	CF_AL BG_AL TO_AL GW_AL	5208 5204 5205 5208	Combination band due to O-H stretching and O-H deformation of absorbed water	5220-5150
5000-4000	CF_AL BG_AL TO_AL GW_AL	4655 4669 4642 4657	Combination band due to aromatic C-H and C=C stretching in Lignin/Extractives	4686
	CF_AL BG_AL TO_AL GW_AL	4410 4409 4409 4409	Combination band due to O-H and C=O stretching	4411
	CF_AL BG_AL TO_AL GW_AL	4279 4279 4277 4277	Combination band due to C-H stretching and CH_2 deformation	4280
	CF_AL BG_AL TO_AL GW_AL	4192 4192 4191 4189	Not assigned	4195

Table 3.20: Some FT-NIR spectral bands of lignin [136]

Spectral range (cm^{-1})	Reference band (cm^{-1})	Band assignment
7000-6000	6874	1st OT of O-H stretching, H-bonded
6000-5000	5963-5980	1st OT of C_{ar}-H stretching
	5890	1st OT of C_{al}-H stretching
	5220-5150	O-H stretching + O-H deformation of absorbed water
5000-4000	4686	C_{ar}-H stretching + C=C stretching
	4411	O-H stretching + C=O stretching
	4280	C-H stretching + CH_2 deformation
	4195	Not assigned

^{1}H-Nuclear magnetic resonance spectroscopic analysis of alkali-lignin samples in d_6-dimethylsulfoxide

^{1}H–NMR spectra of alkali-lignin samples, e.g. CF_AL, BG_AL, TO_AL and GW_AL have been given in Figure 3.12 to Figure 3.16 and spectral data in Table 3.21. ^{1}H-NMR spectrum of CF_AL_acetylated sample was incorporated for comparison.

Lignin may be structurally characterized and classified using ^{1}H-NMR spectroscopy. Acetylation of lignin can improve the spectral resolution of important lignin functionality in ^{1}H-NMR analysis [206]. Several reports have been published on ^{1}H-NMR spectroscopy of lignin, in which acetylated lignin derivatives were analyzed by employing *d*-chloroform as the solvent [76, 205-207]. The investigation of the erythreo and threo forms of lignin's β-O-4 structures was done employing acetylation method. However, derivatization of lignin may cause unwanted chemical modifications in the lignin structure. This complication can be avoided when underivatized lignin is examined. Beside this, there are other difficulties associated with the recording of hydroxyl group protons in underivatized lignin. The immediate area of the prominent methoxyl peak in the spectra of underivatized lignin contains almost all signals from side chain protons attached to carbon atoms. It creates problem to interpret the lignin ^{1}H-NMR spectra in structural terms [206]. It was also observed that lignin phenolic hydroxyl groups in d_6-DMSO solvent can be examined by ^{1}H-NMR spectroscopy, if the sample is "almost bone dry," free of all bases and acids other than minor amounts of lignin-carboxylic acid [76].

Table 3.21: ^{1}H-NMR spectral data and tentative assignment of different protons in underivatized alkali-lignin and acetylated CF_AL samples

Chemical shift/ppm	Observed ^{1}H-NMR peak/ppm					Tentative assignment
	CF_AL	CF_AL_acetylated	BG_AL	TO_AL	GW_AL	
8.0-10.0	-	8.278-8.550	-	-	-	H in phenolic hydroxyl group
7.2-7.9	-	7.069-7.347	7.478-7.518	-	7.234	Aromatic-H in guaiacyl units
6.8–7.2	6.687	6.691-6.858	6.693-6.795	6.698	6.762	Aromatic-H in syringyl units
6.2–6.7	-	-	6.272-6.298	-	-	Certain vinyl protons
4.0-5.5	-	4.442-4.753	4.866	4.872	4.618-4.762	H in aliphatic hydroxyl groups, i.e. α-OH and γ-OH/H_{β} and H_{γ} in several structures
3.3-4.0	3.464	3.375-3.953	3.408-3.719	3.414-3.750	3.456-3.754	H in methoxyl group
2.6-3.2	-	-	-	2.612	-	Benzylic proton in β-β structures/H_{β} in β-1 structure
2.50	2.500	2.507	2.500	2.500	2.500	*d_6*-DMSO
2.2–2.4	-	2.199-2.478	-	-	-	H in phenolic acetate
1.6–2.2	-	1.460-1.883	2.178	-	-	H in aliphatic acetate
<1.6	0.825-1.231	0.729-1.149	0.848-1.230	1.233	0.745-1.230	H in hydrocarbon contaminants

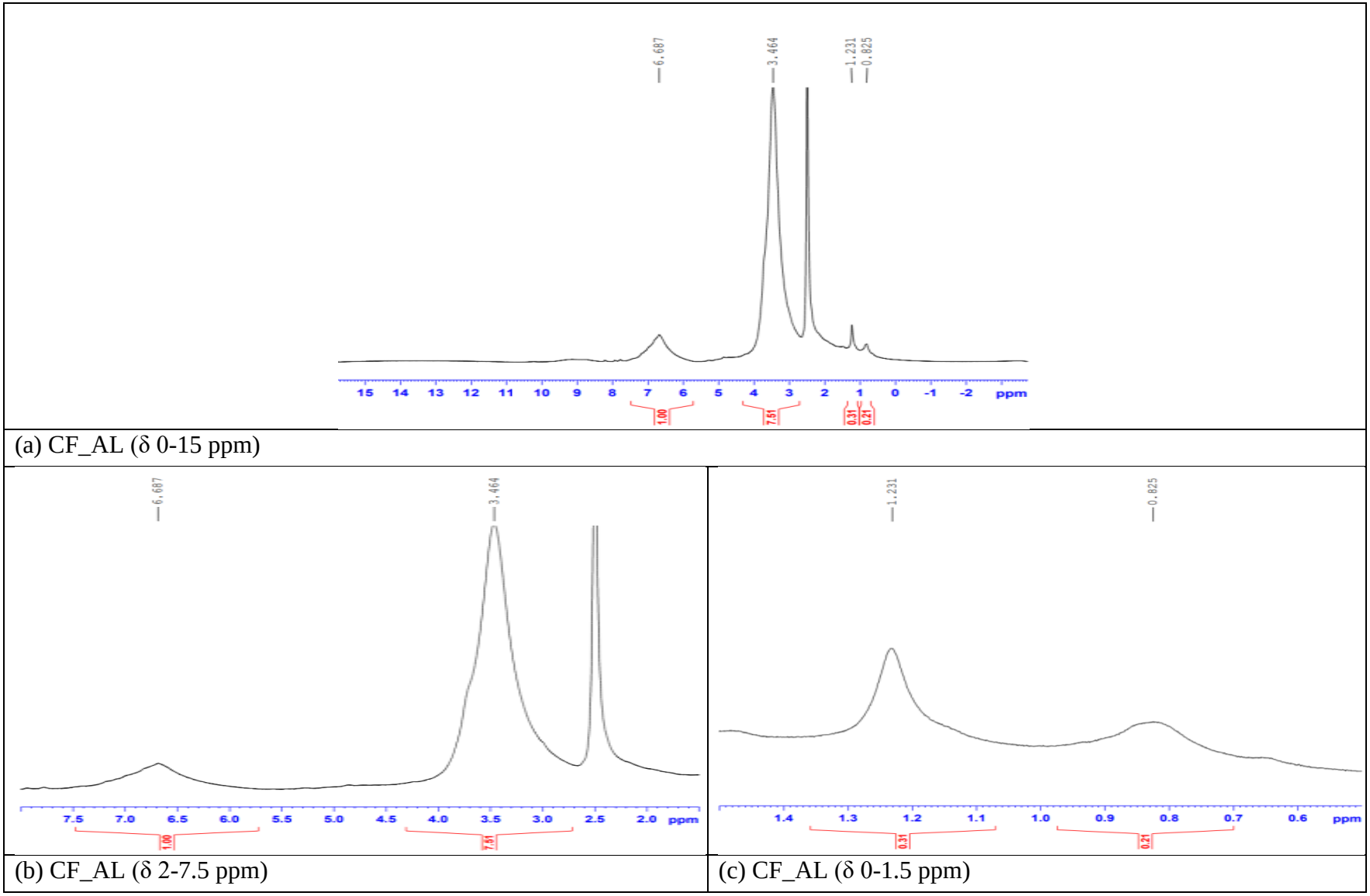

(a) CF_AL (δ 0-15 ppm)

(b) CF_AL (δ 2-7.5 ppm)

(c) CF_AL (δ 0-1.5 ppm)

Figure 3.12: ^{1}H-NMR spectra of CF_AL sample in *d*-DMSO solution at 25 ^{o}C (a) CF_AL (δ 0-15 ppm), (b) CF_AL (δ 2-7.5 ppm) and (c) CF_AL (δ 0-1.5 ppm)

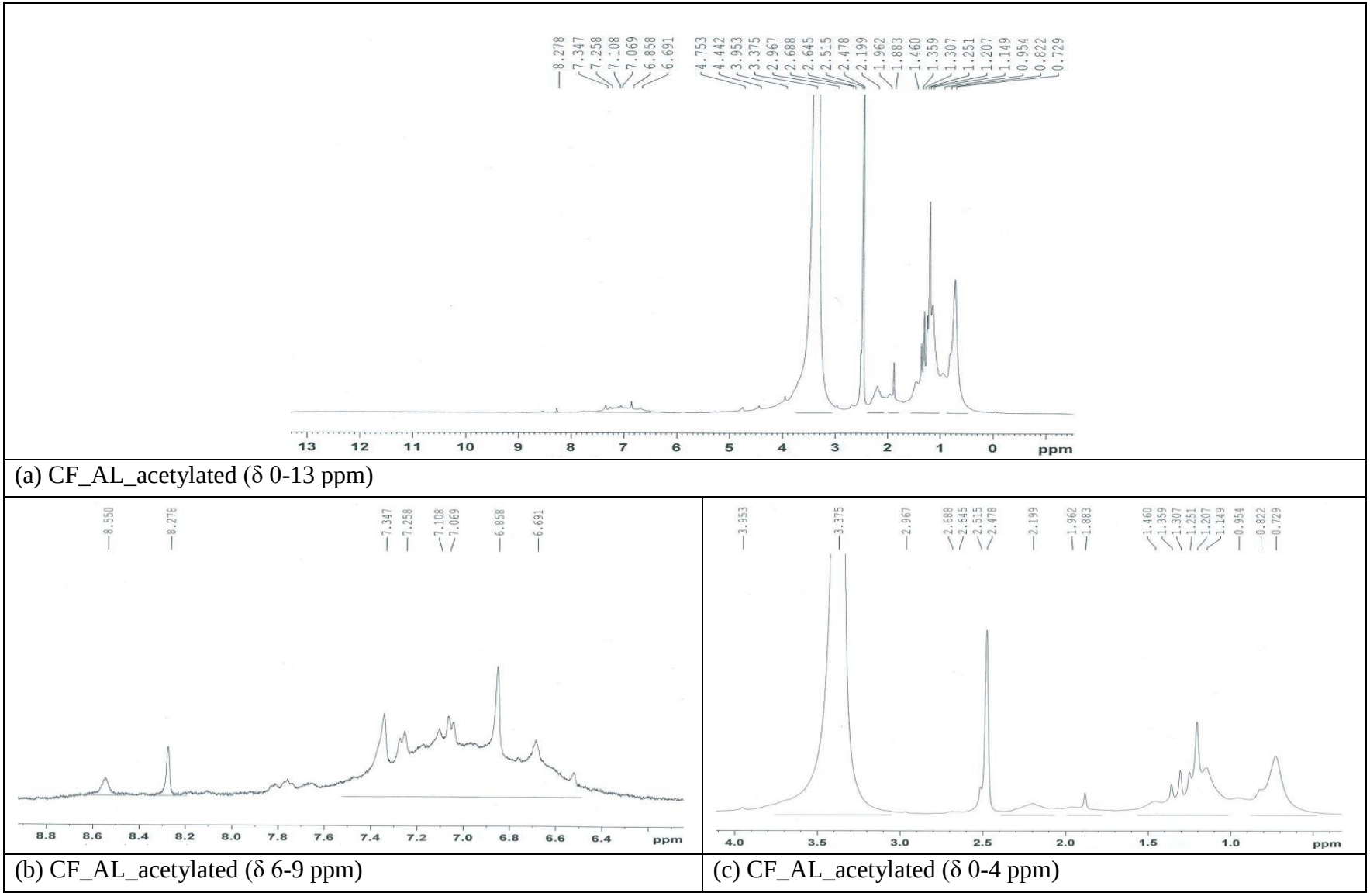

(a) CF_AL_acetylated (δ 0-13 ppm)

(b) CF_AL_acetylated (δ 6-9 ppm)

(c) CF_AL_acetylated (δ 0-4 ppm)

Figure 3.13: ^{1}H-NMR spectra* of CF_AL_acetylated sample in *d*-DMSO solution at 25 ^{o}C (a) CF_AL_acetylated (δ 0-13 ppm), (b) CF_AL_acetylated (δ 6-9 ppm) and (c) CF_AL_acetylated (δ 0-4 ppm)

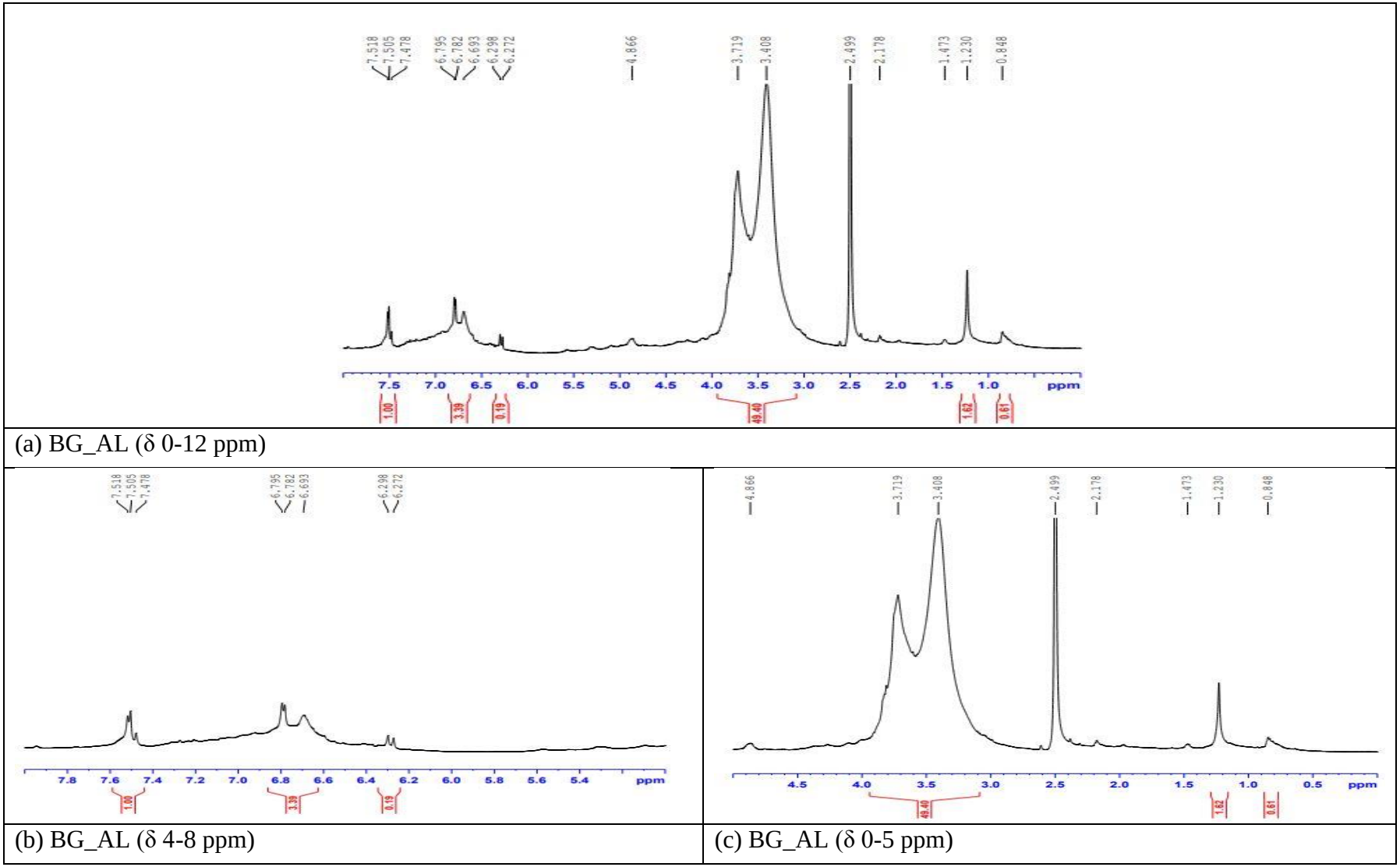

Figure 3.14: ^{1}H-NMR spectra of BG_AL sample in *d*-DMSO solution at 25 ^{o}C (a) BG_AL (δ 0-12 ppm), (b) BG_AL (δ 4-8 ppm) and (c) BG_AL (δ 0-5 ppm)

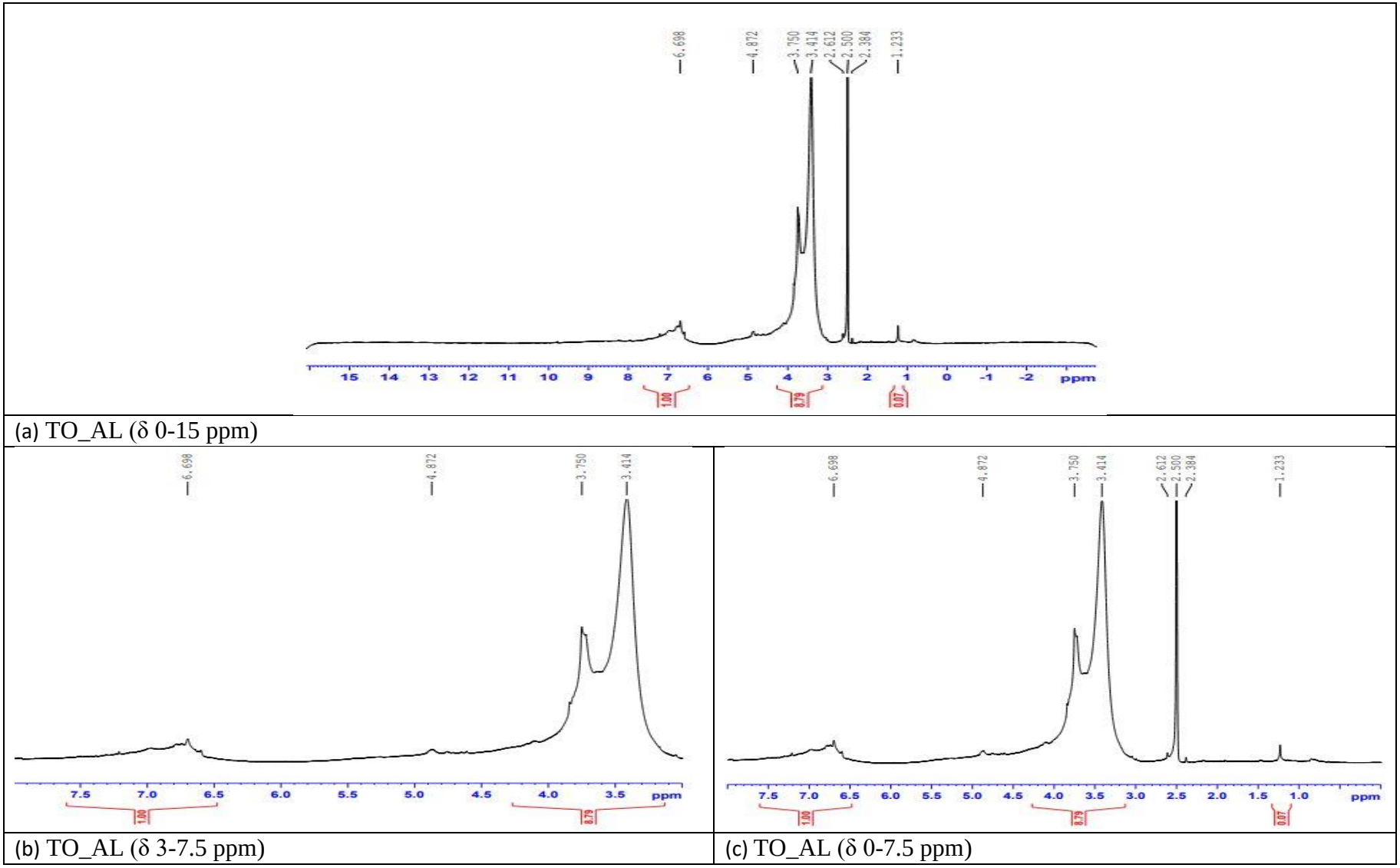

Figure 3.15: ^{1}H-NMR spectra of TO_AL sample in *d*-DMSO solution at 25 ^{o}C (a) TO_AL (δ 0-15 ppm), (b) TO_AL (δ 3-7.5 ppm) and (c) TO_AL (δ 0-7.5 ppm)

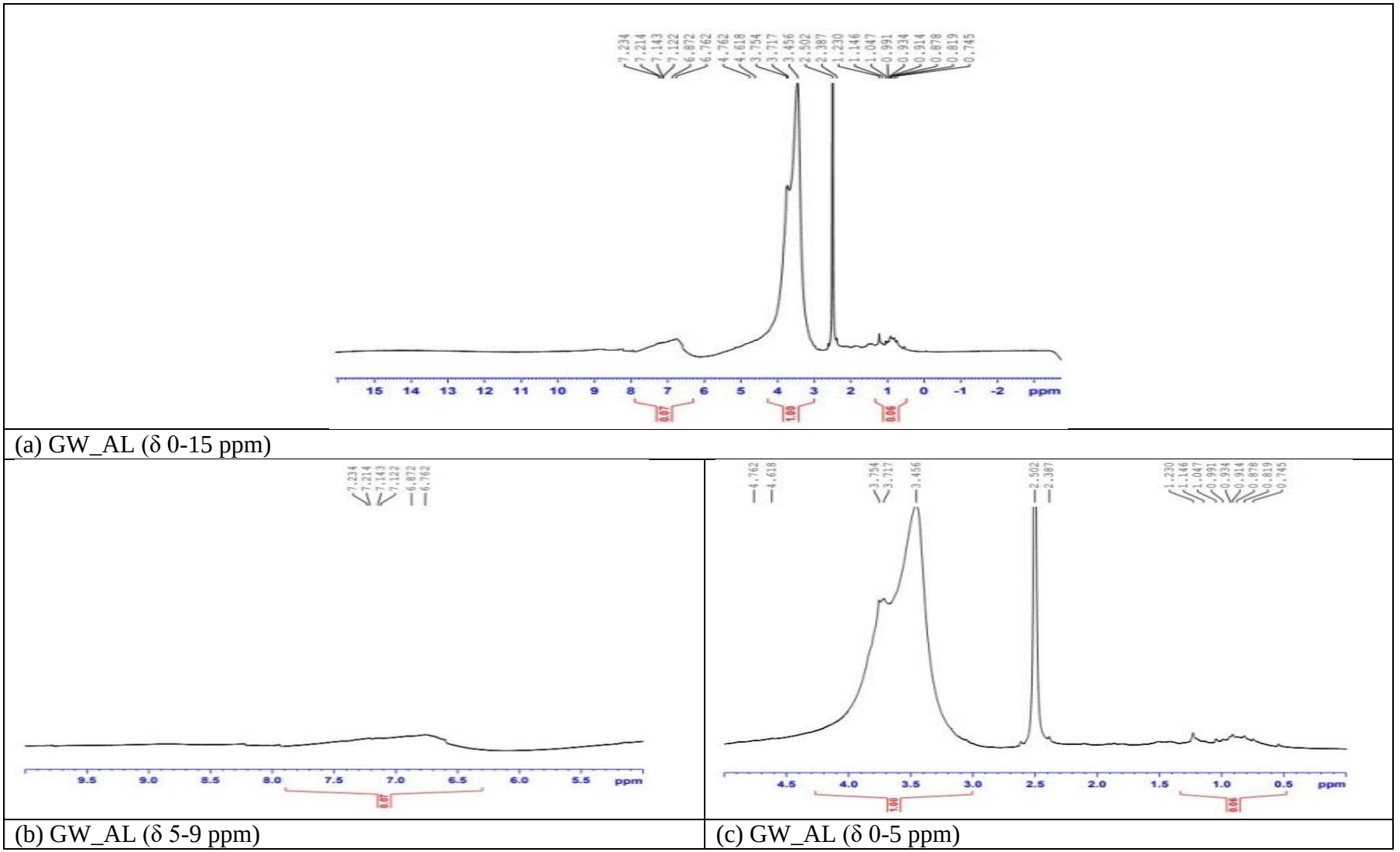

(a) GW_AL (δ 0-15 ppm)

(b) GW_AL (δ 5-9 ppm)

(c) GW_AL (δ 0-5 ppm)

Figure 3.16: ^{1}H NMR spectra of GW_AL in *d*-DMSO solution at 25 ^{o}C (a) GW_AL (δ 0-15 ppm), (b) GW_AL (δ 5-9 ppm) and (c) GW_AL (δ 0-5 ppm)

d$_6$-DMSO could be considered as an excellent solvent for lignin analysis. The chemical shift of hydroxyl protons in this solvent is characteristic and proton exchange is slow.

A few model compounds were also examined in *d*$_6$-DMSO and demonstrated that the signals from alcoholic hydroxyl groups match with other signals in the lignin spectra [76]. This difficulty could be minimized by examining the spectra before and after addition of *d*-TFA (*d*-trifluroacetic acid). The difference spectrum obtained on subtraction of the spectrum recorded after addition of *d*-TFA from the spectrum recorded before the addition. The difference spectrum exhibited three peaks at δ 4.61, δ 5.31 and δ 5.01 ppm. By comparing with model compounds, the peaks as γ-hydroxyl (δ 4.61 ppm; present in β-O-4 structures), α-hydroxyl (δ 5.31 ppm; primarily present in β-O-4 structures) and γ-hydroxyl (δ 5.01 ppm; present in phenylcoumarans structures) in lignin had been assigned [76].

It was observed that ^{1}H-NMR spectrum of CF_AL in *d*$_6$-DMSO exhibited some characteristic peaks of lignin (Table 3.21). Phenolic hydroxyl groups were not detected, and this may be due to contaminants, such as moisture associated with the alkali-lignin, that hindered the detection of the peak under applied experimental conditions. Aromatic protons and the protons in methoxyl group were present (δ 6.687 and δ 3.464 ppm, respectively) in the sample, but no peaks were observed in the range of 4.0-5.5 ppm (mainly, the chemical shifts of H_α, H_β and H_γ in several structures). From Table 3.21, it could be seen that, acetylated CF_AL in *d*$_6$-DMSO exhibited some peaks at δ 8.278-8.550 ppm (H in residual phenolic hydroxyl group), δ 3.375-3.953 ppm (H in methoxyl group), δ 2.199-2.478 ppm (phenolic acetate) and δ 1.460-1.883 ppm (H in aliphatic acetate). Beside these, a few small peaks were detected in the range of δ 4.442-4.753 ppm. These peaks were most likely a sign of residual aliphatic hydroxyl protons in the acetylated lignin sample [76]. H_β and H_γ in several structures of lignin provided signals in the range of δ 4.0-5.5 ppm [206]. While being examined in *d*$_6$-DMSO, the samples BG_AL, TO_AL, and GW_AL exhibited comparable ^{1}H-NMR spectra of CF_AL. TO_AL showed a signal at δ 2.612 ppm, potentially as an indication of the presence of benzylic protons in β-β structures or H_β in β-1 structure.

Field emission-scanning electron microscopic analysis: Surface morphologies of alkali-lignin

Surface morphologies of vacuum-dried free-flowing alkali-lignin powders were analyzed by field emission scanning electron microscope (FE-SEM) at different magnifications (5, 10, 20, 30 and 50 KX) and depicted in Figure 3.17 (a to d).

It could be observed that submicron lignin particles were agglomerated in different sizes and also formed rough surfaces [142-145]. Microscopic cavities were observed in all cases. It was suggested that milled alkali-lignin could be characterized by irregular particle morphology [145]. Irregularly shaped lignin agglomerates could be seen at higher resolutions. Due to agglomerated forms, the particle sizes measured by dynamic light scattering technique were differed significantly in the FE-SEM analysis, as observed from the Figure 3.17. However, further investigations need to be done by dispersing the agglomerated particles with appropriate solvent system followed by solvent evaporation to monitor the actual particle sizes and also shapes.

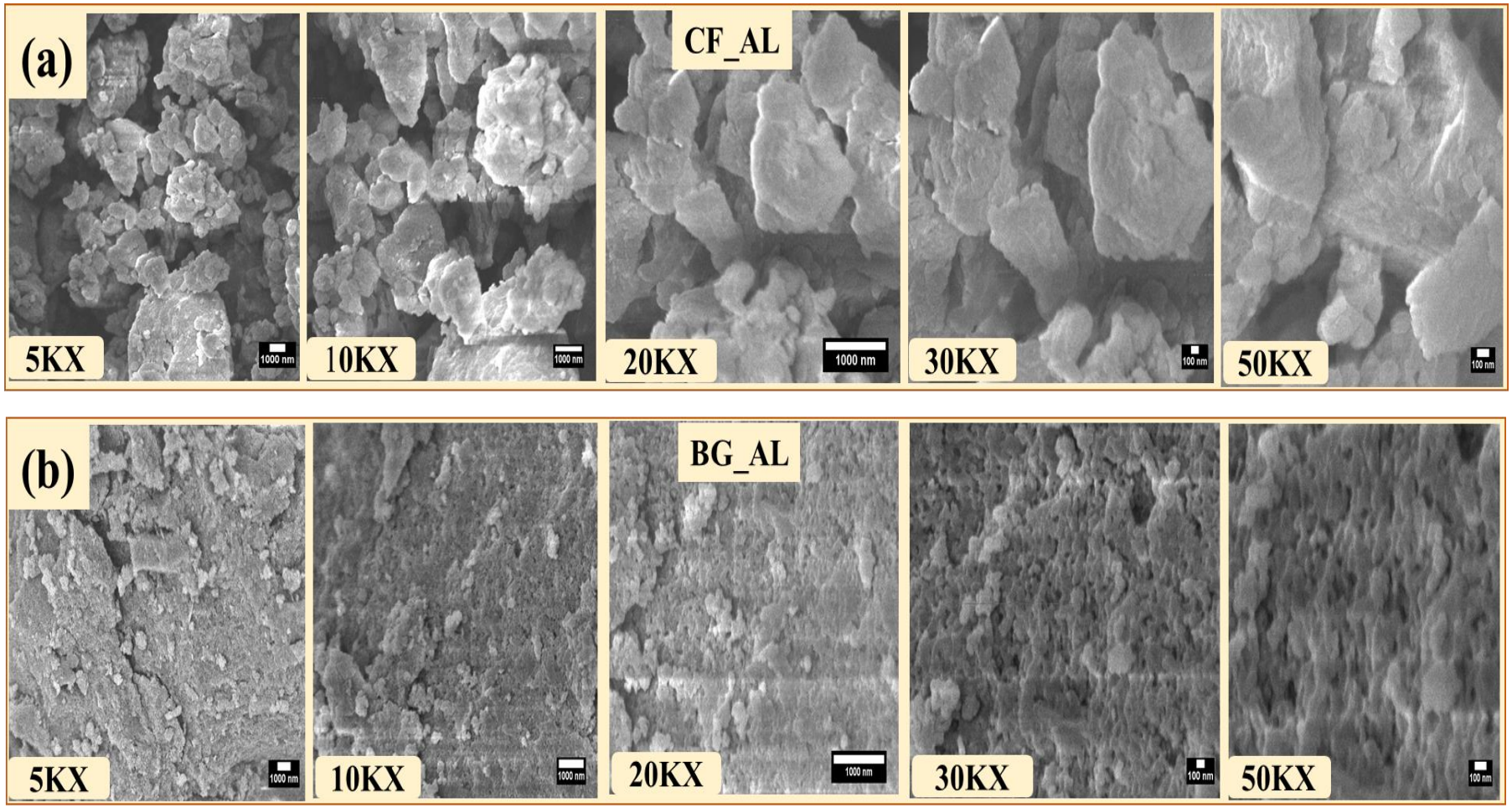

Figure 3.17: FE-SEM images of alkali-lignin particles at different magnifications, i.e., 5, 10, 20, 30 and 50 KX; (a) CF_AL and (b) BG_AL. Scale bar set at 1000 nm for 5 to 20 KX and 100 nm for 30 to 50 KX magnifications.

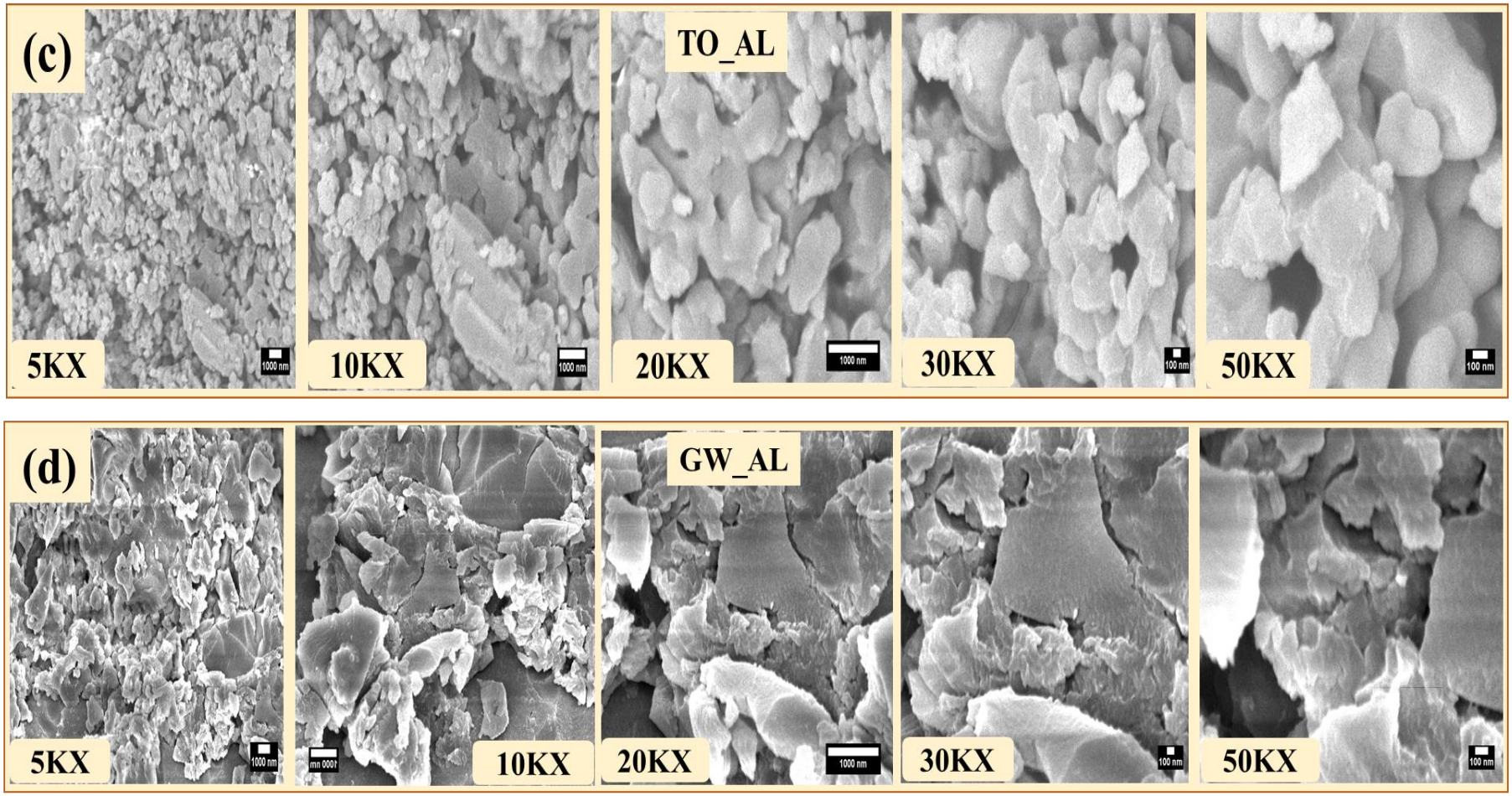

Figure 3.17: FE-SEM images of alkali-lignin particles at different magnifications, i.e., 5, 10, 20, 30 and 50 KX; (c) TO_AL and (d) GW_AL. Scale bar set at 1000 nm for 5 to 20 KX and 100 nm for 30 to 50 KX magnifications.

Simultaneous thermal analysis: Examination of thermal properties

Thermal properties of submicron alkali-lignin samples, CF_AL, BG_AL, TO_AL and GW_AL were investigated by simultaneous thermal analyzer (STA) and obtained thermogravimetric (TG) and differential scanning calorimetric (DSC) thermograms were given separately in Figure 3.18. The test settings, such as atmosphere, gas flow rate, vapor pressure on the sample, heating rate, thermal contact to the sample and crucible, etc., were the same for both TGA and DSC outputs in simultaneous thermal analysis.

It can be observed from Figure 3.18a that the rates of degradation of the sample were different, as the lignin isolated from different sources with different chemical compositions. With increasing temperature from ambient to 850 ^{o}C, the samples lost 5 to 10% of their initial weights up to 105 ^{o}C. These were due to removal of volatiles, e.g. mainly strongly bonded moisture, etc. as reported in several literatures [133]. TO_AL lost 25% of its initial weight below 200 ^{o}C as indicated the structural degradation, e.g. losses of small molecules like H_2O, CO_2, CH_4, CH_3COOH, etc. Other samples were comparatively stable than TO_AL at this temperature. Rapid degradations were stared from 200 ^{o}C and BG_AL lost 30% of its initial weight at 375 ^{o}C, whereas other samples were comparatively stable. CF_AL and GW_AL showed more thermal stability up to 850 ^{o}C and produced 40.33% and 43.67% char, respectively. BG_AL and TO_AL started rapid degradation as the temperature raised from 350 ^{o}C to 600 ^{o}C and lost 50-60% of their initial weights, but CF_AL and GW_AL were comparatively stable than others. Only 19.96% and 26.44% char produced by BG_AL and TO_AL, respectively at temperature 850 ^{o}C. It could be assumed that CF_AL and GW_AL might be used as a good source of carbon and carbon based valuable products due to their char forming properties at higher temperatures.

The initial endothermic shift in the DSC thermogram indicates a glass transition because lignin samples are amorphous polymers that move chain segments when heated. Interestingly, all of the alkali-lignin samples exhibited endothermic peaks centered roughly at about 75 ^{o}C (CF_AL 79.9 ^{o}C, BG_AL 72.0 ^{o}C, TO_AL 67.2 ^{o}C and GW_AL 77.5 ^{o}C) in their DSC thermograms as shown in Figure 3.18b and data were given in Table 3.22. The onset temperatures could be assigned as their glass transition temperature [146].

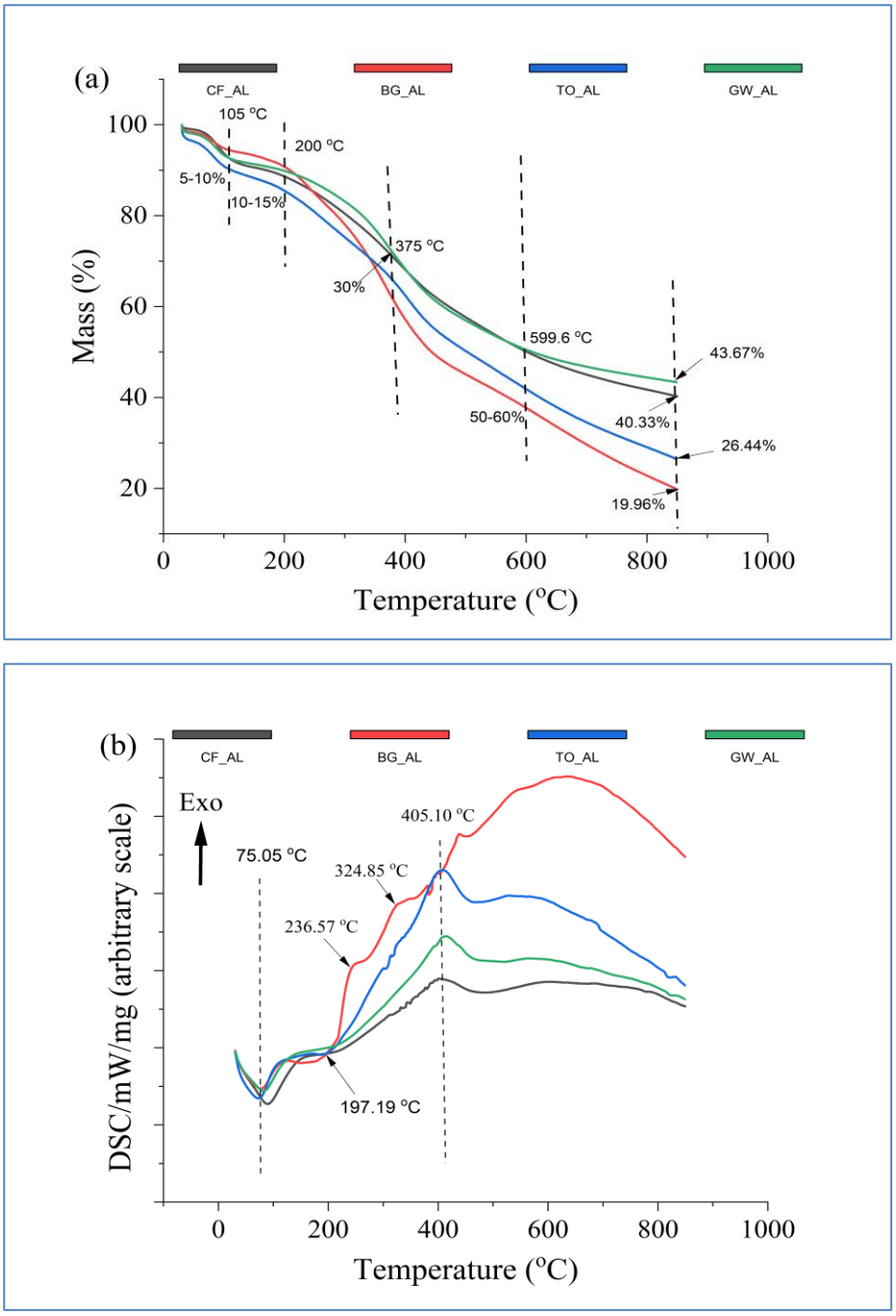

Figure 3.18: Simultaneous thermal analysis of four alkali-lignin samples (a) thermogravimetric analysis and (b) differential scanning calorimetric analysis.

Generally, extrapolated onset temperature has been used as the glass transition temperature, T_g of polymers [133]. The free volume, heat capacity, and thermal expansion coefficient of the samples all abruptly shift in conjunction with the glass transition. It can be seen (Table 3.22) that there were some differences in T_g values of the alkali-lignin samples. CF_AL showed the highest T_g followed by GW_AL and the lowest T_g was obtained for TO_AL.

Table 3.22: Differential scanning calorimetric data of alkali-lignin samples

Alkali-lignin	Glass transition temperature (°C)			Enthalpy change (ΔC_p) J/(g/K)
	Onset	Inflection	End	
CF_AL	79.9	131.1	96.7	1.456
BG_AL	72.0	90.6	83.1	0.530
TO_AL	67.2	88.3	79.1	0.965
GW_AL	77.5	98.7	89.1	0.536

It was observed that the DSC curves, e.g., change in enthalpy against temperature showed a drift in the curve at higher temperatures and associated difficulties with the drift had also been reported [147]. The observed drift was explained by the sample's physical characteristics changing during the STA run. It was shown that the normal T_g value for any given lignin could not be provided with accuracy; for example, the T_g values of dioxane lignin (DL) and milled wood lignin (MWL) are typically approximately 166.85 and 146.85 °C, respectively. Several studies showed the T_g values of coconut fibre lignin were in the range of 140 to 172 °C, in which 2% alkali with anthraquinone and acidic dioxane solutions were used as lignin extracting solvents [148, 149]. The reported values were significantly higher than 79.9 °C as obtained for CF_AL. Similarly, bagasse lignin showed glass transition temperatures in the range of 111 to 150 °C and the T_g values were also higher than BG_AL [90, 150].

Lower glass transition temperature of bagasse lignin (54-74 °C) was also reported [152]. TO_AL and GW_AL showed glass transition temperatures, 67.2 °C and 77.5 °C, respectively and the values were lower than Kraft lignin samples isolated from hardwood and softwood (T_g 93 °C for hardwood and 119 °C for softwood) [153]. Klason lignin, isolated from hardwood and softwood biomasses, showed similar glass transition temperatures and the values were higher than lignin isolated by other methods [154-156]. It means that highly condensed lignin structure, e.g., Klason lignin showed higher glass transition temperature [157]. The molecular weight of lignin, cross-linking density, hydrogen bonding, thermal history of the samples, etc. all affect the glass transition temperature, which can also be impacted by low molecular weight impurities like water, solvents, etc. [133]. However, it could be assume that the prepared alkali-lignin samples with lower glass transition temperatures would facilitate the flow properties and subsequent processing for different industrial applications.

Determination of antioxidant activities and comparison with commercial antioxidants

To assess the antioxidant activity of lignin, the 2,2-diphenyl-1-picrylhydrazyl radical (DPPH*) free radical scavenging assay is frequently used [158]. Results obtained from the measurements in which R^2 values were 0.996 for CF_AL; 0.938 for BG_AL; 0.983 for TO_AL; 0.960 for GW_AL and 0.985 for Ascorbic acid were given in Figure 3.19.

It can be observed that IC_{50} value of CF_AL (6.02 µg/mL) was the lowest among all lignin samples including ascorbic acid (9.52 µg/mL) and thus the most effective alkali-lignin antioxidant among the tested samples. The highest IC_{50} value was obtained for BG_AL (19.57 µg/mL), whereas TO_AL and GW_AL showed IC_{50} values of 16.40 µg/mL and 14.18 µg/mL, respectively. Numerous investigations have been made into the antioxidant activities of various lignin preparations [159-163]. Enzymatic hydrolysis lignin was shown to have lower antioxidant activity than Irganox1010, although alkaline depolymerized enzymatic hydrolysis lignin samples displayed similar IC_{50} values to Irganox1010 [159]. Contrarily, alkali lignin samples extracted with ethanol and ethyl acetate showed more antioxidant activity (IC_{50} 23 µg/mL) than Irganox1010 (IC_{50} 26 µg/mL), leading researchers to draw the conclusion that lignin's antioxidant performance was enhanced by its reduced molecular weight and increased phenolic hydroxyl group concentration. Interestingly, antioxidant activity of ball milled alkali lignin particles, i.e., CF_AL (IC_{50} 6.02 µg/mL), BG_AL (IC_{50} 19.57 µg/mL),TO_AL (IC_{50} 16.40 µg/mL) and GW_AL (IC_{50} 14.18 µg/mL) were significantly higher than the antioxidant activities of commercially available antioxidants, such as sterically hindered primary phenolic antioxidant (Irganox1010; IC_{50} 26 µg/mL), Butylated hydroxyanisole (BHA; IC_{50} 56.3 µg/mL) and Butylated hydroxytoluene (BHT; IC_{50} 38.2 µg/ mL), as well as the depolymerized enzymatic hydrolysis and ethanol and ethyl acetate extracted alkali lignin. The ball-milled alkali-lignin particles produced by the LCF biorefinery system can be used as thermal oxidation stabilizers, conductive and packaging materials, biomaterials, anti-UV agents, and photosensitive materials, along with other things [158].

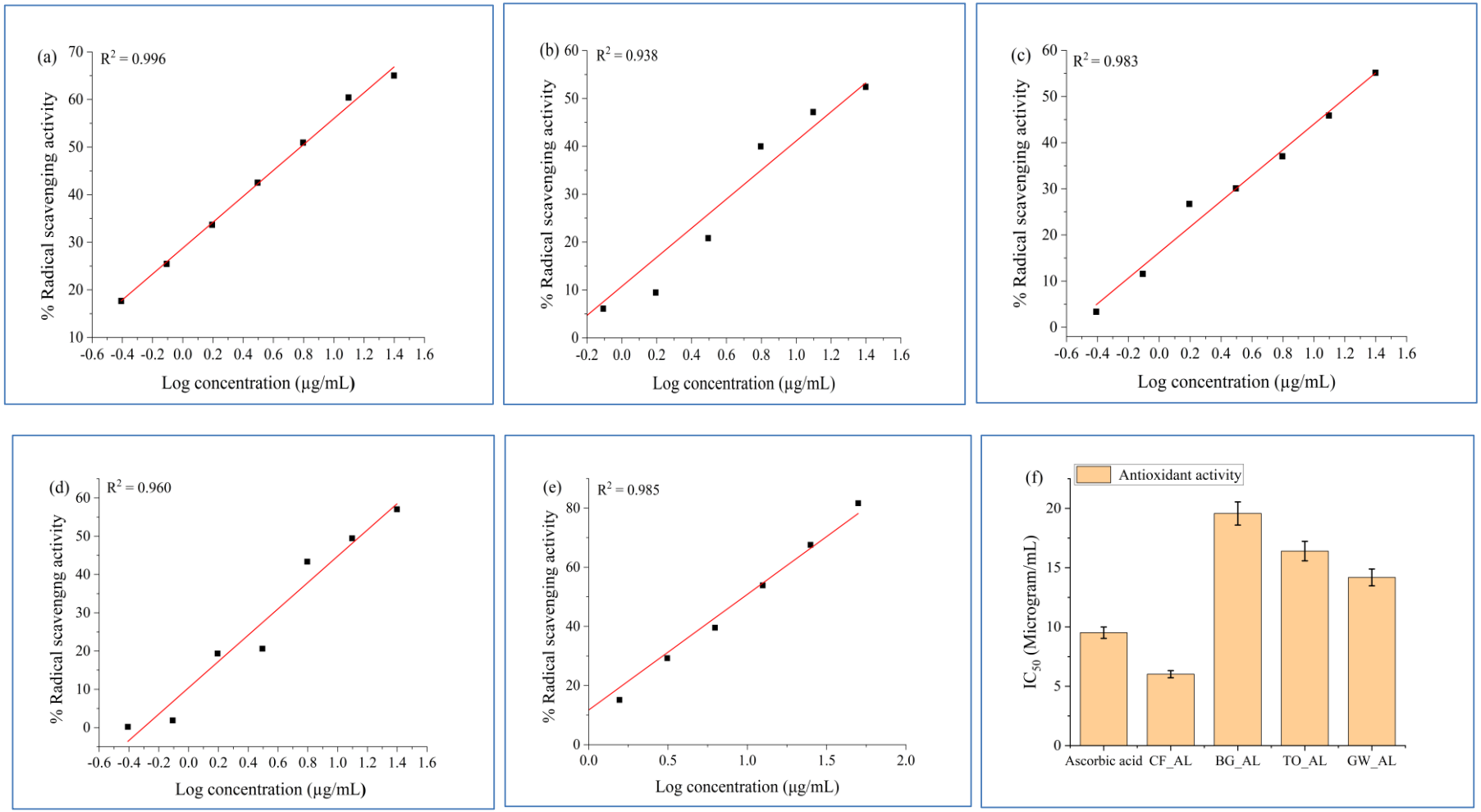

Figure 3.19: Antioxidant activities (AO) of alkali-lignin and ascorbic acid samples, (a) CF_AL (b) BG_AL (c) TO_AL (d) GW_AL (e) Ascorbic acid and (f) Comparison of IC_{50} value of the samples

Diffuse reflectance Ultraviolet-Visible spectroscopic analysis: Kubelka-Munk function for different alkali-lignin particles

Even for particles with submicron length scales, diffuse reflectance spectroscopy can be used to determine the absorption characteristics of the particles [164]. Results of the UV-Vis diffuse reflectance measurements of submicron alkali-lignin particles have been depicted in Figure 3.20. The measured apparent absorbance and Kubelka-Munk functions have been summarized in Table 3.23 and compared with the values found in the literature [165]. It can be observed that all lignin samples absorbed UV radiation ranging from 224 to 428 nm and maximum absorptions exhibited at different wavelengths, i.e., 337 nm for CF_AL (1.7020 AU), 316 nm for BG_AL (0.5640 AU), 302 nm for TO_AL (0.5088 AU) and 334 nm for GW_AL (0.8238 AU).

Generally, electronic transitions in the organic molecules, e.g., lignin involves the bonding, anti-bonding and non-bonding molecular orbitals and transitions occur from lower to higher energy states by absorbing light in UV-Vis range. This process is sensitive to the chemical structure of compounds, e.g., the presence of conjugation in pi-bonded aliphatic and aromatic skeletons (with or without different functional groups, as termed as auxochromes, such as hydroxyl or methoxyl groups) and other light absorbing functional groups, as termed as chromophores, such as ethylene, carbonyl, carboxylic acid or ester groups, etc. [166, 167]. Different lignin preparations contain UV-absorbing functional groups, such as phenolic, carbonyl, carboxylic acid or ester, which make lignin polymer as ultraviolet and visible (UV-Vis) light absorber [168, 169]. However, the Kubelka-Munk function, $F(R_\infty)$ might be used for quantitative evaluation of light absorption properties of lignin by integrating the degree of reflection on the sample surface. In UV-Vis diffuse reflectance spectroscopy, the Kubelka-Munk function can be expressed by following equation 3.5 [165].

$$F(R_\alpha) = \frac{(1- R_\alpha)^2}{2 R_\alpha} = \frac{K}{S} = \frac{2.303\ \varepsilon C}{S} \qquad (3.5)$$

here,

R_∞ = Absolute remittance
$F(R_\infty)$ = Kubelka-Munk function
K = Absorption coefficient
S = Scattering coefficient
ε = Absorptivity
C = Analyte concentration

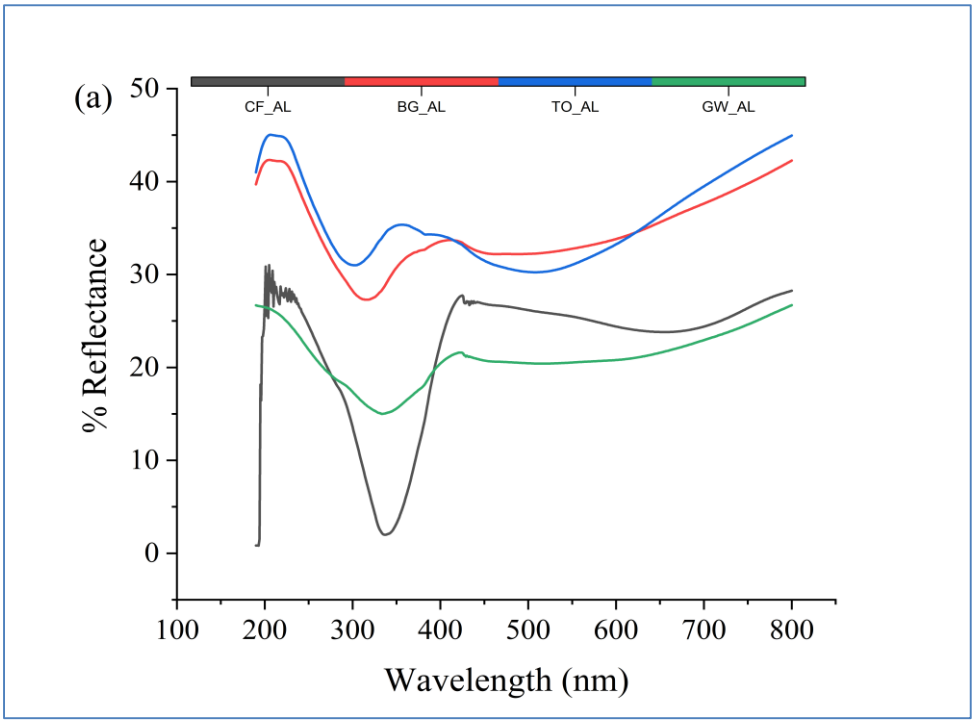

Figure 3.20: UV-Vis diffuse reflectance spectroscopic analysis of four alkali-lignin samples (a) percent reflectance at different wavelengths and (b) Kubelka-Munk functions.

Kubelka-Munk (K-M) functions for the alkali-lignin samples have been derived based on % reflectance and apparent absorbance (calculated from % reflectance) data and given in Table 3.23.

Table 3.23: Comparison of theoretical absorbances and Kubelka-Munk functions at various %reflectance values with alkali-lignin samples

% Reflectance	Theoritical value [163]		Experimental values for alkali-lignin			
	Apparent absorbance [Log $(1/R_\alpha)$]	Kubelka-Munk function $[(1-R_\alpha)^2/2R_\alpha]$	Apparent absorbance [Log $(1/R_\alpha)$]	Kubelka-Munk function $[(1-R_\alpha)^2/2R_\alpha]$	λ_{max} (nm)	Alkali-lignin
100	0	0	-	-	-	-
90	0.046	0.0056	-	-	-	-
80	0.097	0.025	-	-	-	-
70	0.15	0.064	-	-	-	-
60	0.22	0.13	-	-	-	-
50	0.30	0.25	-	-	-	-
40	0.40	0.45	-	-	-	-
30	0.52	0.82	0.5640	0.97	316	BG_AL
			0.5088	0.77	302	TO_AL
20	0.70	1.6	0.8238	2.41	334	GW_AL
10	1.0	4.0	-	-	-	-
1	2.0	49	1.7020	24.28	337	CF_AL

It was observed that the measured Kubelka-Munk functions and apparent absorbances of alkali-lignin samples showed good agreement with the reference values and exhibited higher absorption coefficient in UV regions, i.e., UV-A 315 to 400 nm; UV-B 280 to 315 nm and UV-C 200 to 280 nm. Surprisingly, CF_AL showed the highest Kubelka-Munk function with the highest apparent absorbance value and absorbed strongly in UV regions, i.e., 224 to 428 nm, but other alkali-lignin particles absorbed in both UV and to some extent visible regions. Earlier studies using diffuse reflectance UV-Vis spectroscopy on several lignin samples revealed stronger absorption at the 250 to 280 nm and 280 to 350 nm ranges [169, 170]. Alkali lignin from palm and bamboo exhibits high UV-blocking efficiency, which, according to a comparison of UV absorbance for the samples, is mostly attributable to the presence of functional groups such as phenolic OH, aliphatic OH, and polyunsaturated aromatic structures [171].

Intrinsic viscosity and macromolecular behaviours of alkali-lignin in solution

The measurement of intrinsic viscosity of the alkali-lignin samples using very dilute solution in dimethyl sulfoxide at 25^{o}C, e.g., fulfilling the Debye dilution criterion $C[\eta] < 1$, where $[\eta]$ was the intrinsic viscosity and C was the polymer concentration, were done and given in the Table 3.24.

Table 3.24: Dilute solution viscometric analysis of alkali-lignin in DMSO* at 25 ^{o}C

Sample	Relative viscosity	Inherent viscosity (mL/g)	Specific viscosity	Reduced viscosity (mL/g)	Intrinsic viscosity (mL/g)	Dynamic viscosity (mPa.s)	Kinematic viscosity (mm^2/s)
CF_AL	1.046	22.6	0.046	23.1	22.7	3.000	2.737
BG_AL	1.008	4.0	0.008	4.0	4.0	2.943	2.686
TO_AL	1.034	16.8	0.034	17.0	16.8	3.001	2.738
GW_AL	1.027	13.1	0.027	13.3	13.1	2.964	2.705

*Dynamic viscosity of DMSO at 25 ^{o}C is 1.99 mPa.s.

A polymer coil's effective hydrodynamic volume is measured by intrinsic viscosity, which might alter depending on the solvent or measuring temperature. For a hard and non-swelling sphere intrinsic viscosity, $[\eta]$ in 100 ml/g is given by the Einstein equation 3.6 [170].

$$[\eta] = 0.025\ V \qquad (3.6)$$

Where, *V* is the precise volume of the sphere's substance. *V* in equation 3.6 changes to the volume of the swollen macromolecules per unit weight of solute when the sphere is a macromolecule made up of a porous, solvent-swollen network. Thus, with increased swelling or extension of the macromolecule in the solvent, *V*, increases the intrinsic viscosity, [η]. When, [η] is low for a given molecular weight, the macromolecule or polymer is compact and occupies a small amount of space in the solution. However, several works have been conducted on the determination of intrinsic viscosity of different lignin preparations [171-173].

Karmanov, *et al.* studied the hydrodynamic, scaling, and conformational properties of dilute solutions of dioxane lignin (isolated from *Serratula coronata* L.) in Dimethylformamide in order to establish the topological structure of the macromolecules and reported intrinsic viscosities of the lignin fractions from 4.1 to 10.7 mL/g [171]. Similar intrinsic viscosity values of lignin were also found using *Betula pendula* birch twigs [172]. Goring also studied sodium lignin sulphonate and dioxane lignin (spruce wood lignin preparations of molecular weight 50000) in 0.1M NaCl and pyridine solutions, respectively and reported intrinsic viscosity values were 10 mL/g for lignin sulphonate and 8 mL/g for dioxane lignin. Intrinsic viscosities of Kraft lignin in Dimethylformamide solutions at different temperatures were measured and reported intrinsic viscosities were 6.9 to 8.1 mL/g [173]. The intrinsic viscosity values of different lignin preparations were sufficiently small compared to other polymeric materials and proved the lignin polymers as very compact nature in solution [172, 173].

The intrinsic viscosity, [η] of alkali-lignin samples, i.e., CF_AL (22.7 mL/g), BG_AL (4.0 mL/g), TO_AL (16.8 mL/g) and GW_AL (13.1 mL/g) were higher, except BG_AL, than other lignin preparations as discussed above. It could be assumed that the alkali-lignin preparations were significantly swollen in dimethylsulfoxide at 25 ^{o}C and potentially formed microgel in the solutions. Increased absolute viscosities of alkali-lignin solutions could be considered as an evidence of the microgel formation. So, intrinsic viscosity measurement might be used to evaluate the compactness of lignin polymer obtained from the biorefinery and also be used as a rapid quality monitoring tool for the analysis of different lignin preparations including modified lignin.

Conclusion

- As the LCF biorefinery has been facing unsatisfactory results due to lignin separation and utilization in a techno-economically feasible way, this work has presented an easy and one of the most simplified ways to separate hemicelluloses, cellulosic pulp and alkali-lignin using lower amounts of acid and base from both woods and non-woody LCF biomasses.
- The amounts of isolated lignin were significantly higher than other processes, e.g. uses of ionic liquids, deep eutectic solvents, etc. Recovered hemicelluloses might be used for the production of furfurals, etc. by applying suitable treatment.
- Cellulosic pulp could be used to prepare α-cellulose through eco-friendly bleaching process, e.g., alkaline peroxide bleaching and then further conversions to cellulose hydrogel and other cellulose derivatives.
- The free-flowing submicron alkali-lignin particles were significantly pure and showed excellent physicochemical properties, e.g., high antioxidant activities, superior ultraviolet light absorption properties and also thermal stability for high value applications.
- The alkali-lignin samples could be used as a feedstock for the production of nanolignin of uniform sizes with narrow polydispersity indices. CF_AL showed the highest antioxidant activity and ultraviolet light absorption properties than other lignin and potentially superior quality than commercially available synthetic polymeric antioxidants and ultraviolet light stabilizers, as used in different plastics, rubbers and composite materials, etc.
- Among four alkali-lignin samples, CF_AL and GW_AL showed excellent char forming properties and might be used for the production of carbon fibre of different grades.
- The alkali-lignin samples were soluble in DMSO, THF and partially soluble in acetone and ethanol, etc. and could be modified by different treatments, e.g., chemical modifications in the solution or dispersion states.

References

[73] M. Jablonsky, M. Botkova and J. Adamovska, Prediction of methoxyl groups content in lignin based on ultimate analysis, *Cellulose Chem. Technol.*, 2015, 49(2), 165-168

[74] G. F. Zakis, Functional analysis of lignins and their derivatives, TAPPI PRESS, Atlanta, 1994

[75] S. Beisl, A. Miltner and A. Friedl, Lignin from Micro- to Nanosize: Production Methods, *International Journal of Molecular Sciences*, 2017, *18(6), 1244, DOI: 10.3390/ijms18061244*

[76] S. Li and K. Lundquist, Analysis of hydroxyl groups in lignins by ^{1}H NMR spectrometry, *Nordic Pulp & Paper Research Journal*, 2001, 16, 63-67, doi.org/10.3183/npprj-2001-16-01-p063-067

[77] W. Brand-Williams, M. E. Cuvelier and C. Berset, Use of a free radical method to evaluate antioxidant activity, *LWT - Food Science and Technology*, 1995, 28(1), 25-30, doi.org/10.1016/S0023-6438(95)80008-5

[78] G. Kortüm, W. Braun and G. Herzog, Principles and Techniques of Diffuse-Reflectance Spectroscopy, *Angewandte Chemie*, 1963, 2, 333-341, DOI:10.1002/ANIE.196303331

[79] J. F. Rodríguez, X. Erdocia, F. H. Ramos, M. G. Alriols and J. Labidi, *Separation of functional Molecules in Food by membrane technology*, (ed. C. M. Galanakis), Academic Press, UK, 2019,7, 229–265

[80] P. Azadi, O. R. Inderwildi, R. Farnood and D. A. King, Liquid fuels, hydrogen and chemicals from lignin: A critical review, *Renewable and Sustainable Energy Reviews*, 2013, 5, 506–523, *DOI: 10.1016/j.rser.2012.12.022*

[81] *Y. Z. Lai*, Chemical Modification of Lignocellulosic Materials, (ed. D. N. S. Hon), Marcel Dekker, Inc., New York, 1, 1996, 3, 35-95.

[82] R. A. Young, Encyclopaedia of Materials: Science and Technology, (ed. K.H. J.Buschow, M. C. Flemings, E. J. Kramer, P. Veyssière, R. W. Cahn, B. Ilschnerand S. Mahajan), Elsevier B.V., The Netherlands, Second Edition, 2001, Wood Products: Chemical Degradation, 9691–9694

[83] J. Shakhes, F. Zeinaly, M. A. Marandi and T. Saghafi, The effects of processing variables on the soda and soda-AQ pulping of Kenaf bast fiber, *BioResources*, 2011, 4, 4626-4639

[84] R. C. Francis, S. J. Shin, S. Omori, T. E. Amidon and T. J. Blain, Soda Pulping of Hardwoods Catalyzed by Anthraquinone and Methyl Substituted Anthraquinones, *Journal of wood chemistry and technology*, 2006, 2, 141-152 doi.org/10.1080/02773810600701737

[85] J. B. Sluiter, R. O. Ruiz, C. J. Scarlata, A. D. Sluiter and D. W. Templeton, Compositional Analysis of Lignocellulosic Feedstocks. 1. Review and Description of Methods, *Journal of Agricultural and Food Chemistry*, 2010, 16, 9043–9053, doi.org/10.1021/jf1008023

[86] H. Rabemanolontsoa and S.Saka, Comparative study on chemical composition of various biomass species, *RSC Advances*, 2013, 12, 3946–3956, doi.org/10.1039/C3RA22958K

[87] S.O. Anuchi, K.L.S. Campbell and J.P. Hallett, *Effective pretreatment of lignin-rich coconut wastes using a low-cost ionic liquid*, Sci Rep, 2022, 12, 6108, doi.org/10.1038/s41598-022-09629-4

[88] J. E.G. van Dam, M. J. A. van den Oever, W. Teunissen, E. R. P. Keijsers and A. G. Peralta, Process for production of high density/high performance binderless boards from whole coconut husk: Part 1: Lignin as intrinsic thermosetting binder resin, *Industrial Crops and products*, 2004, 3, 207-216, DOI: 10.1016/j.indcrop.2003.10.003

[89] P. Muensri, T. Kunanopparat, P. Menut and S. Siriwattanayotin, Effect of lignin removal on the properties of coconut coir fiber/wheat gluten biocomposite, *Composites Part A: Applied Science and Manufacturing*, 2011, 2, 173-179, doi.org/10.1016/j.compositesa.2010.11.002

[90] S. Imman, P. Khongchamnan, W. Wanmolee, N. Laosiripojana, T. Kreetachat, C. Sakulthaew, C. Chokejaroenrat and N. Suriyachai, Fractionation and characterization of lignin from sugarcane bagasse using a sulfuric acid catalyzed solvothermal process, *RSC advances*, 2021, 43, 26773-26784, doi.org/10.1039/D1RA03237B

[91] M. S. Jahan and S. P. Mun, Characteristics of Dioxane Lignins Isolated at Different Ages of Nalita Wood (Trema orientalis), *Journal of wood chemistry and technology*, 2007,2, 83-98, DOI: 10.1080/02773810701486865

[92] M. S. Jahan and S. P. Mun, Characteristics of Milled Wood Lignins Isolated from different ages of Nalita Wood (Trema orientalis), *Cellulose chemistry and technology*, 2006, 6, 457-467

[93] R. Rana, R. L. Heyser, R. Finkeldey and A. Polle, FTIR spectroscopy, chemical and histochemical characterisation of wood and lignin of five tropical timber wood species of the family of Dipterocarpaceae. *Wood Sci Technol*, 2010, 44, 225–242, doi.org/10.1007/s00226-009-0281-2

[94] A. U. Israel, R. E. Ogali, O. Akaranta and I. B. Obot, Extraction and characterization of coconut (Cocos nucifera L.) coir dust, *Songklanakarin J. Sci. Technol*., 2011, 33 (6), 717-724

[95] J. Rencoret, A. Gutiérrez, L. Nieto, J. J. Barbero, C. B. Faulds, H. Kim, J. Ralph, Á. T. Martínez and J. C. Del Río, Lignin Composition and Structure in Young versus Adult Eucalyptus globulus Plants, *Plant Physiology*, 2011, 155 (2), 667-682, doi.org/10.1104/pp.110.167254

[96] J. A. Joshua, J.C. Ahiekpor and A. Kuye, Nigerian Hardwood (Nesogordonia papaverifera) Sawdust Characterization: Proximate Analysis, Cellulose and Lignin Contents *Lignocellulose*, 2016, 5(1), 50-58

[97] Z .J. Shi, L. P. Xiao, J. Deng, H. Y. Yang, X. L. Song and R. C. Sun, Isolation and Structural Exploration of Hemicelluloses from the Largest Bambo Species: *Dendrocalamus Sinicus*, *BioResources*, 2013, 8*(*4), 5036-5050

[98] T. M. Santos, M. V. Alonso, M. Oliet, J. C. Domínguez, V. Rigual and F. Rodriguez, Effect of autohydrolysis on Pinus radiata wood for hemicellulose extraction, *Carbohydrate polymers*, 2018, 194, 285-293

[99] Y. Lu, Q. He, G. Fan, Q. Cheng and G. Song, Extraction and modification of hemicellulose from lignocellulosic biomass: A review, *Green Processing and Synthesis*, 2021, 1, 779-804, doi.org/10.1515/gps-2021-0065

[100] T. H. Kim, H. J. Ryu and K. K. Oh, Low acid hydrothermal fractionation of Giant Miscanthus for production of xylose-rich hydrolysate and furfural, *Bioresource Technology*, 2016, 218:367-372, DOI: 10.1016/j.biortech.2016.06.106

[101] W. M. Goldmann, J. Ahola, M. Mikola and J. Tanskanen, Formic acid aided hot water extraction of hemicellulose from European silver birch (Betula pendula) sawdust, *Bioresource technology*, 2017, 232, 176-182

[102] S. M. de Vasconcelos, A. M. P. Santos, G. J. M. Rocha and A. M. Souto-Maior, Diluted phosphoric acid pretreatment for production of fermentable sugars in a sugarcane-based biorefinery, *Bioresource technology*, 2013, 135, 46-52, doi.org/10.1016/j.biortech.2012.10.083

[103] M. Tiboni, A. Grzybowski, G. R. Baldo, E. F. Dias Jr, R. D. Tanner, J. A. Kornfield and J. D. Fontana, Thermopressurized diluted phosphoric acid pretreatment of ligno(hemi)cellulose to make free sugars and nutraceutical oligosaccharides, *Journal of Industrial Microbiology and Biotechnology*, 2014, 41:957-964, DOI 10.1007/s10295-014-1426-3

[104] M. F. Andrade and J. L. Colodette, Dissolving pulp production from sugar cane bagasse, *Industrial Crops and Products*, 2014, 52, 58–64, DOI : 10.1016/j.indcrop.2013.09.041

[105] O. Ajao, M. Marinova, O. Savadogo and J. Paris, Hemicellulose based integrated forest biorefineries: Implementation strategies, *Industrial Crops and Products*, 2018,126, 250-260, doi.org/10.1016/j.indcrop.2018.10.025

[106] A. Tribot, G. Amer, M. A. Alio, H. de Baynast, C. Delattre, A. Pons, J. D. Mathias, J. M. Callois, C. Vial, P. Michaud and C. G. Dussap, Wood-lignin: Supply, extraction processes and use as bio-based material, *European Polymer Journal*, 2019,112, 228-240

[107] S. K. Bose, S. Omori, D. Kanungo, R. C. Francis, N. H. Shin, 2009, Mechanistic Differences Between Kraft and Soda/AQ Pulping. Part 1: Results from Wood Chips and Pulps, *Journal of Wood Chemistry and Technology*, 29, 214-226

[108] Z. Liu, H. Wang and L. Hui, Pulping and Papermaking of Non-Wood Fibers, IntechOpen, 2018, doi:10.5772/intechopen.79017

[109] R. Rinaldi, R. Jastrzebski, M. T. Clough, J. Ralph, M. Kennema, P.C. Bruijnincx and B. M. Weckhuysen, Paving the Way for Lignin Valorisation: Recent Advances in Bioengineering, Biorefining and Catalysis, *Angewandte Chemie*, 2016, 29, 8164-8215, doi.org/10.1002/anie.201510351

[110] D. M. D. Carvalho, M. H. Lahtinen, M. Lawoko and K. S. Mikkonen, Active role of lignin in anchoring wood-based stabilizers to the emulsion interface, *ACS Sustainable Chemistry & Engineering*, 2020, 31, 11795-11804, doi.org/10.1039/D1GC02891J

[111] S. Octave and D. Thomas, Biorefinery: toward an industrial metabolism, *Biochimie*, 2009, 96, 659-664

[112] E. C. Achinivu, R. M. Howard, G. Li, H. Gracz and W. A. Henderson, Lignin extraction from biomass with protic ionic liquids, *Green Chemistry*, 2014, 3, 1114-1119, doi.org/10.1039/C3GC42306A

[113] Y. C. Sun, X. N. Liu, T. T. Wang, B. L. Xue and R. C. Sun, Green process for extraction of lignin by the microwave-assisted ionic liquid approach: toward biomass biorefinery and lignin characterization, *ACS Sustainable Chemistry & Engineering*, 2019, 15, 13062-13072, doi: 10.1021/acssuschemeng.9b02166

[114] A. H. A. Rahim, Z. Man, A. Sarwono, W. S. W. Hamzah, N. M. Yunus and C. D. Wilfred, Extraction and Comparative Analysis of Lignin Extract from Alkali and Ionic Liquid Pretreatment, *Journal of Physics: Conference Series*, 2018, 1123, doi:10.1088/1742-6596/1123/1/012052

[115] M. Lievonen, J. J. Valle-Delgado, M. L. Mattinen, E. L. Hult and K. Lintinen, M. A. Kostiainen, A. Paananen, G. R.Szilvay, H. Setälä and M. Österberg, Simple process for lignin nanoparticle preparation, *Green Chem*, 2015, DOI: 10.1039/C5GC01436K

[116] M. Österberg, M. H. Sipponen, B. D. Mattos and O. J. Rojas, Spherical lignin particles: a review on their sustainability and applications, *Green Chemistry*, 2020, 9, 2712-2733. doi.org/10.1039/D0GC00096E

[117] S. Atifi, C. Miao and W. Y. Hamad, Surface modification of lignin for applications in polypropylene blends, *Journal of Applied Polymer Science*, 2017, doi:10.1002/app.44669

[118] Z. Zhang, V. Terrasson and E. Guénin, Lignin Nanoparticles and Their Nanocomposites, *Nanomaterials*, 2021, 15, 1336, doi.org/10.3390/nano11051336

[119] DLS size distribution and Polydispersity Index (PDI Index) of insulin loaded CS/ALG and CS-g-PAMAM/ALG core-shell nanoparticles, www.rsc.org/suppdata/c5/ra/c5ra17729d/c5ra17729d1.pdf (Last accessed 01.08.2022)

[120] R. H. Müller and K. Peters, Nanosuspensions for the formulation of poorly soluble drugs: I. Preparation by a size-reduction technique. *International Journal of Pharmaceutics*, 1998, 160(2), 229-237, doi.org/10.1016/S0378-5173(97)00311-6

[121] S. Beisl, A. Miltner and A. Friedl, Lignin from Micro- to Nanosize: Production Methods, *International Journal of Molecular Sciences*, 2017, 6, 1244, doi.org/10.3390/ijms18061244

[122] F. Xiong, Y. Han, S. Wang, G. Li, T. Qin, Y. Chen and F. Chu, Preparation and Formation Mechanism of Renewable Lignin Hollow Nanospheres with a Single Hole by Self-Assembly, *ACS sustainable chemistry & engineering*, 2017, 3, 2273-2281, doi.org/10.1021/acssuschemeng.6b02585

[123] L. S. Johansson, J. Campbell, K. Koljonen, M. Kleen and J. Buchert, On surface distributions in natural cellulosic fibers, *Surf. Interface Anal.*, 2004, 36, 706–710

[124] D. Kocaefe, X. Huang, Y. Kocaefe and Y. Boluk, Quantitative characterization of chemical degradation of heat-treated wood surfaces during artificial weathering using XPS, *Surface and Interface Analysis*, 45(2), 639-649, doi.org/10.1002/sia.5104

[125] G. N. Inari, M. Petrissans, J. Lambert, J. J. Ehrhardt and P. Gerardin, XPS characterization of wood chemical composition after heat-treatment, *Surface and Interface Analysis*, 2006, 10, 1336-1342, DOI: 10.1002/sia.2455

[126] D.N.S. Hon, ESCA study of oxidized wood surfaces, *Journal of Applied Polymer Science*, 1984, 29, 2777-2784, DOI:10.1002/APP.1984.070290908

[127] H. Ardelean, S. Petit, P. Laurens, P. Marcus and F. Arefi-Khonsari, Effects of different laser and plasma treatments on the interface and adherence between evaporated aluminium and polyethylene terephthalate films: X-ray photoemission, and adhesion studies, *Applied Surface Science*, 2005, 243(*1-4), 304–318, doi.org/10.1016/j.apsusc.2004.09.122*

[128] K. Ishimaru, T. Hata, P. Bronsveld, D. Meier and Y. Imamura, Spectroscopic analysis of carbonization behavior of wood, cellulose and lignin, *Journal of materials science*, 2007, 42(1), 122–129, doi.org/10.1007/s10853-006-1042-3

[129] A. Aarva, V. L. Deringer, S. Sainio, T. Laurila and M. A. Caro, Understanding X-ray Spectroscopy of Carbonaceous Materials by Combining Experiments, Density Functional Theory, and Machine Learning. Part I: Fingerprint Spectra, *Chemistry of Materials*, 2019, 22, 9243-9255, doi.org/10.1021/acs.chemmater.9b02049

[130] H. Sun, Y. Yang, Y. Han, M. Tian, B. Li, L. Han, A. Wang, W. Wang, R. Zhao and Y. He, X-ray photoelectron spectroscopy analysis of wood degradation in old architecture, *BioResources*, 2020, 3, 6332-6343

[131] O. Faix, Methods in Lignin Chemistry, (ed. S. Y. Lin and C. W. Dence), Springer-Verlog, Berlin Heidelberg, First edition, 1992, 4, 81-106

[132] T. A. Amit, R. Roy and D. E. Raynie, Thermal and structural characterization of two commercially available technical lignins for potential depolymerization via hydrothermal liquefaction, *Current Research in Green and Sustainable Chemistry*, 2021, 4, 100106, doi.org/10.1016/j.crgsc.2021.100106

[133] L. H. Zhao and H. J. Sun, Comparative Study of Two Types of Alkali Lignin from Different Origin, *Advanced Materials Research*, 2011, 299-300:747-750, DOI: 10.4028/www.scientific.net/AMR.299-300.747

[134] M. Schwanninger, J. C. Rodrigues and K. Fackler, A Review of Band Assignments in near Infrared Spectra of Wood and Wood Components, *J. Near Infrared Spectrosc.*, 2011, 19, 287–308, doi.org/10.1255/jnirs.955

[135] J. J. Workman and L. Weyer, Practical Guide to Interpretive Near-Infrared Spectroscopy, CRC Press, Boca Raton, 2007, doi.org/10.1201/9781420018318

[136] *U. P. Agarwal and R. H. Atalla,* Lignin and lignans: advances in chemistry, (ed. C.Heitner,D. DimmelandJ. A. Schmidt), CRC Press, Boca Raton, edition, 2010, 4, 103-136

[137] M. Mancini, Å. Rinnan, A. Pizzi and G. Toscano, Proc. 18th Int. Conf. Near Infrared Spectrosc., (ed. S.B. Engelsen, K. M. Sørensen and F. van den Berg.), IM Publications Open, Chichester, 2019, 77–84

[138] X. Li, C. Sun, B. Zhou and Y. He, Determination of Hemicellulose, Cellulose and Lignin in Moso Bamboo by Near Infrared Spectroscopy, *Scientific reports*, 2015, 1, 1-11, DOI: 10.1038/srep17210

[139] K. Fackler and M. Schwanninger, Polysaccharide Degradation and Lignin Modification during Brown Rot of Spruce Wood: A Polarised Fourier Transform near Infrared Study, *Journal of Near Infrared Spectroscopy*, 2010, 6, 403-416, DOI: 10.1255/jnirs.901

[140] T. Luo, Y. Hao, C. Wang, W. Jiang, X. Ji, G. Yang, J. Chen, S. Janaswamy and G. Lyu, Lignin Nanoparticles and Alginate Gel Beads: Preparation, Characterization and Removal of Methylene Blue, *Nanomaterials*, 2022, 1, 176, doi.org/10.3390/nano12010176

[141] P. K. Mishra and A. Ekielski, A Simple Method to Synthesize Lignin Nanoparticles, *Colloids and Interfaces*, 2019, 3(2), 52, doi.org/10.3390/colloids3020052

[142] A. Geies, M. Abdelazim, A. M. Sayed and S. Ibrahim, Thermal, Morphological and Cytotoxicity Characterization of Hardwood Lignins Isolated by In-Situ Sodium Hydroxide-Sodium Bisulfate Method, *Natural Resources*, 2020, 10, 427-438, DOI: 10.4236/nr.2020.1110025

[143] J. Köhnke, N. Gierlinger, B. Prats-Mateu, C. Unterweger, P. Solt, A. K. Mahler, E. Schwaiger, F. Liebner and W. Gindl-Altmutter, Comparison of four technical lignins as a resource for electrically conductive carbon particles, *BioRes.* 2019, 14(1), 1091-1109

[144] M. E. Eugenio, R. Martín-Sampedro, J. I. Santos, B. Wicklein and D. Ibarra, Chemical, Thermal and Antioxidant Properties of Lignins Solubilized during Soda/AQ Pulping of Orange and Olive Tree Pruning Residues, *Molecules*, 2021, 26(13), 3819, doi.org/10.3390/molecules26133819

[145] S. Arvelakis, P. A. Jensen and K. Dam-Johansen, Simultaneous thermal. analysis (STA) on ash from high alkali biomass, *Energy & Fuels*, 2004, *4, 1066–1076*

[146] H. Váquez-Torres, G. Canché-Escamilla and C. A. Cruz-Ramos, Coconut husk lignin. I. Extraction and characterization, *Journal of applied polymer science*, 1992, 4, 633-644, doi.org/10.1002/app.1992.070450410

[147] J. E. van Dam, M. J. van denOever, W. Teunissen, E. R. Keijsers and A. G. Peralta, Process for production of high density/high performance binderless boards from whole coconut husk: part I: Lignin as intrinsic thermosetting binder resin, *Industrial Crops and Products*, 2004, 3, 207–216

[148] M. A. Khan, S. M. Ashraf and V. P. Malhotra, Development and Characterization of a Wood Adhesive Using Bagasse Lignin, *International Journal of Adhesion and Adhesives*, 2004, 6, 485-493, doi.org/10.1016/j.ijadhadh.2004.01.003

[149] W. Li, N. Sun, B. Stoner, X. Jiang, , X. Lu and R. D. Rogers, Rapid dissolution of lignocellulosic biomass in ionic liquids using temperatures above the glass transition of lignin, *Green Chemistry*, 2011, 8, 2038-2047, doi.org/10.1039/C1GC15522A

[150] R. Leite, Y. M. B. de Almeida, S. M. Sarmento, K. G. Alves, E. F. de Melo and R. M. Souto-Maior, Solvent-fractionated sugar cane bagasse lignin: structural characteristics and electro-spinnability, *e-Polymers*, 2016, 16(2), 137-144, doi.org/10.1515/epoly-2015-0229

[151] S. Kubo and J. F. Kadla, Hydrogen bonding in lignin: a Fourier transform infrared model compound study, *Biomacromolecules*, 2005, 6(5), 2815-2821, DOI: 10.1021/bm050288q

[152] M. Poletto, Assessment of the thermal behavior of lignins from softwood and hardwood species, *Maderas, Cienc. tecnol.*, 2017, 19, 63-74. doi.org/10.4067/S0718-221X2017005000006

[153] G. Jiang, D. J. Nowakowski and A. V.Bridgwater, A systematic study of the kinetics of lignin pyrolysis. *Thermochimica Acta*, 2010, 498(1-2), 61-66, doi.org/10.1016/j.tca.2009.10.003

[154] A. Tejado, C. Pena, J. Labidi, J. M. Echeverria and I. Mondragon, Physico-chemical characterization of lignins from different sources for use in phenol-formaldehyde resin synthesis. *Bioresource technology*, 2007, 98(8), 1655-1663, doi: 10.1016/j.biortech.2006.05.042

[155] M. T. Klein and P. S. Virk, Modeling of lignin thermolysis, *Energy & Fuels*, 2008, 4, 2175–2182, *DOI: 10.1021/Ef800285F*

[156] Z. Qin, H. Liu, L. Gu, R. Sun and X. Wang, Reactive and Functional Polymers, (ed. T. J.Gutiérrez), Springer Nature, Switzerland, 2020, 5, 65-93

[157] L. F. Xiao, W. F. Liu, J. H. Huang, H. M. Lou and X. Q. Qiu, Study on the antioxidant activity of lignin and its application performance in SBS elastomer. *Industrial & Engineering Chemistry Research*, 2021, 60(1):790-797

[158] H. Faustino, N. Gil, C. Baptista and A. P. Duarte, Antioxidant Activity of Lignin Phenolic Compounds Extracted from Kraft and Sulphite Black Liquors. *Molecules*, 2010, 15(12), 9308-9322, doi.org/10.3390/molecules15129308

[159] J. Ponomarenko, M. Lauberts, T. Dizhbite, L. Lauberte, V. Jurkjane and G. Telysheva, Antioxidant activity of various lignins and lignin-related phenylpropanoid units with high and low molecular weight, *Holzforschung*, 2015, 69(6), 795-805

[160] M. E. Eugenio, R. Martín-Sampedro, J. I. Santos, B. Wicklein and D. Ibarra, Chemical, Thermal and Antioxidant Properties of Lignins Solubilized during Soda/AQ Pulping of Orange and Olive Tree Pruning Residues. *Molecules*, 2021, 26(13), 3819, doi.org/10.3390/molecules26133819

[161] A. Alzagameem, B. E. Khaldi-Hansen, D. Büchner, M. Larkins, B. Kamm, S. Witzleben and M. Schulze, Lignocellulosic Biomass as Source for Lignin-Based Environmentally Benign Antioxidants. *Molecules*, 2018, 23(10), 2664, doi.org/10.3390/molecules23102664

[162] S. Bock, C. Kijatkin, D. Berben and M. Imlau, Absorption and Remission Characterization of Pure, Dielectric (Nano-)Powders Using Diffuse Reflectance Spectroscopy: An End-To-End Instruction. *Applied Sciences*, 2019, 9(22), 4933, doi.org/10.3390/app9224933

[163] J. P. Blitz, Modern Techniques in Applied Molecular Spectroscopy, ed. F. M. Mirabella, John Wiley & Sons, Inc., Canada, 1, 1998, 5, 185-219

[164] George Aiken, Aquatic Organic Matter Fluorescence, (ed.P. G. Coble, J. Lead, A. Baker, D. M. Reynolds and R. G. M. Spencer), Cambridge university Press,New York, 2014, 2, 35–74

[165] M. Paulsson and J. Parkås, Review: Light-induced yellowing of lignocellulosic pulps – Mechanisms and preventive methods, *BioResources*, 2012, 7(4), 5995-6040

[166] J. Ponomarenko, T. Dizhbite, M. Lauberts, A. Volperts, G. Dobele and G. Telysheva, Analytical pyrolysis – A tool for revealing of lignin structure-antioxidant activity relationship, *Journal of Analytical and Applied Pyrolysis*, 2015, 113, 360-369, doi.org/10.1016/j.jaap.2015.02.027

[167] E. Shin, J. H. Kim, C. S. Park and K. Won, UV absorbing, antioxidant, and antibacterial activities of commercial lignins. *Journal of Bioscience and Bioengineering*, 2009, 108, S56. https://doi.org/10.1016/j.jbiosc.2009.08.160

[168] H. Zhang, X. Wang, J. Wang, Q. Chen, H. Huang, L. Huang, S. Cao and X. Ma, UV–visible diffuse reflectance spectroscopy used in analysis of lignocellulosic biomass material. *Wood Sci. Technol*., 2020, 54:837–846, doi: 10.1007/s00226-020-01199-w

[169] Y. Wang, X. Xiao, S. Wang, K. Li, Y. Jiang, Y. Ma, T. Zhang and R. Ran, Exploration on UV-Blocking Performance of Lignin from Palm (Trachycarpus Fortunei) Fiber, *Journal of Natural Fibers*, 2021, 18:1, 71-79, doi.org/10.1080/15440478.2019.161230

[170] D. A. I. Goring, The physical chemistry of lignin, *Pure and Applied Chemistry*, 1962, doi:10.1351/pac196205010233

[171] A. P. Karmanov, L. S. Kocheva, V. A. Belyi and V. V. Volodin, Transport Properties and Sizes of Lignin Macromolecules in Solution, *Polymer Science, Series A*, 2019, 61(1):53-60, DOI: 10.1134/S0965545X1901005X

[172] D. Dong and A. L. Fricke, Intrinsic viscosity and the molecular weight of kraft lignin, *Polymer*, 1995, 36(10), 2075-2078, doi.org/10.1016/0032-3861(95)91455-G

[173] L. S. Kocheva, A. P. Karmanov and Y. A. Karmanova, Evaluation of the scaling parameters of lignin macromolecules, *Russ Chem Bull*, 2014, 63, 2036–2039, doi.org/10.1007/s11172-014-0696-2

CHAPTER 4

CHEMICAL MODIFICATION OF ALKALI-LIGNIN SUBMICRON PARTICLES THROUGH ACETOBROMINATION

Chapter 4: Chemical modification of alkali-lignin submicron particles through acetobromination

4.1. Introduction

In the context of lignin, the term "acetobromination" describes a particular chemical modification of lignin that involves the simultaneous addition of bromine and acetyl groups to the intricate structure of lignin polymer. Usually, acetyl bromide has widely been used to acetobrominate lignin by dissolving different types of lignocellulosic biomasses in acetic acid medium and to elucidate the structural features of lignin, analytically, i.e., derivatization followed by a reductive cleavage (DFRC) methodology [174]. The physicochemical characteristics of acetobrominated lignin have not yet been thoroughly investigated, nor is there a simple way for concurrently incorporating bromine and acetyl groups in the technical lignin structure.

As the halogenated organic compounds are intensively used as fungicides, herbicides and insecticides; precursors in the synthesis of pesticides; as intermediates in the synthesis of dyes, agricultural chemicals and also pharmaceuticals, therefore bromination of lignin macromolecule has the potential to prepare such industrially important products [175-178].

However, numerous studies have been conducted on the bromination of various chemical substances [179-184]. Although both organic and inorganic materials have been brominated using molecular bromine, but working with molecular bromine is challenging due to its toxicity and high vapour pressure. N-bromosuccinimide can be used as an alternative and safe brominating reagent, but this compound also being synthesized from molecular bromine or hypobromous acid [179, 180]. Bromination of organic compounds containing hydroxyl and carboxyl functional groups can be done using Appel and Hell-Volhard-Zelinsky reactions, respectively and also applying different biocatalytic processes [180]. There are some other approaches were taken to prepare bromine containing bioactive molecules. Recent works reported the chemical modifications of inactive natural products to convert as bioactive materials by introducing new functionalities, e.g. halogenations [181-184]. As a consequence chemically engineered complex and mostly uncharacterized products containing bromine atom were obtained.

Lignin, as a biological macromolecule, has been considered as a valuable raw material for the preparation of different industrially important products through chemical modifications with various reagents [185-190]. In particular, the bromination of lignin with bromine in a hydrophilic protic solvent, acetic acid, is one of the various lignin modification reactions that involve the bromination of lignin through electrophilic aromatic substitution [186]. Phenolic hydroxyl group in the aromatic ring of lignin structure could enhance the electron density to the positions for electrophilic attack [179, 186, 191, 192].

Bromination of lignin can be performed in different ways. Some earlier works showed that acetyl bromide reacts with wood, straw and similar lignocellulosic biomasses and dissolved them well in acetic acid medium with producing bromine containing lignin [193, 194]. Based on the observation, a lignin determination method by acetyl bromide was proposed [195]. In later works on lignocellulosic materials, the acetyl bromide method was modified to investigate structural features and characteristics including molar mass determination of lignin preparations and compositions of monolignols using derivatization followed by reductive cleavage (DFRC) method. Acetyl bromide is well known to acetylate hydroxyl groups and to replace certain hydroxyl functions with bromine and O-acetylated, C-acetylated and αC-brominated lignin products can be obtained. Cleavages of ether bonds in lignin structure and thus the reduction of molar mass would be expected to take place, when lignin is treated with acetyl bromide [174, 195-197].

In a recent work, equimolecular amounts of two main monomers of lignin, e.g. guaiacol and syringol were mixed with activated brominating agent, e.g., N-bromosuccinimide and an ionic liquid and reacted for predefined time at 25 ^{o}C. Halogenated products were extracted using diethyl ether and ethyl acetate, detected the compounds with bromine substituted aromatic nucleus and then quantified [179]. In another study, lignin model compounds were reacted with bromine in chloroform at 28 ^{o}C for one hour, terminated the reaction adding aqueous sodium sulfite and extracted the products by chloroform. Analysis showed that the reactivity of non-condensed guaiacyl, condensed guaiacyl and syringyl nuclei towards bromine is different [198]. In both cases, bromine was introduced into aromatic nucleus in model compounds of lignin macromolecule.

On the other hand, acetyl bromide can reacts with lignin and model compounds (monomeric and dimeric, etc.) in acetic acid medium and O-acetylated the phenolic and aliphatic hydroxyl groups, C-acetylated in aromatic rings and probable bromine substitution to benzylic hydroxyl groups. Demethylation of aromatic methoxyl groups and cleavage of the ether linkages (β-O-4, α-O-4, etc.) could also be observed during acetobromination of lignin. Bromine substituted aromatic nucleus was not reported in conventional acetyl bromide method [197].

$$CH_3COBr + \text{Lignin} \xrightarrow[CH_3COOH]{45\ ^oC} \text{Acetobrominated-lignin} + H_2O$$

Reaction scheme 4.1(a): Reaction of acetyl bromide with lignin in acetic acid media

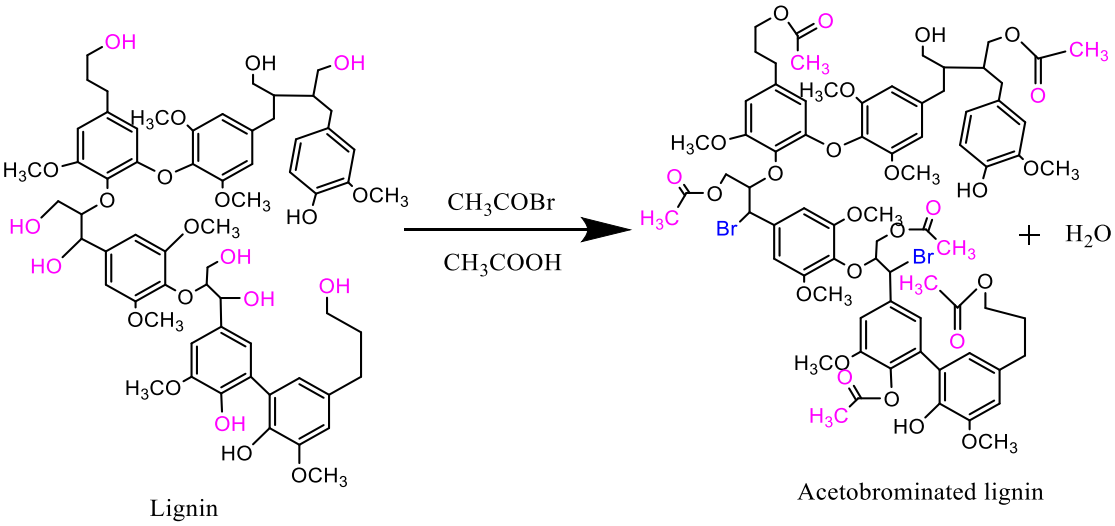

Reaction scheme 4.1(b): Acetobromination of lignin by conventional method

Previous studies demonstrated that the acetic anhydride and bromine molecules can react (reaction scheme 4.2.1) and produce bromoacetic acid and acetyl bromide [199-202]. One mole of acetic anhydride reacts quantitatively with one mole of bromine at 85 ^oC and no hydrogen bromide was evolved. But, further addition of bromine can react with acetyl bromide and forms bromoacetyl bromide and hydrogen bromide (reaction scheme 4.2.2). Hydrogen bromide can catalyse the reaction (reaction schemes 4.2.3 to 4.2.5). It was also reported that the speed of interaction of bromine with acetic anhydride was influenced by the concentration of bromine. The course of the reaction indicated an autocatalytic phenomena and further addition of acetyl bromide caused a considerable acceleration.

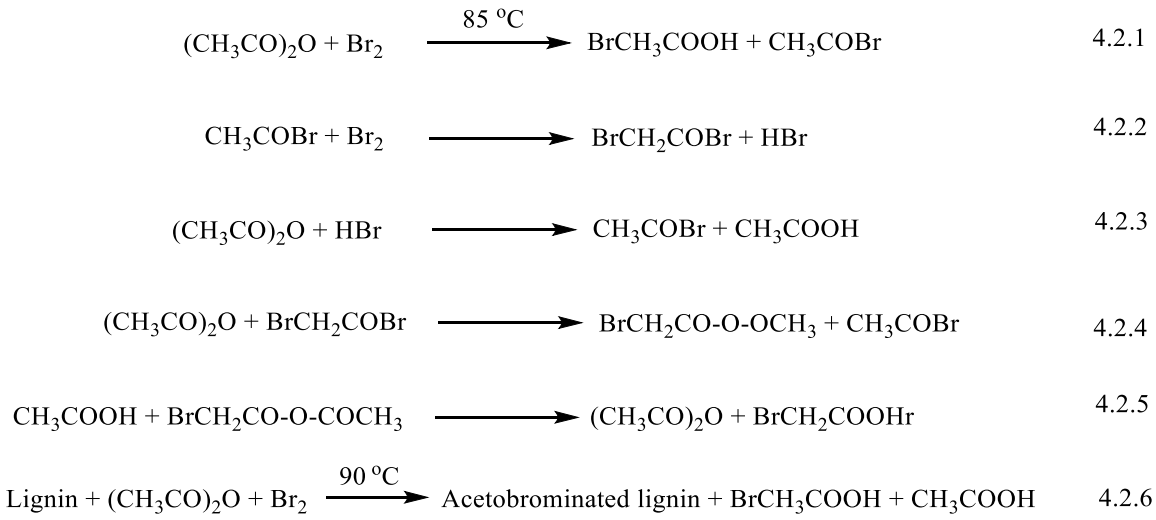

Reaction scheme 4.2: Reactions of acetic anhydride with bromine (equation 4.2.1 to 4.2.5) and reactions of acetic anhydride and bromine with lignin (equation 4.2.6)

Therefore, it was anticipated that acetyl bromide (reaction scheme 4.2.1) produced in-situ would interact with lignin, dissipate during the reaction, and ultimately undergo acetobromination (reaction scheme 4.2.6). Bromoacetic acid, acetic acid, unreacted acetic anhydride, etc. could serve as the reaction medium. Detail investigations on the acetobromination of lignin utilizing acetic anhydride and bromine and characterization of the acetobrominated products need to be performed.

In this work, we have investigated the acetobromination reaction of alkali-lignin using acetic anhydride and bromine in the absence or presence of acetic acid. By applying the flow synthesis process, an effective technique for lignin acetobromination has been created to ensure safety. Acetobromination of alkali-lignin by conventional method were also performed. All acetobrominated alkali-lignin products were separated from the reaction mixtures, purified accordingly and characterized by dfferent instrumental techniques, e.g., SEM-EDX, XPS, FT-MIR-NIR, ^{1}H-NMR, XRD, STA, UV-VIS and DSV. Based on the results obtained a plausible reaction mechanism for lignin acetobromination has been proposed.

4.2. Materials and methods

4.2.1. Materials

Submicron alkali-lignin particles, i.e., CF_AL, BG_AL, TO_AL and GW_AL were used as raw materials in this investigation. Acetyl bromide (Sigma-Aldrich), Glacial acetic acid (Sigma-Aldrich), Bromine (Emparta; ACS reagent), Acetic anhydride (Merck), Dimethyl sulfoxide (Sigma-Aldrich), Tetrahydrofuran (Sigma-Aldrich) and Deionized water (18.2 Mohm) were used as reagents and solvents. Bromocresol green (Sigma-Aldrich) was used as reference standard for SEM-EDX analysis. Densities of dimethylsulfoxide and acetic anhydride were reconfirmed by measuring the densities using an automated density meter (DMA 5000M, Anton-paar, Austria).

4.2.2. Methods

(i) Preparation of acetobrominated alkali-lignin: Conventional method

Alkali-lignin samples, i.e., CF_AL, BG_AL, TO_AL and GW_AL were acetobrominated (reaction scheme 1) by following the procedure described in the literature with some modifications [19, 174]. Moisture-free alkali-lignin particles (0.15 g) were taken in 50 mL glass vial and mixed well with 25 mL glacial acetic acid. Then, 4 mL acetyl bromide was added and stirred at 200 rpm for 3 hours at 25 ^{o}C. After completion of the reaction, acetic acid and residual acetyl bromide were removed by using an efficient rotary evaporator. Products were collected and vacuum dried at 45 ^{o}C until constant weight achieved (Table 4.1).

(ii) Preparation of acetobrominated Coconut fibre alkali-lignin: New methods (i.e., Prepartive method-1 and Preparative method-2)

As the representative sample, moisture-free CF_AL was acetobrominated utilizing varying amounts of acetic anhydride and bromine in the absence or presence of acetic acid. At first, a stock mixture of CF_AL in acetic anhydride was prepared by dissolving 1.5 g of CF_AL in 100 mL acetic anhydride (and small amounts of tetrahydrofuran) with magnetic stirring at 300 rpm for one hour at room temperature. The mixture was then stored into a 250 mL reservoir (R-1). 15 mL pure bromine and 2.5 mL bromine in 23.5 mL acetic acid were taken into another two reservoirs, i.e., R-2 and R-3, respectively. To synthesize the acetobrominated products, continuous flow experiments were conducted

in manual mode by using flow synthesis system (Asia, Syrris, UK) assembled with two syringe pumps, 4 mL PTFE tube reactor, back pressure regulator and a heater. Prepared reactants, i.e., lignin in acetic anhydride (R-1), pure bromine (R-2) and bromine in acetic acid (R-3) were channeled into the tube reactor batch-wise by pumping at specific rates. Residence time was calculated by following equation 4.3:

$$\text{Residence time} = \frac{\text{Volume of the reactor (mL)}}{\text{Flow rate (mL/min)}} \quad (4.3)$$

Pumping was continued for each batch to deliver the calculated amounts of reagents, i.e., lignin (0.15 g) and acetic anhydride and bromine (mole ratios from 1:0.2 to 1:0.6). The reagents were first mixed into a T-piece and then went through the tube reactor. Temperature of the heater was set at 90 ^{o}C and the products were mixed with ice-cooled water. The precipitates were collected by filtration, washed several times with deionized water in order to remove unreacted chemicals, e.g., acetic anhydride, bromine, bromoacetic acid, acetic acid, residual lignin and others. The filtrates, i.e., oily mixtures were stored for the recovery in future works. The precipitates were vacuum dried at 45 ^{o}C until constant weight achieved (Table 4.2). All acetobrominated alkali-lignin samples were readily soluble in tetrahydrofuran, dimethyl sulfoxide, 1,4-dioxane and acetone, but partially soluble in ethanol. Experiments should be carried out inside an efficient fumehood with all personal protection wares.

Characterization of acetobrominated Alkali-lignin

Scanning electron microscopy-energy dispersive X-ray spectroscopic analysis

The Scanning Electron Microscope attached with Energy Dispersive X-Ray Spectrometer (SEM EVO 18, Karl Zeiss, Germany) was employed to study the surface morphology and elemental compositions of moisture-free alkali-lignin and acetobrominated alkali-lignin samples. At first, the samples were mounted on carbon tape with adhesive and sputter-coated with platinum before analysis. Applied electron voltage was 15-20 kV and observations were done with the help of charge compensator. Before the assessment of bromine contents in the synthesized acetobrominated products, SEM-EDX analysis was performed on bromocresol green (structurally comparable to acetobrominated lignin) as reference standard and determined the bromine content with 2.06% relative error and discussed in results and discussion section.

X-ray photoelectron spectroscopic analysis

Surfaces of the selected acetobrominated samples, i.e., CF_AL, CF_AL_AcBr, CF_AL_AcBr-1 and CF_AL_AcBr_AA were analyzed by X-ray photoelectron spectrometer (K-Alpha_KAN, Thermo Fisher Scientific Inc., USA) under high vacuum $2x10^{-9}$ mbar and at room temperature. The moisture-free samples were drop-casted using acetone and dried under vacuum before analysis. The wide scans (200 eV pass energy) were performed to determine the surface elemental composition of the samples. The narrow or high resolution scans (50 eV pass energy) were conducted to evaluate the chemical states or bonding nature of the elements in the samples. The trace elements, e.g. nitrogen, phosphorus and silicon were excluded from high resolution scanning and not considered their contribution in the bond formation in complex molecular architecture of lignin. Gaussian peak profiles were used for the spectral deconvolution of C1s, O1s and Br3d spectra. The C1s peak at 284.82 eV was used as reference to calibrate the binding energy scale. All spectra were reconstructed using OriginPro 2022 software.

Fourier transform mid and near infrared spectroscopic analysis

The moisture-free acetobrominated samples were analyzed in transmission mode using a FT-MIR-NIR Spectrometer (Frontier, Perkin-Elmer, UK) in transmission mode. The MIR spectral range was 400 to 4000 cm^{-1} at a spectral resolution of 4 cm^{-1} and number of scans was 32. The samples were also analyzed by using a Near Infrared Reflectance Accessory (NIRA) attached with the spectrometer. The NIR spectral range was 4,000 to 8,000 cm^{-1} at a spectral resolution of 16 cm^{-1} and number of scans was 32. NIR transparent glass vial was used as sample container. All spectra were recorded, stored in computer memory and reconstructed using OriginPro 2022 software.

Nuclear magnetic resonance spectroscopic analysis

^{1}H-NMR analysis was performed on selected acetobrominated samples, i.e., CF_AL, CF_AL_AcBr, CF_AL_AcBr-1 and CF_AL_AcBr_AA by 600 MHz FT-NMR spectrometer (600 MHz, Ascend, Bruker, Germany) in d_6-DMSO solution (25 mg samples in 0.5 mL d_6-DMSO). Experimental temperature was 25 ^{o}C in the FT mode with the pulse width 10.5 sec (90^{o} pulse), the data acquisition time about 5.4 s without a pulse delay, and the number of scans was 128. ^{13}C-NMR spectra of selected CF_AL and CF_AL_AcBr_AA samples were captured using the same solution. Number of scans was

12000 and data acquisition time was about 12 hours without a pulse delay. Qualitative assessments, e.g., evaluation of aromatic proton and nature of carbon in the samples were done. In order to confirm the bromine substitution in aromatic nucleus, heteronuclear single quantum coherence (HSQC), i.e., ^{13}C-^{1}H correlation NMR spectroscopic experiments were performed on CF_AL_AcBr_AA and CF_AL. In HSQC experiment, a 90^{o} pulse was applied to the ^{1}H nuclei, and a series of ^{13}C pulses were applied to selectively excite the ^{13}C nuclei in a one-bond coupling relationship with the ^{1}H nuclei. Spectral acquisition time was 18 h at 25 ^{o}C. The resulted cross-peaks in the HSQC-NMR spectra were examined and discussed in result and discussion section.

Field emission-scanning electron microscopic analysis

Analyses of the size and morphology of CF_AL and CF_AL_AcBr_AA particles were done by Field Emission Scanning Electron Microscope (JEOL JSM-7610F, Japan). The moisture-free powdered samples were dissolved in tetrahydrofuran and then dispersed in deionized water. A small drop of the dispersion was taken on carbon tape attached with a sample stage, dried using a microwave oven and then sputter-coated with platinum before analysis. The FE-SEM images of the samples were presented and discussed in result and discussion section.

X-ray diffraction analysis

X-ray diffraction (XRD) analysis was performed on CF_AL and acetobrominated CF_AL samples, i.e., CF_AL_AcBr, CF_AL_AcBr-1 and CF_AL_AcBr_AA, under ambient temperature and pressure in the diffraction angle, 2θ ranging from 5 to 90^{o}. The structural analysis was carried out by Thermo Scientific ARL EQUINOX 1000 Benchtop X-Ray Diffractometer (XRD) with a monochromatic copper anode source of Cu-Kα radiation, λ= 0.1548 nm in coplanar asymmetric geometry and operated at 40 kV and 30 mA. The mean crystallite sizes of the ordered domains were estimated by Scherrer's equation 4.4-

$$d = \frac{B\lambda}{\beta \cos\theta} \qquad (4.4)$$

here,

d = Mean crystallite size
B = Dimensionless shape factor
λ = X-ray wavelength (Cu Kα = 0.1548 nm)
β = Full width at half maxima

Simultaneous thermal analysis

Silmultaneous thermal analyses (i.e., thermogravimetric and differential scanning calorimetric analyses) were performed on selected moisture-free acetobrominated alkali-lignin samples using a Simultaneous Thermal Analyzer equipped with a thermobalance and TG-DSC sample carrier (Jupiter F3, Netzsch, Germany). About 10 mg of each sample was placed in an alumina crucible and then measured under a high-purity nitrogen atmosphere (50 ml/min), with the temperature progressively increasing from 30 to 850 °C at a heating rate of 10 °C/min. The thermobalance continuously recorded the mass change during decomposition of the samples with increasing temperature, and the TG characteristics were determined as the percent weight loss related to the initial weight as a function of temperature. The first derivatives of TG (or DTG) were calculated to determine the most intensive mass losses of the samples. Meanwhile, the DSC results were recorded as the changes in heat flow in the sample increased with temperature, and temperature ranges (RT to 240 ^{o}C, 240 to 420 ^{o}C and 420 to 850 ^{o}C) were established for all samples based on the first derivatives of DSC (or DDSC). The DDSC curves were used instead of DTG curves to obtain more information on the thermal phenomena. Maximal values of the energetic effects within the temperature ranges were read from the DSC curves at temperatures corresponding to the characteristic points on the DDSC curves. The thermal changes of all samples were recorded, stored in computer memory, and reconstructed using OriginPro 2022 software.

Ultraviolet-Visible spectroscopic analysis

The powdered acetobrominated samples were dissolved in DMSO at about 10 ppm concentrations and then analyzed by UV-Vis spectrophotometer (Lambda 35, Perkin-Elmer, Singapore). The spectra were acquired from 190 to 800 nm at 1 nm step. UV-Vis spectra of all samples were recorded, stored in computer memory, and reconstructed using OriginPro 2022 software.

Determination of Intrinsic Viscosity

Automated microviscometer (Lovis 2000M, Anton-paar, Austria) was used for the intrinsic viscosity measurement of acetobrominated samples in dimethylsulfoxide. The measurements were done maintaining the temperature at 25 ^{o}C and inclination 35^{o} with 1^{o} steps. Steel made capillary of radius of 1.59 mm was used for all measurements. The

automated microviscometer has the ability to measure absolute viscosity of solution ranging from 0.3 to 10,000 mPa.s with up to 0.5% accuracy, temperature accuracy 0.02 ^{o}C and accuracy of measuring time up to 0.05%. Billmeyer equation 3.3 was used to calculate intrinsic viscosity of acetobrominated alkali-lignin samples.

4.3. Results and discussion

4.3.1. Synthesis of acetobrominated alkali-lignin samples by conventional and new methods (i.e., Preparative method-1 and Preparative method-2)

Alkali-lignin samples, i.e., CF_AL, BG_AL, TO_AL and GW_AL (150 mg each), while reacted with acetyl bromide in acetic acid medium (Conventional method) produced 0.41, 0.25, 0.49 and 0.30 mg of acetobrominated products, e.g., CF_AL_AcBr, BG_AL_AcBr, TO_AL_AcBr and GW_AL_AcBr, respectively (Table 4.1).

Table 4.1: Reactions of acetyl bromide with alkali-lignin submicron particles in acetic acid medium (conventional method)

Sample	Amount (g)	Glacial acetic acid (mL)	Acetyl bromide (mL)	Product obtained (g)	Acronym
CF_AL	0.15	25	4	0.41	CF_AL_AcBr
BG_AL				0.25	BG_AL_AcBr
TO_AL				0.49	TO_AL_AcBr
GW_AL				0.30	GW_AL_AcBr

On the other hand, CF_AL produced 0.23, 0.25, 0.27, 0.28 and 0.30 g of acetobrominated products, i.e., CF_AcBr-1 to CF_AL_AcBr-5, respectively, while pure bromine was added to acetic anhydride-lignin mixture at different mole ratios of acetic anhydride to bromine, i.e., 1:0.2, 1:0.3, 1:0.4, 1:0.5 and 1:0.6, respectively, in the absence of acetic acid (Preparative method-1). Amounts of acetobrominated products (CF_AL_AcBr-1 to CF_AL_AcBr-5) were increased with increasing amounts of bromine (Table 4.2). Interestingly, these amounts were lower than the products generated using conventional acetobromination method. It was potentially due to degradation of lignin under applied reaction conditions in Preparative method-1.

When bromine in acetic acid solution of was used (Preparative method-2) maintaining acetic anhydride to bromine mole ratio of 1:0.2, significantly higher amount of product (CF_AL_AcBr_AA) was obtained (Table 4.2). It was revealed that the presence of acetic

acid as the solvent of bromine in Preparative method-2 showed a positive impact on the conversion process. It was also observed that the solution of bromine in acetic acid made the acetobromination process simpler and safer than using bromine directly into acetic anhydride-lignin mixture because of high volatility of pure bromine. Schematic representation of flow synthesis process for lignin acetobromination (i.e., Preparative method-1 and Preparative method-2) and some photographs of acetobrominated lignin products have been given in Figure 4.1a and 4.1b, respectively.

Table 4.2: Reactions of Coconut fibre alkali-lignin particles (CF_AL) with acetic anhydride and bromine in the absence of acetic acid (i.e., Preparative method-1; SN 1-5) and the presence of acetic acid (i.e., Preparative method-2; SN 6)

SN	Pump-1 flow rate (mL/min)	Pump-2 flow rate (mL/min)	Total flow rate (mL/min)	Residence time (min)	Mole ratio of acetic anhydride to bromine	Product obtained (g)	Product acronym
1	0.465	0.050	0.515	7.76	1:0.2	0.23	CF_AL_AcBr-1
2	0.465	0.075	0.540	7.40	1:0.3	0.25	CF_AL_AcBr-2
3	0.465	0.100	0.565	7.08	1:0.4	0.27	CF_AL_AcBr-3
4	0.465	0.125	0.590	6.78	1:0.5	0.28	CF_AL_AcBr-4
5	0.465	0.150	0.615	6.50	1:0.6	0.30	CF_AL_AcBr-5
6	0.465	0.520	0.985	4.08	1:0.2	0.29	CF_AL_AcBr_AA

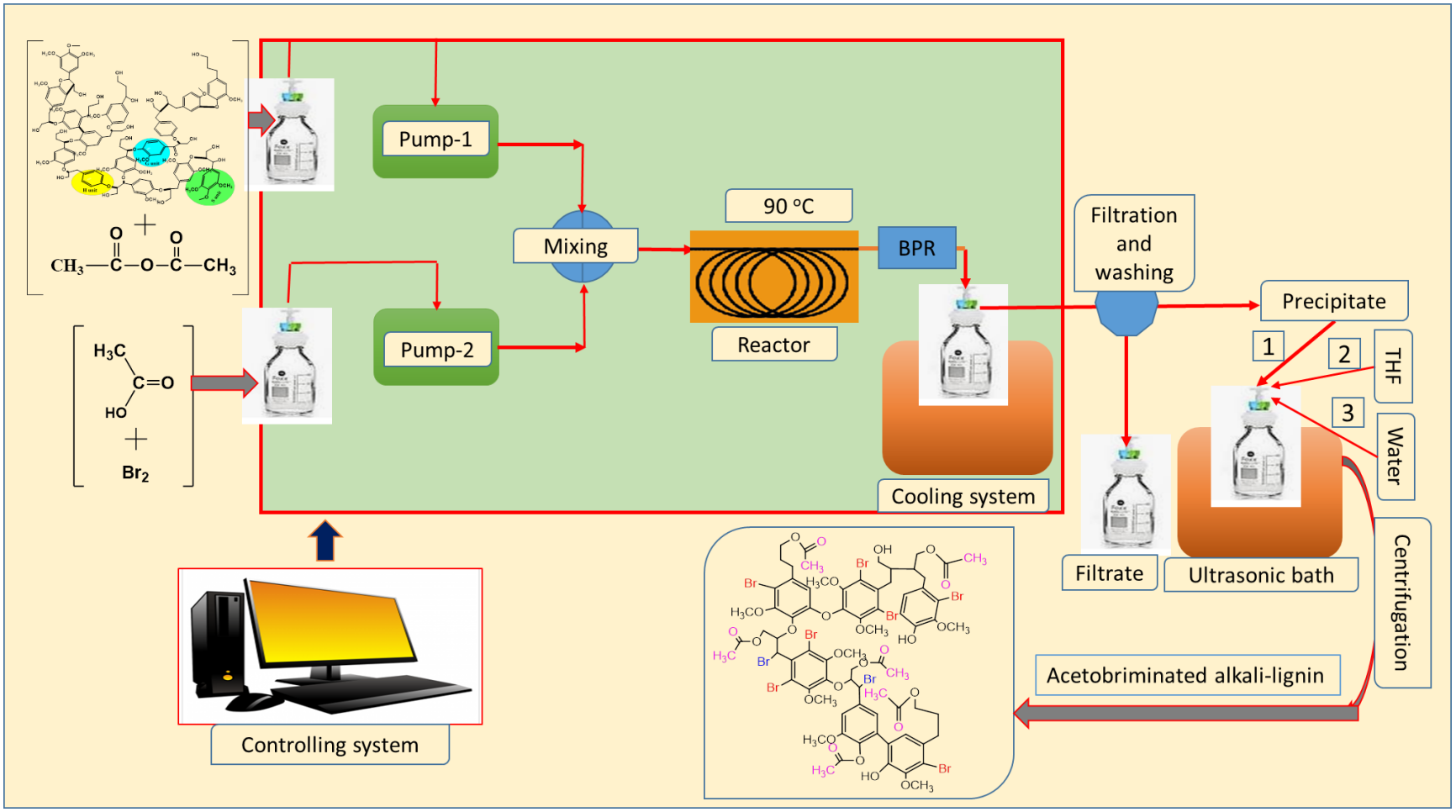

Figure 4.1a: Continuous flow synthesis of acetobrominated alkali-lignin by utilizing acetic anhydride and bromine in the presence or absence of acetic acid. Products of the acetobromination reaction were mixed with ice-cooled deionized water for precipitatation and subsequent recovery of acetobrominated alkali-lignin.

CF_AL

BG_AL

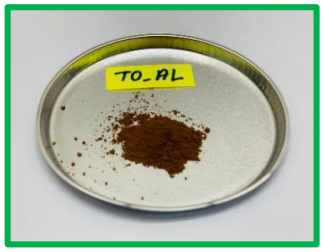

TO_AL

GW_AL

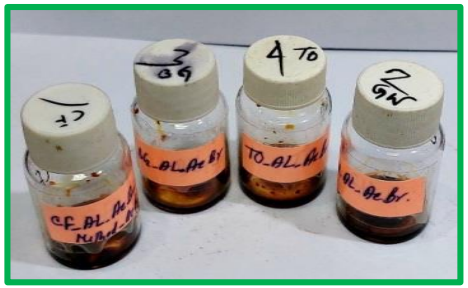

CF_AL_AcBr to GW_AL_AcBr

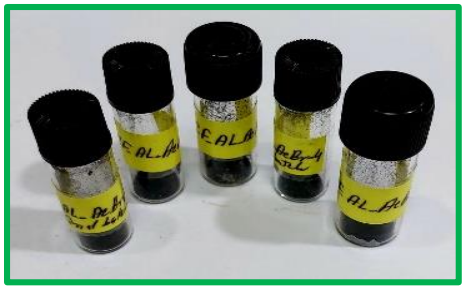

CF_AL_AcBr-1 to CF_AL_AcBr-5

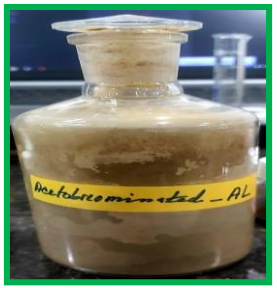

CF_AL_AcBr_AA

CF_AL_AcBr-1 to CF_AL_AcBr-5 in DMSO

CF_AL_AcBr_AA in DMSO

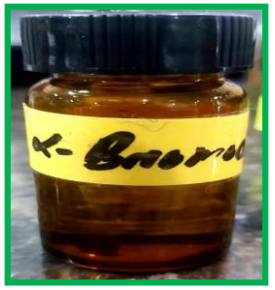

Oily filtrate

Figure 4.1b: Photographs of alkali-lignin and acetobrominated alkali-lignin samples synthesized by conventional and new methods. All of the products were extremely soluble in DMSO at room temperature. Oily filtrate generated during washing of the acetobrominated products synthesized by new methods.

4.3.2. Characterisation of acetobrominated alkali-lignin

Scanning electron microscopy-energy dispersive X-ray spectroscopic analysis: Determination of bromine contents in acetobrominated alkali-lignin

SEM micrographs of acetobrominated lignin products and bromocresol green (as reference standard) have been presented in Figure 4.2(a-k) and Figure 4.2(l) and elemental compositions as atomic and weight percentages in Table 4.3 and Table 4.4, respectively.

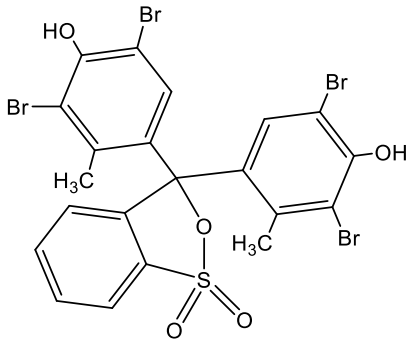

Bromocresol green

Actual atomic percentage of bromine in bromocresol green is 8.88. Thus, the relative error could be measured by following equation 4.5:

$$\text{Relative error} = \left| \frac{\text{Actual value - Expected value}}{\text{Expected value}} \right| \times 100\% \qquad .(4.5)$$

$$\text{Thus, Relative error} = \left| \frac{8.88 - 8.70}{8.70} \right| \times 100 = 2.06\%$$

Table 4.3: SEM-EDX data of bromocresol green (structurally comparable to acetobrominated lignin) as reference standard

Sample	Weight %				Atom %			
	Carbon	Oxygen	Bromine	Sulfur	Carbon	Oxygen	Bromine	Sulfur
Bromocresol green	45.50	13.23	36.22	5.02	72.48	15.79	8.70	3.02

It could be observed that atomic percentages of carbon and oxygen in the surface of CF_AL samples were 66.59 and 33.31%, respectively. After acetobromination by conventional method, atomic percentage of carbon slightly increased from 66.59 to 67.74%, while oxygen percentage decreased from 33.31 to 31.33%.

Only 0.93% bromine atom was added to CF_AL and produced CF_AL_AcBr. Atomic percentages of bromine in BG_AL_AcBr, TO_AL_AcBr and GW_AL_AcBr samples were 0.91, 1.12 and 0.68%, respectively. These amounts of bromine were similar to CF_AL_AcBr and indicated that only small amounts of bromine could be introduced into alkali-lignin structure by conventional acetobrmination method.

On the other hand, higher atomic percentages of bromine (3.08 to 4.20%) could be added to CF_AL by Preparative method-1 and Preparative method-2. At the same time, atomic percentages of carbon increased significantly from 66.69 to 77.25%, while oxygen percentages decreased from 33.31 to 19.25%. Increased mole ratios of bromine in acetic anhydride: bromine solution did not increase the bromine contents significantly in the CF_AL structure, although the product amount increased with increasing bromine concentrations (Table 4.2). Thus, the preparative methods enabled to insert 3.57 ± 0.28% bromine atoms (i.e., 18.64 ± 1.23% weight) into CF_AL under applied reaction conditions.

Lu and Ralph showed that the acetobromination of lignin with acetyl bromide in acetic acid medium can cleanly derivatized lignin sample [203]. In this reaction, benzylic hydroxyl group substituted by bromine and all of the free phenolic and aliphatic hydroxyl groups could be acetylated (reaction scheme 4.1b) under mild conditions, e.g. acetobromination at 25 ^{o}C for three hours. Acetylation of alcohols and phenols with acetyl halides using basic or acidic catalysts is well known, although acetyl bromide is rarely used for preparative reactions. It was also showed that the relative rates of reactions between acetyl bromide and β-aryl ether lignin model compounds under mild conditions are:

Primary γ-OH acetylation >benzyl aryl ether cleavage/bromination > Benzylic secondary α-OH acetylation >Benzylic acetate to benzylic bromide interconversion >>Phenolic-OH acetylation.

According to Iiyama and Wallis, the reactions take place between monomeric lignin models and acetyl bromide during acetobromination of lignin are O-acetylation of phenolic and aliphatic hydroxyl groups, probable C-acetylation of aromatic rings (in presence of perchloric acid), bromine substitution of benzylic hydroxyl groups and demethylation of aromatic methoxyl groups. But, no β-aryl ether cleavage or demethylation was detected during acetobromination by conventional method under mild reaction conditions [196].

Table 4.4: Surface elemental compositions of acetobrominated alkali-lignin samples by SEM-EDX technique

Sample	%Weight			%Atom		
	Carbon	Oxygen	Bromine	Carbon	Oxygen	Bromine
CF_AL	59.68	39.76	-	66.59	33.31	-
CF_AL_AcBr	58.58	36.09	5.33	67.74	31.33	0.93
BG_AL_AcBr	68.02	26.62	5.36	76.59	22.50	0.91
TO_AL_AcBr	63.15	30.38	6.47	72.65	26.23	1.12
GW_AL_AcBr	52.46	43.66	3.88	61.13	38.19	0.68
CF_AL_AcBr-1	59.60	23.97	16.43	74.44	22.48	3.08
CF_AL_AcBr-2	57.96	22.56	19.48	74.47	21.76	3.76
CF_AL_AcBr-3	57.53	21.09	21.37	75.13	20.68	4.20
CF_AL_AcBr-4	58.91	23.55	17.55	74.36	22.31	3.33
CF_AL_AcBr-5	57.46	23.98	18.57	73.43	23.00	3.57
CF_AL_AcBr_AA	61.23	20.33	18.45	77.25	19.25	3.50

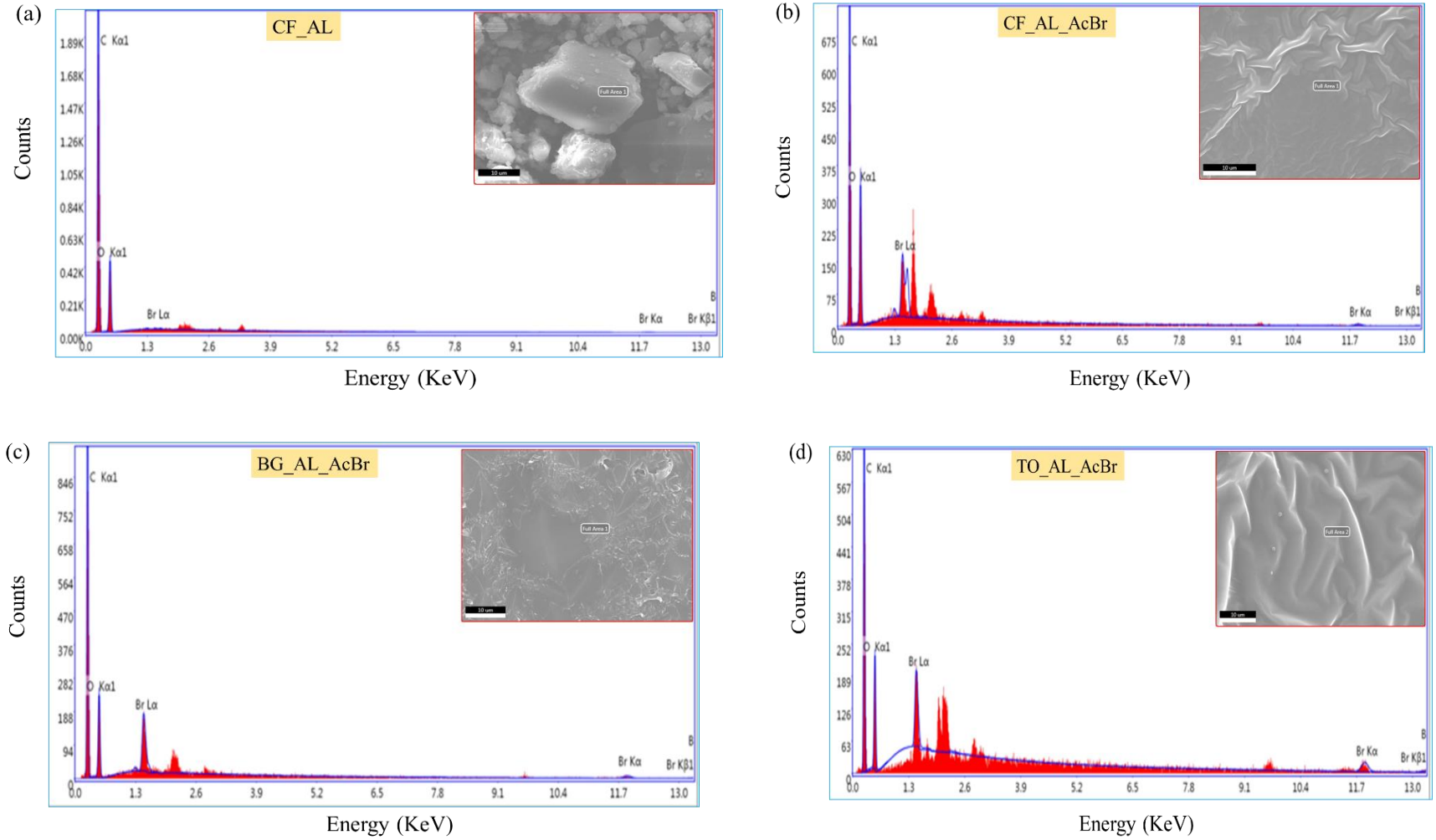

Figure 4.2: SEM-EDX spectra of (a) CF_AL (b) CF_AL_AcBr (c) BG_AL_AcBr and (d) TO_AL_AcBr samples

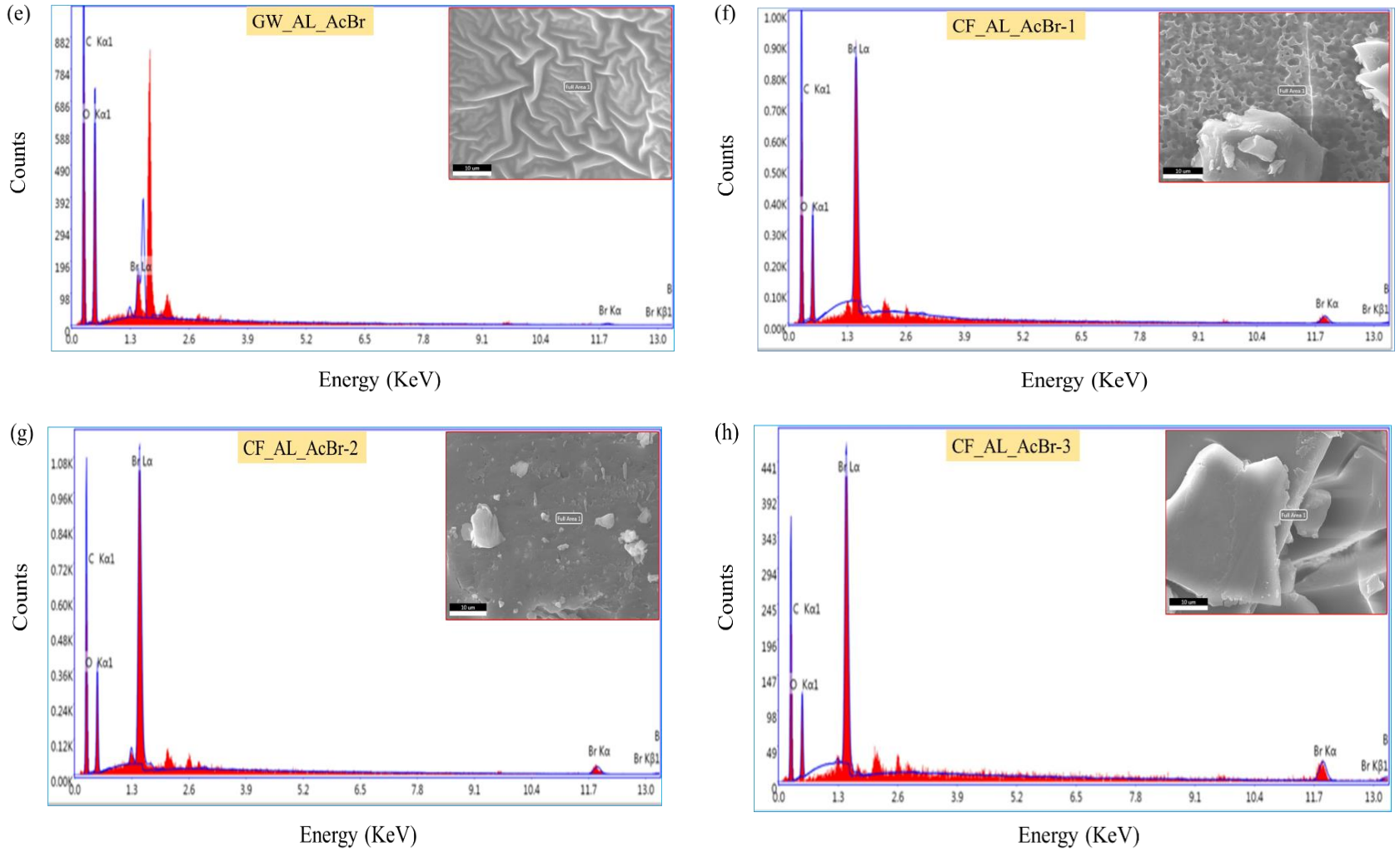

Figure 4.2: SEM-EDX spectra of (e) GW_AL_AcBr, (f) CF_AL_AcBr-1, (g) CF_AL_AcBr-2 and (h) CF_AL_AcBr-3

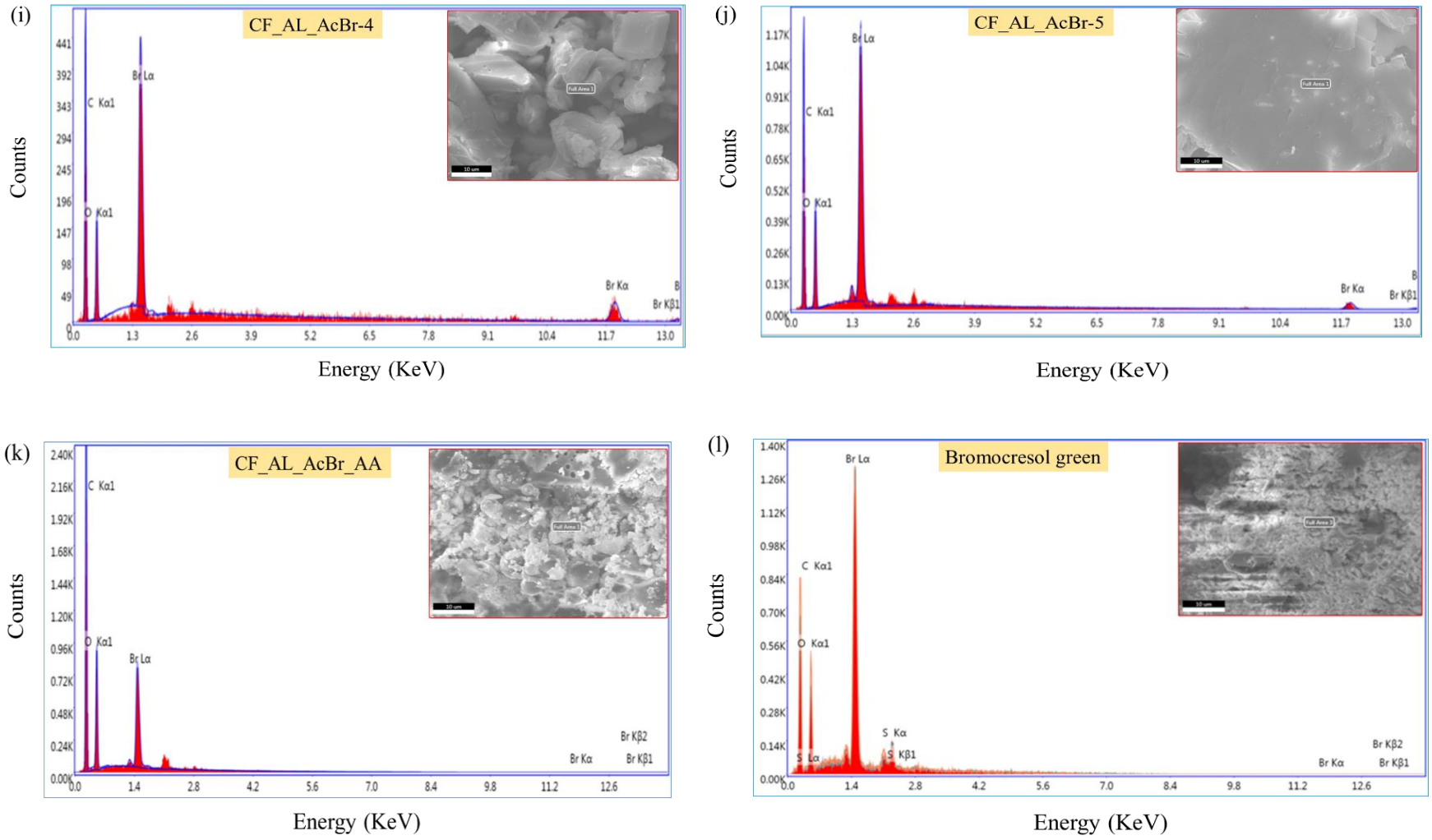

Figure 4.2: SEM-EDX spectra of (i) CF_AL_AcBr-4, (j) CF_AL_AcBr-5, (k) CF_AL_AcBr_AA and (l) Bromocresol green

X-Ray photoelectron spectroscopic analysis: Chemical states of the elements in acetobrominated alkali-lignin samples

Results of the wide scan and high resolution deconvoluted spectra of selected samples, i.e., CF_AL, CF_AL_AcBr, CF_AL_AcBr-1 and CF_AL_AcBr_AA have been presented in Figure 4.3 and Table 4.5 and Figure 4.4 to 4.7 and Table 4.6 to 4.9, respectively.

Table 4.5: Surface elemental compositions (% atom) of CF_AL and acetobrominated samples by X-ray photoelectron spectroscopy

Sample	C	O	Br	O/C	Br/C
CF_AL	62.28	31.30	-	0.50	-
CF_AL_AcBr	61.96	23.68	0.24	0.38	0.003
CF_AL_AcBr-1	63.63	28.51	3.47	0.45	0.054
CF_AL_AcBr_AA	70.31	24.01	5.67	0.34	0.080

It could be observed that surface elemental compositions of the acetobrominated products (Table 4.5) differed from the results obtained by SEM-EDX technique (Table 4.4). This difference was probably due to different interaction volume, e.g., volume of surface of the samples including volume beneath these. The depth of the interaction depends upon the energy of the incident beams, e.g., electron beam in SEM-EDX and X-ray in XPS analyses. Thus, there was a high possibility that the results for various total areas of analysis contributed to the observed difference in surface elemental compositions.

Atomic percentages of bromine increased in the cases of CF_AL_AcBr-1 (3.47%) and CF_AL_AcBr_AA (5.67%) as compared to CF_AL_AcBr (0.24%), which followed similar trends to the results obtained from SEM-EDX analysis. At the same time, atomic percentages of oxygen decreased from 31.30 to 24.01%, while percentages of carbon increased from 62.28 to 70.31%. These results confirmed the incorporation of bromine into CF_AL by conventional and preparative methods for the acetobromination.

The presence of acetic acid in Preparative method-2 facilitated the overall acetobromination reaction and support to introduce higher amount of bromine than conventional and also Preparative method-1.

High resolution deconvoluted spectra of CF_AL, CF_AL_AcBr, CF_AL_AcBr-1 and CF_AL_AcBr_AA could be grouped into C_1 to C_4 for C(1s) and C_5($Br3d_{5/2}$) and

$C_6(Br3d_{3/2})$ for Br3d classes. Based on the deconvoluted spectra obtained, ratios of carbon (1s) in C_1 to C_4 components and bromine (3d) in C_5 and C_6 components could be estimated using corresponding photoelectron (PE) peak areas by Equation 3.4 and given in Table 4.10. It could be observed that the estimated ratios of C(1s) and Br(3d) components showed variation due to acetobromination of CF_AL by Conventional and Preparative methods. C_1 component of CF_AL_AcBr showed no significant change in comparison to CF_AL, but C_2 component increased to some extent, indicated the formation of new C-Br bond in CF_AL. C_3 component was not observed in CF_AL_AcBr, although the ratio of C_4 component increased from 0 to 3.70%. It was potentially due to the acetylation in aliphatic or phenolic hydroxyl groups of CF_AL.

It is interesting that sp^2C-Br bond in bromobenzene gives a C(1s) PE peak at 285.10 eV, but C(1s) PE peak of C-Br in CF_AL_AcBr was found at 286.40 eV. On the other hand, C(1s) PE peak of sp^3C-Br in dibromomethane gives a PE peak at 287.1 eV [33]. Thus, the binding energy of C(1s) in C-Br of CF_AL_AcBr lies between the binding energies of sp^2C-Br in bromobenzene and sp^3C-Br in dibromomethane. So, it could be assumed that a single bromine atom attached to sp^3 C in CF_AL_AcBr structure and formed sp^3 C-Br bond, e.g., α-bromo substituted CF_AL_AcBr. Evidences showed that no bromine substitution occurred in the aromatic rings of the monolgnols during acetobromination of alkali-lignin by conventional method.

Due to the presence of small amount of bromine in CF_AL_AcBr, $C_5(Br3d_{5/2})$ and $C_6(Br3d_{3/2})$ components were observed and showed similarity with Br3d components of Bromanil (Figure 4.8). Binding energies of C_5 ($Br3d_{5/2}$) and $C_6(Br3d_{3/2})$ PE peaks were 70.44 and 71.49 eV, respectively. These binding energies were slightly higher than the binding energies of the Br3d components in Bromanil, e.g., 70.10 eV for $Br3d_{5/2}$ and 71.15 eV for $Br3d_{3/2}$ [204]. No bromide ion (Br^-) detected in the sample as there was no XPS PE peak observed below 70.00 eV.

In the cases of CF_AL_AcBr-1 and CF_AL_AcBr_AA, C_2 components increased to a greater extent from 14.61 to 31.99 and 36.71%, while C_1 component largely decreased from 80.85 to 56.17 and 51.35%, respectively. These were due to probable bromine substitution in the CF_AL structure. At the same time, C_4 components of CF_AL increased from 0 to 11.83 and 11.92% in CF_AL_AcBr-1 and CF_AL_AcBr_AA, respectively, as an indication of the incorporations of acetyl group in CF_AL structure.

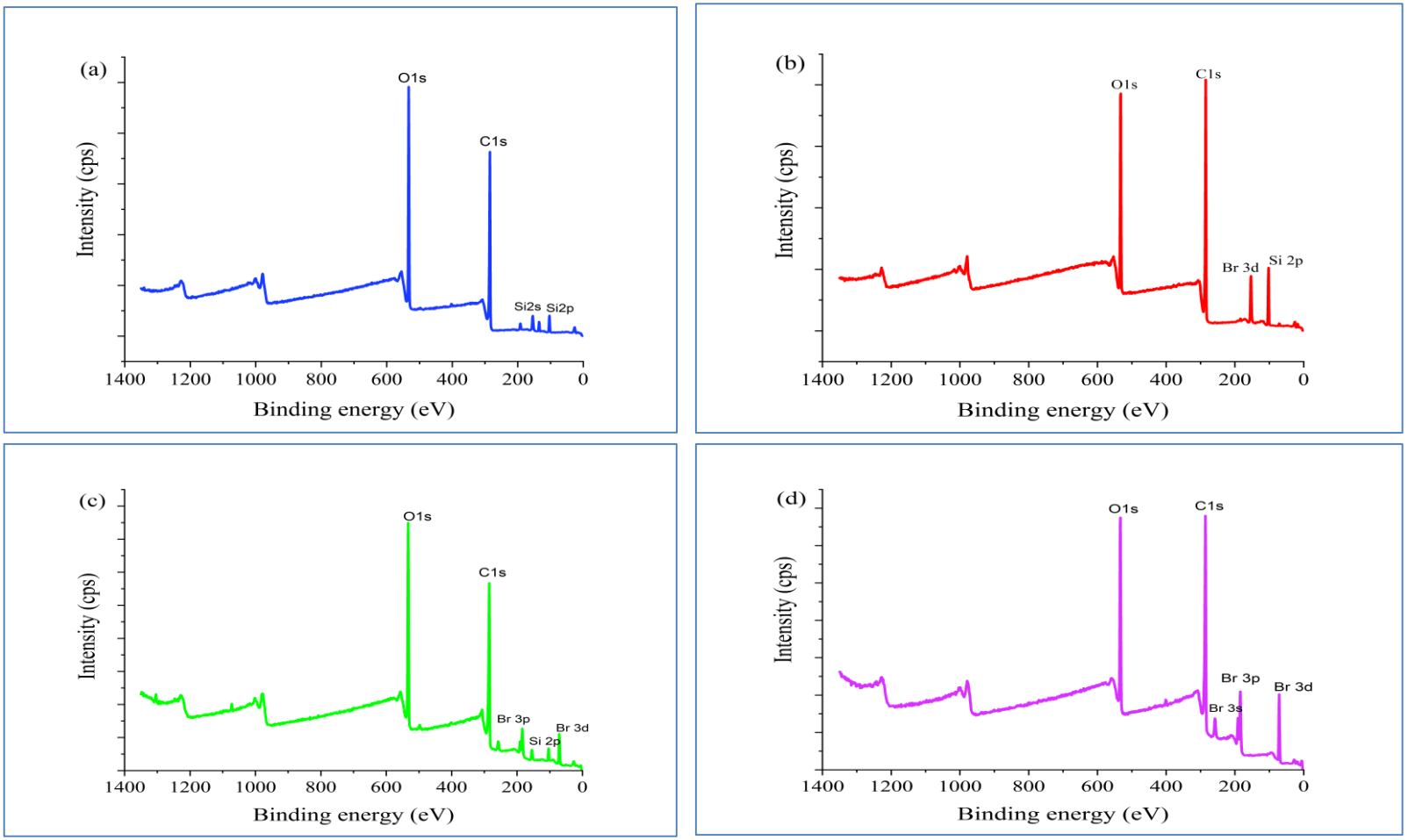

Figure 4.3: XPS wide scan spectra of CF_AL and acetobrominated products (a) CF_AL (b) CF_AL_AcBr (c) CF_AL_AcBr-1 and CF_AL_AcBr_AA

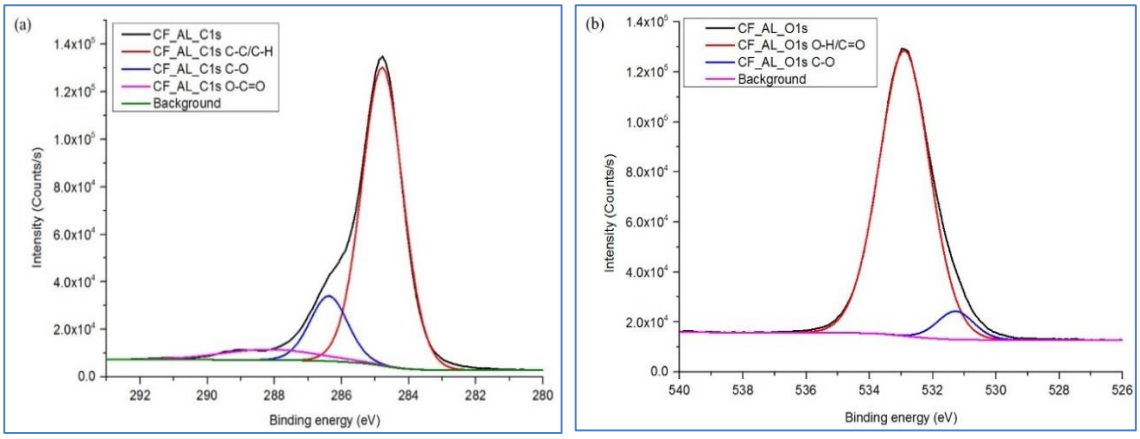

Figure 4.4: XPS high resolution deconvoluted spectra of CF_AL (a) C1s spectra and (b) O1s spectra

Table 4.6: High resolution XPS spectral data of CF_AL

Scan	Peak BE (eV)	Height (CPS)	Height ratio	Peak area (CPS.eV)	Area ratio	Atomic%	Chemical state
C_1	284.79	125709.41	1	195512.13	1	55.19	C1s , C-C/C-H
C_2	286.38	27479.46	0.22	39350.92	0.20	11.12	C1s, C-O
C_3	288.14	4470.13	0.04	16302.36	0.08	4.61	C1s, O-C-O/C=O
C_4	289.35	-	-	-	-	-	C1s, O-C=O/O=COR
O_1	532.90	114164.88	1	232231.25	1	27.14	O1s, -OH/C=O
O_2	531.28	11331.64	0.10	16530.39	0.07	1.93	O1s, C-O

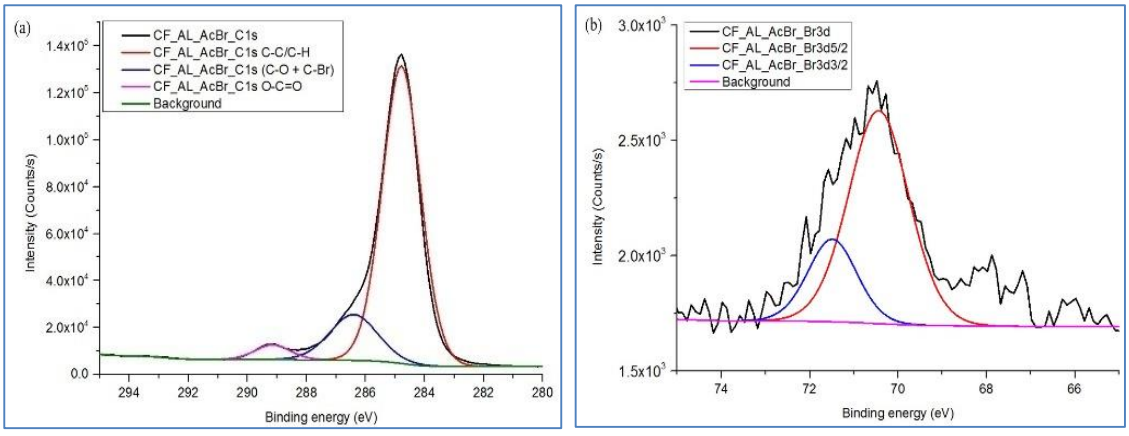

Figure 4.5: XPS high resolution deconvoluted spectra of CF_AL_AcBr (a) C1s spectra and (b) Br3d spectra

Table 4.7: High resolution XPS spectral data of CF_AL_AcBr

Scan	Peak BE (eV)	Height (CPS)	Height ratio	Peak area (CPS.eV)	Area ratio	Atomic%	Chemical state
C_1	284.79	126897.81	1	208922.78	1	48.55	C1s , C-C/C-H
C_2	286.40	19547.41	0.15	40239.67	0.19	10.1	C1s, (C-O + C-Br)
C_3	288.14	-	-	-	-	-	C1s, O-C-O/C=O
C_4	289.15	6298.58	0.05	9593.18	0.05	2.41	C1s, O-C=O/O=COR
C_5	70.44	925.67	1	1608.72	1	0.22	Br3d5/2, C-Br
C_6	71.49	359.19	0.16	504.19	0.2	0.10	Br3d3/2, C-Br

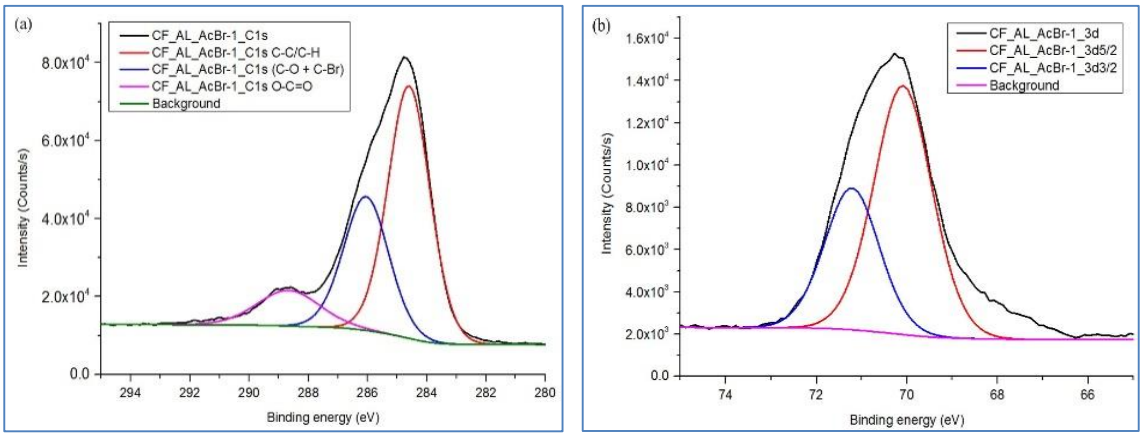

Figure 4.6: XPS high resolution deconvoluted spectra of CF_AL_AcBr-1 (a) C1s spectra and (b) Br3d spectra

Table 4.8: High resolution XPS spectral data of CF_AL_AcBr-1

Scan	Peak BE (eV)	Height (CPS)	Height ratio	Peak area (CPS.eV)	Area ratio	Atomic%	Chemical state
C_1	284.60	64811.68	1	116854.71	1	35.46	C1s , C-C/C-H
C_2	286.05	34358.64	0.53	66556.02	0.57	20.22	C1s, (C-O + C-Br)
C_3	288.14	-	-	-	-	-	C1s, O-C-O/C=O
C_4	288.67	9142.66	0.14	24622.3	0.21	7.49	C1s, O-C=O/O=COR
C_5	70.09	11793.47	1	19228.1	1	1.88	Br3d5/2, C-Br
C_6	71.22	11793.47	0.57	10376.72	0.54	1.02	Br3d3/2, C-Br

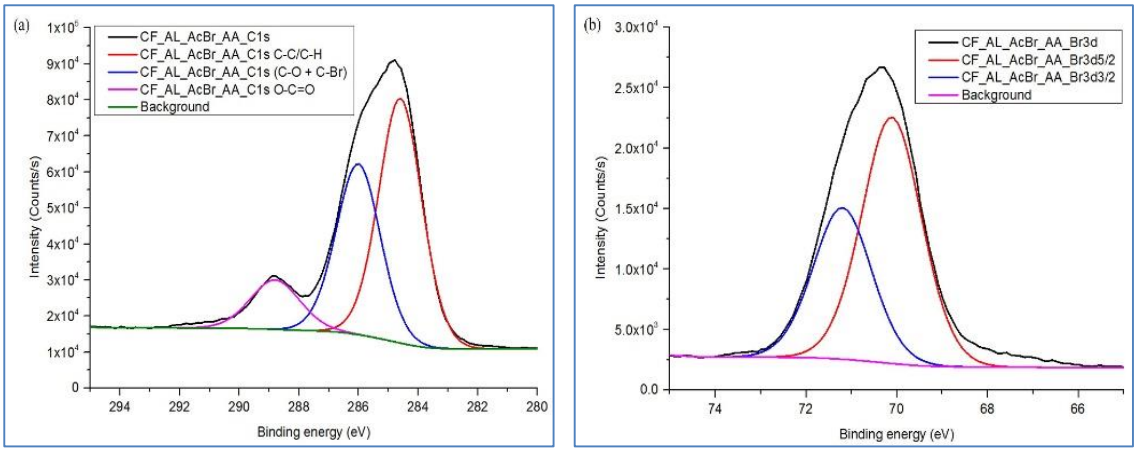

Figure 4.7: XPS high resolution deconvoluted spectra of CF_AL_AcBr_AA (a) C1s spectra and (b) Br3d spectra

Table 4.9: High resolution XPS spectral data of CF_AL_AcBr_AA

Scan	Peak BE (eV)	Height (CPS)	Height ratio	Peak area (CPS.eV)	Area ratio	Atomic %	Chemical state
C_1	284.60	67869.22	1	125185.03	1	35.91	C1s , C-C/C-H
C_2	286.01	47409.97	0.70	89498.39	0.71	25.70	C1s, (C-O + C-Br)
C_3	288.14	-	-	-	-	-	C1s, O-C-O/C=O
C_4	288.80	13705.52	0.20	29075.21	0.23	8.36	C1s, O-C=O/O=COR
C_5	70.11	20368.18	1	34112.16	1	3.16	Br3d5/2, C-Br
C_6	71.20	12532.14	0.62	20564.53	0.6	1.90	Br3d3/2, C-Br

Table 4.10: Percentages of C1s and Br3d components of carbon and bromine and their chemical states in CF_AL and its selectrd acetobrominated products.

Scans for C1s and Br3d components	Chemical states	Binding energy, eV [124-126, 204]	Percentages of C1s and Br3d components in alkali-lignin			
			CF_AL	CF_AL_AcBr	CF_AL_AcBr-1	CF_AL_AcBr_AA
*C_1	C-C, C-H/ C=C, =C-H	284.60-284.79 (284.80)	80.85	80.74	56.17	51.35
C_2	C-O-C/ C-OH/ (C-O + C-Br)	286.01-286.40 (286.10-286.30)	14.61	15.55	31.99	36.71
C_3	C=O/O-C-O	288.08 (288.00)	4.53	-	-	-
C_4	O-C=O/ O=COR	288.80-289.15 (288.35-289.50)	-	3.70	11.83	11.92
C_5 ($Br3d_{5/2}$)	C-Br	70.11-70.44 (70.10)	-	76.14	64.95	62.38
C_6($Br3d_{3/2}$)	C-Br	71.22-71.49 (71.15)	-	23.86	35.05	37.62
Br3d	Br-	- (68.50-69.20)	Not detected	ND	ND	ND

*C1s in (C-C/C-H) and (C=C/=C-H) has been mentioned as C1sC-C/C-H in spectral curves.

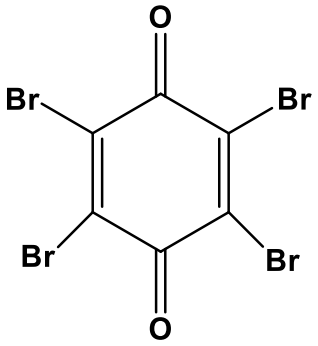

Figure 4.8: Structure of bromanil

Thus, increased amounts of C_2 and C_4 component proved that the acetobromination of CF_AL occurred successfully by Preparative method-1 and Preparative method-2. Preparative method-2 introduced more bromine and acetyl groups into CF_AL in comparison to Preparative method-1. Thus, the presence of acetic acid as solvent for bromine showed a positive impact on the acetobromination of CF_AL by acetic anhydride and bromine.

C(1s) XPS PE peaks were appeared at 286.01 and 286.05 eV in CF_AL_AcBr-1 and CF_AL_AcBr_AA, respectively. These binding energies were higher than the binding energy of C(1s) in sp^2C-Br of bromobenzene (285.10 eV), but significantly lower than the binding energy of C(1s) in sp^3C-Br of dibromomethane (287.1eV). From these data it could be inferred that the bromine atom was added in the aromatic nucleus of monolignols in CF_AL_AcBr-1 and CF_AL_AcBr_AA. The presence of phenolic or methoxyl oxygen could increase the binding energies of C(1s) in sp^2C-Br bond in aromatic ring of the monolignols. C_1 components of CF_AL_AcBr-1 and CF_AL_AcBr_AA largely decreased than CF_AL_AcBr, which was an indication of the degradation of CF_AL structure (e.g., breaking of linkages, e.g., β-O-4, α-O-4, etc.) and bromine substituition in the aromatic rings by Preparative methods.

Fourier transform mid and near infrared spectroscopic analysis: Evaluation of fundamental, overtone and combination bands

FT-MIR spectra of acetobrominated alkali-lignin samples, i.e., CF_AL_AcBr, BG_AL_AcBr, TO_AL_AcBr, GW_AL_AcBr and selected acetobrominated alkali-lignin samples, i.e., CF_AL_AcBr, CF_AL_AcBr-1 and CF_AL_AcBr_AA have been given in Figure 4.9. The spectral data of the samples have been given in Table 4.11(a-b). FT-NIR spectra of acetobrominated alkali-lignin samples have been given in Figure 4.10.

The FT-NIR spectra of CF_AL, BG_AL, TO_AL and GW_AL were incorporated for comparison. The NIR spectral data have been stated in Table 4.12.

The acetobromination of four alkali-lignin samples using conventional method resulted in a drop in the intensities of O-H stretching bands (at about 3410 cm^{-1}), which was a sign of successful acetobromination (Figure 4.9). Thus, aliphatic and phenolic hydroxyl groups of the alkali-lignin samples were acetylated along with bromine substitution in benzylic hydroxyl group. Absorption bands of aliphatic C-H stretching were seen at 2970 and 2894 cm^{-1}, with the latter perhaps produced by methoxyl groups [84]. Absorption bands of medium intensity at around 1752 cm^{-1} were visible in the CF_AL_AcBr, BG_AL_AcBr, TO_AL_AcBr, and GW_AL_AcBr samples. These absorption bands may have been caused by C=O stretching in the phenolic and aliphatic acetate groups. Aliphatic acetates often absorb radiation at a lower frequency than phenolic acetates. Weak absorption bands at about 1600 cm^{-1} were caused by aromatic C-H skeletal vibrations, whereas, aliphatic C-H asymmetric deformation exhibited weak absorption peaks at 1464 cm^{-1}. On the other hand, Figure 4.9(f) showed that the acetobrominated samples, such as CF_AL_AcBr-1 made using the Preparative method-1, displayed comparable absorption bands, but were significantly different from those made using Conventional method in terms of the O-H stretching band at 3428 cm^{-1}. It was due to incomplete acetylation (and related bromine substitution in benzylic hydroxyl group) in aliphatic and phenolic hydroxyl groups of CF_AL structure. Similarly, incomplete acetylation was also observed in the case of CF_AL_AcBr_AA, as synthesized by Preparative method-2. Table 4.11(b) showed different absorption bands of CF_AL, CF_AL_AcBr, CF_AL_AcBr-1 and CF_AL_AcBr_AA samples. It could be observed from Table 4.11b and Figure 4.9(f) that CF_AL_AcBr-1 and CF_AL_AcBr_AA samples exhibited absorption peaks centered at around 1742 cm^{-1}, whereas, CF_AL_AcBr showed absorption peak at 1752 cm^{-1}.

CF_AL did not exhibit any absorption band in this region. Weak absorption bands at about 604 cm^{-1} were observed in the CF_AL_AcBr, CF_AL_AcBr-1, and CF_AL_AcBr_AA samples, which may have resulted from the C-Br stretching. Intensity of the C-Br stretching band at 604 cm^{-1} of CF_AL_AcBr was comparatively higher than CF_AL_AcBr-1 and CF_AL_AcBr_AA, as an indication of different chemical environment of bromine, e.g., bromine attached to the side chain or aromatic nucleous in lignin structure. X-ray photoelectron spectroscopic analysis of the samples also supported this fact. Therefore, it could be inferred that the acetobromination of alkali-

lignin by Conventional and Preparative methods happened following different mechanisms.

It could be observed from Figure 4.10 that acetobromination changed the intensities of some overtone and combination bands of alkali-lignin samples. First overtone bands of O-H stretching at around 6872 cm^{-1} had lower intensities in the case of acetobrominated lignin samples made using the conventional method, but first overtone bands of C_{al}-H stretching had higher intensities. In all instances, the intensity of the combination bands at about 5220 cm^{-1} (O-H stretching + O-H deformation of absorbed water) decreased. While the intensities of the combination bands (O-H stretching + C=O stretching) at 4411 cm^{-1} marginally increased, the intensities of the combination bands (C_{ar}-H + C=C) stretching at about 4686 cm^{-1} did not vary considerably. Since the acetobromination reaction replaced hydroxyl groups of lignin, the insertion of the acetyl group and bromine (in lignin side chain) might be utilized to explain changes in the band intensities. CF_AL_AcBr, BG_AL_AcBr, TO_AL_AcBr and GW_AL_AcBr showed similar NIR bands as seen in Figure 4.10(e). On the other hand, acetobromination of CF_AL sample by Preparative methods also changed the intensities of some overtone and combination bands similarly, as seen from Figure 4.10(f). Interestingly, the intensities of the combination bands (C_{ar}-H + C=C) stretching of CF_AL_AcBr-1 and CF_AL_AcBr_AA at about 4672 cm^{-1} decreased in comparison to CF_AL_AcBr (Figure 4.10f). This change potentially happened due to electrophilic substitution reaction led to bromination in aromatic nucleus of monolignols.

First overtone bands of C_{al}-H stretching in CF_AL_AcBr-1 and CF_AL_AcBr_AA showed comparavely lower intensity than CF_AL_AcBr, as an indication of partial acetylation. The incorporation of acetyl groups into the lignin structure enhanced the combination bands of (O-H + C=O) stretching at 4404 cm^{-1} in intensity.

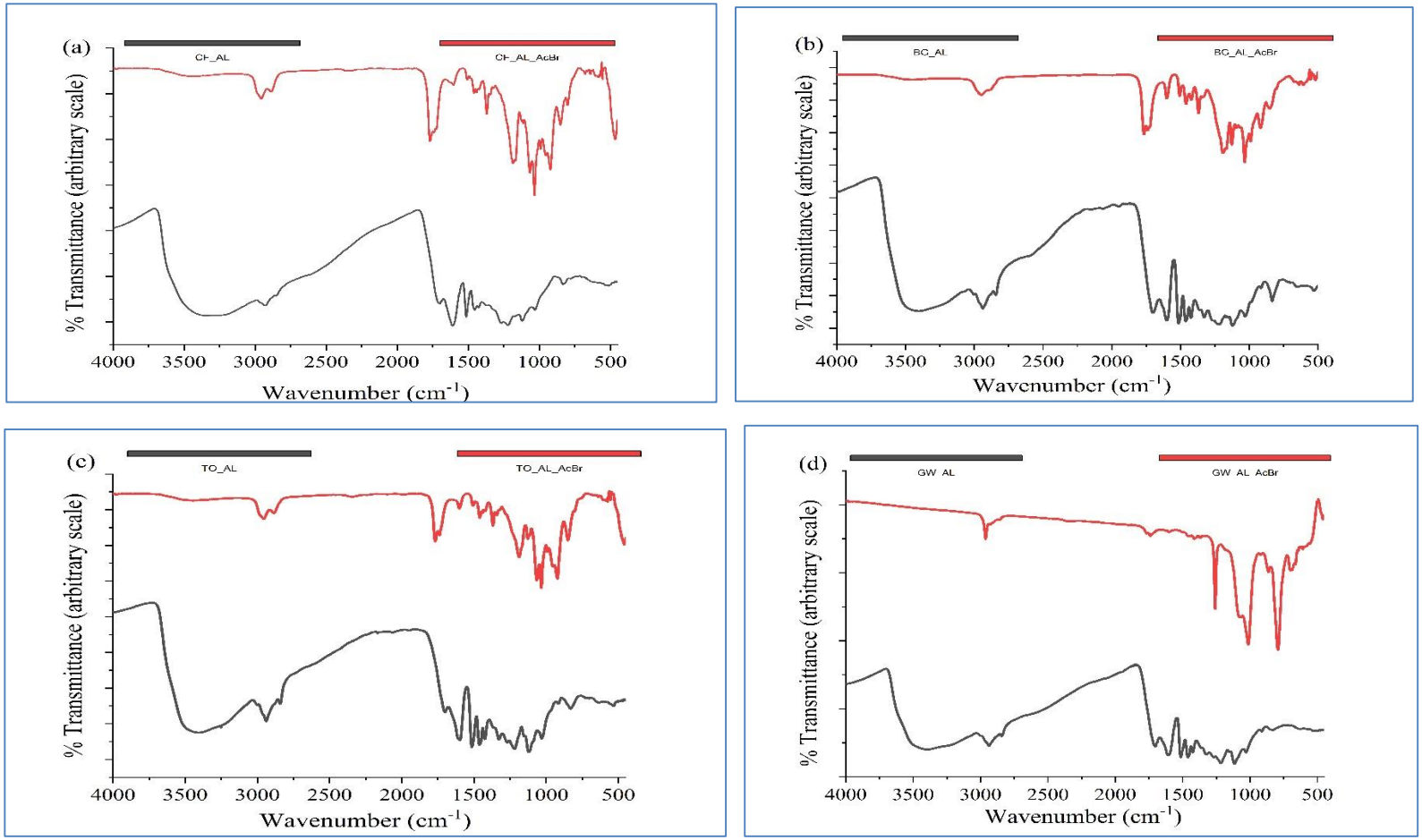

Figure 4.9: FT-MIR spectra of four acetobrominated alkali-lignin samples synthesized by conventional method (a) CF_AL and CF_AL_AcBr (b) BG_AL and BG_AL_AcBr (c) TO_AL and TO_AL_AcBr and (d) GW_AL and GW_AL_AcBr.

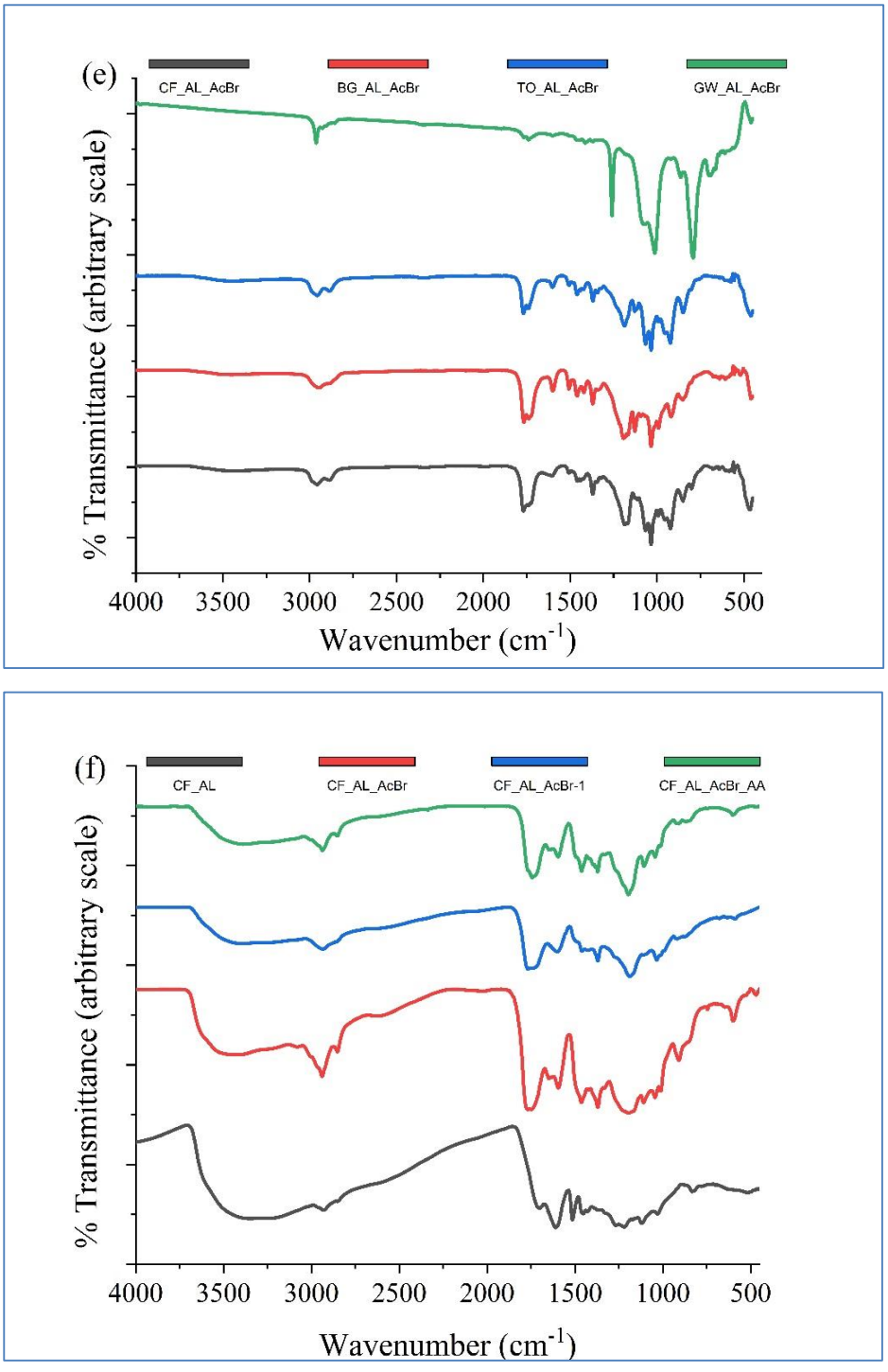

Figure 4.9: FT-MIR spectra of (e) four acetobrominated alkali-lignin samples synthesized by conventional method and (f) selected acetobrominated samples synthesized by new methods, i.e., CF_AL_AcBr (Conventional method), CF_AL_AcBr-1(Preparative method-1) and CF_AL_AcBr_AA (Preparative method-2). FT-MIR spectrum of CF_AL was included for comparison.

Table 4.11(a): FT-MIR spectral data and band assignment of acetobrominated alkali-lignin samples synthesized by Conventional method

Wavenumber range (cm^{-1})	Obtained band (cm^{-1})	Band assignment	Reference band (cm^{-1})
4000-3000	-	O-H stretching	3460-3412
3000-2000	2970	Methyl C-H (asymmetric stretch + deformation overtone)/Out of plane stretching	2972-2952
	2894	Methyl C-H symetric stretching	2882-2862
2000-1000	1752	C=O stretching in acetate groups	1738-1709
	1600	Aromatic skeletal vibrations plus C=O stretching	1605-1593
	1464	C-H deformation combined with aromatic ring vibration/C-C stretch in a ring	1470-1460
	1376	Methyl C-H asym/sym bending	1370-1365
	1188	Phenolic C-O stretch	1266-1180
	1056	C-O stretching vibrations in ether	1075-1000
1000-500	925	Aromatic C-H bending/out of plane deformation	925-915
	798	Skeletal C-C vibrations	832-817
	687	C-Br stretching	750-550

Table 4.11(b): FT-MIR spectral data and tentative assignment of the bands of acetobrominated alkali-lignin samples synthesized by Preparative methods

Wavenumber range (cm^{-1})	Obtained band (cm^{-1})	Band assignment	Reference band (cm^{-1})
4000-3000	3410	O-H stretching, H-bonded	3460-3412
3000-2000	2944	$-CH_3$/ $-CH_2-$ (asymmetric stretch + deformation overtone)/Out of plane stretching	2972-2952
	2852	$-CH_2-$ in plane stretching; twisting	2882-2862
2000-1000	1752	C=O stretching in acetate groups	1738-1709
	1601	Aromatic skeletal vibrations plus C=O stretching	1605-1593
	1459	C-H deformation; assymetric in $-CH_3$/ $-CH_2-$	1470-1460
	1363	Aliphatic C-H stretch in $-CH_3$/Phenolic OH (bending)	1370-1365
	1203	Phenolic C-O stretch	1266-1180

	1102	C-O stretching vibrations in secondary alcohols	1150-1075
	1040	C-O stretching vibrations in primary alcohols/Bromine substituted aromatic ring	1075-1000
1000-500	914	Aromatic C-H bending/out of plane deformation	925-915
	826	C-H bending/out of plane in position 2 and 6 of S and all positions of H units/Di or tetra-substituted aromatic ring	832-817
	604	C-Br stretching	750-550

Table 4.12: FT-NIR spectral data and tentative assignment of the bands of acetobrominated lignin samples

Wavenumber (cm^{-1})	Obtained band (cm^{-1})	Band assignment	Reference band (cm^{-1})
7000-6000	6925	1st OT of O-H stretching	6913
6000-5000	5988	1st OT of C_{ar}-H stretching	5963-5980
	5784	1st OT of C_{al}-H stretching	5795
	5220	O-H stretching + O-H deformation of absorbed water	5150-5220
5000-4000	4672	(C_{ar}-H + C=C) stretching	4686
	4404	(O-H + C=O) stretching	4411

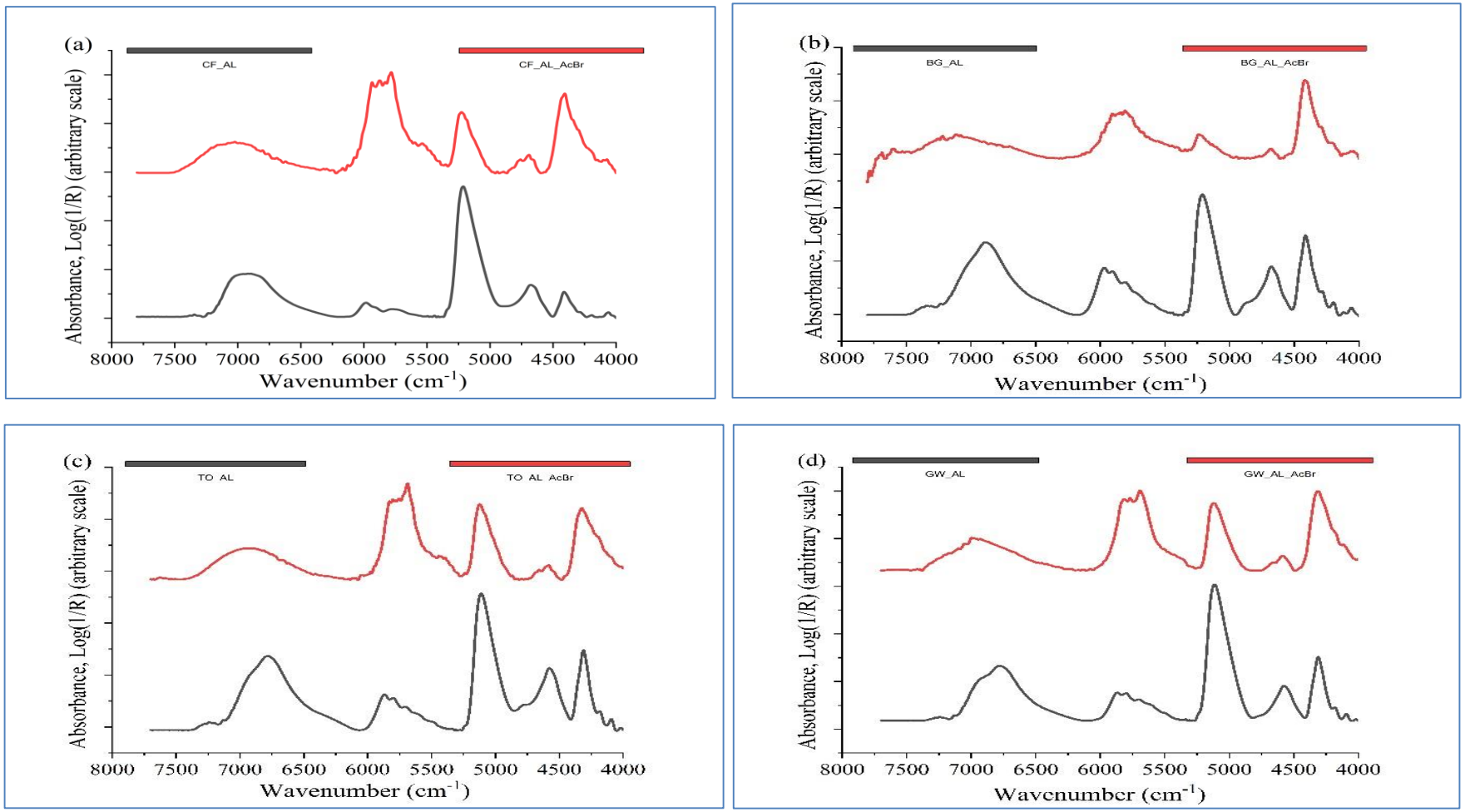

Figure 4.10: FT-NIR spectra of acetobrominated lignin samples (a) CF_AL and CF_AL_AcBr (b) BG_AL and BG_AL_AcBr (c) TO_AL and TO_AL_AcBr (d) GW_AL and GW_AL_AcBr. The spectra of related alkali-lignin samples were included for comparison.

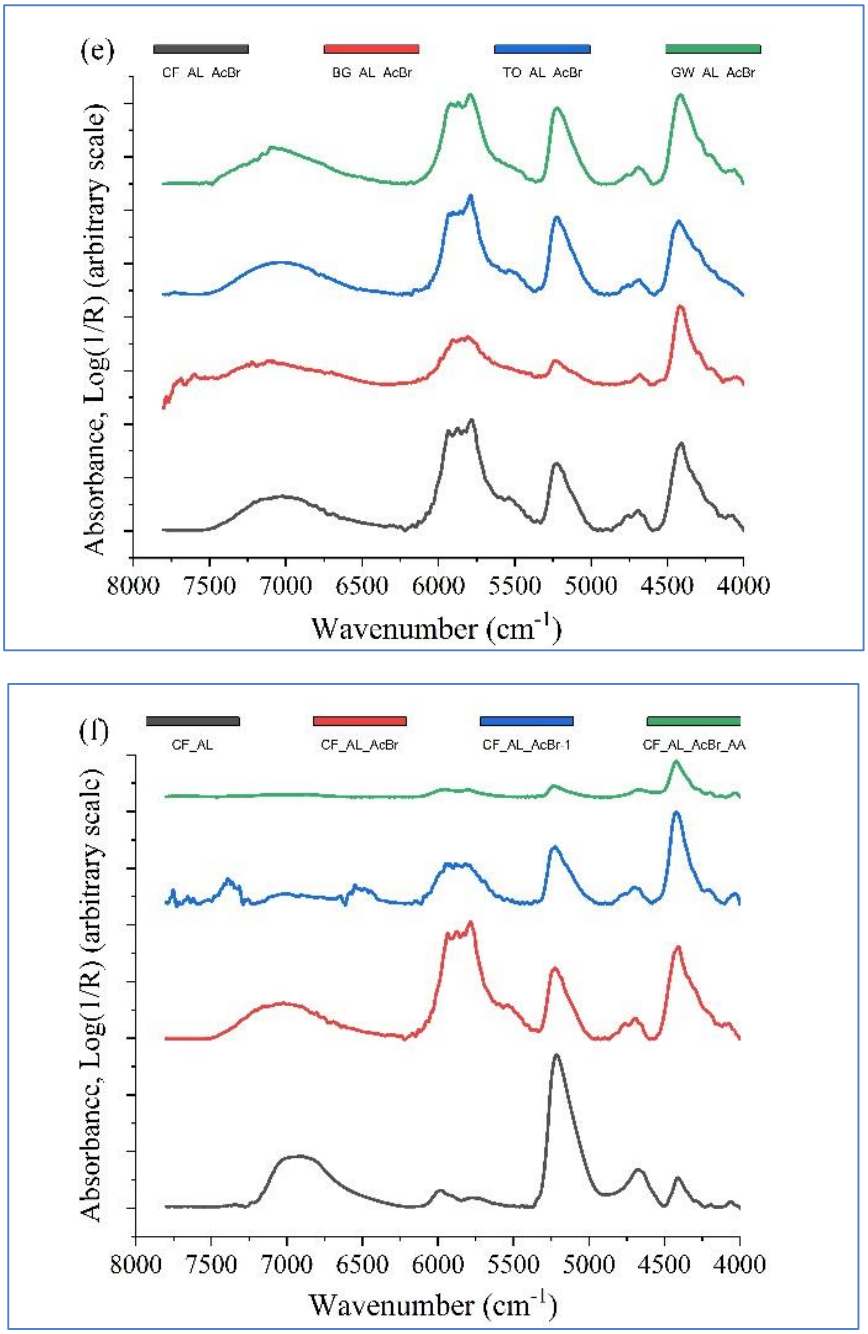

Figure 4.10: FT-NIR spectra of (e) four acetobrominated alkali-lignin samples synthesized by Conventional method and (f) selected acetobrominated samples, CF_AL_AcBr (Conventional method), CF_AL_AcBr-1 (Preparative method-1) and CF_AL_AcBr_AA (Preparative method-2). NIR spectrum of CF_AL was included for comparison.

Nuclear magnetic resonance spectroscopic analysis: Structural features of acetobrominated products

^{1}H–NMR spectra of CF_AL, CF_AL_acetylated and acetobrominated alkali-lignin samples, i.e., CF_AL_AcBr, CF_AL_AcBr-1 and CF_AL_AcBr_AA were given in Figure 4.11 and spectral data were incorporated in Table 4.13. ^{13}C–NMR spectra of CF_AL and CF_AL_AcBr_AA samples were given in Figure 4.12 and spectral data with tentative assignment of the peaks were presented in Table 4.14. 2D ^{13}C-^{1}H HSQC NMR spectra of CF_AL and CF_AL_AcBr_AA were given in Figure 4.13 and spectral data were presented in Table 4.15. All of the peaks have been assigned tentatively.

It could be observed that acetobromination of lignin improved the spectral resolution of key lignin functionalities similar to acetylation [76]. Table 4.11 showed that, like acetylated CF_AL, phenolic and aliphatic acetates were found in the spectra of CF_AL_AcBr-1 and CF_AL_AcBr_AA. However, in the case of CF_AL_AcBr, phenolic acetate was absent. It was potentially due to low reactivity of phenolic hydroxyl group towards acetylation in comparison to α and γ hydroxyl groups [203]. The inclusion of acetyl groups in the CF_AL structure was also supported by high resolution XPS spectra (Table 4.10).

Interestingly, the peaks in the range of δ 2.612 to 3.165 ppm were seen in all acetobrominated samples, but not in CF_AL or CF_AL_acetylated samples as an indication of improved functionality due to bromination in lignin side-chains. These peaks could be assigned for proton in α-carbon in β-1 structures or benzylic protons in β-β structures [76, 206]. All samples showed the peaks of methoxyl protons in specified ranges, i.e., δ 3.3 to 4.0 ppm. The introduction of electronegative bromine atoms into the CF_AL structure led to a slight deshielding effect on the aromatic protons of the monolignols. As a result, higher chemical shift values (from δ 6.687 to δ 7.014-7.234 ppm) were observed in comparison to CF_AL. At the same time, the peak intensity of aromatic protons in CF_AL greatly decreased due to acetobromination.

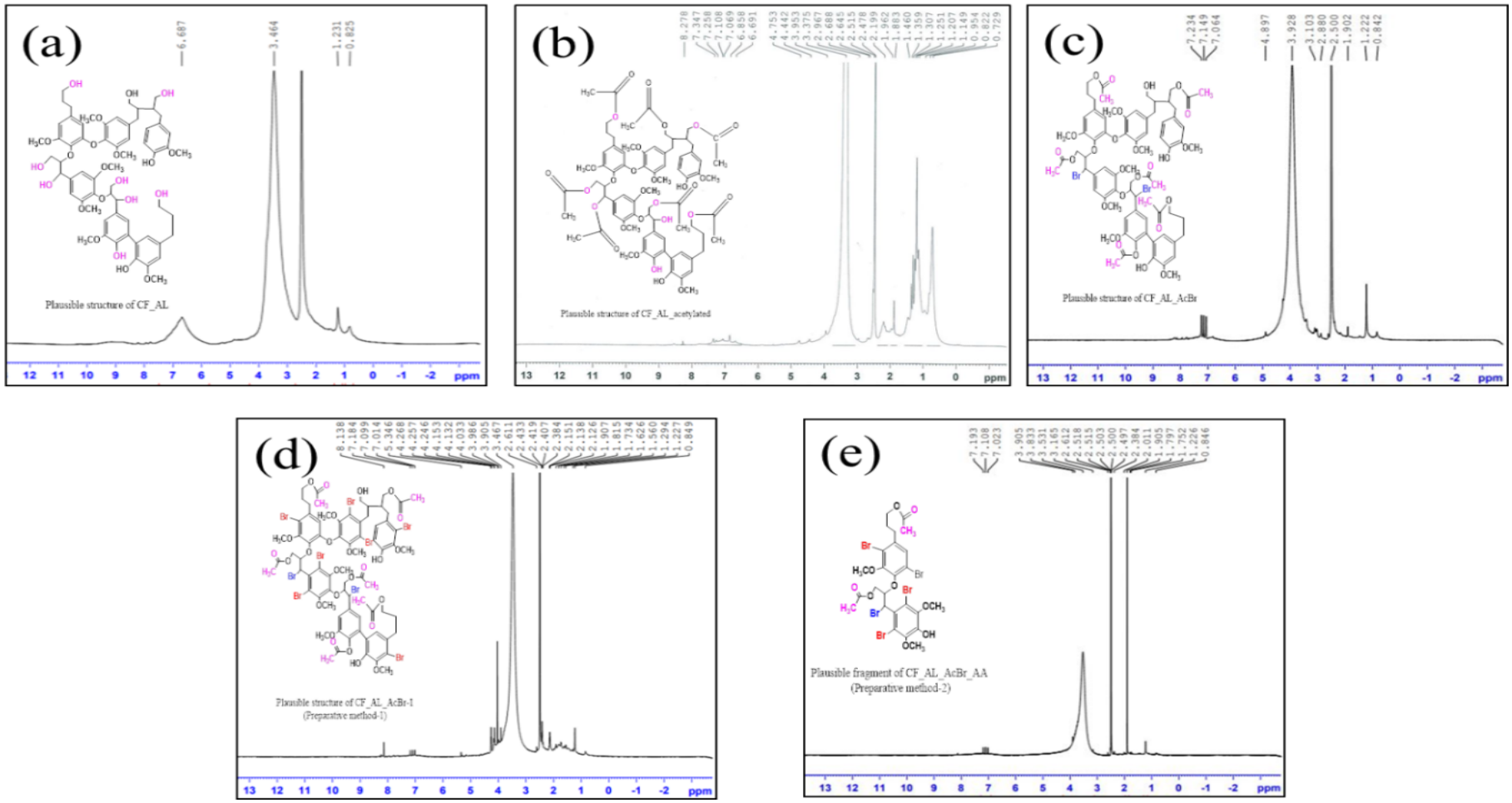

Figure 4.11: ^{1}H-NMR spectra of CF_AL, CF_AL_acetylated and selected acetobrominated samples (a) CF_AL (b) CF_AL_acetylated (c) CF_AL_AcBr (d) CF_AL_AcBr-1 and (e) CF_AL_AcBr_AA. Plausible structures of related products have been incorporated in the figures.

Table 4.13: ^{1}H-NMR data and tentative assignment of different protons in acetobrominated coconut fibre alkali-lignin samples

Chemical shift/ppm	Observed ^{1}H-NMR peak/ppm					Tentative assignment [205-207]
	CF_AL	CF_AL_acetylated	CF_AL_AcBr	CF_AL_AcBr-1	CF_AL_AcBr_AA	
8.0-10.0	-	8.278	-	8.134	-	Proton in residual phenolic hydroxyl group
6.8–7.2	6.687	7.069-7.347	7.064-7.234	7.014-7.184	7.023-7.193	Residual protons in bromine substituted aromatic nucleus in guaiyacyl units.
6.2–6.7	-	6.691-6.858	-	-	-	Aromatic proton in syringyl units
4.0-5.5	-	4.442-4.753	4.897	4.033-4.268; 5.346	3.905	H_{α}, H_{β} and H_{Y} in several structures, i.e., H_{α} in β-O-4 and β-5 structures. Residual aliphatic hydroxyl groups may contribute in this region.
3.3-4.0	3.464	3.375-3.953	3.928	3.467	3.531	Proton in methoxyl group
2.6-3.2	-	-	2.880-3.103	2.611	2.612-3.165	Proton in β-1 structures/ Benzylic protons in β-β structures (potentially bromine substituted side-chain of lignin)
2.50	2.507	2.507	2.500	2.500	2.500	d_6-DMSO peak
2.2–2.4	-	2.199-2.478	-	2.384-2.433	2.384	Proton in phenolic acetate
1.6–2.2	-	1.460-1.883	1.902	1.907-2.151	1.752-2.011	Proton in aliphatic acetate
<1.6	0.825-1.231	0.729-1.149	0.842-1.222	0.849-1.227	0.846-1.226	Protons (-CH_2-/-CH_3) in aliphatic hydrocarbon side chain.

The chemical shift of a brominated carbon (saturated aliphatic) in ^{13}C-NMR spectrum typically falls within a specific range, δ 25 to 65 ppm, which can be influenced by the electronic environment and the molecular structure of the compound. In acetobrominated alkali-lignin samples, bromine atom could be attached to the aromatic nucleus or side-chain of the lignin structure (Table 4.14). ^{13}C-NMR spectrum of C-Br in saturated aliphatic side-chains generally resonates at δ 25 to 65 ppm, whereas, C-Br in aromatic nucleus typically resonate at somewhat higher chemical shifts, often in the range of δ 110 to 150 ppm. On the other hand, ^{13}C-NMR peaks of acetyl groups in lignin structure would appear in the range of δ 168.5 to 171.6 ppm [206, 207]. It could be observed that applied acetobromination reactions changed the chemical structure of lignin and concurrent incorporation of bromine in aromatic nucleus (δ 112.97 to 123.61 ppm) and side-chains of lignin (δ 61.06 ppm) along with acetylation of primary aliphatic hydroxyl (δ 174.46 ppm), secondary aliphatic hydroxyl (δ 172.19 ppm) and phenolic hydroxyl groups (δ 168.42 ppm) occurred successfully.

The position of cross-peaks in the 2D ^{13}C-^{1}H HSQC NMR spectrum corresponded to the chemical shift of the attached hydrogen and carbon atoms in lignin structure (Figure 4.13) [208-210]. It could be observed that no significant ^{13}C-^{1}H correlation (one-bond coupling) was present in aromatic region, e.g., δC/δH 110-120/6-8 ppm in the case of CF_AL_AcBr_AA, whereas, CF_AL showed ^{13}C-^{1}H correlation in this range (Figure 4.15c). These phenomena indicated that the bromination in aromatic rings of CF_AL occurred through electrophilic aromatic substitution and produced CF_AL_AcBr_AA. If bromination in the aromatic rings of the monolignols were incomplete, ^{13}C-^{1}H correlation would be present in the HSQC NMR spectrum.

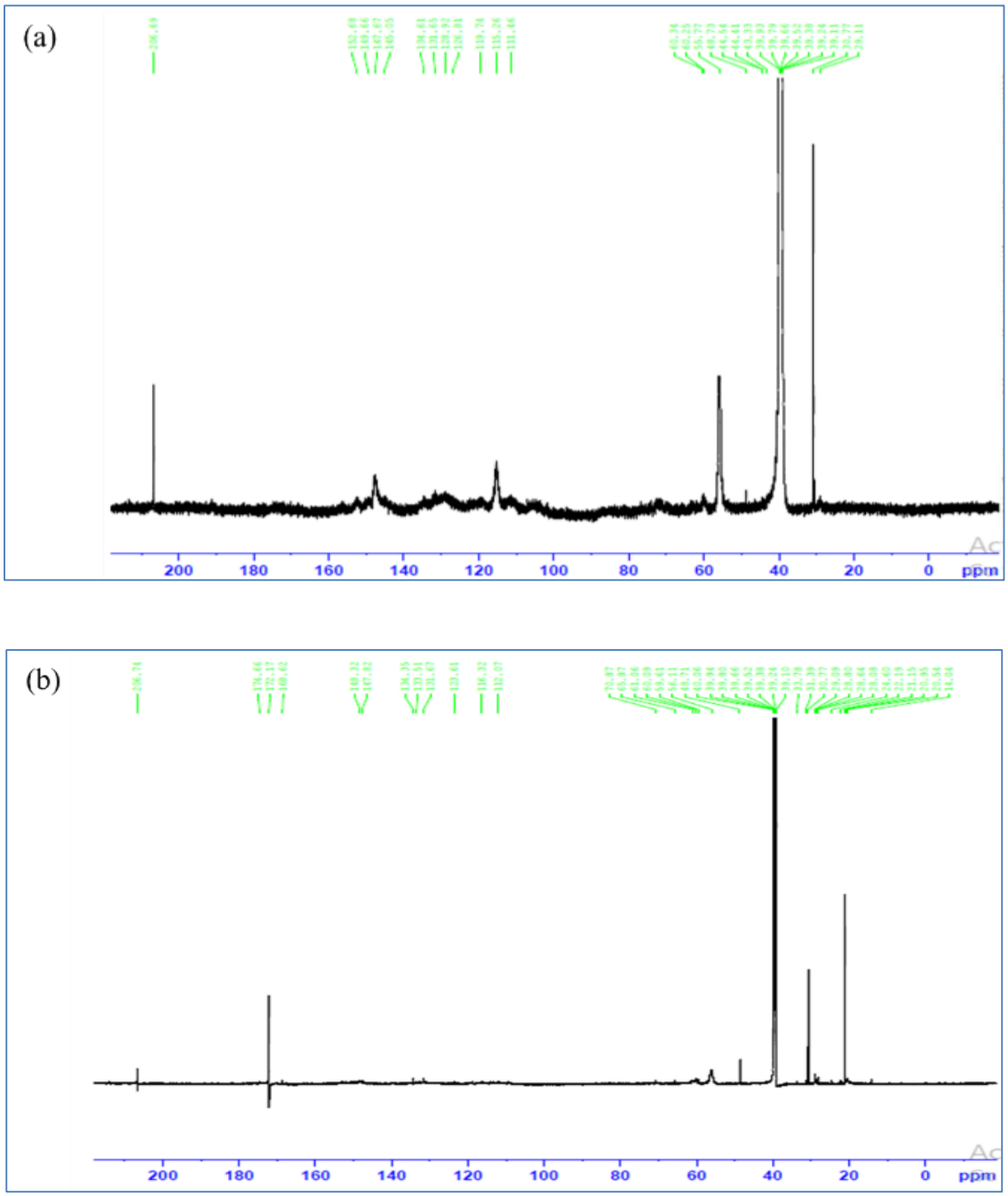

Figure 4.12: ^{13}C-NMR spectra of (a) CF_AL and (b) CF_AL_AcBr_AA (δ 0 to 220 ppm).

Table 4.14: ^{13}C-NMR data and tentative assignment of different peaks of CF_AL and CF_AL_AcBr_AA samples in *d_6*-DMSO solution

SN	Observed ^{13}C-NMR peak/ppm		Tentative assignment [34, 37]
	CF_AL	CF_AL_AcBr_AA	
1	206.69	206.74	Carbon in carbonyl group of ketones
2	-	174.46	C=O in aliphatic acetates (generated from primary hydroxyl group)
3	-	172.19	C=O in aliphatic acetates (generated from secondary hydroxyl group)
4	-	168.42	C=O in aromatic acetates (generated from phenolic hydroxyl group)
5	152.68	-	C-3/C-5 in β-O-4 S unit
6	149.66	148.32	C-3 in etherified G unit; potentially bromine substituted carbon in aromatic ring
7	147.67	147.82	C-4 in G unit; potentially bromine substituted carbon in aromatic ring
8	134.61	134.35	C-1 in β-O-4 G unit
9	131.65	131.67	C-1 in non-etherified 5-5
10	128.92	-	C-2/C-6 in H unit
11	126.81	-	C-5/C-5′ in non-etherified 5–5 unit
12	119.74	123.61	C-6 in G unit (etherified and nonetherified) (potentially bromine substituted carbon in aromatic ring)
13	115.26	116.92	C-5 in G unit (etherified and nonetherified) (potentially bromine substituted carbon in aromatic ring)
14	111.46	112.97	C-2 in G unit (potentially bromine substituted carbon in aromatic ring)
15	-	70.87	C_α in G type β-O-4 units (threo)
16	-	65.87	C_Υ in β-5 and β-O-4 with α-C=O
17	60.25-60.36	61.06	C_Υ in G type β-O-4 units; potentialy bromine substituted carbon in lignin's side-chain
18	55.77	56.12	Aromatic -OMe in G and S units
19	39.11-39.93	39.10-40.96	-CD_3 in *d_6*-DMSO
20	28.75-29.01	28.80-33.78	-CH_3 /-CH_2- in lignin side chain; potentialy bromine substituted carbon
21	-	20.54-22.19	-CH_3 in acetyl groups

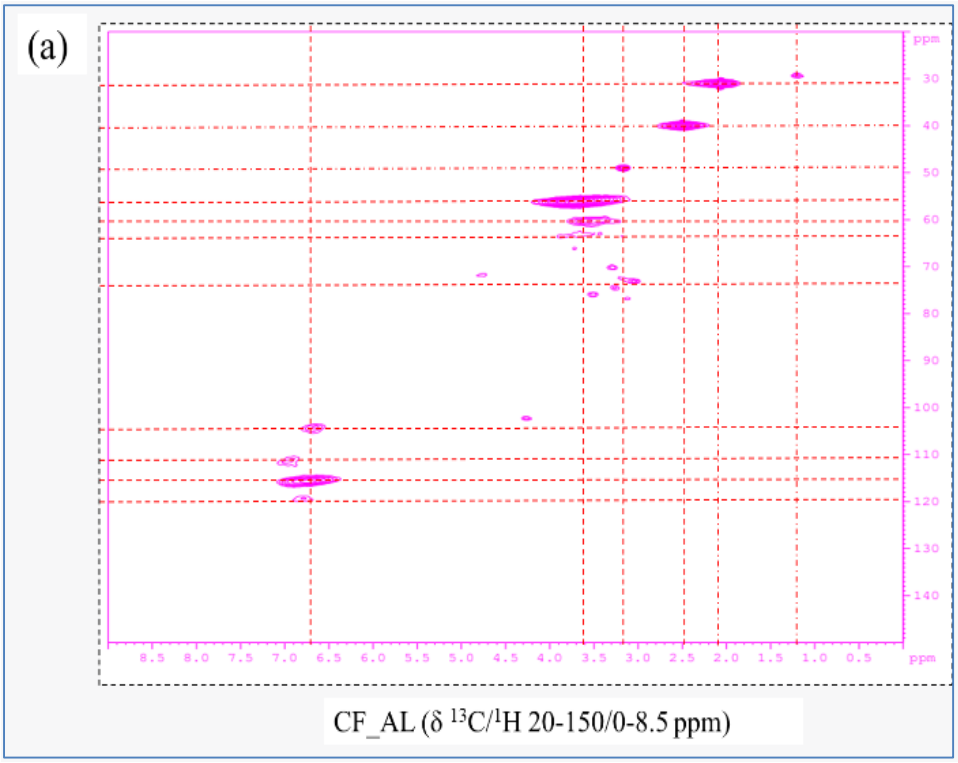

Figure 4.13: ^{13}C-1H correlation spectra of CF_AL in d_6-DMSO solution (a) HSQC full spectrum of CF_AL (b) spectrum of CF_AL in aliphatic region.

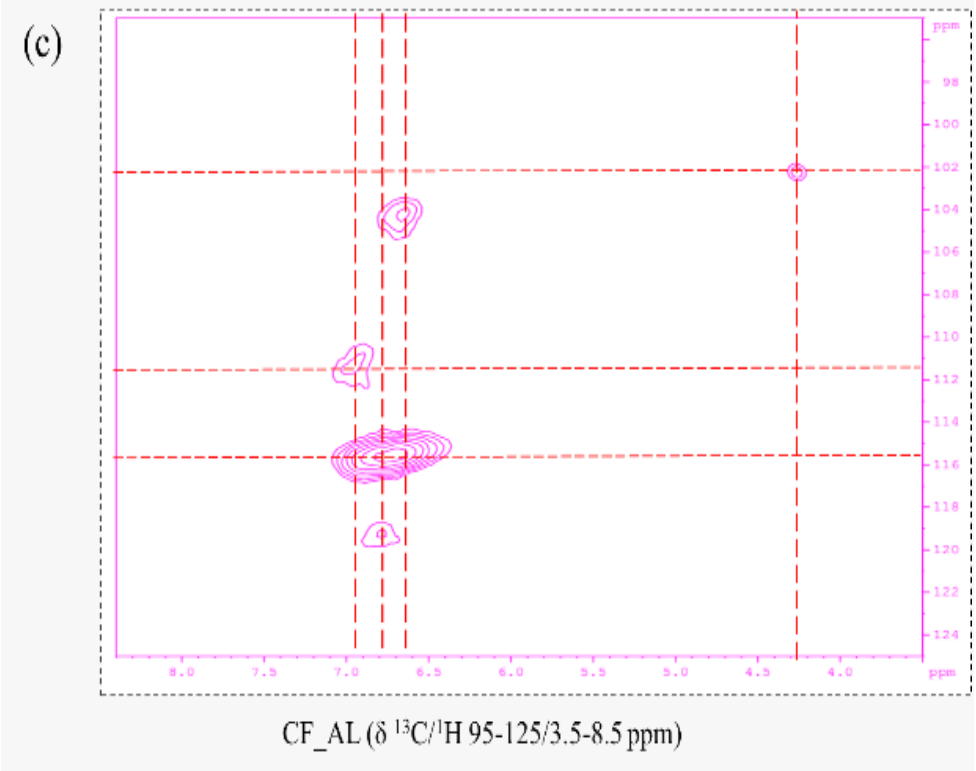

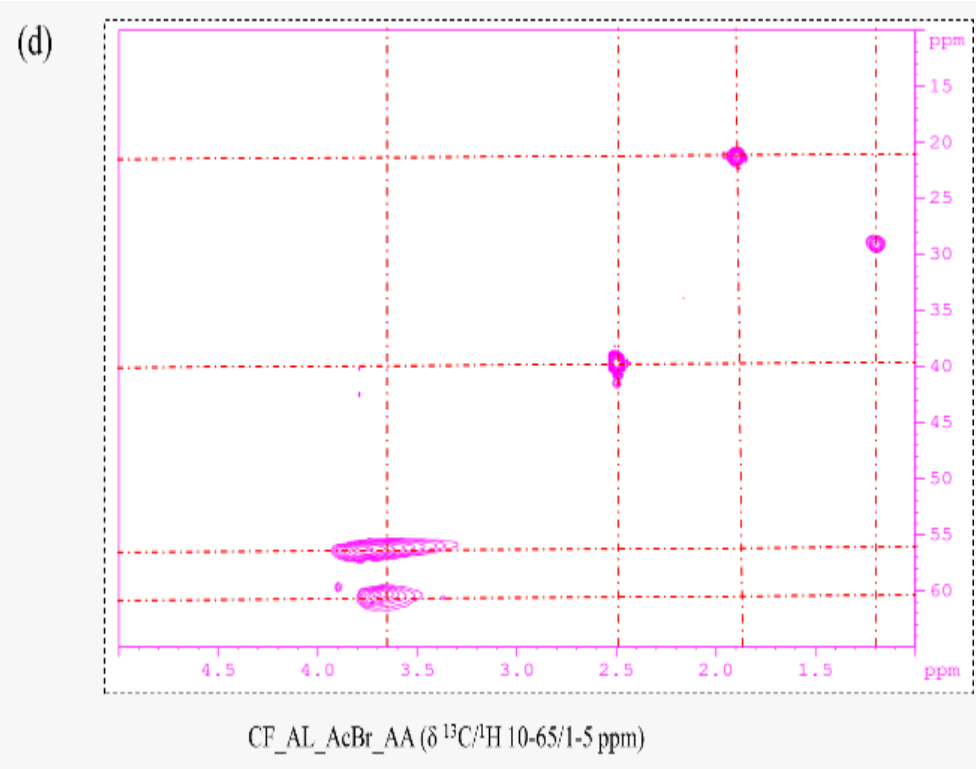

Figure 4.13: ^{13}C-^{1}H correlation spectra of (c) CF_AL in aromatic region and (d) CF_AL_AcBr_AA in aliphatic region. No ^{13}C-^{1}H correlation was observed in the aromatic region of CF_AL_AcBr_AA

Table 4.15: ^{1}H-^{13}C HSQC-NMR spectral data of CF_AL and CF_AL_AcBr_AA tentative assignment of the peaks

$^{13}C/^{1}H$ spectral region (ppm)	HSQC peaks, δC/ δH (ppm)		Tentative assignment
	CF_AL	CF_AL_AcBr_AA	
Aliphatic (0-95/ 0-6.0)	-	20.00/1.95	$-CH_3$ in acetyl groups
	29.01/1.20	29.06/1.20	$-CH_3$ and $-CH_2-$ in aliphatic side chain
	31.00/2.20	-	$-CH_3$ in acetyl groups
	39.93/2.50	40.01/2.50	d_6-DMSO
	49.20/3.30	-	-
	55.77/3.75	56.03/3.742	Carbon in methoxyl groups and C-O in interunit linkages
	60.36/3.44	60.10/3.70	β-O-4
	62.20/3.52	-	β-O-4
	69.01/3.20	-	β-O-4
	70.10/3.30	-	β-β
	72.01/4.20	-	β-O-4
	72.10/4.74	-	β-β
	75.01/3.20	-	α-O-4
	76.03/3.52	-	α-O-4
	77.02/3.10	-	α-O-4
Aromatic (96-175/ 6.0-8.0)	105.10/6.60	-	Carbon in aromatic ring
	111.46/6.90	-	Carbon in aromatic ring
	115.26/6.70	-	Carbon in aromatic ring
	119.00/6.60	-	Carbon in aromatic ring

^{13}C-^{1}H correlation in the side-chain regions, e.g., δC/δH 20-80/1.5-5.5 in HSQC NMR spectra indicated the presence of inter-unit linkages in CF_AL and CF_AL_AcBr_AA samples. Both spectra showed HSQC NMR peaks corresponding to methoxyl groups, e.g., ^{13}C-^{1}H δ 55.77/3.46 ppm for CF_AL and ^{13}C-^{1}H for δ 56.12/3.53 ppm for CF_AL_AcBr_AA. In the case of CF_AL, ^{13}C-^{1}H correlation was observed in aromatic region (Figure 4.13c). Cross-peak at δ 61.06/3.16 (Figure 4.13d) could be assigned for C-Br bond in CF_AL_AcBr_AA, which was formed due to bromination in saturated aliphatic side-chains. A plausible structure (containing β-O-4 lingkage) of acetobrominated alkali-lignin could be represented as follows-

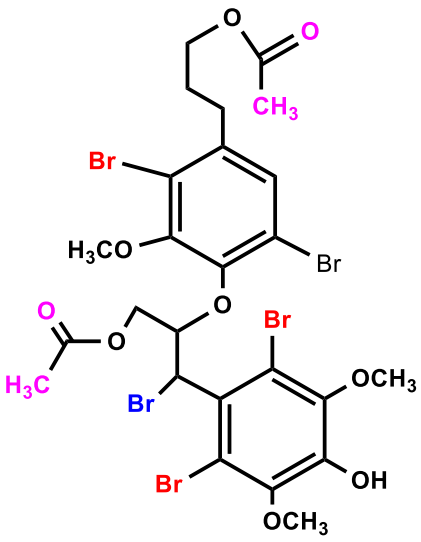

Figure 4.14: A plausible structure of acetobrominated alkali-lignin fragment containing β-O-4 lingkage. Bromine atoms (substituted in lignin's side chain and aromatic nucleus) have been presented in blue and red color, respectively.

Field emission-scanning electron microscopic analysis: Surface morphology and particle sizes

Surface morphology of the selected samples, i.e., CF_AL and CF_AL_AcBr_AA were analyzed by field emission-scanning electron microscope (FE-SEM) and depicted in Figure 4.15 (a-b). Particle size distributions of CF_AL_AcBr_AA have been presented in Figure 4.15(c). It was suggested that milled CF_AL could be characterized by irregular particle morphology [211, 212]. Figure 4.15(a) showed that the CF_AL particles were agglomerated in different irregular sizes and formed rough surfaces, whereas CF_AL_AcBr_AA showed spherical shapes (Figure 4.15b). Reduction of particle sizes of CF_AL_AcBr_AA than CF_AL could be seen seen from the micrographs. Microscopic cavities were also observed in all cases. Thus, the applied acetobromination reaction could significantly change the CF_AL particles's size and morphology.

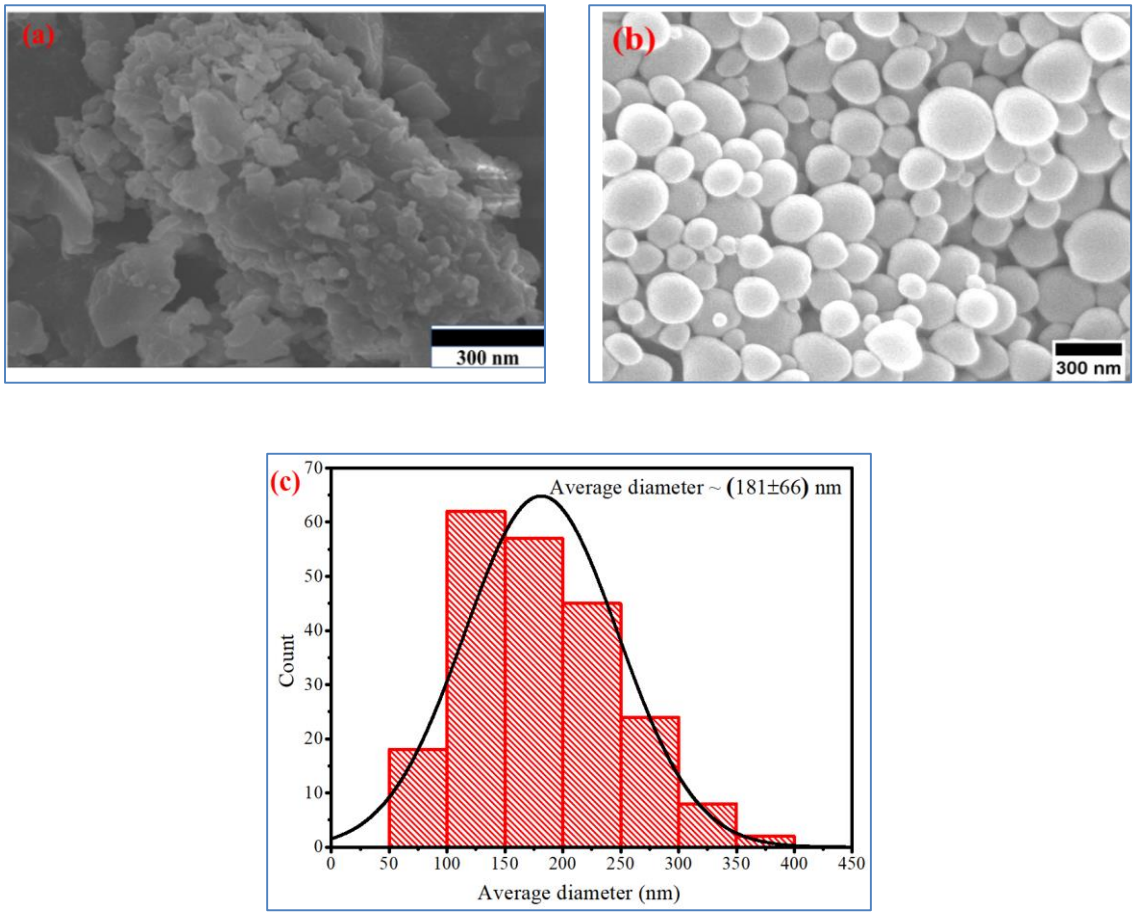

Figure 4.15: Field emission-scanning electron micrographs of (a) CF_AL in 3K and (b) CF_AL_AcBr_AA in 50K magnifications. Particle size distributions of (c) CF_AL_AcBr_AA. Formation of spherical particles was clearly seen from the micrograph (b).

X-ray diffraction analysis: Evaluation of crystallinity of acetobrominated products

X-ray powder diffraction investigations were carried out on CF_AL and its acetobrominated products in order to get a deeper insight into the sample's crystallinity. The X-ray diffractograms of the samples have been presented in Figure 4.16. It could be observed that substantial regions beneath the curves supporting the assumption that the acetobrominated products were amorphous in nature like base lignin (CF_AL).

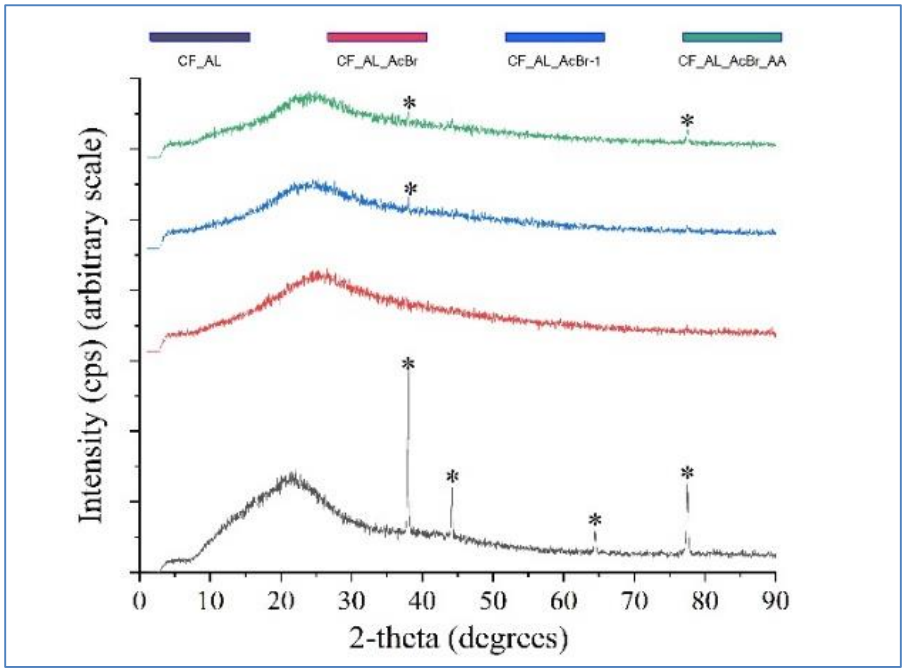

Figure 4.16: X-ray deffractogram of acetobrominated alkali-lignin samples. (*Peaks due to sample stage).

For CF_AL, the 2-theta value was 22.13. Conversely, the 2-theta values for CF_AL_AcBr, CF_AL_AcBr-1, and CF_AL_AcBr_AA were 25.31, 23.53, and 23.71, respectively. As a result, the acetobrominated compounds' diffraction angles increased relative to CF_AL. It is noteworthy that the most prominent peaks of CF_AL_AcBr_AA and CF_AL_AcBr_AA were nearly identical at 2-theta values. The mean size of the ordered domains for CF_AL and acetobrominated products calculated using Scherrer's equation 2 with B = 0.9, were displayed in Table 4.16. Previous research showed that lignin samples with mean crystallite sizes comparable to CF_AL and acetobrominated products exist [213]. The observed variation can be explained in terms of different structural features due to acetobromination in different conditions. However, the applied acetobromination methods did not change the amorphous nature of base CF_AL.

Table 4.16: Maximum peak location of CF_AL and its acetobrominated products in X-ray diffractograms and mean crystallite sizes

Sample	2-Theta	Full width half maxima	Mean crystallite size (nm)
CF_AL	22.13	13.93	0.61
CF_AL_AcBr	25.31	18.57	0.46
CF_AL_AcBr-1	23.53	14.34	0.59
CF_AL_AcBr_AA	23.71	11.03	0.77

Simultaneous thermal analysis: Examination of thermal properties

The thermal properties of acetylated and acetobrominated alkali-lignin samples, such as CF_AL_AcBr, CF_AL_AcBr-1, and CF_AL_AcBr_AA, were investigated using a simultaneous thermal analyzer (STA). The obtained thermogravimetric (TG) analysis curves, as well as the differential thermogravimetric (DTG) analysis curves have been shown in Figures 4.17. The differential scanning calorimetry (DSC) curves, as well as the first derivative differential scanning calorimetry (DDSC) curves, of the samples have been presented in Figures 4.18.

Simultaneous thermal analysis was also performed on CF_AL to enable comparison among samples. The test settings, such as atmosphere, gas flow rate, vapour pressure on the sample, heating rate, thermal contact to the sample and crucible, were kept the same for both thermogravimetric analysis (TGA) and differential scanning calorimetry (DSC) outputs. Obtained thermogravimetric analysis (TG) curves and first derivatives, indicated that the rates of degradation of the samples were different due to the lignin being modified by different techniques.

The TG curves for all samples showed a gradual weight loss as the temperature increased (Figure 4.17a). In the analyzed temperature range (room temperature to 850 °C), CF_AL exhibited the highest weight loss, approximately 37%, compared to CF_AL_AcBr, CF_AL_AcBr-1, and CF_AL_AcBr_AA up to 380 °C, indicating a greater number of thermolabile functional groups in its structure, including strongly absorbed moisture. CF_AL also experienced a weight loss of around 20% of its initial weight at 105 °C, whereas the weight losses of acetobrominated samples were insignificant, around 2%, suggesting that the acetobrominated samples have a lower affinity for moisture absorption than CF_AL. Among the acetobrominated samples, CF_AL_AcBr and CF_AL_AcBr_AA retained approximately 95% of their initial weights up to 200 °C, indicating higher thermal stability, while CF_AL_AcBr-1 lost around 12% of its initial weight. Faster degradation rates were observed for all samples from 200 to 380 °C, where CF_AL_AcBr_AA showed more thermolabile properties. Residual masses of CF_AL and CF_AL_AcBr were about 42% each, whereas, 35% and 30% for CF_AL_AcBr-1 and CF_AL_AcBr_AA, respctively. Due to the breakdown of different chemical bonds, the samples' weight loss intensities differed significantly. These changes were revealed in the DTG characteristics (Figure 4.17b).

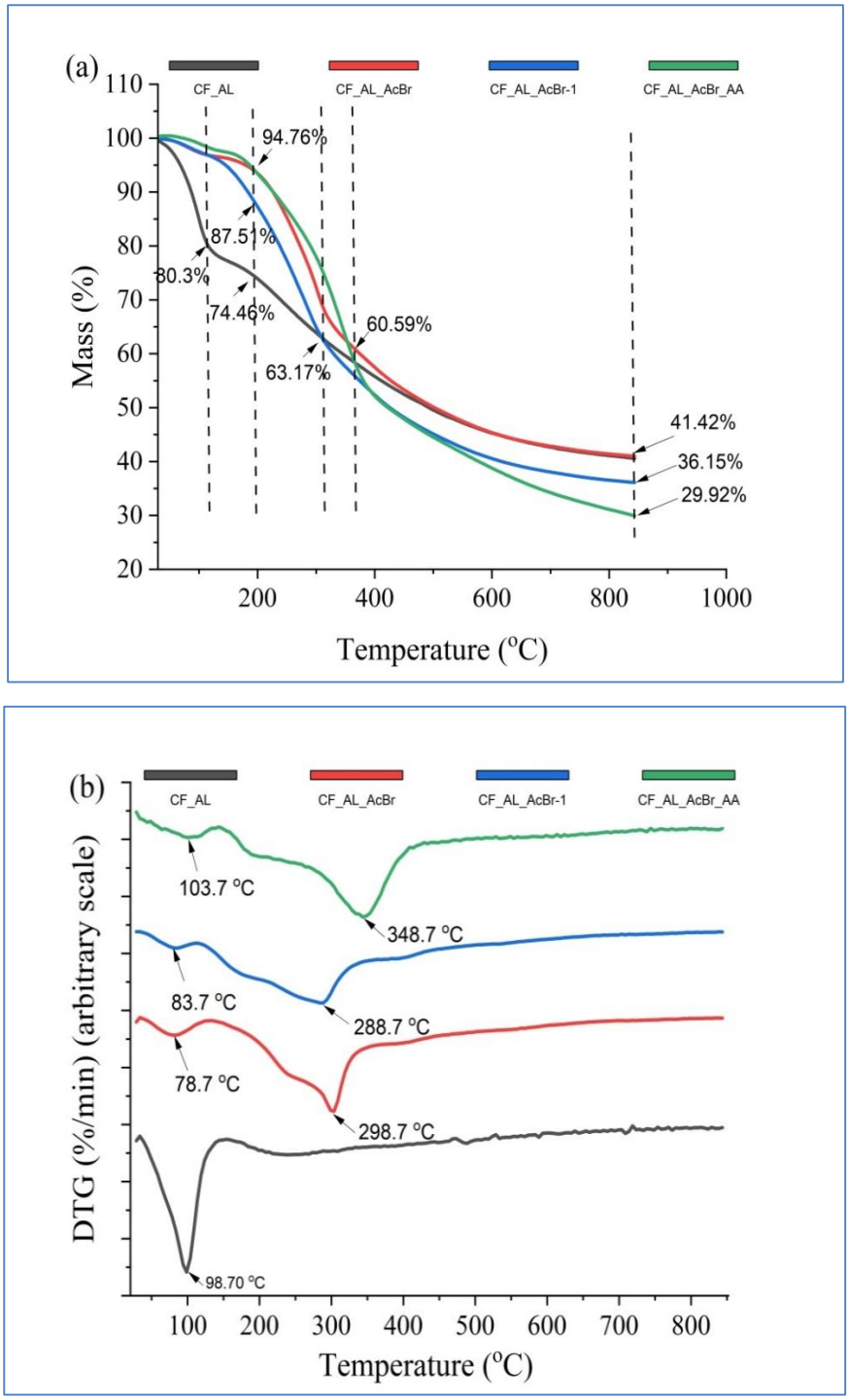

Figure 4.17: Simulteneous thermal analysis of CF_AL and selected acetobrominated CF_AL samples (a) Thermogravimetric (TG) analysis curves and (b) Differential thermogravimetric (DTG) analysis curves

All samples showed endothermic changes below 105 °C and CF_AL showed the highest intensity of weight loss among the samples. Acetobrominated samples, however, showed the second endothermic changes at higher temperaturess, i.e., CF_AL_AcBr at 298.7 °C, CF_AL_AcBr-1 at 288.7 °C and CF_AL_AcBr_AA at 348.7 °C. CF_AL did

not show any sharp changes at higher temperature. These changes could be explained by the presence of different functional groups in lignin and acetobrominated lignin structures and subsequent decompositions with increasing tempertures. Generally, alkali lignin, i.e., CF_AL contains aliphatic and phenolic hydroxyl groups, methoxyl groups, etc. and different ether chemical linkages in its complex structure. By substituting hydroxyl groups with acetyl groups and bromine, along with other chemical linkages created in the lignin structure, as seen through XPS analysis, acetobromination of CF_AL incorporated both into the lignin structure.

When CF_AL was heated (around 100 ºC), it undergoes thermal degradation resulting in faster weight loss due to the release of water, carbon dioxide, and other volatile compounds (Figure 4.17a). The degradation rate gradually decreased as the temperature increased. At higher temperatures, the aromatic ring structure of lignin also begins to break down, leading to the formation of smaller aromatic compounds. However, earlier studies showed that, when acetylated lignin is heated below 100 °C, it may undergo slight weight loss due to the evaporation of water molecules and other low molecular weight compounds [214]. The acetylated lignin structure remains relatively stable at this temperature range. As the temperature increases, more significant decomposition processes begin. In the case of acetylated lignin, the initial decomposition step may involve the cleavage of the acetyl groups from the lignin structure. This process can occur between 200 to 300 °C, depending on the degree of acetylation. At higher temperatures, more significant decomposition steps occur, and the lignin structure starts to break down into smaller fragments. In general, the thermal decomposition of acetylated lignin leads to the formation of various volatile compounds, such as acetic acid, acetone, and phenols, etc. The residue left after decomposition is mainly composed of carbon and ash.

The presence of bromine atoms could increase the thermal stability of the acetobrominated lignin (Figure 4.17b). Earlier studies showed that Polybrominated diphenyl ethers (PBDEs) are thermally stable and can withstand high temperatures without significant decomposition. The thermal stability of PBDEs is attributed to the high bond dissociation energies of the C-Br bonds in their structure, which make them resistant to thermal degradation. The compounds can begin to decompose and release bromine atoms at temperature range 200 to 250 °C, with significant decompositions occur at temperatures above 300 °C. At higher temperatures, PBDEs can completely

decompose into smaller and more volatile compounds [215]. Thermal stability of PBDEs increases with increasing degree of bromination.

The synthesized product by Preparative method-2, i.e., CF_AL_AcBr_AA also demonstrated the maximum thermal stability among the acetobrominated samples due to its higher bromine content (5.67% atoms) than the others. Acetobrominated lignin's thermal breakdown profiles resembled those of PBDEs, suggesting that it might be employed as a flame retardant in a variety of consumer goods, including electronics, textiles, and plastics [215, 216].

The differential scanning calorimetry (DSC) curves and first derivative differential scanning calorimetry (DDSC) curves of the samples are presented in Figure 4.18(a–f).

DSC characteristics and especially their first derivatives could provide more detail information, due to higher sensitivity and the fact that they display all reactions with heat transfer, even those without weight loss, as opposed to TG and DTG. All acetobrominated samples showed exothermic phase transitions at around 46 ºC indicating the first crystallization temeparature and no endothermic peaks were observed for the samples below this temperature. This phenomenon could be explained by the difference in sensitivity of TG and DSC analysis techniques. The DSC is more sensitive to small changes in heat flow compared to the TGA, which is more sensitive to changes in mass. Therefore, in the cases where mass change associated with an endothermic transition is small, it may be detected by the TG, until after the exothermic transition which generates a larger heat flow and is more easily detected by the DSC. As the temperature continues to increase, the mass change associated with the endothermic transition becomes more pronounced and is eventually detected by the TG. CF_AL shwed glass transition temperature of 79.9 ºC as discussed in earlier section. On the other hand, CF_AL_AcBr exhibited multiple exothermic transitions with peaks at 126, 218, 299, and 409 ºC. In contrast, CF_AL_AcBr-1 displayed transitions at 126, 289, and 444 ºC, with a weak signal at 218 ºC. CF_AL_AcBr_AA demonstrated exothermic transitions at around 100 ºC, with a faint peak at 128 ºC. No significant change observed in the temperature range around 150 to 600 ºC. At higher temperatures of 669 and 788 ºC, baseline shifts were evident. On the other hand, CF_AL displayed a broad endothermic transition at around 98 ºC and two exothermic peaks at 264 and 749 ºC. The differences in the thermal breakdown profiles and phase transitions observed in the heat flow curves could be attributed to various factors, including crystallizations, potential chemical reactions and also decompositions of the samples.

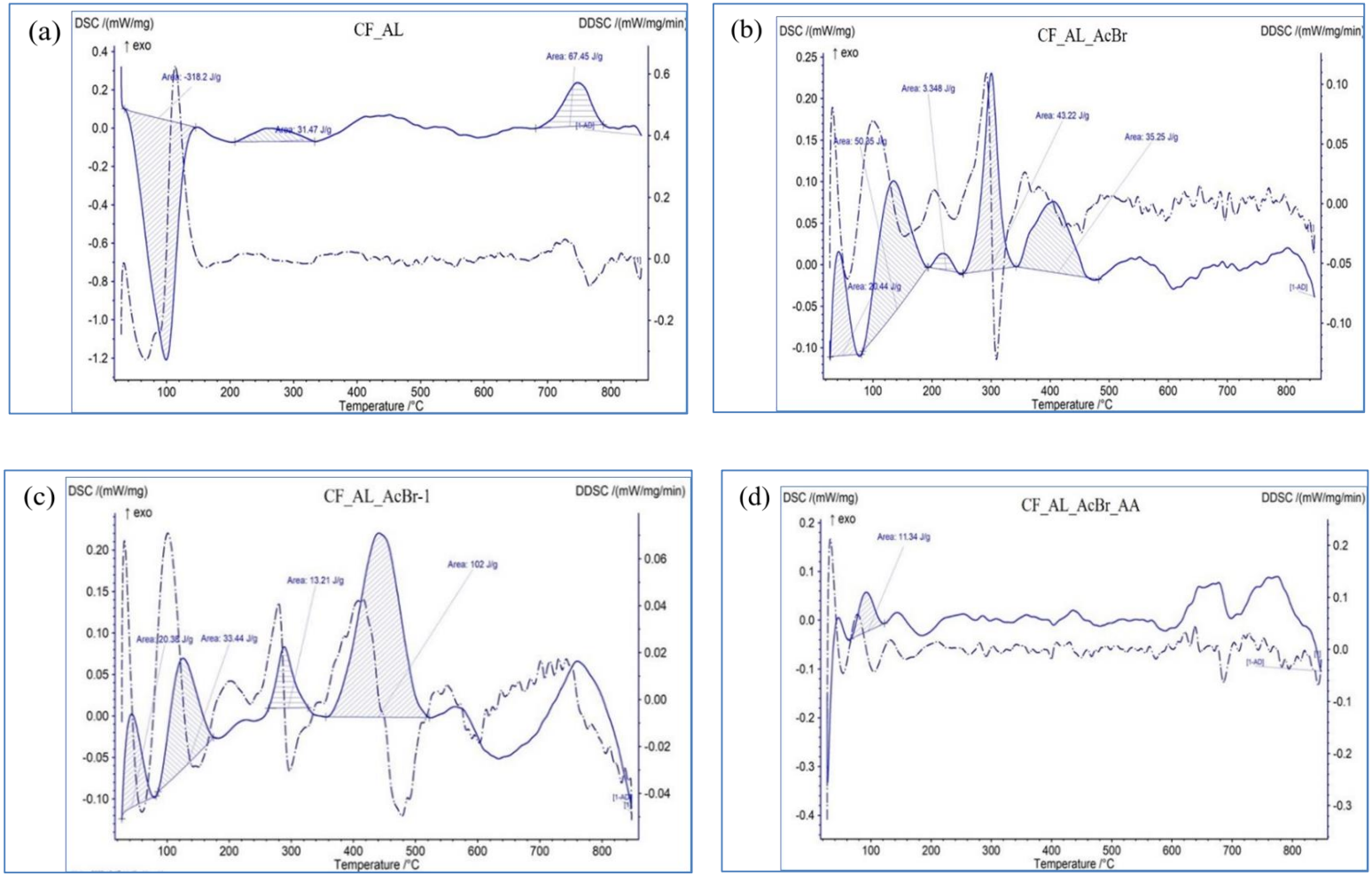

Figure 4.18: Differential scanning calorimetric (DSC) and first derivatives of DSC (DDSC) analyses of CF_AL and acetobrominated CF_AL samples (a) CF_AL (b) CF_AL_AcBr (c) CF_AL_AcBr-1 and (d) CF_AL_AcBr_AA

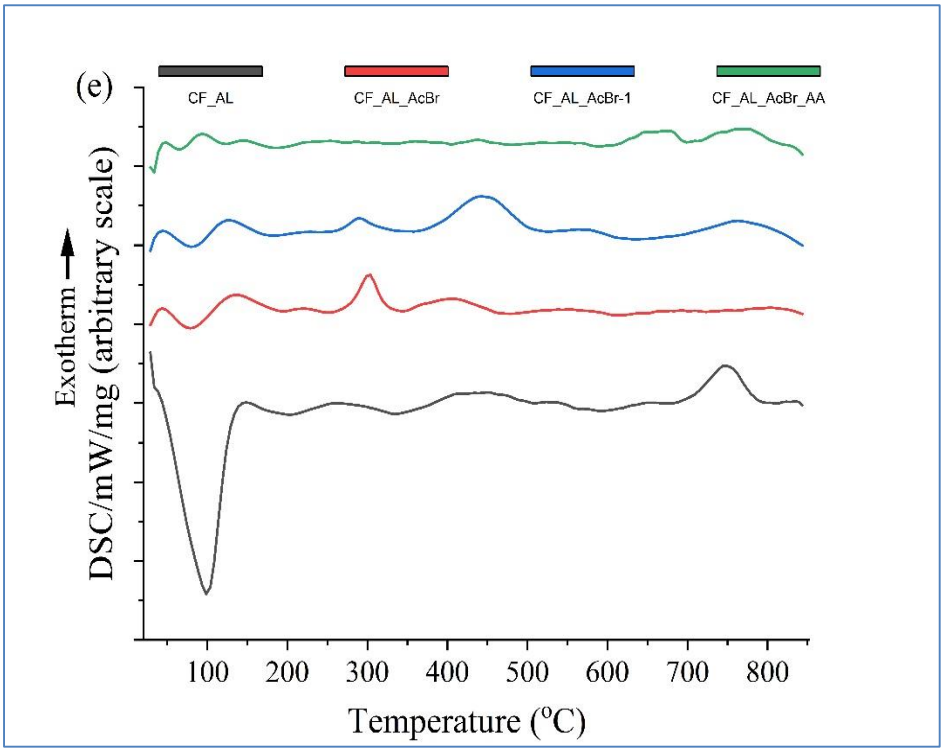

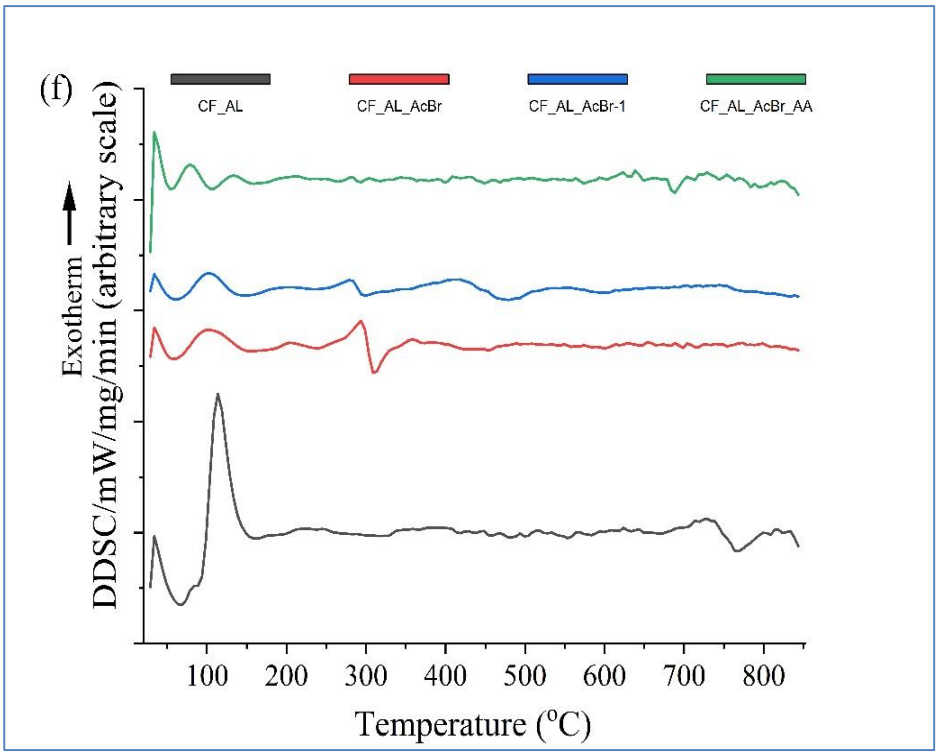

Figure 4.18: Differential scanning calorimetric (DSC) and first derivatives of DSC (DDSC) analyses of CF_AL and acetobrominated CF_AL samples (e) comparison of DSC characteristics and (f) comparison of DDSC characteristics.

Ultraviolet-Visible spectroscopic analysis: Light absorption characteristics of acetobrominated products

UV-Vis spectroscopic analysis of CF_AL and synthesized acetobrominated samples in DMSO at 10 ppm concentrations have been done and depicted in Figure 4.19. Table 4.17 displays the UV-Vis absorption peaks obtained from different electronic transitions in selected samples. All of the samples exhibited absorption of radiation in both the ultraviolet (200 to 400 nm) and visible (400 to 700 nm) regions. CF_AL displayed a broad and intense absorption peak at 256 nm, which can be attributed to the π - π^* transition in the C=C bonds of the aromatic ring. A weak absorption peak at 323 nm can be assigned to the π - π^* transition in the -OCH_3 group attached to the aromatic ring (Ar-OCH_3) of guaiyacyl and syringyl units of lignin [217]. The intensity of this peak is related to the degree of methoxylation of lignin. The absorption peak at 446 nm can be attributed to the π - π^* transition in the C=O groups present in the lignin structure. The UV-Vis spectra of acetobrominated lignin samples showed changes in the absorption peaks and intensities, indicating the formation of new chromophores and conjugated structures. These changes may be attributed to the incorporation of acetyl and bromine groups to the structure of CF_AL.

Interestingly, CF_AL_AcBr exhibited different changes than the other samples and displayed a broad absorption band (ranging from 250 to 400 nm) centered around 323 nm. This broad absorption band was likely due to the extensive conjugation that occurred while the hydroxyl groups were fully acetylated (and brominated accordingly) during acetobromination via the conventional method. On the other hand, the absorption spectra of CF_AL_AcBr-1 and CF_AL_AcBr_AA exhibited similar characteristics to CF_AL. Both samples exhibited two major absorption peaks, one in ultraviolet and the other in visible regions, as observed in the case of CF_AL. Higher absorbances of CF_AL_AcBr-1 and CF_AL_AcBr_AA at around 464 nm indicated higher acetyl groups incorporated in the CF_AL structure. Notably, in the UV region, the absorption peaks slightly shifted to lower wavelengths (blue shift), while in the visible region, the peaks slightly shifted to higher wavelengths (red shift). The shifts of the absorption peaks observed in CF_AL_AcBr-1 and CF_AL_AcBr_AA compared to CF_AL may be attributed to the presence of both the bromine and acetyl groups. Additionally, the reduction in intensity of the peaks at 323 nm may suggest demethylation in lignin.

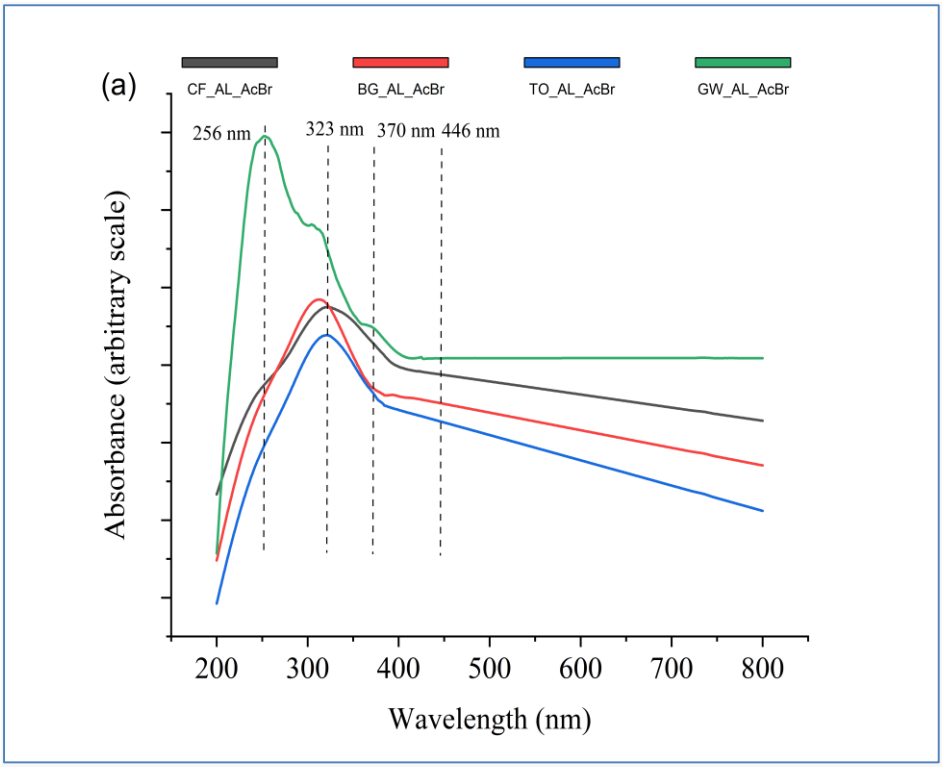

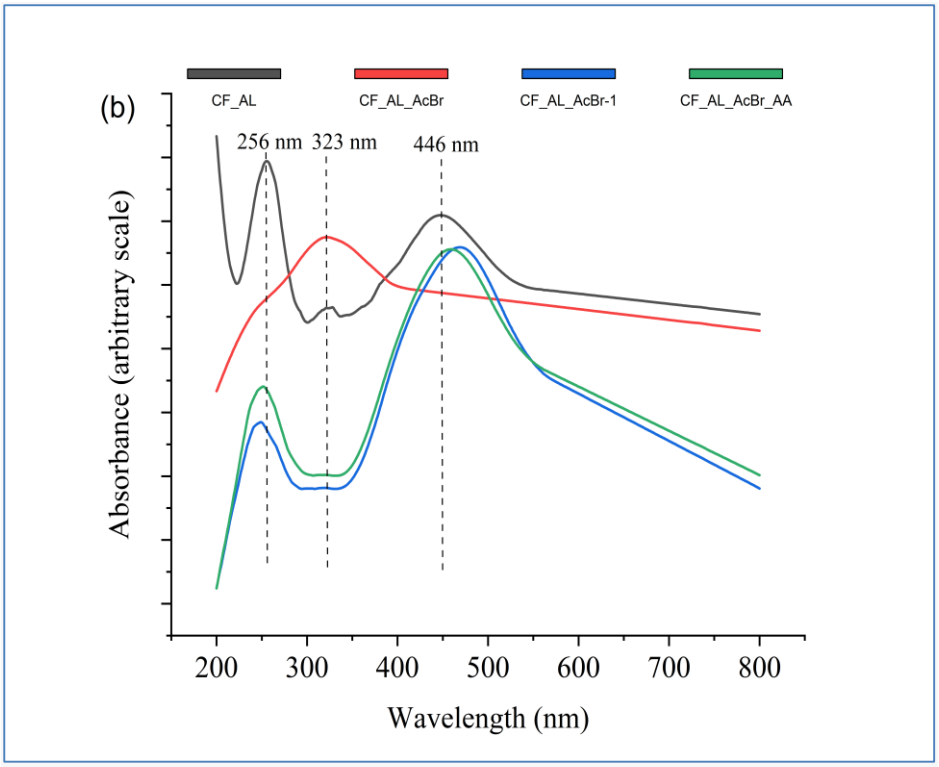

Figure 4.19: UV-Vis spectroscopic analysis acetobrominated samples in DMSO at 10 ppm concentrations (a) Acetobrominated alkali-lignin synthesized by conventional method and (b) selected acetobrominated samples synthesized by new methods. The spectrum of CF_AL was incorporated for comparison.

Table 4.17: UV-Vis spectral data and band assignment of CF_AL and acetobrominated CF_AL samples

Sample	Absorption at wavelengths (nm)	Wavelength of maximum absorption (nm)
CF_AL	256 (broad); 323 (weak); 446 (broad)	λ_{max} 256 nm
CF_AL_AcBr	250 nm (shoulder), 323 (broad)	λ_{max} 323 nm
CF_AL_AcBr-1	250 (broad), 323 (very weak) and 460 (broad)	λ_{max} 460 nm
CF_AL_AcBr_AA	250 (broad), 323 (very weak) and 464 (broad)	λ_{max} 464 nm

It could be observed that the nature of the electronic transitions in acetobrominated lignin is similar to that in unmodified lignin, with the pi-electrons in the aromatic rings being responsible for the absorption of UV-Vis radiation. However, the presence of the bromine and acetyl groups can affect the distribution of electrons in the lignin structure and alter the energy levels of the electronic transitions. This can lead to changes in the UV-Vis spectra of acetobrominated lignin compared to unmodified lignin. It can be concluded that the acetobromination of lignin using the conventional method differs significantly from the preparative methods employed in this study.

Determination of intrinsic viscosity and macromolecular behaviours in solution

The intrinsic viscosities of CF_AL and its acetobrominated products (CF_AL_AcBr, CF_AL_AcBr-1 and CF_AL_AcBr_AA) were measured in very dilute solutions of dimethyl sulfoxide at 25 °C and the results are presented in Table 4.18. Results showed that acetobromination led to a significant increase in the intrinsic viscosity values of CF_AL, although the substitution of hydroxyl groups with acetyl group and bromine atom reduced the number of available hydroxyl groups for intermolecular hydrogen bonding. In addition to this, several factors such as molecular weight, molecular shape, and solvent interactions could also affect the intrinsic viscosity [218, 219].

Increased molecular size resulting from acetobromination may increase the intrinsic viscosity of unmodified lignin. However, if depolymerization occurred during acetobromination, intrinsic viscosity would decrease. Moreover, the presence of acetyl groups and bromine could also affect the intermolecular forces, resulting in changes in intrinsic viscosity compared to the base lignin.

XPS analysis showed that the developed acetobromination methods decreased the C-C/ C-H bonds (C_1 component) from 80.85% in CF_AL to 56.17 and 51.35% in CF_AL_AcBr-1 and CF_AL_AcBr_AA, respectively. Concentration of these bonds slightly decreased in the case of CF_AL_AcBr. Total concentration of C-Br bonds (C_2 component) and acetyl groups (C_3 component) increased by following order:

CF_AL_AcBr_AA > CF_AL_AcBr-1 > CF_AL_AcBr

The presence of acetic acid as reaction media in Conventional and Preparative method-2 could enhance the depolymerization of CF_AL during acetobromination, resulting lower intrinsic viscosity values of CF_AL_AcBr and CF_AL_AcBr_AA in comparison to CF_AL_AcBr-1. Decreased intrinsic viscosity of CF_AL_AcBr_AA than CF_AL_AcBr was due to enhanced depolymerization of lignin during acetobromination at increased reaction temperature, i.e., 90 ^oC in acetic acid media. For a complete understanding of how reaction conditions and substituents affect the intrinsic viscosity of acetobrominated alkali-lignin and related depolymerization phenomena, more research may be required.

Table 4.18: Dilute solution viscometry on CF_AL and acetobrominated CF_AL samples in DMSO at 25 ^oC (Density of DMSO at 25 ^oC was 1.09594 g/mL).

Sample	Relative viscosity	Inherent viscosity (mL/g)	Specific viscosity	Reduced viscosity (mL/g)	Intrinsic viscosity (mL/g)	Dynamic viscosity (mPa.s)	Kinematic viscosity (mm^2/s)
CF_AL	1.046	22.6	0.046	23.1	22.7	3.000	2.737
CF_AL_AcBr	1.126	118.7	0.126	126.0	165.0	3.535	3.224
CF_AL_AcBr-1	1.546	217.8	0.546	273.0	231.6	4.508	4.111
CF_AL_AcBr_AA	1.121	66.8	0.121	70.8	67.8	3.128	2.856

4.3.3. Plausible mechanisms for acetobromination of alkali-lignin using acetic anhydride-bromine in presence or absence of acetic acid

The mechanism of acetobromination through conventional and new methods, i.e., Preparative method-1 and 2, involved the formation of bromoacetylated derivatives of alkali-lignin, such as CF_AL_AcBr, CF_AL_AcBr-1, and CF_AL_AcBr_AA. XPS and other studies have provided evidences that bromine atoms can be attached in both lignin's side chain and aromatic nucleus of the constituting monolignols. Additionally, hydroxyl groups may be substituted with acetyl groups. However, there is no evidence to suggest that the conventional method, as depicted in Reaction scheme 4.1b, introduces bromine

into the aromatic nucleus. Therefore, the following steps may explain the concurrent incorporation of bromine in both the side chain and aromatic nucleus of lignin, as well as the acetylation of hydroxyl groups.

Step-1: In the absence of moisture, acetic anhydride can react with bromine to produce acetyl bromide, acetyl hypobromite, or bromoacetic acid, as depicted in the reaction scheme 4.3. Acetyl hypobromite, being less stable [220], is prone to rearrangement into bromoacetic acid.

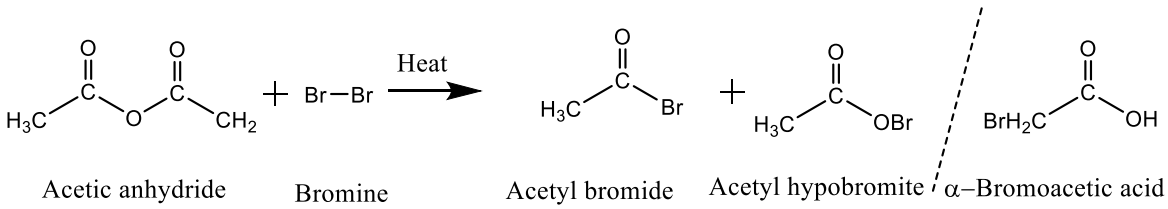

Reaction scheme 4.3: Plausible reaction of bromine with acetic anhydride in absence of Moisture

]

Step-2: In the second step, the nucleophilic substitution reaction between lignin and acetyl bromide (generated in-situ) proceeded in a manner similar to the conventional mehod, leading to acetylation and bromine substitution in the carbon atoms of lignin's side chain, as shown in the reaction scheme 4.4.

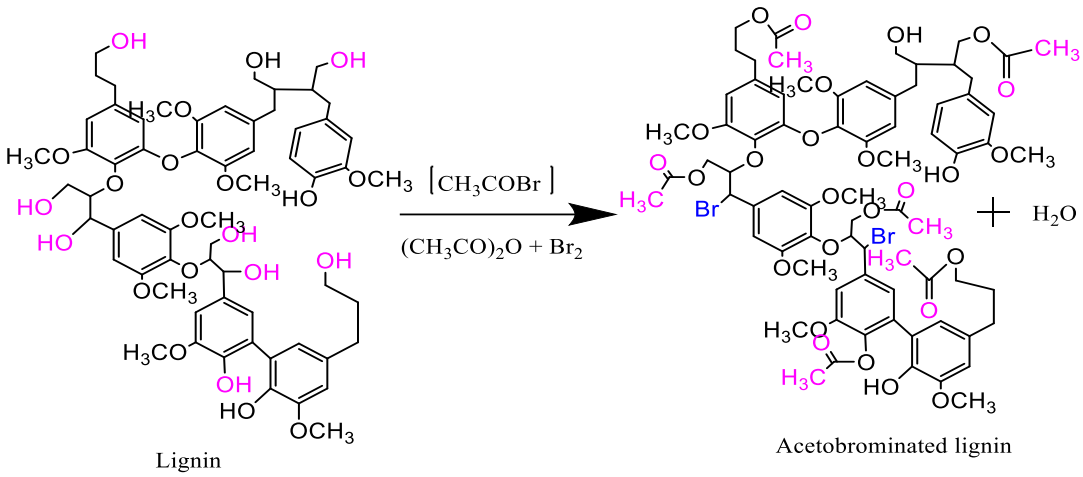

Reaction scheme 4.4: Nucleophilic substitution reaction of acetyl bromide (generated in-situ) in lignin according to conventional method (substitution of hydroxyl groups from α and Ɣ positions of lignin). Acetyl group and bromine in lignin's side chain have been shown in pink and blue color, respectively.

Step-3: Acetyl hypobromite (produced in step-1), has the potential to generate a bromonium ion, can attack aromatic rings of the monolignols in suitable positions and subsequently trigger the electrophilic substitution, i.e., bromination in the aromatic nucleus, as illustrated in the Reaction scheme 4.5.

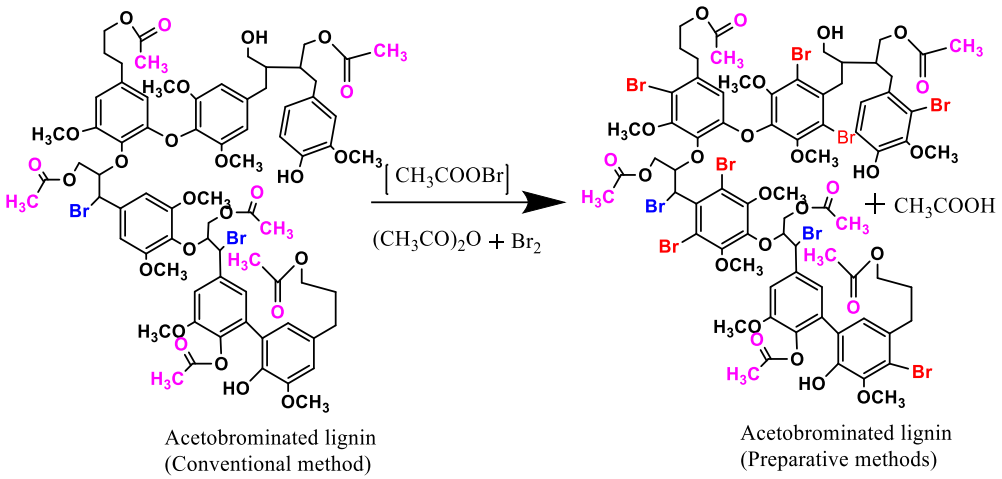

Reaction scheme 4.5: The electrophilic aromatic substitution reaction (bromination) by acetyl hypobromite (generated in-situ) in the lignin structure (attached bromine atoms in the aromatic nucleus have been shown in red color).

The presence of acetic acid in Preparative method-2 facilitated the acetobromination reaction following similar mechanism as described above and supported to introduce more bromine and acetyl groups into lignin structure. XPS studies also supported this fact. Furthermore, depolymerization of alkali-lignin structure could also be observed during acetobromination by new method, i.e., Preparative method-2 due to degradation of different ether linkages under applied reaction conditions [221]. Therefore, different acetobrominated fragments might be generated. Potential substructures of alkali-lignin and corresponding acetobrominated fragments have been presented in Figure 4.20 (a-f) and Figure 4.20 (g-l). Thus, it can be concluded that the reaction mechanism of lignin acetobromination through conventional and new methods differed significantly.

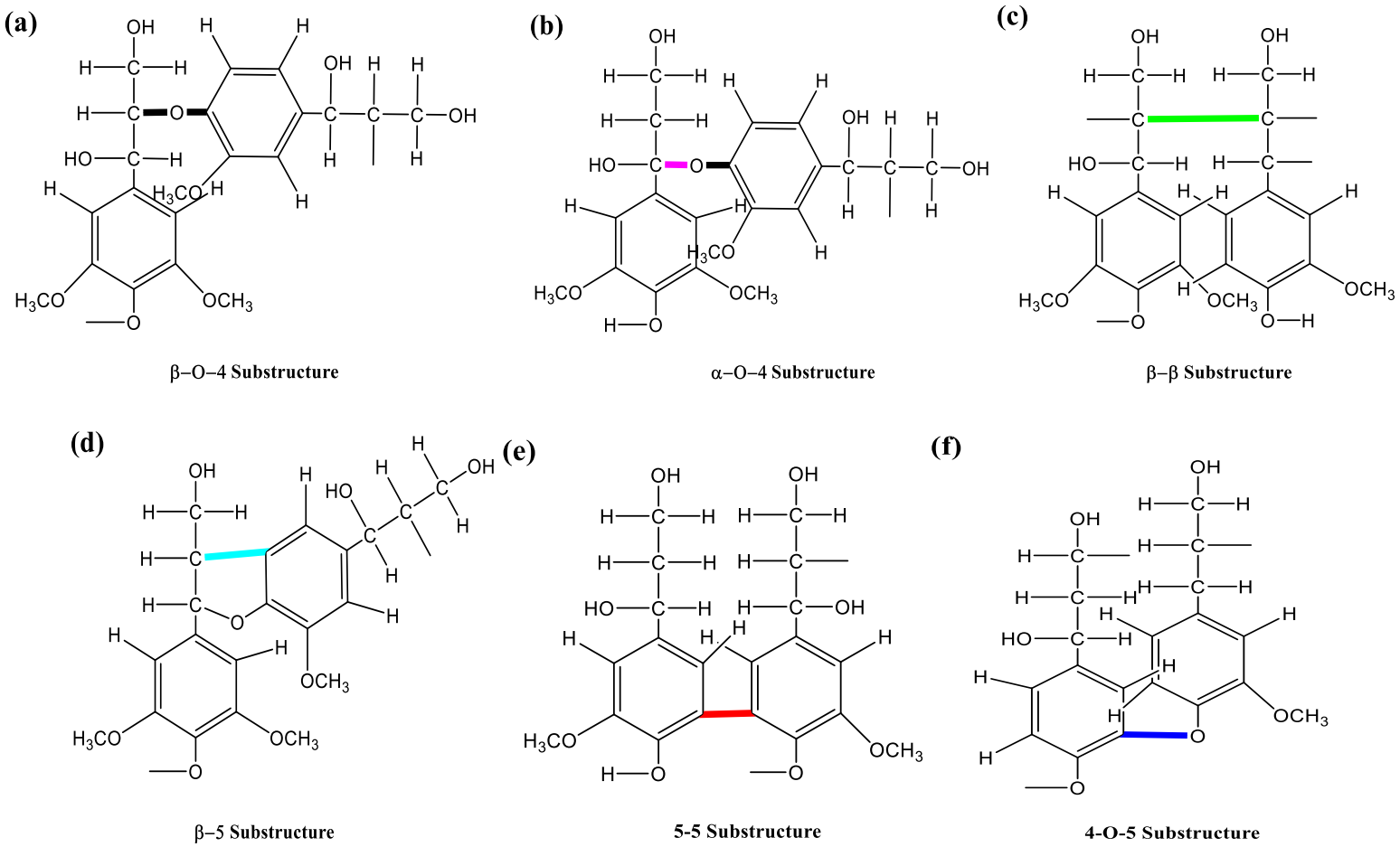

Figure 4.20 (a-f): Potential substructures of alkali-lignin

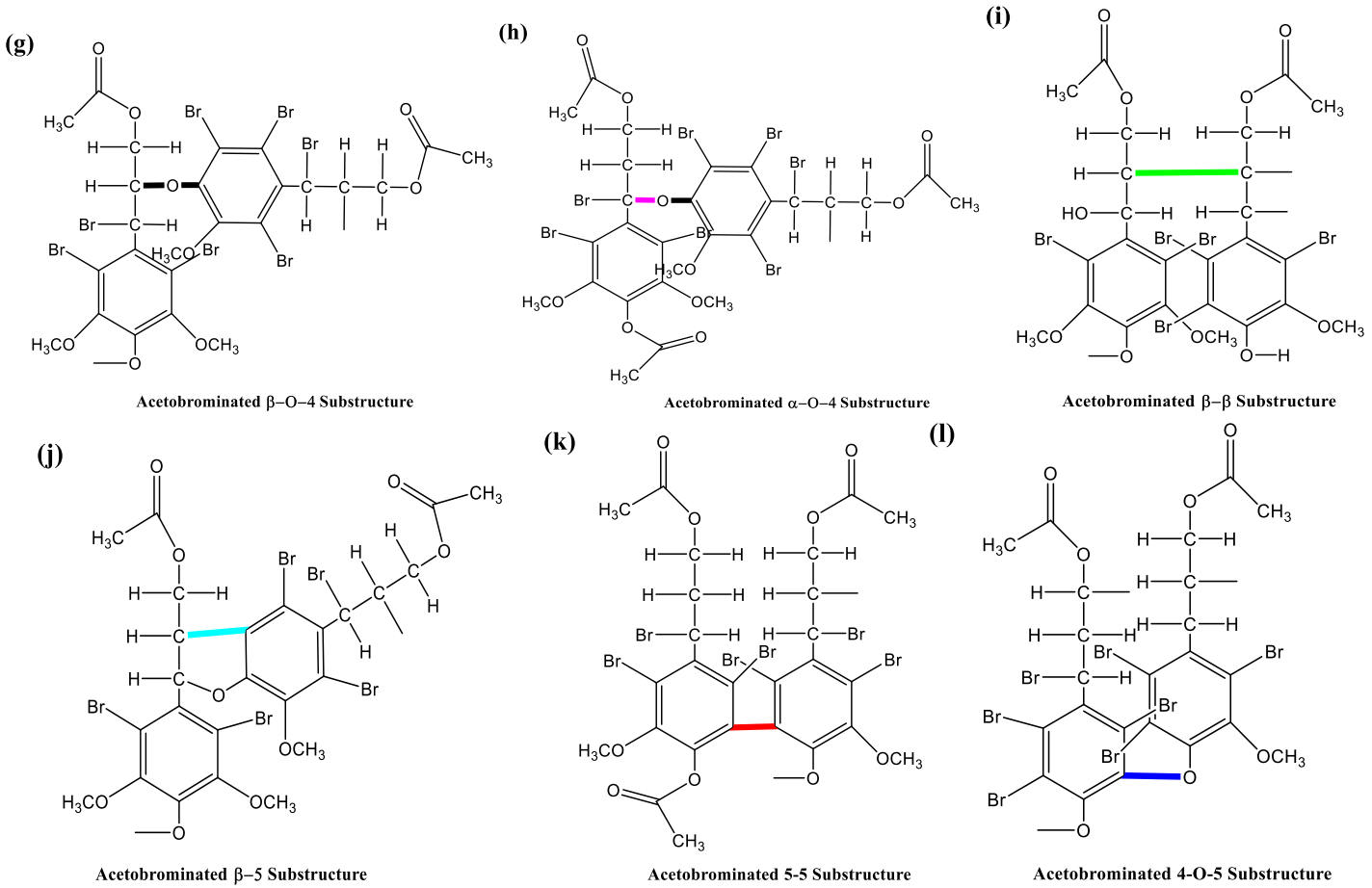

Figure 4.20(g-l)**:** The incorporation of acetyl groups and bromine atoms in the corresponding substructures of alkali-lignin stated in Figure 4.20(a-f)

The use of acetic acid in Preparative method-2 could act as a reaction medium and may facilitate the acetobromination reaction following similar mechanism as described and could introduce more bromine and acetyl groups into lignin structure as determined by XPS technique. At the same time, depolymerisation of lignin was observed in Preparative method-2 under applied reaction temperature, i.e., 90 ºC as indicated by the measurement of intrinsic viscosity. More research is still needed to investigate the degradation nature of alkali-lignin during acetobromination and to identify potential fragments or acetobrominated products.

4.4. Conclusion

- The synthesis of acetobrominated lignin in preparative scale offered a promising approach to modify lignin. The described acetobromination of lignin was a chemical modification technique that involved the addition of acetyl and bromine groups to the complex lignin structure and might be considered as one of the most unexplored techniques for lignin modification.
- The synthesis of acetobrominated lignin involved the use of acetic anhydride and bromine (as reagents) in presence or absence of acetic acid (as solvent) and reaction occurred among the lignin hydroxyl groups, aromatic nucleus, acetyl group and the bromine. The preparative acetobromination procedures could introduce about 17 to 22% (w/w) bromine into complex lignin structure in comparison to conventional procedure (about 5% w/w). Apart from bromine, significant amounts of acetyl group also incorporated in the lignin structure as revealed by XPS study. Various reaction conditions, including temperature, time, and solvent selection could be adjusted to control the degree of substitution and optimize the desired properties of the resulting products.
- Acetobromination presented several advantages for enhancing lignin's properties and expanding its potential applications. Since, lignin has several beneficial properties, such as its abundance and renewable nature, its solubility limitations restrict its potential applications. The complex and heterogeneous chemical structure of lignin is one of the main causes of its low solubility. As the lignin is made up of various phenolic compounds linked together through a complex network of chemical bonds such as ether and carbon-carbon linkages, contribute to lignin's rigidity and resistance to dissolution in most solvents.

- The solubility of lignin can vary depending on the factors such as lignin type, molecular weight, method of isolations, structural modifications, and the presence of impurities. Furthermore, lignin's hydrophobic nature adds to its solubility challenges. Hydrophobic compounds tend to repel water and are more likely to dissolve in non-polar solvents. Since lignin has a high degree of hydrophobicity, it tends to aggregate and form complex three-dimensional structures when exposed to water, making it difficult to dissolve. Another factor that affects lignin solubility is its molecular weight. Lignin has a wide range of molecular weights, ranging from several thousand to over a hundred thousand Daltons. Higher molecular weight lignin tends to have lower solubility due to increased intermolecular interactions. Overcoming the solubility challenge is a crucial step in harnessing lignin's full potential and maximizing its value as a sustainable and renewable feedstock.
- By incorporating acetyl groups, acetobrominated lignin gained increased hydrophobicity along with improved solubility in various organic solvents. Thus, the new modification technique opened up new possibilities for lignin utilization in industries such as coatings, adhesives, and polymer composites, where compatibility with organic matrices is essential.
- Additionally, the presence of bromine groups introduced reactive sites that can be further functionalized, enabling the synthesis of tailored lignin derivatives with desired properties. The functionalization of lignin through acetobromination can unlock the potentials for creating lignin-based polymers with improved mechanical strength, thermal stability, hydrophobicity, chemical resistance and ultraviolet light absorption properties.
- More interestingly, the synthesized acetobrominated lignin products showed extream solubilities in acetone, tetrahydrofuran (THF) and dimethylsulfoxide (DMSO). The synthesized products were moderately soluble in ethanol and insoluble in water. These types of solubility behavior might be considered as a promising property to prepare lignin nanoparticles by anti-solvent precipitation method.
- Therefore, it becomes possible to utilize this abundant natural resource in a broader range of applications, such as the production of adhesives, flame and fire retardants, coatings, polymer additives, carbon materials, and specialty chemicals.
- More research is still needed to fully understand the properties of acetobrominated lignin and utilization of acetobrominated lignin in the following fields-

(i) Adhesives: Acetobrominated lignin might be used as a binder in adhesive formulations, particularly for wood products. The modified lignin may improve the water resistance and mechanical properties of the adhesive.

(ii) Coatings: Acetobrominated lignin may be used as a coating material for various substrates, including paper, textiles, and metals. The modified lignin may provide improved adhesion, water resistance, and barrier properties.

(iii) Carbon materials: Acetobrominated lignin might be explored as a precursor for the production of carbon materials, such as activated carbon and carbon fibers.

(iv) Polymer additives: Acetobrominated lignin might be used as a polymer additive, particularly for improving the flame retardancy and thermal stability of the polymer matrices.

(v) Bio-based materials: Acetobrominated lignin has potential as a bio-based material for various applications, including packaging, composites, and functional materials. The modified lignin may provide improved properties and sustainability compared to unmodified lignin.

4.5. References

[174] J. Asikkala, T. Tamminen and S. D. Argyropoulos, Accurate and reproducible determination of lignin molar mass by acetobromination, *Journal of Agricultural and Food Chemistry*, 2012, 60(36), 8968–8973, doi:10.1021/jf303003d

[175] D. Ioffe and R. Frim, Bromine, Organic Compounds, 1-26, doi.org/10.1002/0471238961.0218151325150606.a01.pub2

[176] G. W. Gribble, Natural Organohalogens: A New Frontier for Medicinal Agents? *J. Chem. Educ.* 2004, 81, 10, 1441, doi:10.1021/ed081p1441

[177] F. C. M. Lobo, A. R. Franco, E. M. Fernandes and R. L. Reis, An Overview of the Antimicrobial Properties of Lignocellulosic Materials, *Molecules*, 2021, 26(6), 1749, doi:10.3390/molecules26061749

[178] C. Torres-Duarte and R. Vazquez-Duhalt, Applications and Prospective of Peroxidase Biocatalysis in the Environmental Field, E. Torres and M. Ayala, (eds) Biocatalysis Based on Heme Peroxidases. Springer, Berlin, Heidelberg, 2010, pp.179-206, doi:10.1007/978-3-642-12627-7_8

[179] A. Sequeiros, L. Serrano and J. Labidi, Bromination of guaiacol and syringol using ionic liquids to obtain bromides, *Journal of Chemical Technology & Biotechnology*, 2016, 91(6), 1809–1815, doi:10.1002/jctb.4773

[180] A. V. Fejzagić, J. Gebauer, N. Huwa, T. Classen, Halogenating Enzymes for Active Agent Synthesis: First Steps Are Done and Many Have to Follow, *Molecules*, 2019, 24(21):4008, doi:10.3390/molecules24214008

[181] I. Carletti, B. Banaigs, P. Amade, Matemone, a New Bioactive Bromine-Containing Oxindole Alkaloid from the Indian Ocean Sponge *Iotrochota purpurea*, *Journal of Natural Products*, 2000, 63(7), 981–983. doi:10.1021/np990408d

[182] S. N. Lopez, I. A. Ramallo, M. G. Sierra, S. A. Zacchino, R. L. E. Furlan, Chemically engineered extracts as an alternative source of bioactive natural product-like compounds, Proceedings of the National Academy of Sciences, 2007. 104(2), 441–444, doi:10.1073/pnas.0608438104

[183] I. A. Ramallo, M. O. Salazar, L. Mendez, R. L. E. Furlan, Chemically Engineered Extracts: Source of Bioactive Compounds, *Acc. Chem. Res.*, 2011, 44(4), 241–250, doi:10.1021/ar100106n

[184] L. Méndez, M. O. Salazar, I. A. Ramallo, R. L. E. Furlan, Brominated Extracts As Source of Bioactive Compounds. *ACS Comb. Sci.* 2011, 13(2), 200–204, doi:10.1021/co100073k

[185] R. Rinaldi, R. Jastrzebski, M. T. Clough, J. Ralph, M. Kennema, A. P. C. Bruijnincx and B. M. Weckhuysen, Paving the Way for Lignin Valorisation: Recent Advances in Bioengineering, Biorefining and Catalysis. *Angewandte Chemie* International Edition, 2016, 55(29), 8164-8215, doi.org/10.1002/anie.201510351

[186] J. J. Meister, Modification of lignin, *Journal of Macromolecular Science*, Part C: *Polymer Reviews*, 2002, 42:2, 235-289, DOI: 10.1081/MC-120004764

[187] A. E. Kazzaz, Z. H. Feizi and P. Fatehi, Grafting strategies for hydroxy groups of lignin for producing materials, *Green Chem*., 2019, 21, 5714, DOI: 10.1039/c9gc02598g

[188] S. Elangovan, A. Afanasenko, J. Haupenthal, Z. Sun, L. Yongzhuang, A. K. H. Hirsch and K. Barta, From Wood to Tetrahydro-2-benzazepines in Three Waste-Free Steps: Modular Synthesis of Biologically Active Lignin-Derived Scaffolds, *ACS Central Science*, 2019, 5 (10), 1707-1716, DOI: 10.1021/acscentsci.9b00781

[189] W. Lan and J. S. Luterbacher, A Road to Profitability from Lignin via the Production of Bioactive Molecules, *ACS Cent. Sci*. 2019, 5, 10, 1642–1644, doi.org/10.1021/acscentsci.9b00954

[190] R. Liu, L. Dai, C. Xu, K. Wang, C. Zheng and C. Si, Lignin-based micro-/nanomaterials and composites in biomedical Applications, *ChemSusChem*, 2020, doi:10.1002/cssc.202000783

[191] P. Jeschke, The unique role of halogen substituents in the design of modern agrochemicals, *Pest Manag Sci*. 2010, 66(1):10-27, doi: 10.1002/ps.1829

[192] W. Zhao, L. Xiao, G. Song, R. Sun, L. He, S. Singh, B. Simmons and G. Cheng, *Green Chem*., 2017, 19, 3272-3281, doi:10.1039/c7gc00944e

[193] P. Karrer and F. Widmer, Polysaccharides. IX. Cellulose and Lignin, *Helv. Chim, Acta*, 1921, 4, 700-702, doi:10.1039/ca9212000761

[194] D. E. Pearson, R. D. Wysong, C. V. Breder, Ortho bromination of phenols, *The Journal of Organic Chemistry*, 1967, 32(7), 2358–2360, doi:10.1021/jo01282a063

[195] D. B. Johnson, W. E. Moore and L. C. Zank, The spectrophotometric determination of lignin in small wood samples. *Tappi*, 1961, 44(11):793– 798

[196] K. Iiyama, and A. F. A. Wallis, Determination of lignin in herbaceous plants by an improved acetyl bromide procedure, *Journal of the Science of Food and Agriculture*, 1990, 51(2), 145-161, doi.org/10.1002/jsfa.2740510202

[197] R. Hatfield and R. S. Fukushima, Can Lignin Be Accurately Measured? *Crop Science*, 2005, 45(3), 832-839, doi.org/10.2135/cropsci2004.0238

[198] Y. Ogata, Y. Furuya and K. Okano, The Bromination of Aromatic Compounds with a Mixture of Peroxyacetic Acid and Bromine in Acetic Acid, *Bulletin of the Chemical Society of Japan*, 1964, 3(7), doi.org/10.1246/bcsj.37.960

[199] K. J. P. Orton, H. B. Watson and H. I. Hughes, CCCXXIX. The interaction of bromine with acetic anhydride. Part II. *Journal of the Chemical Society (Resumed)*, 1927, 2458–2465, doi:10.1039/jr9270002458

[200] H. B. Watson, CCCCVI. The Interaction of Bromine with Acetic Anhydride. Part III. Arrest of the Reaction. A Comparison with the Brominntion of Acetone., *Journal of the Chemical Society (Resumed)*, 1927, 3065-3068, doi.org/10.1039/JR9270003065

[201] H. B. Watson and E. H. Roberts, CCCLXVII. The Interaction of Bromine with Acetic Anhydride. Part IV. Bromination and Chlorination compared, *Journal of the Chemical Society (Resumed)*, 1928, 2779-2786, doi:10.1039/jr9280002779

[202] W. 1. Burnett, CXXV. An Accident With Acetic Anhydride and Bromine, *J. Chem. Educ*. 1975, 52(6), A322, doi.org/10.1021/ed052pA322

[203] F. Lu and J. Ralph, Reactions of Lignin Model ß-Aryl Ethers with Acetyl Bromide, *Holzforschung*, 1996, 50(4):360-364, doi.org/10.1515/hfsg.1996.50.4.360

[204] J. F. Moulder, W. F. Stickle, P. E. Sobol and K. D. Bomben, Handbook of X-ray Photoelectron Spectroscopy (ed. J. Chastain), Perkin-Elmer Corporation, United States of America, 1992, 1-260

[205] O. Faix, Methods in Lignin Chemistry, (ed. S. Y. Lin and C. W. Dence), Springer-Verlog, Berlin Heidelberg, First edition, 1992, 4, 81-106

[206] K. Lundquist, 1H NMR spectral studies of lignin: Results regarding the occurrence of beta-5 structures, beta-beta structures, non-cyclic benzyl aryl ethers, carbonyl groups and phenolic groups, *Nordic Pulp & Paper Research Journal*, 1992, 7(1), 4-8a, doi.org/10.3183/npprj-1992-07-01-p004-008

[207] C. L. Chen and D. Robert, Characterization of lignin by 1H and 13C NMR spectroscopy, *Methods in Enzymology*, 1988, 161,137–174, doi:10.1016/0076-6879(88)61017-2

[208] Zhou, S., Huang, G. Extraction, structure characterization and biological activity of polysaccharide from coconut peel. *Chem. Biol. Technol. Agric.* **10**, 15 (2023). https://doi.org/10.1186/s40538-023-00391-x

[209] Rencoret J, Marques G, Gutierrez A, Nieto L, Santos JI, Jimenez-Barbero J, Martínez ÁT, del Río JC. HSQC-NMR analysis of lignin in woody (Eucalyptus globulus and Picea abies) and non-woody (Agave sisalana) ball-milled plant materials at the gel state 10th EWLP, Stockholm, Sweden, August 25–28, 2008.

[210] Zhao C, Huang J, Yang L, Yue F, Lu F. Revealing structural differences between alkaline and kraft lignins by HSQC NMR. Industrial & Engineering Chemistry Research. 2019 Mar 19;58(14):5707-14.

[211] Latham, K.G., Matsakas, L., Figueira, J., Rova, U., Christakopoulos, P. and Jansson, S., 2021. Examination of how variations in lignin properties from Kraft and organosolv extraction influence the physicochemical characteristics of hydrothermal carbon. *Journal of Analytical and Applied Pyrolysis*, *155*, p.105095.

[212] R. A. C. Gomide, A. C. S. de Oliveira, D. A. C. Rodrigues, C. R. de Oliveira, O. B. G. de Assis, M. V. Dias, S. V. Borges, Development and Characterization of Lignin Microparticles for Physical and Antioxidant Enhancement of Biodegradable Polymers, *Journal of Polymers and the Environment*, 2020, 28, 1326–1334, doi.org/10.1007/s10924-020-01685-z

[213] M. Altarawneh, A. Saeed, M. Al-Harahsheh and B. Z. Dlugogorski, Thermal decomposition of brominated flame retardants (BFRs): Products and mechanisms, *Progress in Energy and Combustion Science*, 2019, *70*, 212-259, doi.org/10.1016/j.pecs.2018.10.004

[214] P. Shao-hong, C. Lie-qiang, L. Liu-bin and X. Ming-quan, Thermal Decomposition of Decabromodipheny1 Ether During the TempPS Resin in Fire, *Procedia Engineering*, 2011, 11, 349-354, doi.org/10.1016/j.proeng.2011.04.668

[215] J. H. Shin and Y. J. Baek, Analysis of polybrominated diphenyl ethers in textiles treated by brominated flame retardants, *Textile Research Journal, 2012*, 82(13), 1307-1316. doi:10.1177/0040517512439943

[216] P. Boguta, Z. Sokołowska and K. Skic, Use of thermal analysis coupled with differential scanning calorimetry, quadrupole mass spectrometry and infrared spectroscopy (TG-DSC-QMS-FTIR) to monitor chemical properties and thermal stability of fulvic and humic acids. *PLoS One*. 2017, 12(12):e0189653, doi: 10.1371/journal.pone.0189653

[217] G. Aufischer, R. Süss, B. Kamm and C. Paulik, Depolymerisation of kraft lignin to obtain high value-added products: antioxidants and UV absorbers, *Holzforschung*, 2022, 76(9), 845-852, doi.org/10.1515/hf-2022-0023

[218] D. Dong and A. L. Fricke, Intrinsic viscosity and the molecular weight of kraft lignin, *Polymer*, 1995, 36(10), 2075-2078, doi.org/10.1016/0032-3861(95)91455-G

[219] D. A. I. Goring, The physical chemistry of lignin, *Pure and Applied Chemistry*, 1962, doi:10.1351/pac196205010233

[220] J. J. Reilly, D. J. Duncan, T. P. Wunz, R. A. Patsiga, Isolation and properties of acetyl hypobromite. *The Journal of Organic Chemistry*, 1974, 39(22), 3291-3292, doi:10.1021/jo00936a032

[221] F. Lu and J. Ralph, Reactions of Lignin Model ß-Aryl Ethers with Acetyl Bromide, *Holzforschung*, 1996, 50(4):360-364, doi.org/10.1515/hfsg.1996.50.4.360

CHAPTER 5

RECOVERY OF PRETREATMENT CHEMICALS FROM WASTE LIQUORS OF THE BIOREFINERY

Chapter 5: Recovery of Pretreatment Chemicals from Waste Liquors of the Biorefinery

5.1. Introduction

Pretreatment is one of the fundamental unit activities in a biorefnery system. Therefore, it is essential to evaluate the pretreatment stage along with all relevant machinery and processing options in a proposed biorefinery technique. Finding appropriate and sustainable production techniques require the use of tools like life-cycle analysis and techno-economic assessments. A number of challenges have been identified for implementation of successful future biorefneries, e.g., scale-up to industrial scale, construction and design, biomass availability, logistics and supply, maturity of a process, etc. [222, 223].

However, vast amounts of lignocellulosic biomass are being processed for the pulp production. Different pulping processes are used depending on the fibre materials and the desired end products. Chemical pulping is by far the most common method for pulping wood both in Europe and in the United States. Chemical pulps have a low yield, but the pulp produced is of very high quality. The most common process, e.g., the kraft process, accounts for more than 80% of all chemical pulp produced both in the United States and in Europe. In this process, the virgin materials are mixed with a chemical solution, called white liquor, in a digester, where they are pressurized and heated to dissolve the lignin from the wood. After being dissolved, the virgin material is separated into individual fibers, e.g. pulp and the chemical mixture, e.g. black liquor, is concentrated in an evaporator. Then, it is burned in a recovery boiler, where the energy is recovered, often cogenerating both steam and electricity, which is then used as process energy [224].

The characteristics of the wastewater generated from various processes of the pulp and paper industry depend upon the type of process, type of the wood materials, process technology applied, management practices, internal recirculation of the effluent for recovery, and the amount of water to be used in the particular process. The kraft process, which involves turning wood into wood pulp and ultimately bleached pulp, is used to make industrial paper. Pollution from the pulp and paper industry being created from two steps, e.g. pulping and bleaching processes. These processes generate volatile organic compounds, reduced sulfur compounds, organochlorine compounds, fine and coarse particulates, NO_x, SO_x, etc. [225, 226].

Table 5.1: Potential pollutants from pulping industries [225, 234, 239].

Main input	Processing step	Environmental pollutants
Raw material/wood	Wood preparation	Solid wastes and wastewater
Chemicals/energy	Pulp manufacture	Air emissions and wastewater
Process water	Pulp washing/screening	Dissolved material, residual chemicals, and waste water
Chemicals/energy	Pulp bleaching	Air emissions, dissolved material, residual chemicals, and waste water
Energy	Pulp drying	Air emissions
Energy/water/chemicals	Paper manufacture	Solid wastes, dissolved materials, residual chemicals, and wastewater

Major organic constituents of black liquor are lignin, carboxylic acids, and hemicelluloses are high-priority candidates for further processing and production of platform chemicals and value-added products. The treated liquor contains modified lignin, residual carbohydrates, and degradation products thereof, like hydroxy carboxylic acids. Modern kraft pulp mills have already produced and marketed a variety of bio-based products besides the main revenue, cellulose [228].

On the other hand, in sulfite process, depending on the raw material used, the main components present in the spent liquor are sugars from hemicelluloses, e.g. xylose, mannose, etc. and lignosulfonates. This spent liquor could be used to prepare lignosulfonates, xylitol, ethanol, polyhydroxybutyrate or polybutylene-succinate, hydrogen and furfural, etc. Oher compounds present in the liquor such as furans, acids and inorganic pollutants can complicate the valorization options [229].

It was shown that the pulp and paper mill effluents were chemical compounds, mostly degraded lignin, cellulose, hemicelluloses and extractives which contain phenols, enol ethers, mercaptides, stilbene, quinone derivatives, chlorinated phenols, acetic acid, formic acid, acetaldehyde, methanol, furfural, methyl glyoxal, etc. and also contain a large numbers of organochlorine compounds [230]. These effluents might cause significant pollution, if discarded in the environment without proper treatment. Pollution from the pulp and paper industry can be minimized by various internal process changes and different management measures [231-233].

However, lignin is a common waste product generated during chemical pulping and biorefinery processes aimed at producing various products from lignocellulosic biomass. Although lignin has limited value as a standalone product, there are ongoing efforts to

develop processes and technologies to convert it into high-value products, which would increase the economic and environmental sustainability of the pulping and biorefinery processes [234, 235]. The specific fate of lignin produced during biorefinery processes depends on the process used and the goals of the biorefinery [236, 237].

Table 5.2: Pretreatment of lignocellulosic biomass and lignin recovery from waste liquor

Pretreatment process	Applied conditions	Lignin isolation from black/waste liquors
Alkali-AQ process	(NaOH/KOH + AQ), pH 13-14, elevated temperature	Acid precipitation
Kraft process	($NaOH + Na_2S$); pH 13-14, elevated temperature	Acid precipitation
Sulfite process	($H_2SO_3 + HSO_3^-$) with Ca^{2+}, Mg^{2+} Na^+, or NH_4^+; pH 1.5 to 5, elevated temperature, alkali concentration	Membrane filtration
Bioethanol process	Modrerate to elevated temperatures, pH, time, uniform mixing, nutrient supplimentation, inhibitor mitigation, etc.	Precipitation at neutral or acidic conditions
Deep eutectic solvents	Moderate to elevated temperatures, time, and pressure	Liquid-liquid extraction by organic solvents
Ionic liquids	Moderate to elevated temperatures, time, and pressure	Organic solvents
Hydrolysis	Acidic, alkaline, or enzymatic hydrolysis conditions at moderate to elevated temperatures	Acid precipitation
Organosolv	Organic acid-based, alcohol/water-based, and mixed solvents; elevated temperature	Precipitation by aqueous dioxane solution

One of the most common biorefinery processes is the production of cellulosic ethanol, which involves breaking down plant biomass's cellulose and hemicelluloses into sugars that can be fermented into ethanol. The waste liquor generated during bioethanol production is known as stillage, vinasse, or spent wash, depending on the process used. There are two main types of waste liquor, (i) thin stillage and (ii) thick stillage. Thin stillage is the liquid portion that remains after the solids have been separated from the fermented mash during distillation. It contains residual sugars, organic acids, minerals, and enzymes. Thick stillage is the concentrated; high-solids fraction remaining after the thin stillage has been concentrated through evaporation. It contains a higher concentration of organic compounds and minerals than thin stillage. Managing waste liquor can be challenging since it is high in organic matter and nutrients, potentially

harming the environment if not properly treated. However, it can also be a valuable resource for biogas production, animal feed, or fertilizer [238-243].

To secure long-term sustainability of the envisioned material-driven phase III lignocellulosic feedstock biorefinery system, a crucial step involves treating the spent liquors resulting from the separation of alkali-lignin. This treatment process aims to recover the chemicals employed during the separation processes of pulp, hemicellulose and lignin, while simultaneously transforming the spent liquors into a valuable resource, e.g., fertilizer for agricultural applications.

In this study, the applied treatment on spent liquors involved a crystallization process that enabled the extraction of salts which were abundant in potassium, nitrogen, and phosphorus (NPK). These elements can be considered as essential nutrients for plant growth and are commonly found in NPK-fertilizers. While the focus of the treatment process was to recover valuable chemicals, i.e., phosphoric acid and potassium hydroxide, and convert the spent liquors into a fertilizer resource by adding ammonium hydroxide, it was possible that not all substances present in the spent liquors could be completely extracted or transformed. These irrecoverable substances may include trace potassium, phosphate and ammonium ions, degraded organic compounds, or other components that were not targeted for the cryatallization. In this case, the liquors containing irrecoverable valuable nutrients were concentrated, making them a nutrient-rich fertilizer blend suitable for use as another NPK-fertilizer product. All products were analyzed by different instrumental methods.

5.2. Materials and methods

5.2.1. Materials

In this study, ammonium hydroxide (Merck, India) was ued to recover the pretreatment chemicals (phosphoric acid and potassium hydroxide) and degraded organics from the spent liquors (generated after the separation of alkali-lignins from black liquors of the biorefinery, as shown in Table 3.4).

5.2.2. Methods

Recovery of chemicals, i.e., acid, base and degraded organics as NPK-salts and liquid NPK-fertilizers

After the separations of alkali-lignin, spent liquors or filtrates were obtained, typically measuring around 250 mL and having a pH of approximately 2.5. To initiate the processes for recovery of used chemicals, i.e., acid, base and degraded organics, necessary amounts of ammonium hydroxide (or a mixture of ammonium and potassium hydroxides) were added to the spent liquors. This addition served to neutralize the acidic pH of the filtrates. By adjusting the pH to a neutral level, four salts were crystallized and recovered by filtration method. The salts were air dried and stored for analysis.

Furthermore, the filtrates, which represent the liquid fertilizers, i.e., CF_LF, BG_LF, TO_LF and GW_LF, underwent a distillation process. This distillation process aimed to separate the desired components from liquid fertilizers for further analysis and utilization. After the distillation, the resulting residues were obtained. These residues contained the concentrated form of the desired components. To remove any remaining moisture and prepare them for analysis, the residues were dried in an oven at a temperature of 105 °C. The drying process helped to ensure the residues, i.e., CF_LF-S, BG_LF-S, TO_LF-S and GW_LF-S were in stable and dry state suitable for subsequent analysis.

Characterization of the cystallized salts and liquid fertilizers

Scanning electron microscopy-energy dispersive X-ray spectroscopic analysis

Analyses of the morphology and compositions of prepared crystallized salts, *i.e.*, CF_SF, BG_SF, TO_SF and GW_SF were done by scanning lectron microscope attached with energy dispersive x-ray spectrometer applying electron voltage 15 kV. The moisture-free crystalline salts were set/mounted on carbon tape with adhesive and sputter-coated with platinum before analysis. Observation was done with the help of charge compensator. The same method was applied to analyze the solid contents of liquid fertilizers, *i.e.,* CF_LF-S, BG_LF-S, TO_LF-S and GW_LF-S.

X-ray photoelectron spectroscopic analysis

Surfaces of all crystallized salts, e.g. CF_SF, BG_SF, TO_SF and GW_SF were analyzed by x-ray photoelectron spectrometer under high vacuum ($2x10^{-9}$ mbar) and at room temperature. The moisture-free salt samples were drop-casted using ethanol and dried under vacuum before analysis. The wide scans (200 eV pass energy) were performed to determine the surface elemental composition of salt samples. All spectra were reconstructed using OriginPro 2022 software.

X-ray diffraction analysis

X-ray diffraction (XRD) analysis was performed on the crystalized salts, i.e., CF_SF, BG_SF, TO_SF and GW_SF under ambient temperature and pressure in the diffraction angle, 2θ ranging from 5 to 80^{o}. A Rigaku X-ray Diffractometer with Ni-filtered Cu Kα radiation (λ = 0.1548 nm) was used at 40 kV and 40 mA. X-ray diffraction patterns were generated as a plot of intensities (counts) of the scattered x-rays at specified angles by the salt samples. All deffractograms were reconstructed using OriginPro 2022 software. Identification of phases was achieved by comparing the acquired data with reference database.

Determination of physicochemical properties of liquid fertilizers and their solid contents

All liquid fertilizers were analyzed by different physicochemical methods. pH of the liquids were determined at 25 ^{o}C using a bench top pH meter (Hach, USA). Densities were measured at 25 ^{o}C by using a density meter (DMA 5000M, Anton-paar, Austria). Refractive indices were measured at 25 ^{o}C by a digital refractometer (Abbemet; Anton-paar, Austria). Moisture contents were determined by Karl-Fisher Titrator (Metrohm, Switzerland) and solid contents were obtained by difference. Dynamic and kinematic viscosities were measured at 25 ^{o}C by using a microviscometer (Lovis 2000 M/ME, Anton-paar, Austria). Ash contents were measured by muffle furnace at 850 ^{o}C for six hours.

5.3. Results and discussion

Recovery of chemicals from waste liquor as crystalline salts and liquid NPK-fertilizers

The spent liquors, despite their acidic nature, were not discarded but rather utilized for the recovery of valuable components, including phosphoric acid, potassium hydroxide, and degraded organics. The recovery processes aimed to transform these spent liquors into usable forms, such as NPK-salts and liquid NPK-fertilizers. The volume and pH of the spent liquors and the amounts of recovered NPK salts and liquid NPK fertilizers were given in Table 5.3.

Table 5.3: Recovery of chemicals from spent liquors as NPK-fertilizers

Ex-free biomass sample	Spent liquors	Recovered salts and liquid fertilizers	
	Volume (mL) and pH	Crystallized NPK-salts (g)	Solid contents of liquid NPK-fertilizer (%)
CF	250; 2.5	1.03	41.29
BG	250, 2.5	2.43	29.50
TO	250; 2.4	2.56	27.72
GW	250; 2.5	2.47	24.80

The pH of the black liquors obtained from the biorefinery was approximately 13.5, resulting from the digestion of used lignocellulosic biomass with 4% w/v potassium hydroxide solution. To separate the lignin from these alkaline black liquors containing soluble lignin, degraded organics and KOH, phosphoric acid was used to adjust the pH to around 2.5. This adjustment facilitated the occurrence of the following reaction:

$$\text{Lignin(aq) + Degraded organics(aq) + KOH(aq)} \xrightarrow{H_3PO_4(aq)} \text{Lignin(s) + Lignin residue(aq) + Degraded organics(aq) + } KH_2PO_4(aq) + K_2HPO_4(aq) + H_2O(l) \quad (5.1)$$

After the separation of lignin precipitates through filtration, the resulting filtrates contained soluble lignin residue, potassium and phosphate ions, degraded organics, and excess phosphoric acid. Apart from lignin residue and degraded organics, addition of ammonium hydroxide to the filtrates neutralized the excess phosphoric acid and enhanced the crystallization as NPK salts according to following plausible reaction-

$$K^+(aq) + H_2PO_4^-(aq) + HPO_4^{2-}(aq) + H_3PO_4(aq) \xrightarrow{NH_4OH(aq)} KH_2PO_4(s) + K_2HPO_4(s) + (NH_4)H_2PO_4(s) + (NH_4)_2HPO_4(s) + (NH_4)KHPO_4(s) + H_2O(l) \quad (5.2)$$

The crystalized salts from four spent liquors were separated by filtration method, subsequently air-dried and presented as CF_SF, BG_SF, TO_SF and GW_SF. The filtrates contained residual K^+, NH_4^+, $H_2PO_4^-$, HPO_4^{2-} along with soluble lignin and degraded organics in aqueous solutions were referred to as liquid NPK fertilizers, i.e., CF_LF (solid content: 41.29%), BG_LF (solid content: 29.50%), TO_LF (solid content: 27.72%) and GW_LF (solid content: 24.80%). The components of liquid NPK fertilizer could be recovered through straightforward processes such as distillation or drying, resulting in the formation of solid residues, i.e., CF_LF-S, BG_LF-S, TO_LF-S and GW_LF-S, respectively. However, regardless of the specific compositions of the crystallized salts or liquid fertilizers, it could be assumed that these materials consisted of ammonium, phosphates and potassium ions, and degraded organics. As a result, they possessed significant potential for the utilization as valuable fertilizers.

Evaluation of properties of the recovered materials

Scanning electron microscopy-energy dispersive X-ray spectroscopic analysis: Determination of nitrogen, phosphorus and potassium (NPK) contents in crystallized salts

Elemental compositions of crystallized salts (CF_SF, BG_SF, TO_SF and GW_SF) were done by SEM-EDX technique and the resultant micrographs and elemental compositions were given in Figure 5.1 and Table 5.4. Table 5.4 reveals that the surface of crystallized NPK salts contained approximately 4 to 7% atomic percentages of carbon. These carbon atoms originated from degraded organic materials. All crystallized salts consisted of nitrogen (approximately 4 to 18% atoms), phosphorus (around 14 to 20% atoms), and potassium (0.08 to 18% atoms). However, BG_SF exhibited a lower concentration (0.08% atoms) of potassium compared to other crystallized salts.

Table 5.4: Elemental composition of crystallized salts by SEM-EDX technique

Sample	Nitrogen (%)		Phosphorus (%)		Potassium (%)		Carbon (%)		Oxygen (%)	
	Atom	Weight	Atom	Weight	Atom	Weight	Atom	Weight	Atom	Weight
CF_ SF	17.63	13.05	20.40	33.39	1.62	3.35	3.83	2.43	56.52	47.78
BG_SF	17.50	13.59	16.77	28.81	0.08	0.17	3.78	2.52	61.87	54.90
TO_SF	5.23	3.27	18.28	25.22	17.73	30.88	6.95	3.72	51.81	36.92
GW_SF	3.34	2.28	14.25	21.51	13.59	25.91	7.42	10.20	51.40	40.09

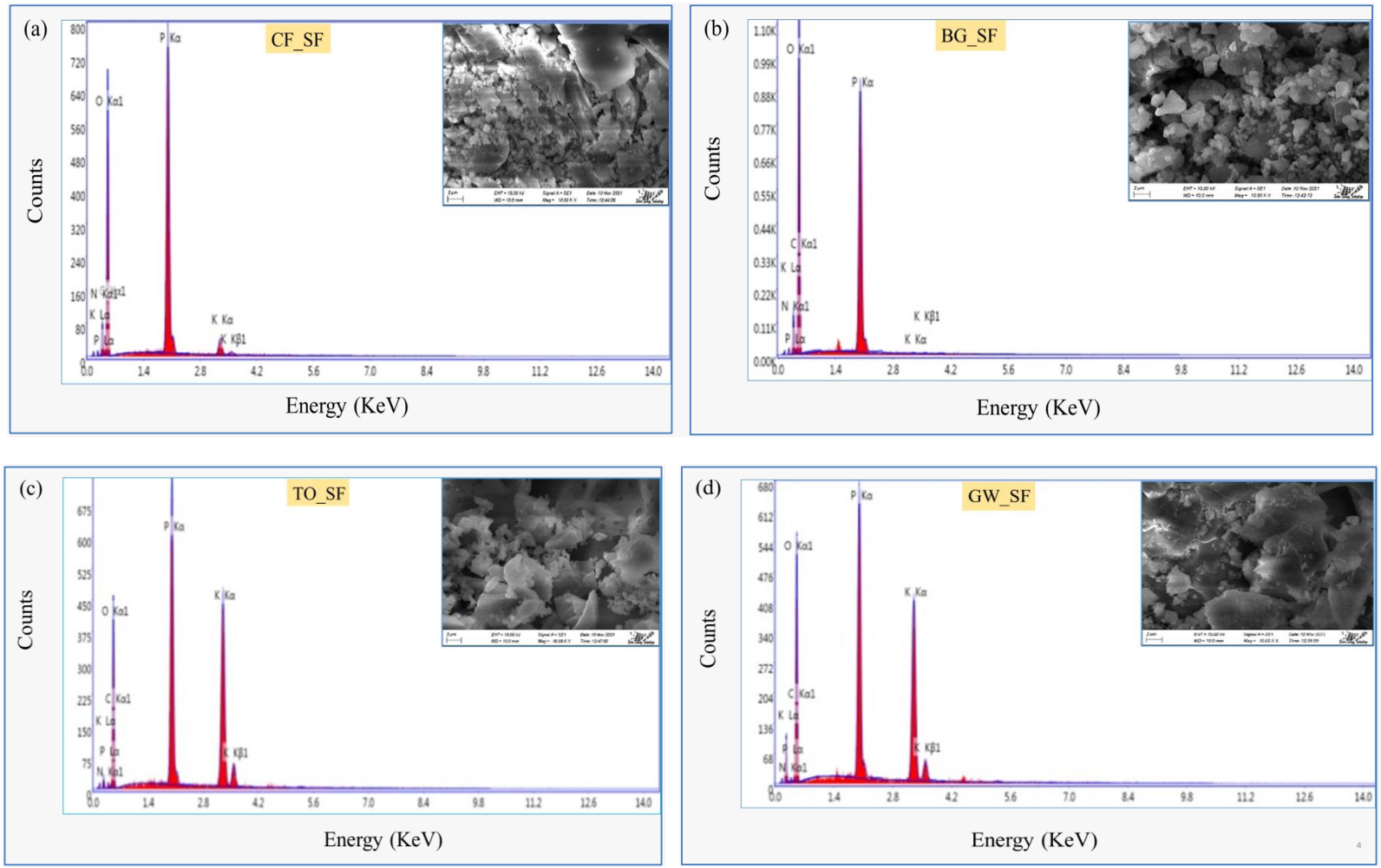

Figure 5.1: Scanning electron microscope-energy dispersive x-ray spectra of crystallized salts (a) CF_SF (b) BG_SF (c) TO_SF and (d) GW_SF

X-Ray photoelectron spectroscopic analysis: Wide scan spectral analysis

Results of the XPS wide scan spectra of CF_SF, BG_SF, TO_SF and GW_SF have been presented in Figure 5.2 and Table 5.5. It could be observed that surface elemental compositions of the crystallized salts differerd from the results obtained by SEM-EDX technique (Table 5.4). XPS wide scan spectra revealed the presence of nitrogen, phosphorus, carbon, and oxygen atoms in all samples. However, potassium atoms were not detected in CF_SF and BG_SF. The variation in surface elemental compositions could be attributed to differences in the interaction volumes, including the sample surface and underlying volume. The depth of interaction could be influenced by the energy of the incident beams, such as the electron beam in SEM-EDX and the X-ray beam in XPS analyses.

Table 5.5: Surface elemental compositions of the crystalline salts by XPS technique

Sample	Nitrogen (% atom)	Phosphorus (% atom)	Potassium (% atom)	Carbon (% atom)	Oxygen (% atom)
CF_SF	2.60	1.41	-	71.21	24.72
BG_SF	10.31	13.76	-	20.85	55.09
TO_SF	3.02	6.46	3.44	52.84	34.24
GW_SF	1.19	16.77	6.20	20.12	53.62

Therefore, variations in the total analysis areas likely contributed to the observed differences. Additionally, it is worth considering that the samples were analyzed using the ethanol drop-cast method in the XPS technique [245]. The differences in solubility may have influenced the measurement of the actual concentrations of the elements.

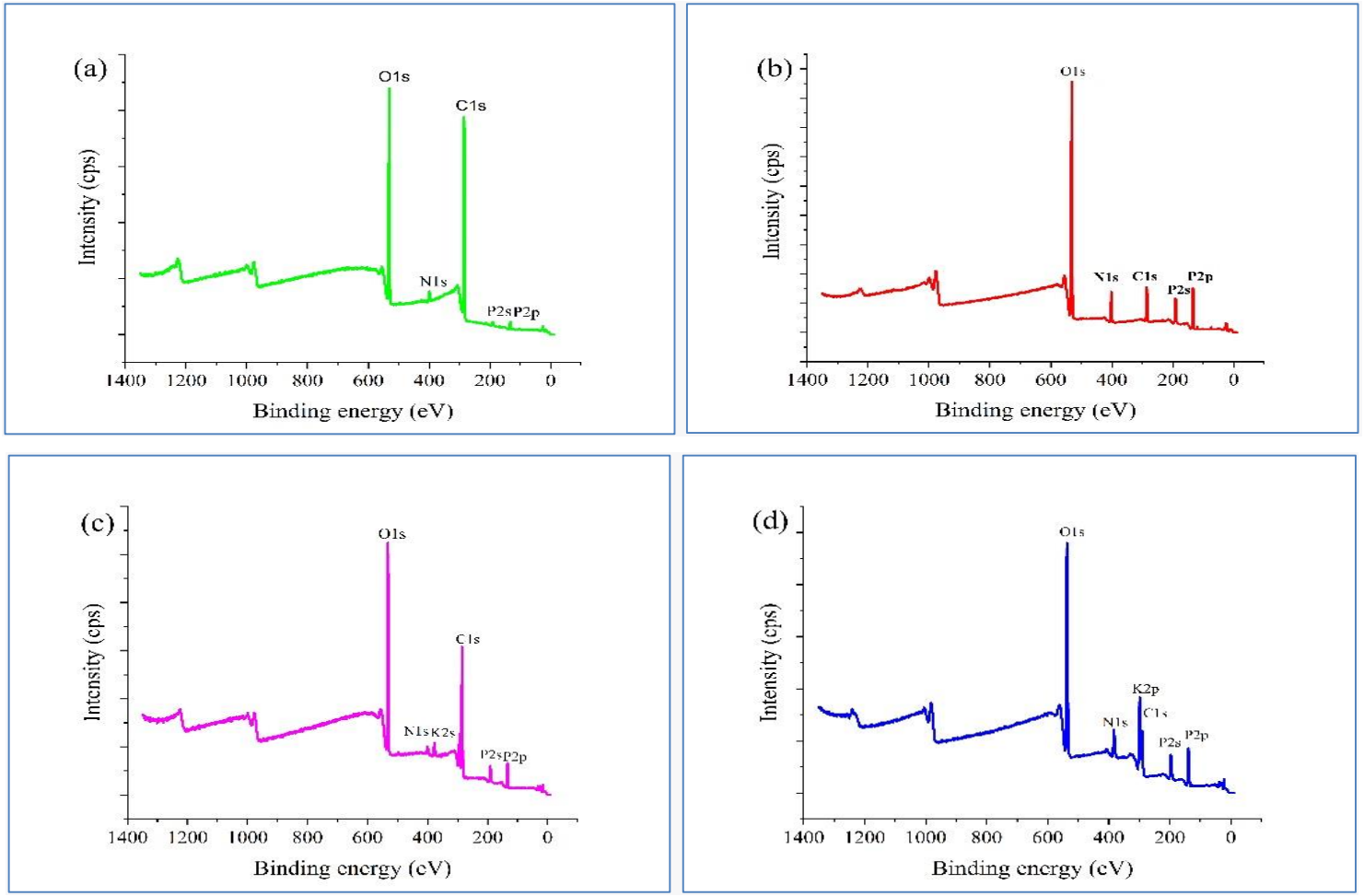

Figure 5.2: XPS wide scan spectra of crystallized salts from black liquors after separation of alkali-lignin samples (a) CF_SF (b) BG_SF (c) TO_SF and (d) GW_SF

X-Ray diffraction analysis for the identification of crystallized salts

The XRD diffractograms and corresponding data for CF_SF, BG_SF, TO_SF, and GW_SF have ben presented in Figure 5.3 and Table 5.7, respectively. The XRD pattern of CF_SF exhibited prominent peaks at 2θ angles of 16.74°, 23.83°, 29.13°, 33.78°, and 45.22°. Specifically, the peak at 16.74° corresponded to the (101) crystal plane, while the peaks at 23.83°, 29.13°, 33.78°, and 45.22° could be attributed to the (200), (112), (202), and (312) crystal planes, respectively. These findings closely matched the crystal structure of potassium ammonium hydrogen phosphate, $K(NH_4)HPO_4$ [238]. The relative intensities of the peaks provided valuable insights into the crystallographic structure and preferred orientation within the material, with the (200) plane exhibiting the highest intensity. Moreover, the sharpness of the peaks indicated a large crystallite size [247]. Similar observations of sharp peaks and large crystallite sizes were made for BG_SF, TO_SF, and GW_SF, despite their distinct crystal structures: Phosphammite, $(NH_4)_2(PO_3OH)$ structure for BG_SF [240]; potassium dihydrogen phosphate, KH_2PO_4 structure for TO_SF [249]; and archerite, $(K,NH_4)H_2PO_4$ structure for GW_SF [242]. The corresponding diffraction angles and crystal planes for BG_SF, TO_SF, and GW_SF were listed in Table 5.5, with the highest peak intensities observed at 23.63° for plane (002) in BG_SF, 23.84° for plane (200) in TO_SF, and 23.83° for plane (200) in GW_SF.

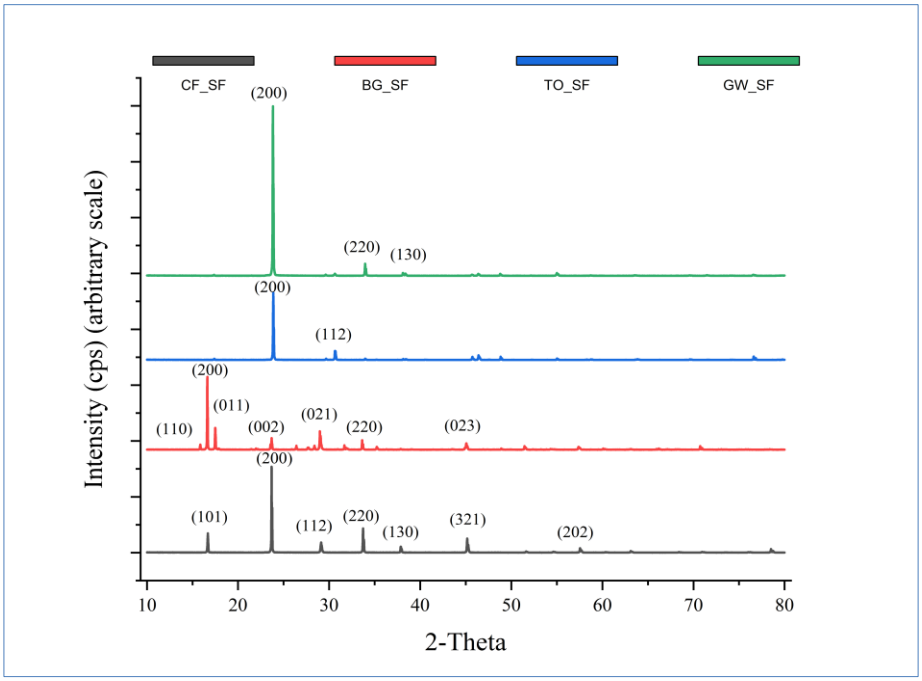

Figure 5.3: X-ray diffractogram of crystallized salts recovered from the spent liquors after the separation of alkali-lignin samples.

The applied crystallization or recovery technique did not yield a specific salt; instead, it was observed that multiple compounds could be crystallized by the conditions applied. Despite this variability, all of the salts obtained have the potential to be utilized as fertilizers, potentially requiring further modifications or enhancements to optimize their efficacy.

Table 5.6: XRD data of crystallized salts from the black/spent liquors after separation of the alkali-lignin samples

Salt	Crystalline peak at 2θ	(hlk) value	d, Å	Intensity	Identified salt
CF_SF	16.74	(101)	5.30775	69.30	$K(NH_4)HPO_4$
	23.83	(200)	3.75265	96.54	
	29.13	(112)	3.06456	29.81	
	33.78	(202)	2.65387	11.19	
	45.22	(312)	2.00603	56.32	
BG_SF	16.63	-	-	100.00	$(NH_4)_2(PO_3OH)$ (Phosphammite)
	17.59	(200)	-	37.46	
	23.63	(002)	3.36741	50.00	
	29.02	(021)	3.05824	45.00	
	33.68	-	-	19.66	
TO_SF	23.84	(200)	3.72976	100.00	KH_2PO_4
	30.71	(112)	2.91567	93.20	
GW_SF	23.83	(200)	3.73051	100.00	$(K,NH_4)H_2PO_4$ (Archerite)
	34.09	(220)	2.63787	23.00	

Physicochemical properties of liquid NPK-fertilizers

Liquid fertilizers were analyzed using various physical methods, and their properties are presented in Table 5.7. Elemental compositions of the solid residues of liquid fertilizers (CF_LF-S, BG_LF-S, TO_LF-S and GW_LF-S) were done by SEM-EDX technique and the resultant micrographs and elemental compositions were given in Figure 5.4 and Table 5.8.

The pH of the liquid fertilizers was neutral. CF_LF had a higher density, while BG_LF, TO_LF, and GW_LF had slightly lower densities. CF_LF had higher ash content due to lower amounts of crystallized salts (CF_SF) recovered. On the other hand,

BG_LF, TO_LF, and GW_LF exhibited lower ash contents. CF_LF had a significantly higher solid content, which can be attributed to a greater presence of carbon materials according to XPS analysis. CF_LF also had higher dynamic viscosity, while BG_LF, TO_LF, and GW_LF had lower viscosities.

Table 5.7: Properties of liquid fertilizers obtained from the biorefinery

Parameter	Unit	CF_LF	BG_LF	TO_LF	GW_LF
Color	-	Deep orange	Deep orange	Deep orange	Deep orange
pH	-	6.86	6.92	6.95	6.91
Density	Kg/m^3	1.246	1.175	1.170	1.140
Refractive index	nD	1.363	1.363	1.361	1.359
Moisture content	%	58.71	70.50	72.49	75.20
Solid content	%	41.29	29.50	27.72	24.80
Ash content	%	13.34	10.93	9.14	7.29
Dynamic viscosity	mPas	6.408	3.269	3.198	2.613
Kinematic viscosity	mm^2/s	5.142	2.782	2.733	2.292

Scanning electron microscopy-energy dispersive X-ray spectroscopy: Elemental composition of the solid contents of liquid NPK-fertlizers

Elemental compositions of the solid contents of liquid NPK-fertilizers (CF_LF, BG_LF, TO_LF and GW_LF) were analyzed by SEM-EDX technique and the resultant micrographs and elemental compositions were given in Figure 5.4 and Table 5.8. Table 5.8 reveals that the surface of solid residues contained approximately 9 to 15% atomic percentages of carbon, while the crystallized salts exhibited lower percentages ranging from 4 to 7%. The higher carbon percentages in the solid residues indicated the presence of degraded organics at higher amounts in comparison to crystallized salts. Additionally, the solid residue of the liquid fertilizers contained nitrogen (around 12 to 17% atoms), phosphorus (around 12 to 15% atoms), and potassium (around 3 to 9% atoms) [244].

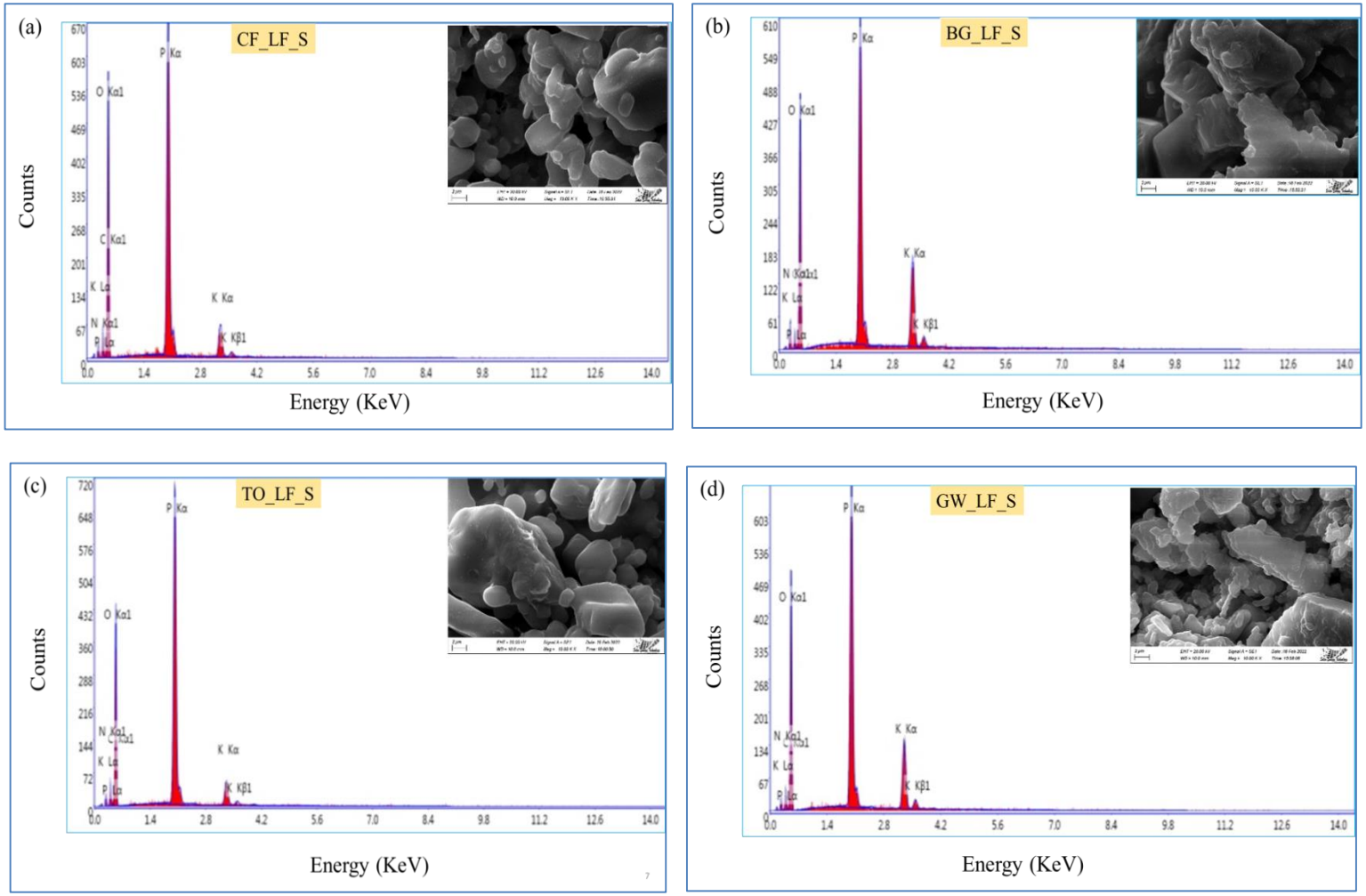

Figure 5.4: Energy dispersive x-ray spectra of solid contents of the liquid fertilizers (a) CF_LF-S (b) BG_LF-S (c) TO_LF-S and (d) GW_LF-S

Table 5.8: Elemental composition of solid contents of liquid fertilizers by SEM-EDX technique

Sample	Nitrogen (%)		Phosphorus (%)		Potassium (%)		Carbon (%)		Oxygen (%)	
	Atom	Weight	Atom	Weight	Atom	Weight	Atom	Weight	Atom	Weight
CF_LF-S	16.08	12.76	13.34	23.40	1.61	3.56	9.81	6.67	59.16	53.61
BG_LF-S	12.15	9.46	12.11	20.85	4.34	9.44	14.69	9.81	56.72	50.45
TO_LF-S	17.39	13.60	15.33	26.51	1.56	3.40	9.92	6.65	55.80	49.84
GW_LF-S	15.13	11.57	14.03	23.72	3.75	8.01	8.73	5.73	58.36	50.97

The described properties can be used to evaluate the performance of liquid NPK fertilizers. However, the liquid NPK fertilizers might offer several advantages compared to traditional solid fertilizers, including ease of application, faster nutrient availability, and improved nutrient uptake efficiency. A balanced NPK ratio, such as 10-10-10 or 20-20-20, is often suitable for general plant growth and maintenance. This balanced ratio provides equal proportions of nitrogen, phosphorus, and potassium and is commonly used as a standard or all-purpose fertilizer for many crops. The preferred NPK ratios for plants can vary depending on the specific plant species, growth stage, and environmental conditions [251, 252]. Different crops have different nutrient requirements, and their optimal NPK ratios may vary based on the factors such as soil fertility, crop management practices, and regional climate. However, the NPK ratios in the recovered NPK containing salts/materials could be adjusted by adding different chemicals, e.g., urea, ammonium phosphates, potassium hydrogen phosphates, etc. to achieve the preferred NPK ratios.

5.4. Conclusion

- The proposed material-driven biorefinery has focused on efficiently utilizing diverse lignocellulosic feedstocks to extract maximum value and produce a range of valuable products, including lignin and NPK-containing materials, which is often regarded as a low-value material or waste byproduct.
- In order to ensure the long-term viability of the biorefinery, the spent liquors produced after the separation of alkali-lignin have been further treated to recover the used chemicals by crystalizing as salts that were rich in potassium, nitrogen, and phosphorus as well as degraded organics for use as fertilizer.
- Overall, the utilization of ammonium hydroxide (and potassium hydroxide, if necessary) in the treatment of generated spent liquors showcased the biorefinery's efforts to optimize resource utilization and adopt sustainable practices. By recovering the used chemicals in the pretreatment process and transforming the spent liquors into a fertilizer resource, the biorefinery demonstrated its commitment to a sustainable and circular approach. Instead of discarding the spent liquors as waste, this strategy enabled their conversion into a valuable product that could contribute to improving soil fertility and supporting agricultural productivity.

- Additionally, this approach aligned with the principles of resource efficiency and environmental stewardship, such as no waste generation and promoted the reuse of materials within the biorefinery system. This approach exemplified a sustainable and environmentally responsible practice, supporting the biorefinery's goals of maximizing resource utilization and generating no waste.

5.5. References

[222] M. Galbe, O, Wallberg, Pretreatment for biorefineries: a review of common methods for efficient utilisation of lignocellulosic materials, *Biotechnol Biofuels*, 2019, 12, 294, doi.org/10.1186/s13068-019-1634-1

[223] M. Kaltschmitt, Biomass as Renewable Source of Energy, Possible Conversion Routes, *Encyclopedia of Sustainability Science and Technology,* 2017, *1–38,* doi:10.1007/978-1-4939-2493-6_244-3

[224] L. Reyes, C. Nikitine, L. Vilcocq and P Fongarland, Green is the new black: a review of technologies for carboxylic acid recovery from black liquor, *Green Chemistry,* 2020, 22, 8097-8115, doi:10.1039/d0gc02627a

[225] B. K. Ince, Z. Cetecioglu and Orhan Ince, Pollution Prevention in the Pulp and Paper Industries, *Environmental Management in Practice*, 2011, DOI: 10.5772/23709

[226] A. Haile., G. G. Gelebo, T. Tesfaye, et al., Pulp and paper mill wastes: utilizations and prospects for high value-added biomaterials, *Bioresour. Bioprocess*, 2021, 8, 35, doi.org/10.1186/s40643-021-00385-3

[227] R. Alén, M. Hupa and T. Noopila, Combustion Properties of Organic Constituents of Kraft Black Liquors, *Holzforschung,* 1992, 46(4), 337–342, doi:10.1515/hfsg.1992.46.4.337

[228] R. Alén, Pulp Mills and Wood-Based Biorefineries, Industrial Biorefineries & White Biotechnology, ed. A. Pandey, R. Höfer, M. Taherzadeh, M. Nampoothiri and C. Larroche, Elsevier, Amsterdam, 1st edn, 2015, ch 3A, 91–126, doi:10.1016/B978-0-444-63453-5.00003-3

[229] C. Rueda, P. A. Calvo, G. Moncalián, G. Ruiz, A. Coz, Biorefinery options to valorize the spent liquor from sulfite pulping. *Journal of Chemical Technology & Biotechnology*, 2014, 90(12), 2218-2226, doi:10.1002/jctb.4536

[230] P. Singh, N. Srivastava, P. Singh, S. Geetha, N. Usharani, R. S. Jagadish, A. Upadhyay, Effect of Toxic Pollutants from Pulp & Paper Mill on Water and Soil Quality and its Remediation, *International Journal of Lakes and Rivers*, 2019, 12(1), 1-20

[231] T. Chen, Y. Li, L. Lei, M. Hong, Q. Sun, and Y. Hou, Influence of residual black liquor in pulp on wastewater pollution after bleaching process, *BioRes*., 2017, 12(1), 2031-2039.

[232] D. D. Mandal, G. Singh, S. Majumdar. *et al.*, Challenges in developing strategies for the valorization of lignin—a major pollutant of the paper mill industry, *Environ Sci Pollut Res* 2023, **30**, 11119–11140, doi.org/10.1007/s11356-022-24022-4

[233] S. Dagar, S. K. Singh and M. K. Gupta, Economics of advanced technologies for wastewater treatment: Evidence from pulp and paper industry. *Front. Environ. Sci*., 2022, 10:960639, doi: 10.3389/fenvs.2022.960639

[234] H. Wang, Y. Pu, A. Ragauskas and B. Yang, From lignin to valuable products-strategies, challenges, and prospects, *Bioresource Technology*, 2019, *271*: 449-461, doi.org/10.1016/j.biortech.2018.09.072

[235] Z. Fang and R. L. Smith (ed.), Production of Biofuels and Chemicals from Lignin, *Biofuels and Biorefineries*, 2016, 6, DOI 1.1007/978-981-10-1965-4_13

[236] S. Sharma, M. Tsai, V. Sharma, P. Sun, P. Nargotra, B. K. Bajaj, C. Chen and C. Dong, Environment Friendly Pretreatment Approaches for the Bioconversion of Lignocellulosic Biomass into Biofuels and Value-Added Products, *Environments*, 2013, *10*(1), 6, doi.org/10.3390/environments10010006

[237] A. Barraga´n-Ocaña, H. Merritt, O. E. Sa´nchezEstrada, J. L. Me´ndez-Becerril, M. del Pilar LongarBlanco, Biorefinery and sustainability for the production of biofuels and value-added products: A trends analysis based on network and patent analysis. *PLoS ONE*, 2023, 18(1): e0279659, doi.org/10.1371/journal.pone.0279659

[238] M. Zieli ´nska, K. Bułkowska, W. Mikucka, Valorization of Distillery Stillage for Bioenergy Production: A Review, *Energies*, 2021, 14(21), 7235, doi.org/10.3390/en14217235

[239] K. Sankaran, M. Premalatha, M. Vijayasekaran, V. T. Somasundaram, DEPHY project: Distillery wastewater treatment through anaerobic digestion and phycoremediation—A green industrial approach. *Renewable and Sustainable Energy Reviews*, 2014, 37, 634–643, doi: 10.1016/j.rser.2014.05.062

[240] A. C. Wilkie, K. J. Riedesel, J. M. Ownes. Stillage characterization and anaerobic treatment of ethanol stillage from conventional and cellulosic feedstocks, *Biomass and Bioenergy*, 2000, 19(2), 63-102, doi.org/10.1016/S0961-9534(00)00017-9

[241] W. Den, V. K. Sharma, M. Lee, G. Nadadur and R. S. Varma, Lignocellulosic Biomass Transformations via Greener Oxidative Pretreatment Processes: Access to Energy and Value-Added Chemicals, *Frontiers in Chemistry*, 2018, 6, 337170, doi.org/10.3389/fchem.2018.00141

[242] M. A. Hubbe, E. M. A. Becheleni, A. E., Lewis, E. M. Peters, W. Gan, G. Nong, S. Mandal and S. Q. Shi, Recovery of inorganic compounds from spent alkaline pulping liquor by eutectic freeze crystallization and supporting unit operations: A Review**,** *BioRes. 2018*, 13(4), 9180-9219

[243] L. Pola, S. Collado, P. Oulego and M. Díaz, Kraft black liquor as a renewable source of value-added chemicals. *Chemical Engineering Journal*, 2022, *448*, 137728, doi.org/10.1016/j.cej.2022.137728

[244] L. L. Messa, G. A. Contieria and R. Faez, Sugarcane Bagasse Fibers Derivatives and Their Application in Chitosan-Based Composite Films for NPK Fertilizer Release, 2023, *J. Braz. Chem. Soc*., 34(5), 653-663, doi.org/10.21577/0103-5053.20220135

[245] F. A. Stevie, R. Garcia, S. Jeffrey, J. G. Newman and C. L. Donley, Sample handling, preparation and mounting for XPS and other surface analytical techniques, J. *Vac. Sci. Technol. A*, 2020, 38, 063202, doi: 10.1116/6.0000421

[246] Del Butler, Fluid Fertilizer Foundation Technology Workshop Ortho/Low Poly Products, Production & Characteristics, 2014, https://fluidfertilizer.org/technology-workshop-presentations, (Last assessed: 27.06.2023)

[247] R. J. Farrauto and M. C. Hobson, Catalyst Characterization, *Encyclopedia of Physical Science and Technology*, 2003, 501-526, doi.org/10.1016/B0-12-227410-5/00087-9

[248] Phosphammite mineral data, http://webmineral.com/data/Phosphammite.shtml, (Last assessed: 27.06.2023)

[249] K. Jančaitienė and R. Šlinkšienė, KH2PO4 crystallization from potassium chloride and ammonium dihydrogen phosphate, *Polish Journal of Chemical Technology*, 2016, 18, 1, 1—8, 10.1515/pjct-2016-0001

[250] L R. Frost, X. Yunfei and S. J. Palmer, Are the 'cave' minerals archerite (K,NH_4) H_2PO_4 and biphosphammite (K,NH_4)H_2PO_4 identical? A molecular structural study, *Journal of Molecular Structure*, 2011, 1001(1-3), 49–55, doi:10.1016/j.molstruc.2011.06.015

[251] E Solihin , A Yuniarti , M Damayani and S Rosniawaty, Application of liquid organic fertilizer and N, P, K to the properties of soil chemicals and growth of rice plant, IOP Conf. Series: *Earth and Environmental Science*, 2019, 393:012026, doi:10.1088/1755-1315/393/1/012026

[252] T. P. Hignett, Physical and Chemical Properties of Fertilizers and Methods for their Determination, *Developments in Plant and Soil Sciences*, 1985, 284–316, doi.org/10.1007/978-94-017-1538-6_22

CHAPTER 6

ASSESSMENT OF SUSTAINABILITY OF THE MATERIAL-DRIVEN PHASE III LCF BIOREFINERY SYSTEM

Chapter 6: Assessment of Sustainability of the Material-driven Phase III LCF Biorefinery System

6.1. Mass balance of the material-driven biorefinery system and atom economy

Mass balance is the fundamental and indispensable tool for any biorefinery system operated in continuous, semi-continuous or batch modes. It enables an efficient resource utilization, product quality control, process optimization, compliance with regulations, economic viability, and safety. Biorefineries must rigorously apply mass balance principles to achieve their sustainability and profitability goals while minimizing environmental impact. The general equation 6.1 could be used to calculate mass balance of the developed material-driven biorefinery process by evaluating it as a closed system-

$$\frac{dM}{dt} = \sum m\_input - \sum m_{output} + \sum m\_generation - \sum m\_consumption \quad (6.1)$$

here,

$\frac{dM}{dt}$ = the rate of change of mass within the system over time or accumulation

$\sum m\_input$ = the total mass entering the system per unit of time

$\sum m\_output$ = the total mass leaving the system per unit of time

$\sum m\_generation$ = mass that is generated within the system during a process

$\sum m\_consumption$ = mass that is consumed within the system during a process

It was considered that the sequential transformations and fractionations of biomass would take place in the closed system (batch mode) and therefore, $\sum m\_generation$ and $\sum m\_consumption$ would be zero. For simplification, the accumulation $\frac{dM}{dt}$ may be considered as zero when the biorefinery system reached at pseudo-steady-state conditions. Thus, equation 6.1 could be written as-

$$\sum m\_input = \sum m\_output \quad (6.2)$$

A simple schematic diagram for mass balance of the material-driven phase III lignocellulosic feedstock biorefinery system has been represented in Figure 6.1.

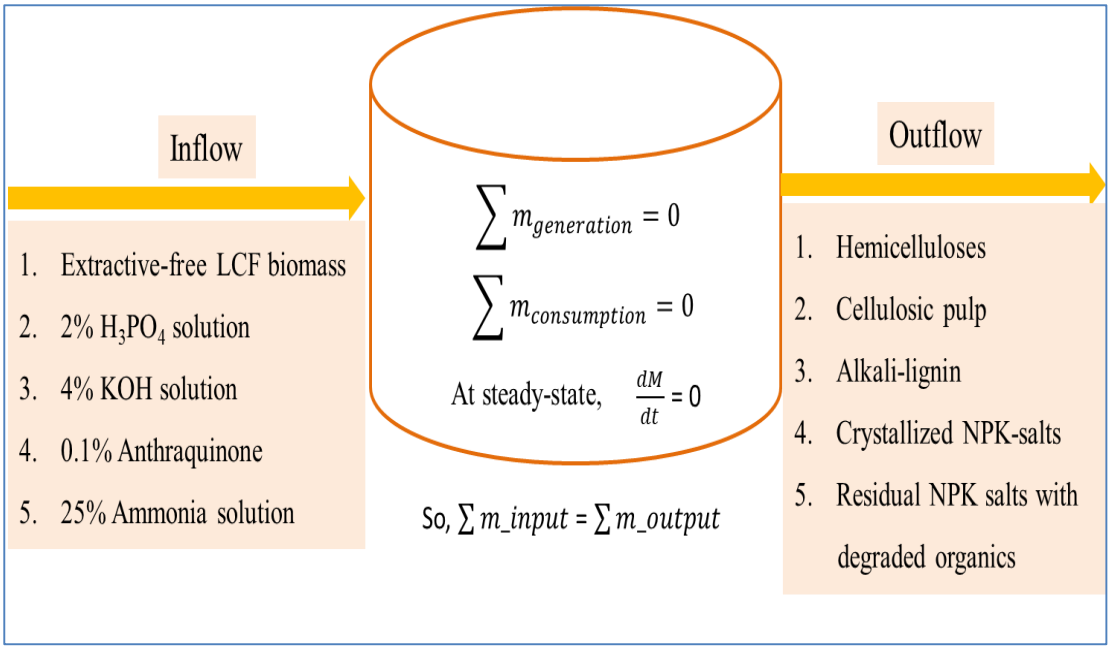

Figure 6.1: A schematic diagram representing mass balance of the material-driven phase III lignocellulosic feedstock biorefinery system considering at steady-state conditions. Extractive-free lignocellulosic feedstock will be converted to their structural components (continuous, semi-continuous or batch mode operations) by interacting with pretreatment chemicals and sequentially recovered all of the materials by different techniques without generating any waste.

According to steady-state circumstances, internal variables like concentrations, temperatures and mass fluxes would not change over time in a continuous biorefinery system. Due to the system's balanced input and outflow rates and the absence of a net change in the mass content over time, the rate of mass accumulation can be regarded as zero at this point. Nevertheless, in practice, achieving a true steady-state may be difficult since a number of outside influences, such as equipment wear, variations in feedstock quality, etc., may cause some fluctuations. It is possible to have approximate calculations and comprehend the behavior of the system under steady-state conditions by using the assumption of zero accumulation when calculating the mass balance of such biorefinery system. Stable steady-state conditions for a continuous biorefinery system can be ensured by reaching process equilibrium, constant feedstock input, stable operating conditions, constant output streams, and continuous operation. But, reaching at the steady-state conditions in a batch mode biorefinery operation is not possible, because it involves a finite start and end time with no continuous feed or discharge of materials. However, a pseudo-steady-state condition can be achieved in batch mode biorefinery system. Once the initial batch ingredients have been thoroughly mixed and the reaction

or transformation has progressed to a point where process variables, e.g., feedstock quality, concentrations, temperatures and time are no longer changing significantly, the system may be considered to reach at pseudo-steady-state conditions. At these conditions, quality of the products and optimization of process variables to maximize yields, minimize wastes and improved energy efficiency along with process safety can be ensured in batch mode biorefinery operation. In the developed biorefinery system, the input pretreatment chemicals sequentially converted the extractive-free lignocellulosic biomass (i.e., coconut fibre) and subsequently recovered the structural components in a technologically feasible way. At the same time, pretreatment chemicals were also recovered as discussed earlier. The attainment of 96.2% atom economy indicated that the biorefinery system was intricately engineered to maximize the utilization of atoms from raw materials, establishing it as a more sustainable and efficient approach (Scheme 6.1).

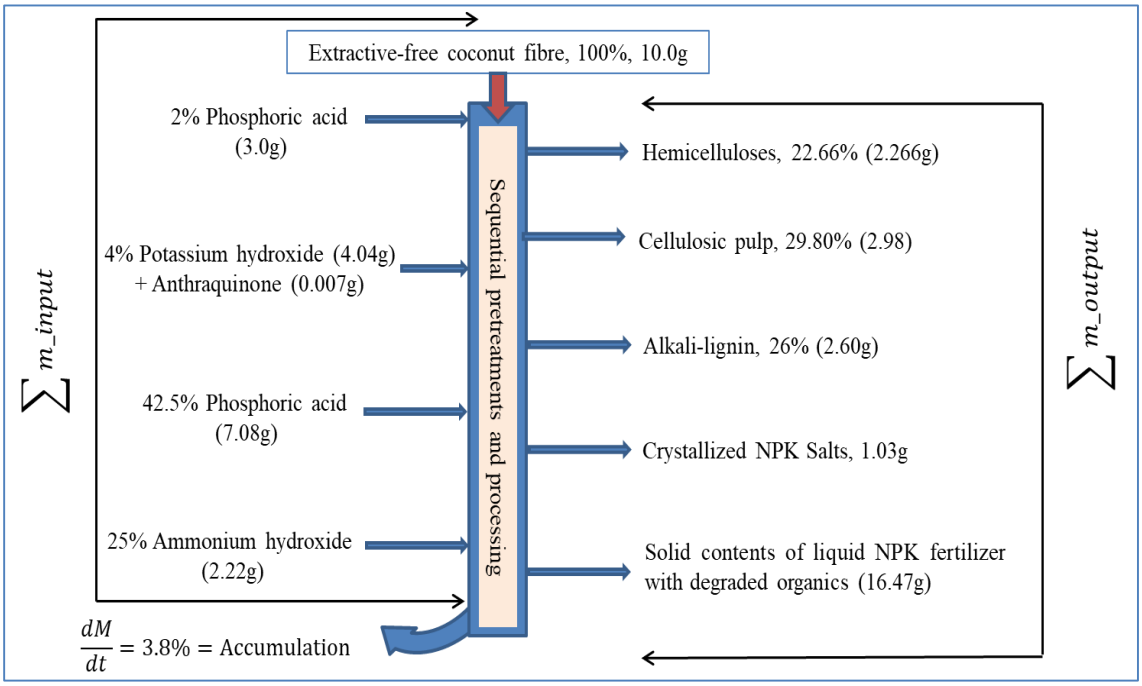

Scheme 6.1: Mass balance of the proposed material-driven phase III lignocellulosic feedstock biorefinery process (Batch mode operation).

The technical steps included in the biorefinery system (batch mode operation) have been stated in Table 6.1.

Table 6.1: Technical steps of the material-driven phase III lignocellulosic feedstock biorefinery system (batch mode operation)

SN	Steps	Description of technical steps (in brief)
1	Selection of lignocellulosic feedstock	Nonwood and woody biomasses including their waste forms were used as feedstock. Mixed samples of similar particle sizes may be used.
2	Preparation of feedstock	After washing and cleaning, sundrying was considered as a method of drying of the biomasses to reduce the moisture content below 10%. Crushing/grinding and then screening of particles of less than 100 mesh can be used in the biorefinery process.
3	Removal of extractives	Thermo-pressurized extractions of water and ethanol soluble materials may be considered as a preferred way to ensure the purity of structural components of biomass before subjected to sequential acid-base pretreatment.
4	Sequential pretreatment on feedstock	Thermo-pressurized sequential acid-base pretreatment on extractive-free biomasses has been applied to deconstruct/separate the structural components.
5	Fractionation and separation of components	Separation of structural components and recovery of pretreatment chemicals could be done by- (i) Vacuum filtration (ii) Precipitation and centrifugation (iii) Crystallization and (iv) Drying techniques
6	Process integration and optimization	Integrated and optimized the overall process for four different samples (Laboratory scale)
7	Product diversification and value addition applying well established method for modifications	The biorefinery system have the potential to produce diversified products, (i) Hemicellulose-based hydrogel-NPK slow release fertilizer, Furfurals, etc. (ii) Cellulosic pulp, cellulose-based hydrogel and cellulose derivatives (iii) Alkali-lignin, lignin-based hydrogels and derivatives (iv) Crystallized NPK-salts (v) Liquid NPK-fertilizer, etc.

Assessing the economic viability of a biorefinery involves a thorough examination of its financial components. The feasibility of a biorefinery project usually depends on a multitude of factors, including the availability of feedstock, the efficiency of technology including energy balance, current market conditions, and regulatory considerations.

6.2. General conclusion

In the light of ongoing challenges faced by the lignocellulosic feedstock biorefineries, this study introduced a straightforward and highly simplified method for isolating hemicelluloses, cellulosic pulp, and alkali-lignin from both woody and non-woody lignocellulosic biomass resources. The biorefinery approach employed reduced quantities of acid and base compared to the conventional methods and recovered efficiently. Apart from the cellulosic pulps and hemicelluloses, the alkali-lignin and obtained NPK-fertilizers might be used in different industrial and agricultural applications. The enhanced atom economy of the developed biorefinery system can be assessed as a technologically and economically viable strategy for promoting sustainability.

The developed Material-driven Phase III Lignocellulosic-feedstock Biorefinery System holds immense promise for the utilization and modification of lignin, a complex and abundant biomass component. Lignin, traditionally regarded as a waste product in the pulping and paper industry, is now recognized as a valuable resource with various potential applications. Through material-driven biorefinery approaches, lignin could be efficiently extracted from lignocellulosic biomass and transformed into a range of high-value products, such as platform chemicals, and advanced materials. This process not only maximizes the utilization of different lignocellulosic-feedstock but also offers a sustainable alternative to fossil-based resources, reducing greenhouse gas emissions and environmental impacts.

The modification of lignin is a critical aspect of its utilization. Lignin is a highly complex and heterogeneous polymer, which makes it challenging to process and incorporate into value-added products. However, through innovative technique such as functionalization, lignin could be tailored to meet specific application requirements. One of the key advantages of lignin lies in its aromatic structure, which provides opportunities for the synthesis of aromatic chemicals and materials. By selectively breaking down lignin into its constituent monomers, such as phenolic compounds, it is

possible to produce renewable alternatives to petroleum-derived chemicals. The lignin-derived compounds can be further transformed into resins, adhesives, plastics, and other materials, thereby replacing their fossil-based counterparts and promoting a circular economy.

Moreover, the utilization of lignin in biofuel production has gained significant attention. Lignin can be processed into bio-oil through pyrolysis or liquefaction, which can serve as a renewable substitute for fossil fuels. Furthermore, lignin-based carbon materials, such as activated carbon and carbon fibers, possess excellent adsorption and mechanical properties, making them suitable for various applications including energy storage, water treatment, and structural reinforcement. However, despite the substantial progress made in lignin valorization, several challenges remain. The heterogeneity and structural complexity of lignin necessitate further advancements in depolymerization techniques to obtain well-defined and consistent lignin fragments. Additionally, the development of efficient separation and purification methods is crucial to obtain high-purity lignin fractions for targeted applications. Furthermore, the scale-up and commercialization of lignin-based products require improvements in cost-effectiveness and process efficiency. Collaboration between academia, industry, and government institutions is essential to address these challenges and accelerate the transition towards lignin-based biorefineries.

In conclusion, the sequential acid-base pretreatment based material-driven phase III lignocellulosc biorefinery approach offers a promising avenue for the utilization and modification of lignin. By leveraging its inherent properties and employing innovative processing techniques, lignin can be transformed into a wide range of valuable products, contributing to a more sustainable and bio-based economy. Continuous research and development efforts in this field will unlock the full potential of lignin as a renewable resource and drive the transition towards a more environmentally friendly future.

6.3. Future prospects

The following works on the Material-driven Phase III Lignocellulosic-feedstock Biorefinery System are now under investigations-

- ***Effects of sequential acid-base pretreatment under different conditions:***
    - Effects of the variation of lignocellulosic feedstock to recover structural components in the biorefinery system.
    - Effects of particle sizes of the lignocellulosic feedstock, phosphoric acid concentration, digestion time and temperature on the isolation and structural changes of hemicelluloses and cellulose.
    - Effects of alkali concentration, digestion time and temperature on the isolation of alkali-lignin and more efficient lignin recovery processes from black liquor.
- ***Applications of submicron-sized alkali-lignin:*** Applications of submicron alkali-lignin particles to enhance ultraviolet light absorption, retard air and thermal oxidation during processing and boast up thermal properties of different polymeric matrices including plastics, rubber, bitumen, etc.
- ***Applications of submicron-sized acetobrominated alkali-lignin:***
    - Applications of acetobrominated alkali-lignin particles to enhance flame and fire retardant properties of plastics, rubber and composite materials.
    - Applications of acetobrominated alkali-lignin particles to prepare control release insecticides and pesticide formulations.
- ***Applications of NPK-fertilizers in agriculture:*** Applications of NPK-fertilizers to plant and monitor the growth profile in pot experiments.
- ***Evaluation of bleachability of recovered cellulosic pulps through ecofriendly bleaching process.***
- ***Characteristics of recovered hemicelluloses.***
- ***Cellulose and hemicellulose-based product formulations.***
- ***Technoeconomical feasibility of the biorefinery system***
    - Pilot study of the developed material-driven biorefinery system.
    - Detail calculations on the mass and energy balances of the biorefinery system.
    - Evaluation of technoeconomic feasibility of the overall system.

Appendix

Appendix

A 1: Calculations for determining empirical formula of alkali-lignin using elemental analysis data

The simplest empirical formula of phenyl propane unit (C_6-C_3), taking out only the OCH_3 group:

$$C_9H_{nH}O_{nO}\ (OCH_3)n_{OCH3}$$

Percent of C, H and O contents included into OCH_3group have been given below-

$[C_{OCH3}] = [OCH_3]*12.01/31.035 = 0.387 * [OCH_3]$
$[H_{OCH3}] = [OCH_3]* 3.024/31.035 = 0.097 * [OCH_3]$
$[O_{OCH3}] = [OCH_3]*16.00/31.035 = 0.515 * [OCH_3]$

Carbon percentage in C_9 unit, subtracting carbon in OCH_3 group:

$[C_9] = [C] - 0.387\ [OCH_3]$(i)

Index of methoxyl group, n_{OCH3}can be found as follows-

$[C_9]/[OCH_3] = 9 *12.01/n_{OCH3}*31.035$

So, $n_{OCH3}= 3.48\ [OCH_3]/[C_9]$ (ii)

Similarly,

$n_H= 107.7\ ([H] -0.097\ [OCH_3])/[C_9]$ (iii)

$n_O= 6.75\ ([O] – 0.515\ [OCH_3])/\ [C_9]$ (iv)

If, the methoxyl content is known, the n_{OCH3},n_H and n_O could be calculated and thus simple empirical formula of lignin could be established.

General empirical formula of lignin: $C_9H_{nH}O_{nO}\ (OCH_3)n_{OCH3}$

Calculations of C, H and O indices and establishment of empirical formula:

(i) Coconut fibre alkali-lignin (CF_AL)

$[C_9] = [C] - 0.387\ [OCH3] = 55.11-(0.387 \text{ x } 15.05) = 49.28\%$

So, $n_{OCH3}= 3.48[OCH_3]/[C_9] = 3.48 \text{ x } 15.05/49.28 = 1.06$

$n_H= 107.7\ ([H] -0.097\ [OCH_3])/[C_9] = 107.7\ (4.871-0.097 \text{ x } 15.05)/49.28 = 7.45$

$n_O= 6.75\ ([O] – 0.515\ [OCH_3])/[C_9] = 6.75\ (40.019 – 0.515 \text{ x } 15.05)/49.28 = 5.88$

Empirical formula of CF_AL: $C_9H_{7.45}O_{5.88}\ (OCH_3)_{1.06}$

(ii) Bagasse alkali-lignin (BG_AL)

$[C_9]$ = [C] - 0.387 $[OCH_3]$ = 60.22- (0.387 x 16.07) = 54.00%

So, n_{OCH3}= 3.48$[OCH_3/[C_9]$ = 3.48 x 16.07/54.00 = 1.03

n_H = 107.7 ([H] -0.097 $[OCH_3]$)/$[C_9]$ = 107.7 (5.619-0.097 x 16.07)/54.00 = 8.09

n_O= 6.75 ([O] – 0.515 $[OCH_3)/[C_9]$ = 6.75 (34.161 – 0.515 x 16.07)/54.00 = 3.23

Empirical formula of BG_AL: $C_9H_{8.09}O_{3.23}(OCH_3)_{1.03}$

(iii) Trema orientalis alkali-lignin (TO_AL)

$[C_9]$ = [C] - 0.387 $[OCH_3]$ = 58.72 -0.387 x 17.03 = 52.13%

So, n_{OCH3}= 3.48$[OCH_3]/[C_9]$ = 3.48 x 17.03/52.13 = 1.13

n_H= 107.7 ([H] -0.097 $[OCH_3]$)/$[C_9]$ = 107.7 (5.47-0.097 x 17.03)/52.13 = 7.88

n_O= 6.75 ([O] – 5.515 $[OCH_3]$)/$[C_9]$ = 6.75 (35.81 – 0.515 x 17.03)/52.13 = 3.50

Empirical formula of TO_AL: $C_9H_{7.88}O_{3.50}(OCH_3)_{1.13}$

(iv) Dipterocarpus turbinatus (GW_AL)

$[C_9]$ = [C] - 0.387 $[OCH_3]$ = 58.61-0.387 x 15.49 = 52.61%

So, n_{OCH3}= 3.48$[OCH_3]/[C_9]$ = 3.48 x 15.49/52.61 = 1.02

n_H = 107.7 ([H] -0.097 $[OCH_3]$)/$[C_9]$ = 107.7 (5.315-0.097 x 15.49)/52.61 = 7.80

n_O= 6.75 ([O] – 5.515 $[OCH_3]$)/$[C_9]$ = 6.75 (36.075 – 0.515 x 15.49)/52.61 = 3.60

Empirical formula of GW_AL: $C_9H_{7.80}O_{3.60}(OCH_3)_{1.02}$

A 2: Calculations for determining antioxidant activity of four alkali-lignin samples and Ascorbic acid by 2,2-Diphenyl-1-picrylhydrazyl (DPPH) method

Table A 2.1: Antioxidant activity of CF_AL (Absorbance of the blank = 0.475)

Concentration (µg/mL)	Log concentration	Sample absorbance	% of Scavenging	IC_{50} Value (µg/mL)
25	1.398	0.166	65.05	6.02
12.5	1.097	0.188	60.42	
6.25	0.796	0.233	50.95	
3.125	0.495	0.273	42.53	
1.562	0.194	0.315	33.68	
0.781	-0.107	0.354	25.47	
0.391	-0.408	0.391	17.68	

Table A 2.2: Antioxidant activity of BG_AL

Concentration (µg/mL)	Log concentration	Sample absorbance	% of Scavenging	IC_{50} Value (µg/mL)
25	1.398	0.226	52.42	19.57
12.5	1.097	0.251	47.16	
6.25	0.796	0.285	40.0	
3.125	0.495	0.376	20.84	
1.562	0.194	0.430	9.47	
0.781	-0.107	0.446	6.11	
0.391	-0.408	0.453	4.63	

Table A 2.3: Antioxidant activity of TO_AL

Concentration (µg/mL)	Log Concentration	Sample absorbance	% of Scavenging	IC_{50} Value (µg/mL)
25	1.398	0.213	55.16	16.40
12.5	1.097	0.257	45.89	
6.25	0.796	0.299	37.05	
3.125	0.495	0.332	30.11	
1.562	0.194	0.348	26.74	
0.781	-0.107	0.420	11.58	
0.391	-0.408	0.459	3.37	

Table A 2.4: Antioxidant activity of GW_AL

Concentration (µg/mL)	Log concentration	Sample absorbance	% of Scavenging	IC_{50} Value (µg/mL)
25	1.398	0.204	57.05	14.18
12.5	1.097	0.240	49.47	
6.25	0.796	0.269	43.37	
3.125	0.495	0.377	20.63	
1.562	0.194	0.383	19.37	
0.781	-0.107	0.466	1.89	
0.391	-0.408	0.474	0.21	

Table A 2.5: Antioxidant activity of Ascorbic acid

Concentration (µg/mL)	Log Concentration	Sample absorbance	% of Scavenging	IC_{50} Value (µg/mL)
50	1.699	0.087	81.68	9.52
25	1.398	0.154	67.58	
12.5	1.097	0.219	53.89	
6.25	0.796	0.287	39.58	
3.125	0.495	0.336	29.26	
1.562	0.194	0.403	15.16	
0.781	-0.107	0.444	6.53	
0.391	-0.408	0.465	2.11	

A 3: Applied methods for the analysis of lignocellulosic biomass

A 3.1. Introduction

All lignocellulosic biomasses consist of non-structural and structural components. Non-structural components are those which are non-chemically bound to the complex biomass matrices. Broadly, these components include resin, waxes, chlorophyll, protein, ash, etc. The non-structural components are also called extractives and can be removed by different solvents, e.g., water, ethanol, etc. applying exhaustive extraction processes. Removal of non-structural components is essential as they could potentially interfere the downstream analysis of the biomass samples.

A 3.2. Preparation of sample for compositional analysis [66]

Collected lignocellulosic biomass samples were sundried to reduce the moisture content below 10% and then grounded to fine powder. Powdered samples of 40-60 mesh were used for compositional analysis according to NREL/TP-510-42620.

A 3.3. Determination of extractives [67]

An exhaustive extraction process is complete when most or all of the extractable materials have been extracted from the biomass samples. Usually, an exhaustive extraction process is complete within 24 h of extraction. Soxhlet apparatus and accelerated solvent extractor can be used for the exhaustive extraction purposes. After removal of the non-structural components as extractives, the lignocellulosic biomass residue is called extractive-free biomass. Extractive-free lignocellulosic biomasses contain structural components, e.g., components those are chemically bound and formed the biomass matrices. These components are celluloses, hemicelluloses and lignin.

All measurement needs to be performed and calculated as oven-dried weight (ODW) of biomass basis, e.g., moisture-free samples. Water and ethanol soluble extractives of the biomass samples were determined following the procedure described by National Renewable Energy Laboratory No. NREL/TP-510-42619.

Extraction by Accelerated Solvent Extractor

Procedure

- The collection tubes were dried at 105 ± 5 °C using a convection oven for 12 h. After cooling in a desiccator, the weight of the tubes was recorded to the nearest 0.1 mg.
- Placed two appropriately sized glass filters in the bottom of a labeled extraction cells, tamped down one at a time. A tamping rod was fitted each extraction cells. Polypropylene filter cloth was used to cut filters.
- About 2 g of oven-dried samples, i.e., Coconut fibre (CF), Baggase (BG), *Trema orientalis* (TO) and *Dipterocarpus turbinatus* (GW) of samples to a tared extraction cells. Placed the cell in the automatic extractor and extraction performed accordingly.

Operation and software details

Using the Dionex ASE system and ASE software, program the following parameters:
Pressure: 1500 PSI
Temperature: 100 ^{o}C
Preheat time: 0
Heat time: 5 minutes (automatic software default)
Static time: 7 minutes
Flush volume: 150%
Purge time: 120 seconds
Static cycles: 3

Saved one program for 100% water and another for 95% ethanol.

After completing the extraction, the extraction cells were to cooled to room temperature, vacuum dried up to constant weight achieved and calculated the water and ethanol soluble extractives.

A 3.4. Total ash contents [68]

Total ash contents were determined by heating of each sample in a muffle furnace at 575 ± 25 ^{o}C for 4 h following NREL/TP-510-42622 method. 2 g of each lignocellulosic biomass samples, i.e., Coconut fibre (CF), Baggase (BG), *Trema orientalis* (TO) and *Dipterocarpus turbinatus* (GW) were heated in the muffle furnace at 575 ± 25 ^{o}C for 4 h. After cooling the ash contents were measured gravimetrically.

A 3.5. Determination of Klason lignin [69]

Klason lignin and acid insoluble ash contents were measured by NREL/TP-510-42618 method. Briefly, 300 ± 2 mg of oven-dried lignocellulosic biomass samples, i.e., Coconut fibre (CF), Baggase (BG), *Trema orientalis* (TO) and *Dipterocarpus turbinatus* (GW) were taken in pressure tubes. 3.00 ± 0.01 ml 72% H_2SO_4 solution was added to each tube and mixed uniformly with a glass rod. Pressure tubes were placed in a water bath at 30 ± 3 ºC for 60 min and stirred after 5-10 min interval. Pressure tubes were removed after 60 min hydrolysis. Then, the mixtures were diluted to 4% H_2SO_4 concentration by adding de-ionized water to 84 ± 0.04 ml. Vacuum filtration of the mixtures were done using previously weighted Gooch type II filtering crucible. 50 ml of each filtrate was transferred in storage bottle for ASL analysis. 50 ml de-ionized water was further added for washing the acid insoluble lignin. After drying the crucible containing acid insoluble residues at 105 ± 3 ºC in convection oven for 4 h, then cooled in a desiccator. The acid insoluble lignin was calculated and reported as klason-lignin of the lignocellulosic biomass.

A 3.5.1. *Measurement of acid insoluble ash*

The crucible with dried klason-lignin was placed in a muffle furnace at 575 ± 25 ºC for 4 h. After ashing, the crucible was cooled in a desiccator and then weight loss was measured. The residue was reported as acid insoluble ash.

A 3.5.2. *Measurement of acid soluble lignin*

Acid soluble lignin of the samples was determined using a simple gravimetric technique. After six months' preservation of the stored filtrate in the 50 mL centrifuge tube, interestingly, acid soluble lignin was precipitated and settled down. The precipitate was collected by vacuum filtration using Gooch type III crucible. The crucible was then dried in a convection oven at 105 ± 3 ºC until constant weight achieved. The residue was reported as acid soluble lignin.

A 3.6. Determination of holocellulose content [70]

About 2 g extractive-free dried biomass sample was taken in 250 mL conical flask and then 80 mL distilled water was added with magnetic stirring. Temperature of the pulp mixture was set at 75 ± 5 ºC for 6 h. 0.5 mL acetic acid and 2.6 mL 25% (w/v)

$NaClO_2$ solution were added into the mixture 3 to 5 times in every hour (pH of the mixture was sat at 4 using CH_3COOH-CH_3COONa buffer).

After completion of delignification, the mixture was filtered and the residue (holocellulose) was washed several times with distilled water. The holocellulose was then dried under vacuum at 70 ^oC for 96 h or until constant weight achieved. Yield was calculated as oven-dried basis.

A 3.6.1. Determination of α-cellulose content [71]

About 1 g of dried holocellulose sample was taken in 250 mL round bottom flask and 50 mL 17.5 w/v % NaOH solution was added. The mixture was stirred by magnetic stirrer at 250 rpm for 30 min. 50 mL distilled water was added to it and further stirred for another 30 min and then filtered. Residue was washed three times with distilled water and then 50 mL 10% CH_3COOH solution was used for further washing. Finally, the residue was washed with distilled water and then dried in vacuum at 70 ^oC for 96 h or until constant weight achieved. Yield was calculated as oven dried basis.

A 3.6.2. Determination of hemicellulose content [72]

Hemicellulose contents were determined from the difference between holocellulose and α-cellulose contents of each biomass.

A 3.7. Microscopic observation of biomass samples

Optical micrograph of biomass samples were taken by optical microscope (Karl-Zeiss, Germany) at 100X magnification.

Figure A 3.7.1. Extractive-free lignocellulosic biomass samples

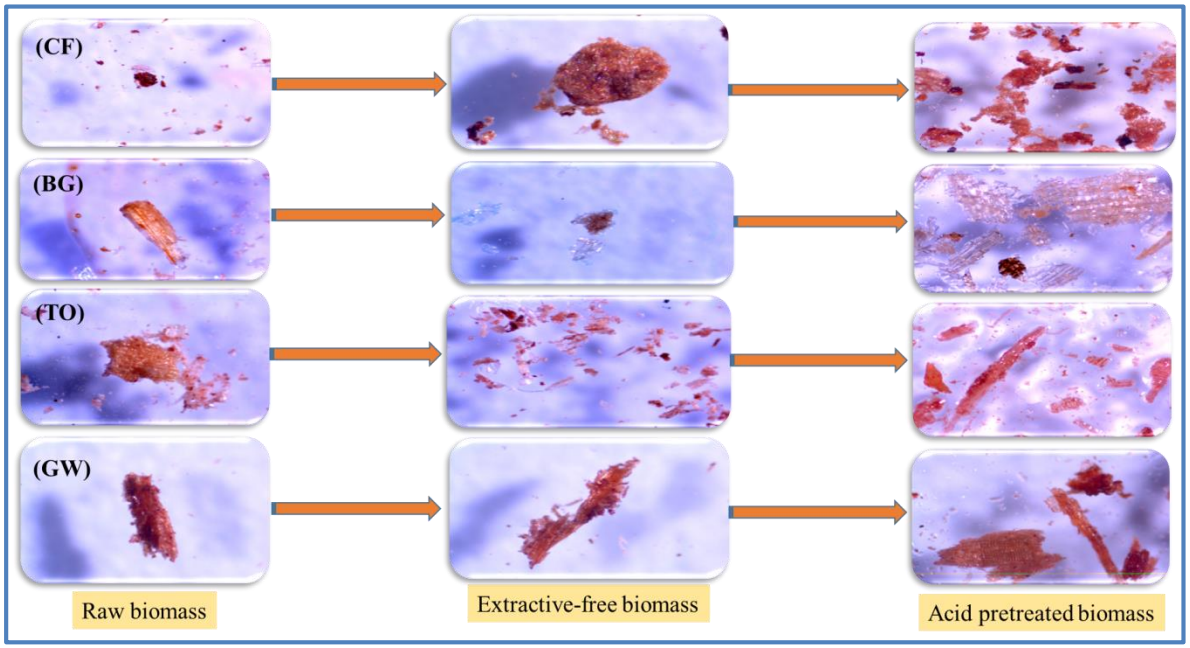

Figure A 3.7. 2: Optical micrographs of powdered raw biomass sample (left position in the Figure). Intermolecular forces among the non-structural and structural constituents in the complex lignocellulose matrices were broaken/loosen caused by the removals of water and ethanol extractives and dilute acid pretreatment. Sowllen structures could be seen from the micrographs of extractive-free (mid position) and acid pretreated biomass (right position).

A 4: Some figures on FT-NIR analysis of lignocellulosic biomass components recovered at different pretreatment phases

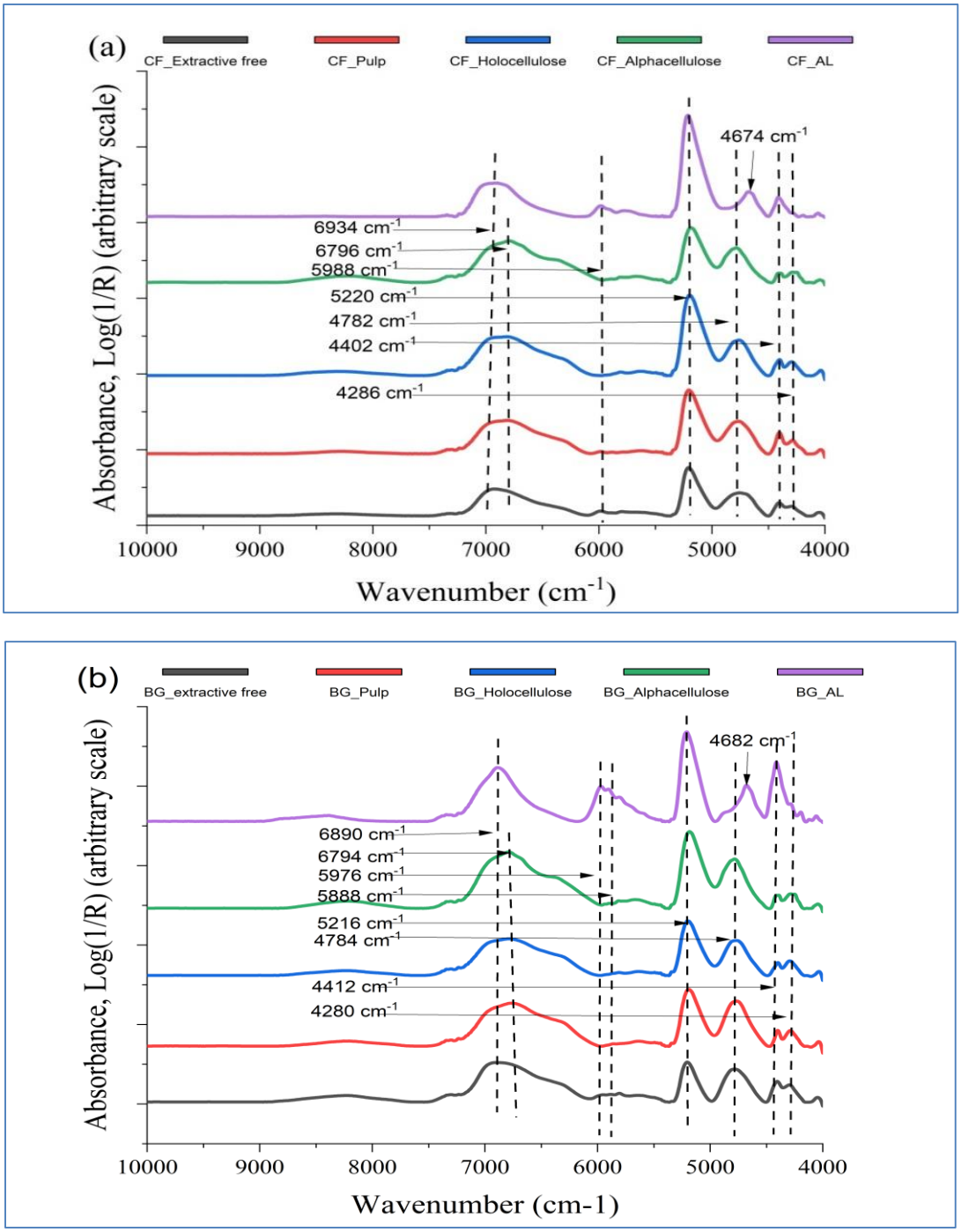

Figure A 4: FT-NIR spectra of isolated components, i.e., cellulosic pulp, holocellulose, α-cellulose and alkali-lignin of lignocellulosic biomass, (a) coconut fibre (extractive-free) and (b) bagasse (extractive-free). First overtone bands of aromatic C-H stretching in isolated alkali-lignin samples could be seen at 5988 and 5976 cm^{-1}, respectively with higher absorbances. Combination bands of (C_{ar}-H stretching + C=C stretching) in both alkali-lignin samples could also be seen at 4674 and 4682 cm^{-1}.

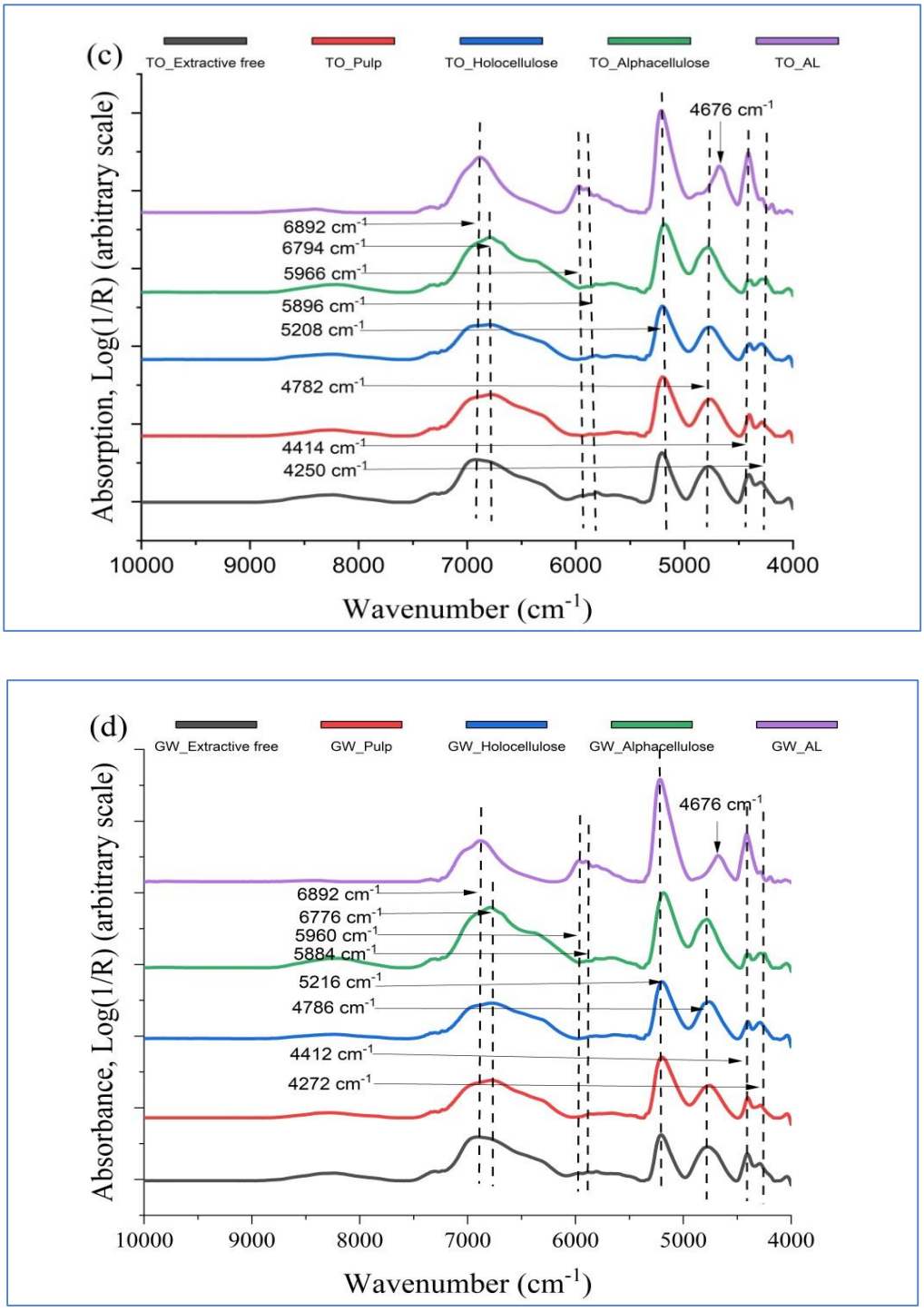

Figure A 4: FT-NIR spectra of isolated components, i.e., cellulosic pulp, holocellulose, α-cellulose and alkali-lignin of lignocellulosic biomass, (c) *Trema orientalis* (TO) (extractive-free) and (d) *Dipterocarpus turbinatus* (GW) (extractive-free). First overtone bands of aromatic C-H stretching in isolated alkali-lignin samples could be seen at 5966 and 5960 cm^{-1}, respectively with higher absorbances. Combination bands of (C_{ar}-H stretching + C=C stretching) in both alkali-lignin samples could also be seen at same wavenumber, 4676 cm^{-1}.

A 5: Particle size analysis of alkali-lignin samples in DMSO-Water system at 0.15 and 0.20 mg/mL concentrations by dynamic light scattering technique

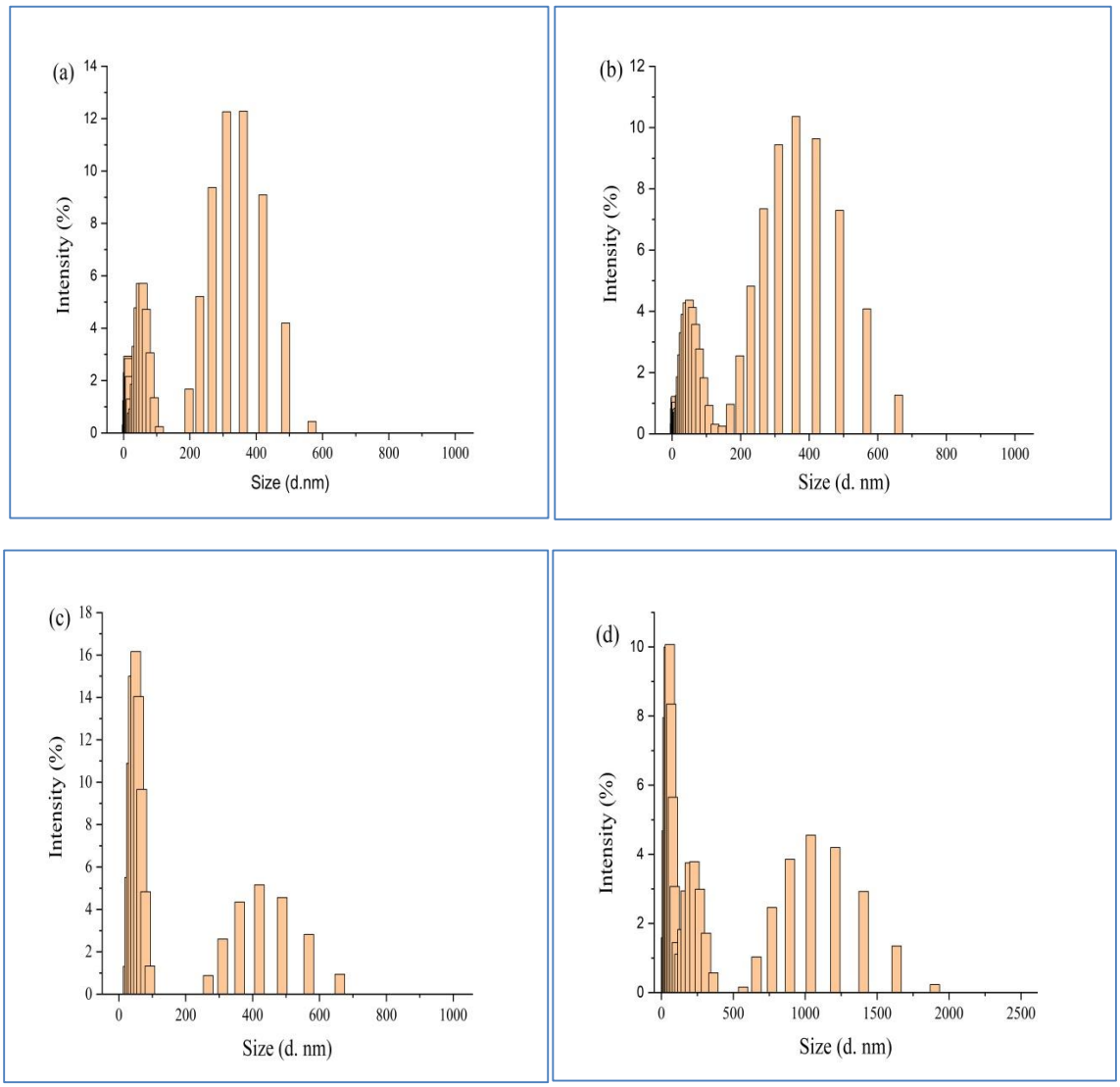

Figure A 5: Particle sizes and distributions of alkali-lignin samples in DMSO-Water Systems, (a) CF_AL at 0.15 mg/mL concentration, (b) CF_AL at 0.20 mg/mL concentration, (c) BG_AL at 0.15 mg/mL concentration and (d) BG_AL at 0.20 mg/mL concentration

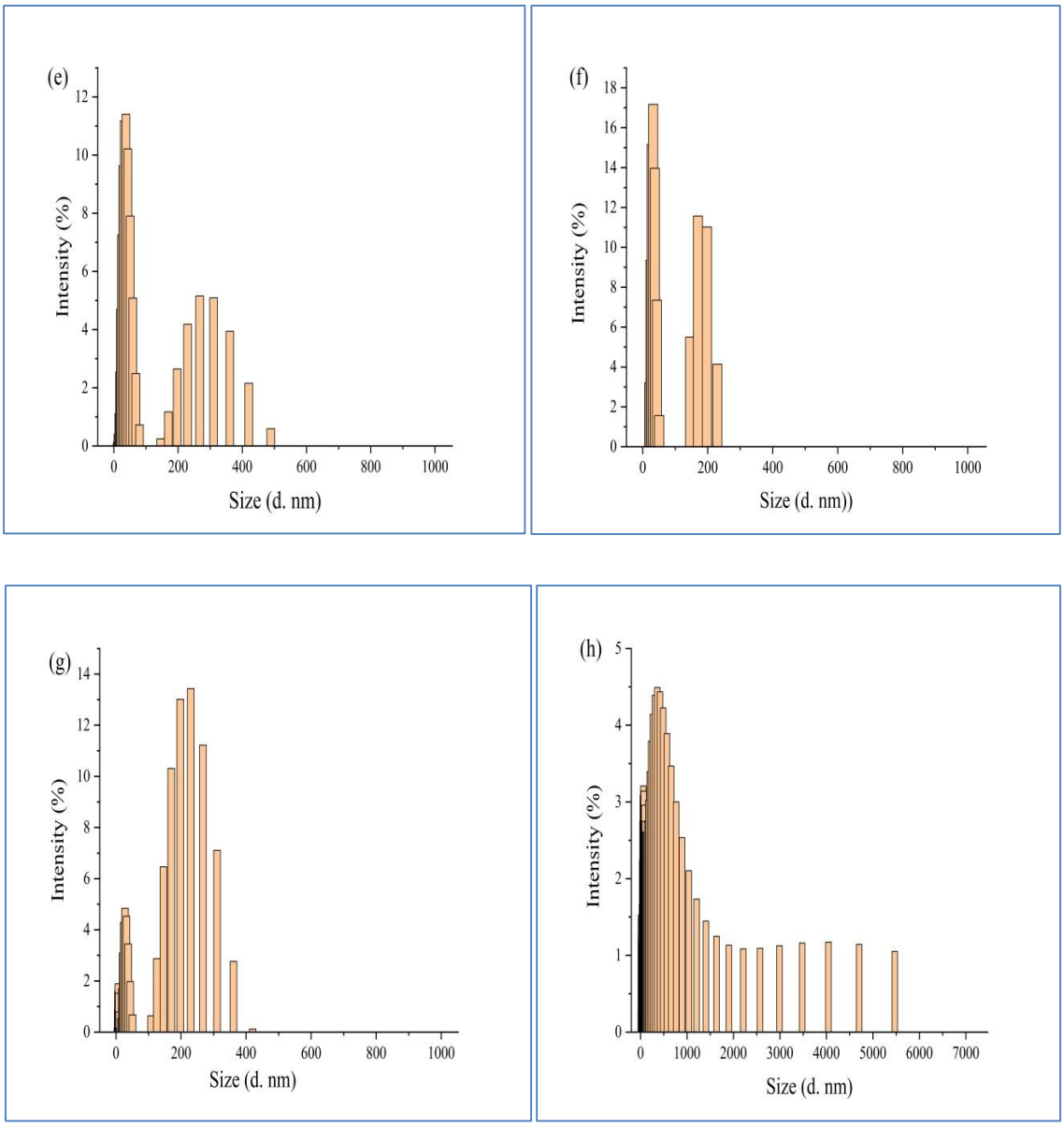

Figure A 5: Particle sizes and distributions of alkali-lignin samples in DMSO-Water systems, (e) TO_AL at 0.15 mg/mL concentration, (f) TO_AL at 0.20 mg/mL concentration, (g) GW_AL at 0.15 mg/mL concentration and (h) GW_AL at 0.20 mg/mL concentration.

A 6: Schematic diagram of some instruments used in the research work

The following instruments have been used for the characterization and properties determination of lignocellulosic biomass, lignin, modified lignin, recovered NPK-containing materials and others. Basic principles of the instruments are well established. Only schematic diagram of the instruments with some related figures on the analysis have been given below-

AD 6.1: Elemental analyzer

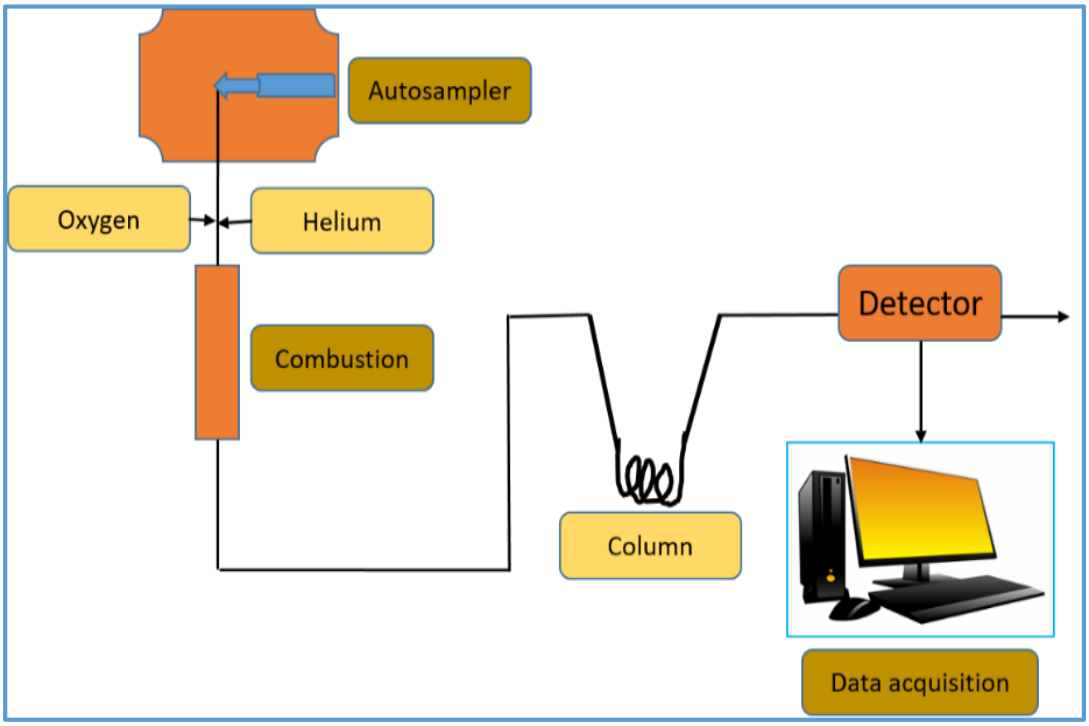

Figure AF 6.1: Schematic diagram of an Elemental Analyzer

AD 6.2: X-ray photoelectron spectrometer

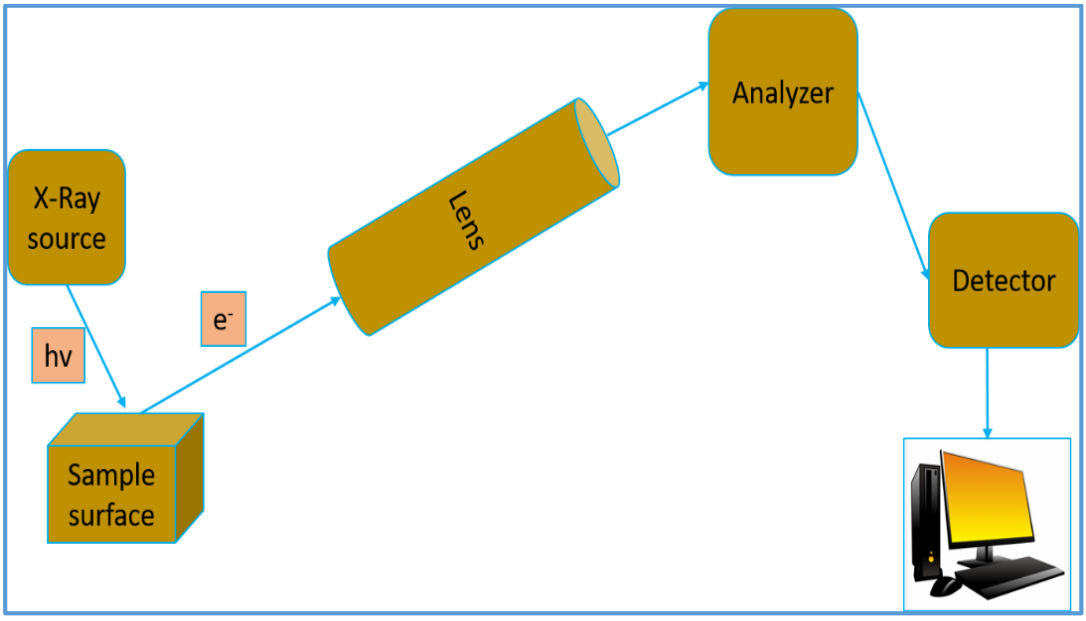

Figure AF 6.2.1: Schematic diagram of X-Ray Photoelectron Spectrometer

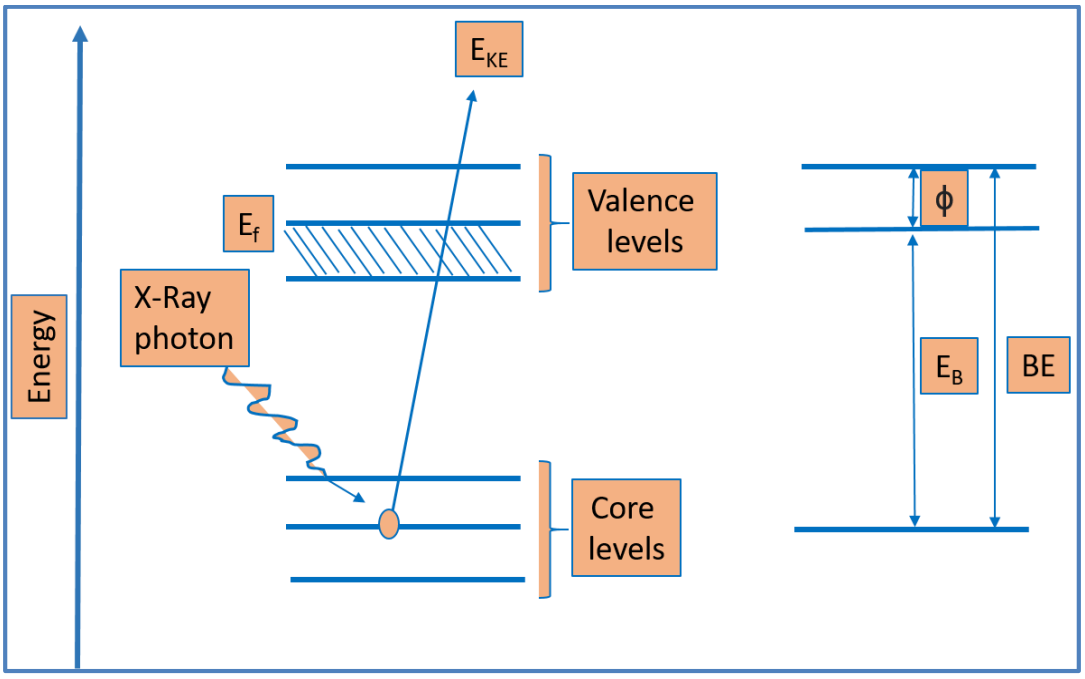

Figure AF 6.2.2: Schematic diagram for energy-material interaction in X-Ray Photoelectron Spectrometer

AD 6.3: Scanning electron microscopy-energy dispersive X-ray spectrometer

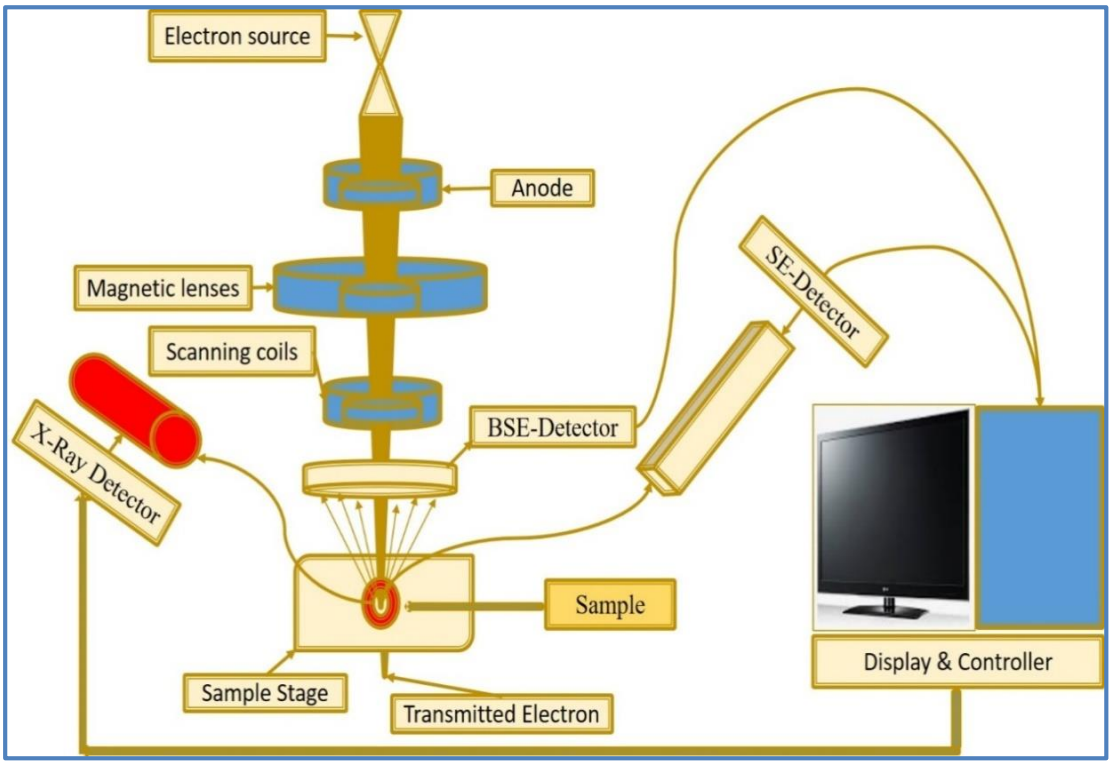

Figure AF 6.3.1: Schematic diagram of Scanning Electron Microscope

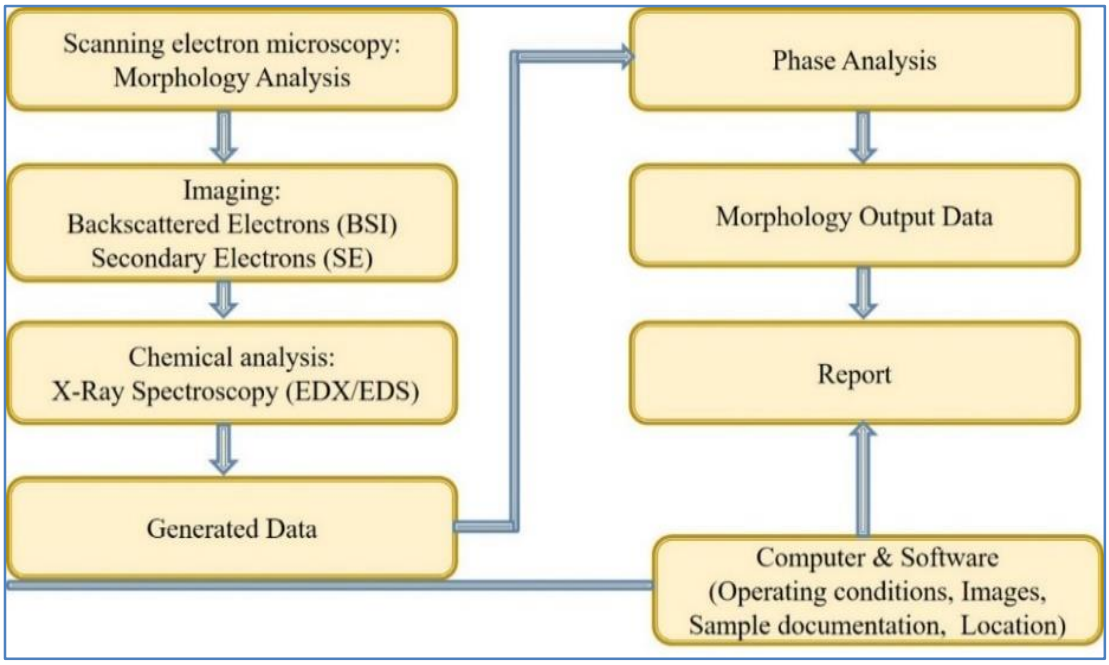

Figure AF 6.3.2: SEM morphology method with chemical analysis of materials

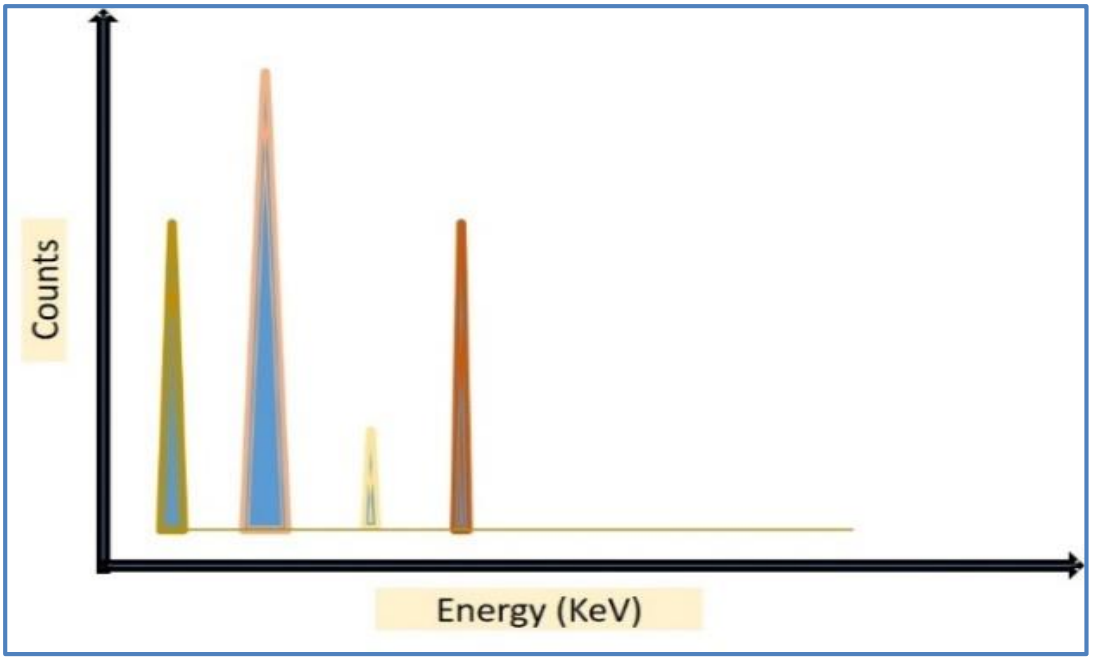

Figure AF 6.3.3: Graphical representation of EDX Spectrum

AD 6.4: Dynamic light scettering based particle size analyzer

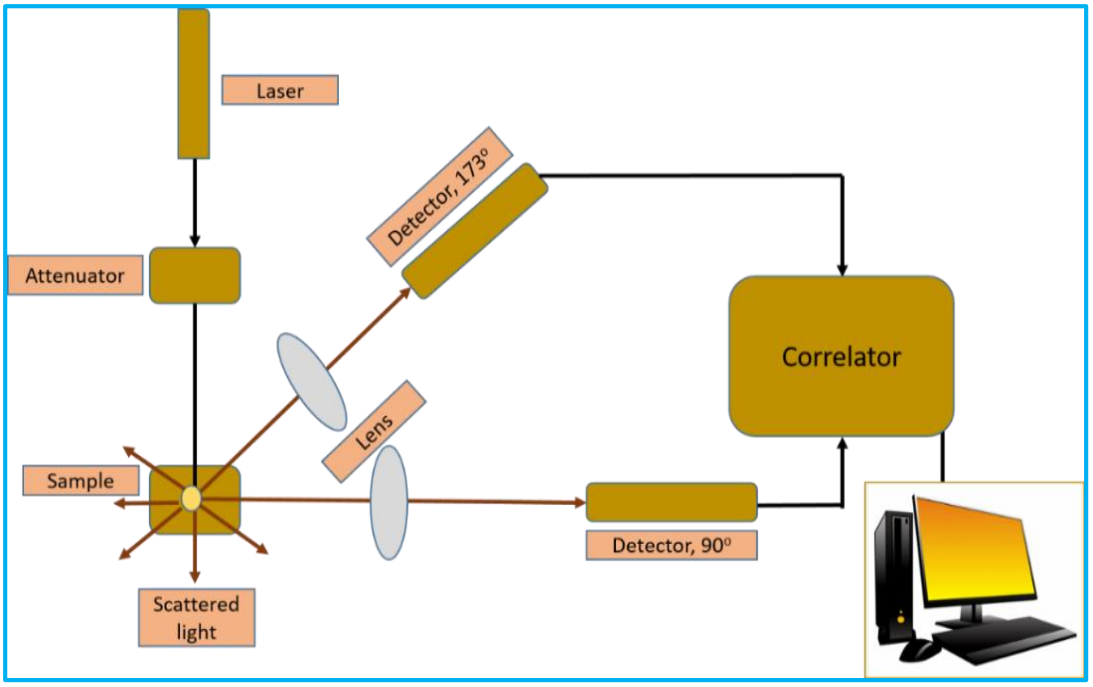

Figure AF 6.4: Schematic diagram of Dynamic Light Scattering based Particle Size Analyzer

AD 6.5: Fourier transform mid and near infrared spectrometer

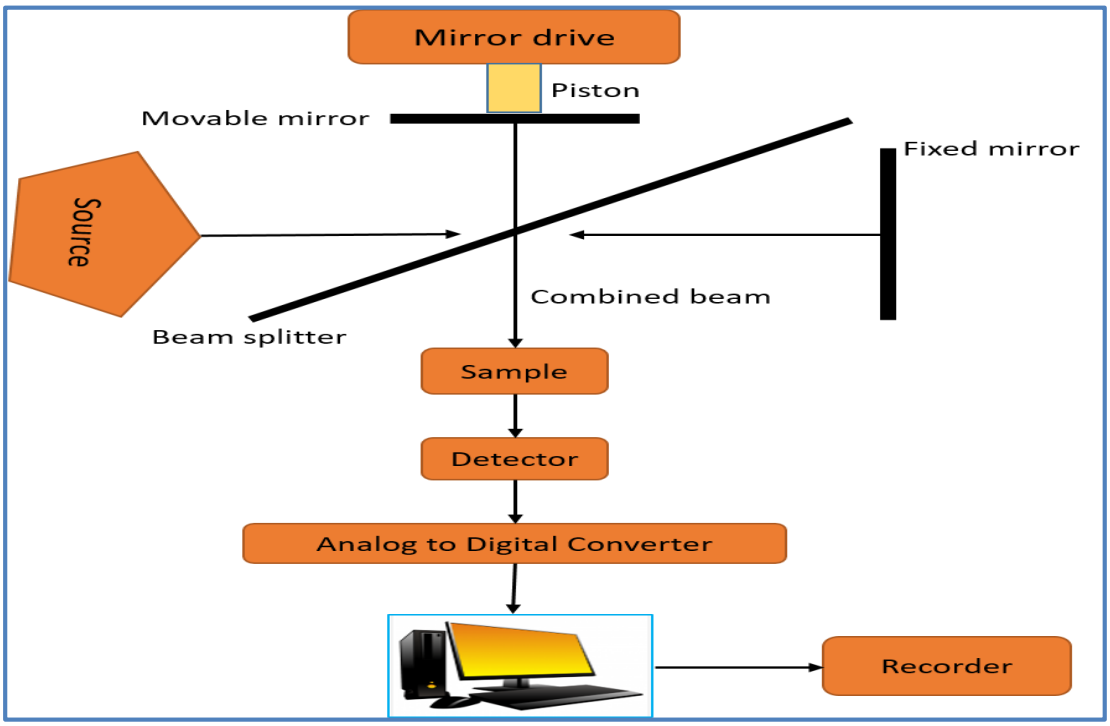

Figure AF 6.5: Schematic diagram of FT-MIR-NIR spectrometer

AD 6.6: Nuclear magnetic resonance spectrometer

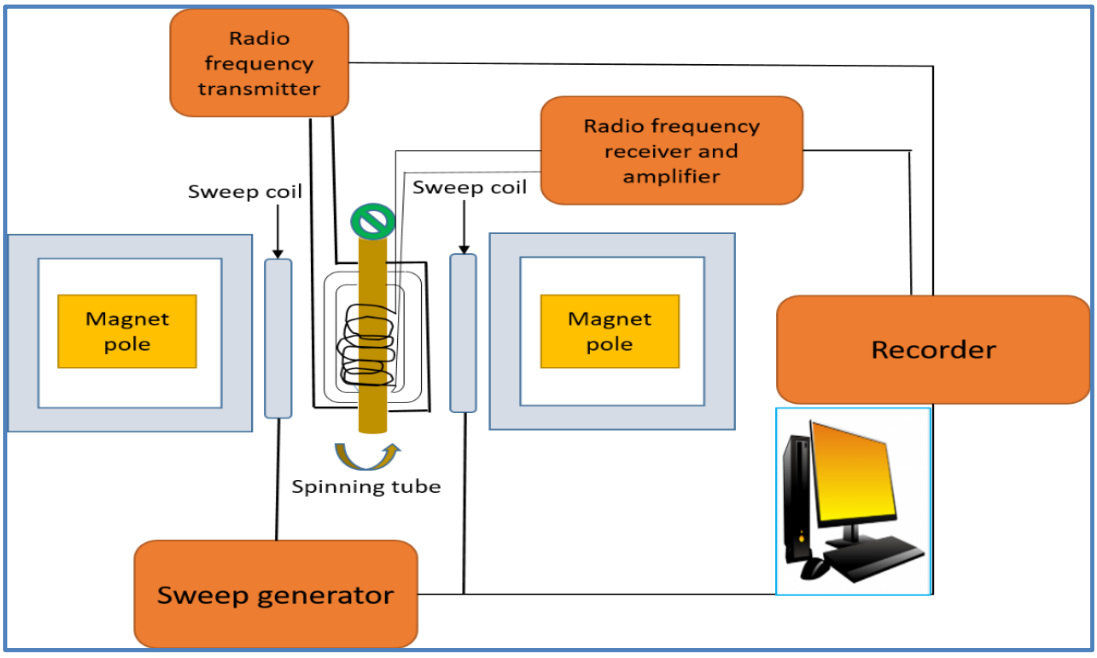

Figure AF 6.6: Schematic diagram of Nuclear Magnetic Resonance Spectrometer

AD 6.7: X-ray diffractometer

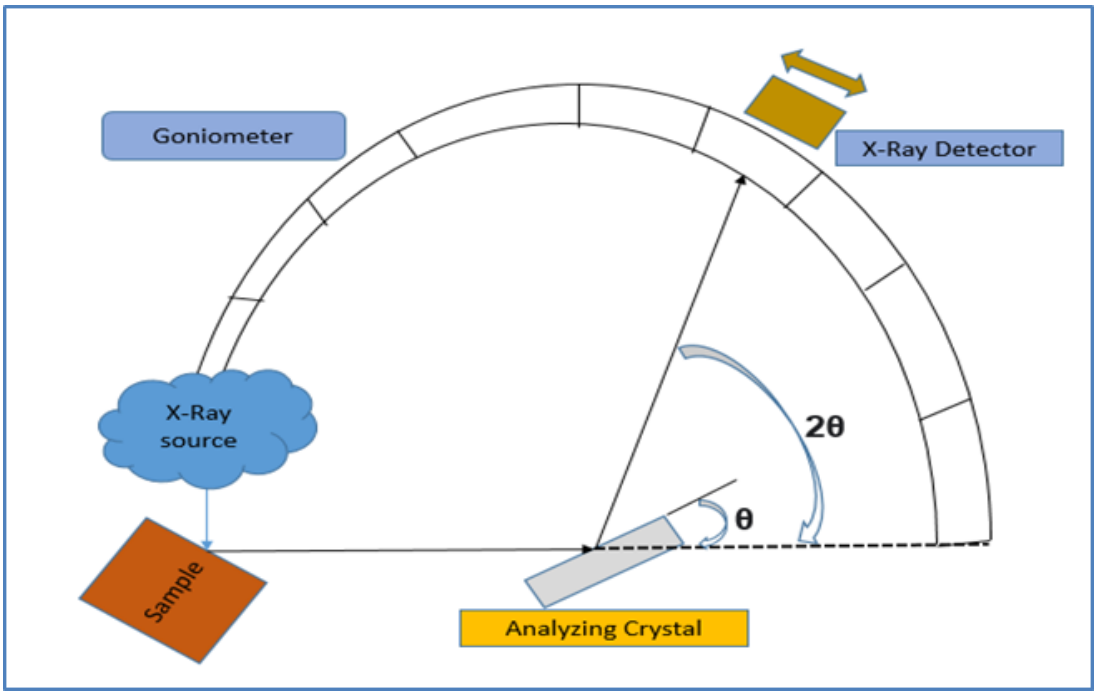

Figure AF 6.7.1: Schematic diagram of X-Ray diffractometer

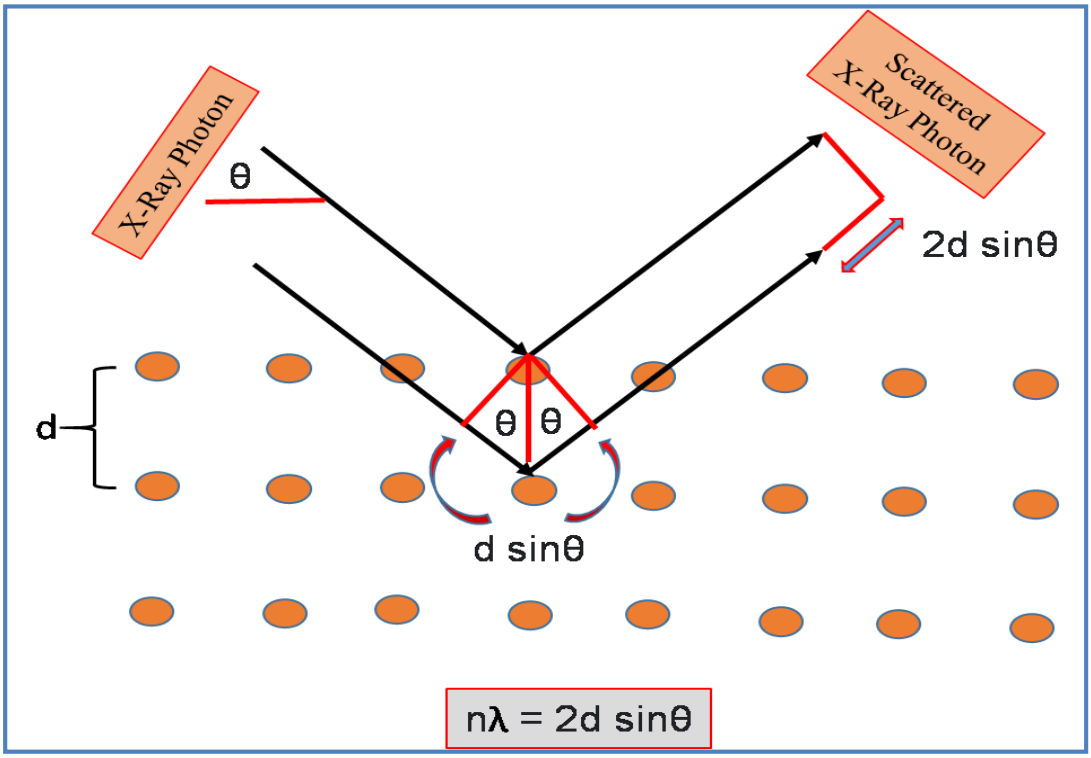

Figure AF 6.7.2: Schematic diagram of X-Ray diffraction of crystalline materials

AD 6.8: Simulteneous thermal analyzer

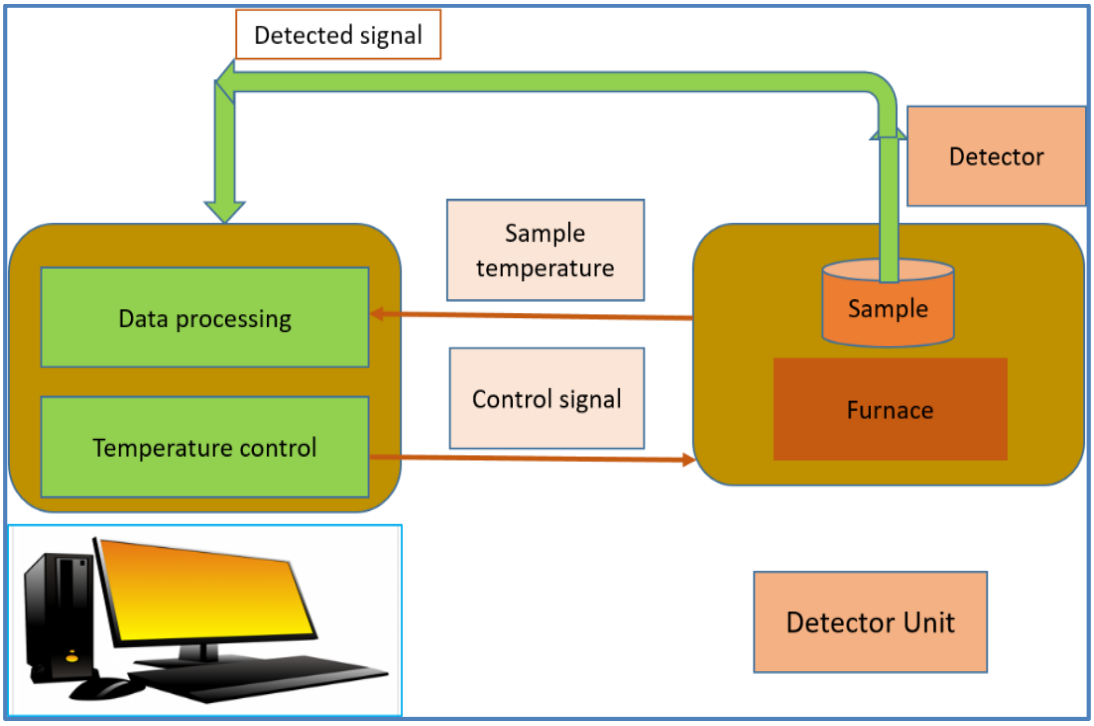

Figure AF 6.8: Schematic diagram of a Simulteneous thermal analyzer

AD 6.9: Double beam Ultraviolet-Visible spectrophotometer coupled with an Integrating sphere

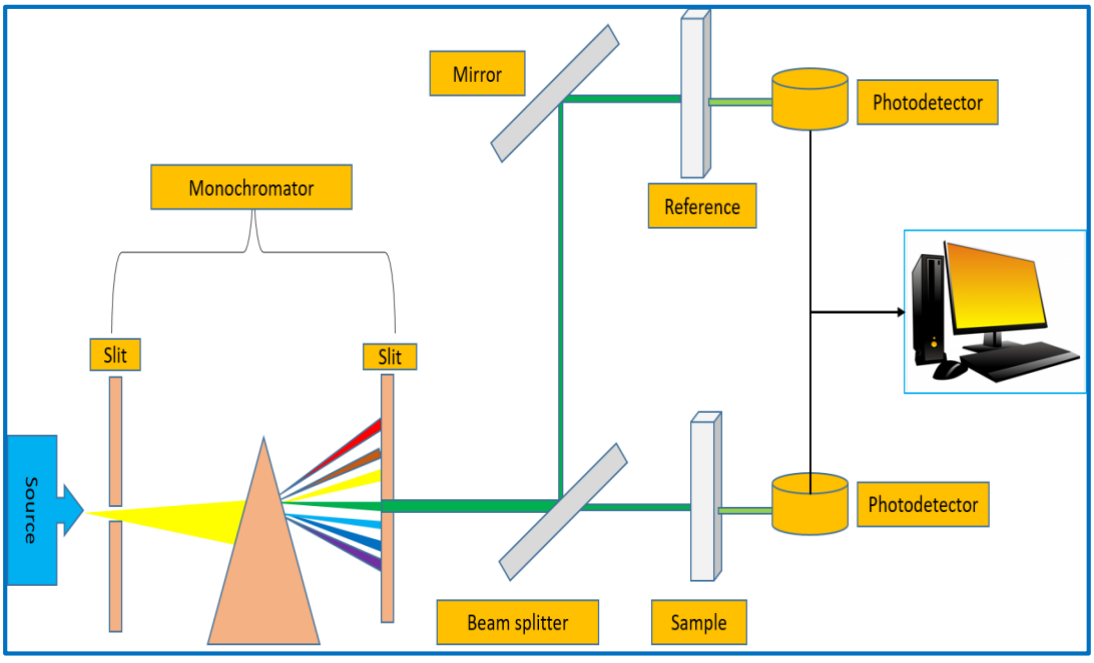

Figure AF 6.9.1: Schematic diagram of UV-Vis Spectrophotometer

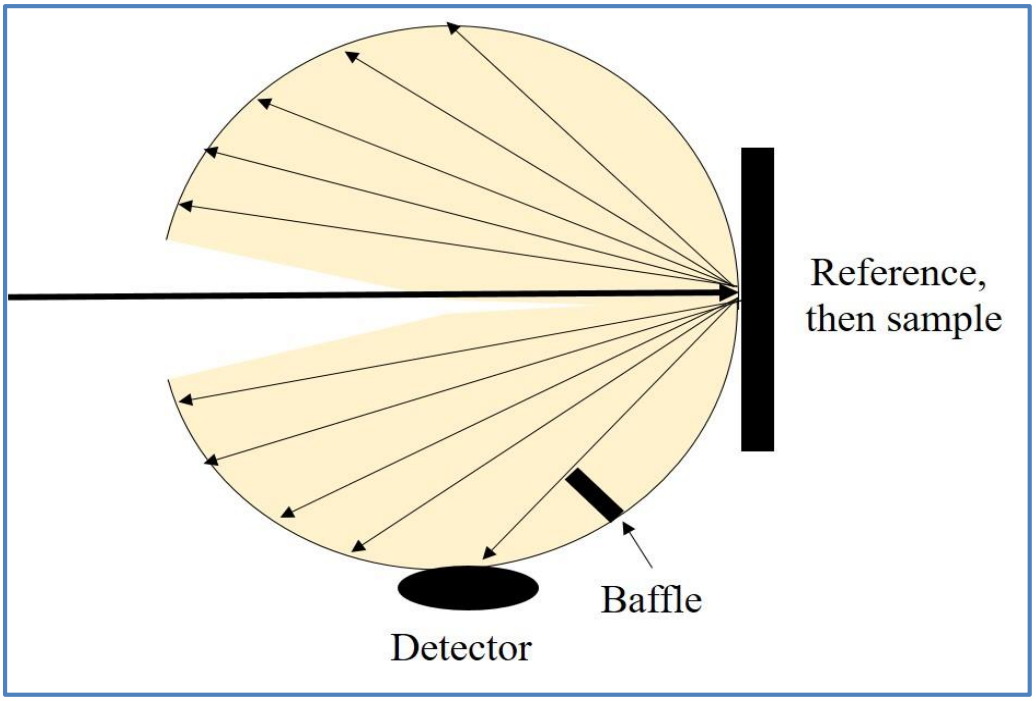

Figure AF 6.9.2: Schematic diagram of an integrating sphere attached with UV-Vis spectrophotometer for diffuse reflectance spectroscopic analysis

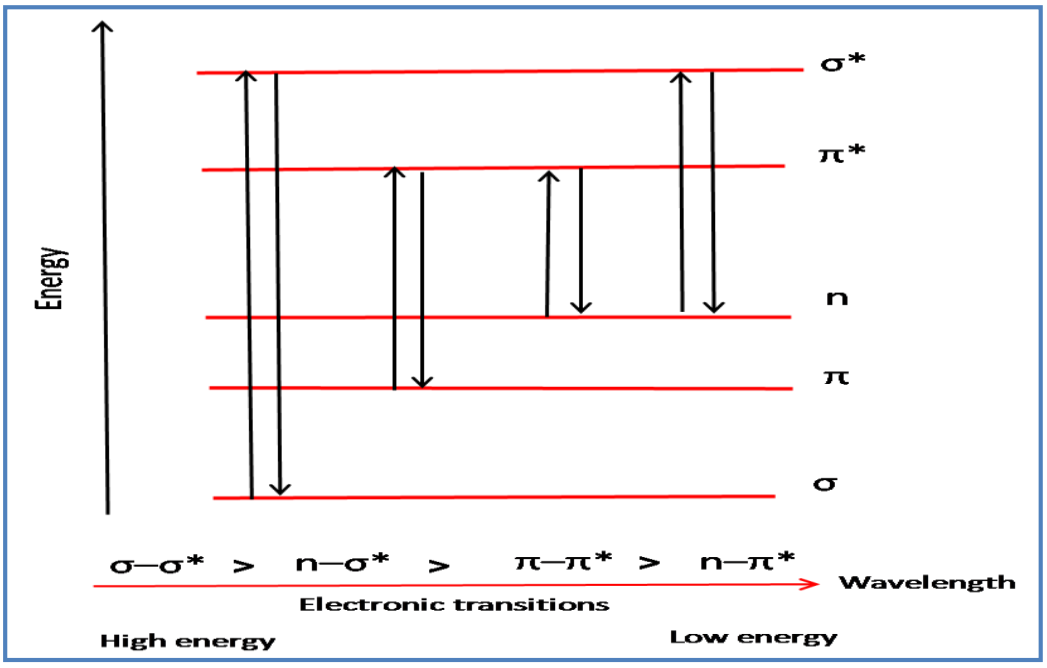

Figure AF 6.9.3: Electronic transitions in molecular orbitals

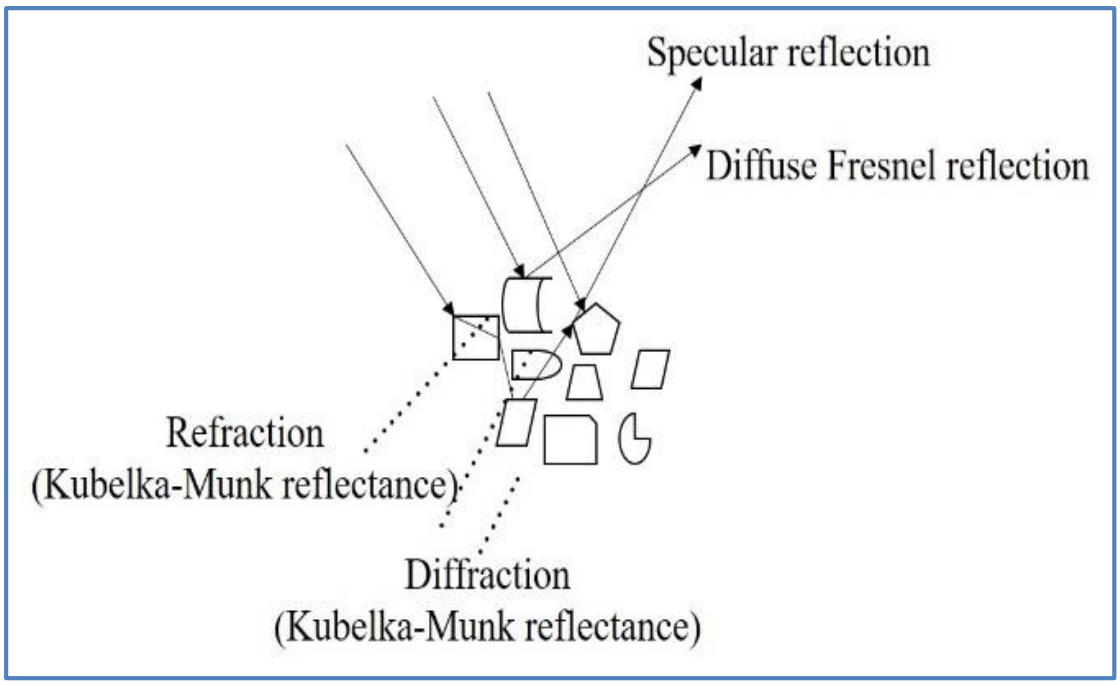

Figure AF 6.9.4: Optical phenomena in UV-Vis diffuse reflectance spectroscopy

AD 6.10: Automated Microviscomerter (Rolling-ball type)

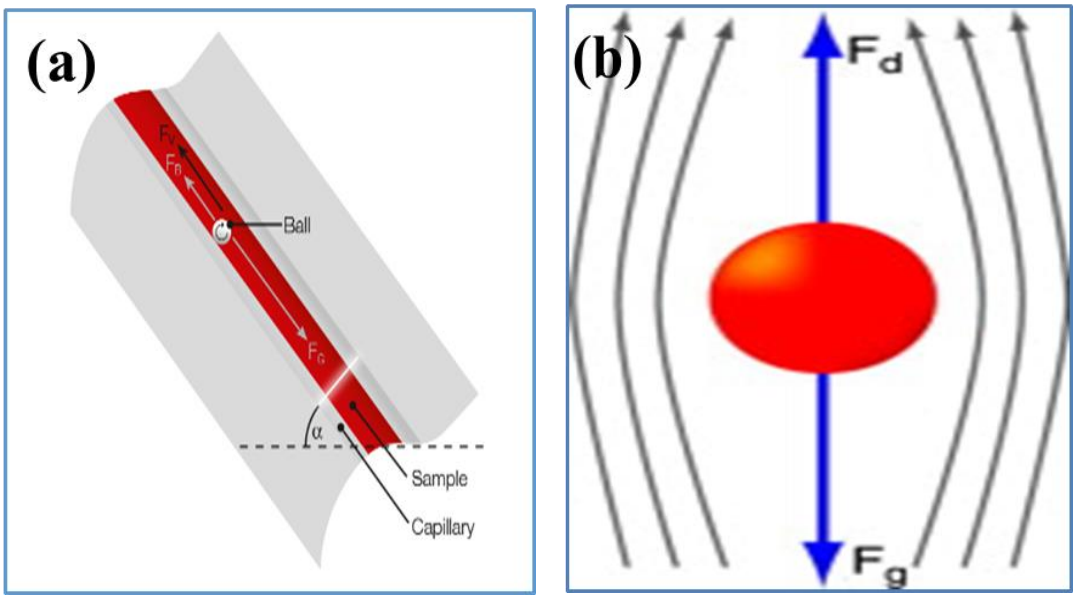

Figure AF 6.10: Automated Microviscometer (a) the inclination angle of the capillary and (b) forces acted on the rolling ball. A portion of the gravitational force (F_g), which depends on the angle, drives the ball downwards. As opposing forces (F_d), the buoyancy inside the sample and the viscous forces of the liquid slow the ball down. (https://www.anton-paar.com/corp-en/products/details/rolling-ball-viscometer-lovis-2000-mme)